Glassy Behaviour in Simple Systems

Lexie Davison

New College
University of Oxford

Thesis submitted for the Degree of Doctor of Philosophy at the University of Oxford

· Trinity Term 2001 ·

"The ice is music, the glass is noise..."

J. Tyndall, 1863

Glassy Behaviour in Simple Systems

Lexie Davison

New College

A thesis submitted in partial fulfillment of the requirements for the Degree of Doctor of Philosophy at the University of Oxford

Trinity Term 2001

Abstract

In this thesis we study several different models which display glassy behaviour. Firstly, we investigate a simple, purely topological, cellular model for which the Hamiltonian is non-interacting but the dynamics are constrained. We find a non-thermodynamic transition to a glassy phase in which the energy fails to reach the equilibrium value below a characteristic temperature which is dependent on the cooling rate. This model involves activated processes and displays two-step relaxation in both the energy and the correlation functions; the latter also exhibit signs of aging. The relaxation time can be well-fitted at all temperatures by an offset Arrhenius law. Some predictions of Mode-coupling Theory are tested with some agreement found, but no convincing evidence that this description is the most fitting. By defining a suitable response function, we find that the equilibrium Fluctuation-Dissipation Theorem (FDT) is upheld for all but very short waiting-times, despite the fact that the system is not in equilibrium.

This topological model is simplified to a hexagonally-based spin model, which also displays glassy behaviour, involves activated processes and exhibits two-step relaxation. This is a consequence of reaction-diffusion processes on two different time-scales, one temperature-independent and the other an exponential function of inverse temperature. We study two versions of this model, one with a single absorbing ground state, and the other with a highly degenerate ground state. These display qualitatively similar but quantitatively distinct macroscopic behaviour, and related but different microscopic behaviour. We extend this work to a square lattice, and find that the geometry of the lattice has a considerable impact on the behaviour, and to three dimensions, which provides support for the reaction-diffusion classification of the early behaviour. We find observable-dependent FDT plots; the observable can be chosen such that FDT is upheld for a region whilst the system is out of equilibrium — this observation is supported by some preliminary results for one-dimensional kinetically-constrained Ising chains.

Contents

Acknowledgements

I would like to extend my sincere thanks to my supervisor, Prof David Sherrington, for his support and guidance throughout the course of my DPhil. I would also like to thank my collaborators, Dr Juan Pedro Garrahan and Dr Arnaud Buhot, who have been a pleasure to work with.

I have thoroughly enjoyed my three years as a graduate student — this is largely due to the people who make up the Theory department. I'd particularly like to mention the two Toms, with whom I shared an office; their comments and insights have been invaluable, and their patience throughout my regular gripes and moans nothing short of saintly! It has been a pleasure sinking many Blue Hawaiians with them and the rest of the the DoC crew: Miraculous Joe, Steph, Seb, Andy and the two Petes. My heartfelt thanks also goes to Adrian for his help, encouragement, LaTeX expertise and irreverent emails which brighten up my days.

Beyond the confines of the department my thanks go to: Laura, for unstinting friendship and general maintenance of my sanity through many coffees, lunches and rapid-response emails; Leigh, for nights out in London unraveling that sanity and many years of being my partner in crime; Ed, for his incredible patience and for never failing to thoroughly spoil me; house-mates Colm and Susie, for fireworks and vodka jelly parties; Chloe, who made swimming large bodies of water almost fun; and the rest of the London crowd — Sam, Grant and Harry — who managed to wine, dine and dance the night away with me on numerous occasions.

Lastly I must thank my parents, whose love and support has given me the confidence to try my hand at anything and everything, be it a theoretical physics DPhil or a four hour swim, and who are always ready to listen. This thesis is dedicated to them.

Publications

The research presented in this thesis is original work by the author unless expressly stated otherwise. Much of the work has appeared in the following publications:

- L. Davison and D. Sherrington, Journal of Physics A **33** (2000), pp 8615-8625
- L. Davison, D. Sherrington, J. P. Garrahan and A. Buhot, Journal of Physics A **34** (2001), pp 5147-5182

L. Davison is grateful for the support of EPSRC(UK) research studentship 98311155.

List of Figures

Chapter 1

Introduction

Examples of glassy behaviour are everywhere in our world, with disordered materials playing significant rôles in a wide range of applications. Ordinary window glass has obvious impact in building applications and most optical fibres are made from a highly purified form of the same substance (vitreous silica). Amorphous silicon is used widely in the electronics industry, particularly in photovoltaic cells, and recently amorphous metal alloys have made an impact in the same field. Synthetic polymers have in many cases no crystallinity at all, and all have at least some amorphous character. One might be forgiven for thinking that with glassy behaviour so abundant, it must be well understood; in fact, relaxation in liquids and glasses is one of the oldest problems in condensed matter theory and remains as yet unsolved.

The history of this field is long and has relied heavily on phenomenology[1]. With the advent of technology computer simulations have contributed much to the body of knowledge within the field. Since glassy behaviour itself is a wide-ranging phenomenon, the models developed in order to attempt to understand it are also wide-ranging. One requires either disorder or frustration within the model, but that can be achieved explicitly through the Hamiltonian, or it can be introduced through the dynamics. In addition the interactions may be local or infinite-range. These loose requirements inevitably result in a great many extremely diverse models leading to glassy behaviour.

The ethos of this thesis is minimalism: we wish to study the simplest possible models in order to establish the relevant physics, with the hope that the findings may also then be applicable to a wider range of models. Thus for the early part of this thesis (Chapter 2) we focus on a purely topological model that is a simplified version of a two-dimensional soap froth. We look for glassy signatures within this model, and also study the results within the context of the predictions of Mode-coupling Theory (MCT), some features of which will be reviewed briefly in Section 1.1.

This topological model can be further simplified by introducing an underlying hexagonal lattice. One then finds oneself dealing with a three-state spin-model (Chapter 3) which is somewhat more tractable than the original topological model,

[1] For an interesting short introduction see [1], which contains within many historical references.

and has natural connections with both kinetically-constrained Ising models and reaction-diffusion models; thus the general review that follows in this introductory chapter will cover both of these areas as well as that of glasses. As the reader will no doubt be aware, each of these three topics is a vast field in of itself, and each attracts specialist study; therefore this review cannot be and is not intended to be entirely comprehensive, but merely sufficient to remind the reader of the relevant features that one should bear in mind throughout this thesis. The remainder of the thesis deals with extensions of this work to a square lattice (Chapter 4), with some comparison to common kinetically-constrained models (Chapter 4), and to three dimensions (Chapter 5). Chapter 6 presents the concluding remarks of this thesis.

1.1 Glasses

The simplest description of a glass is that of a liquid that has become so viscous it can no longer flow. This ties in neatly with the experimentalists' viewpoint that a substance undergoes a glass transition when its viscosity reaches the (somewhat arbitrary) value of 10^{13} Poise. However, the most suitable definition for our purposes, and one which shall be used throughout this thesis, is that a system is in a glassy state if it fails to equilibrate over even the longest time-scale that one can probe through experiment. To elaborate, the normal experimental method of preparation of a glass is cooling of a viscous liquid. Under cooling from high temperatures, a liquid may crystallise at a characteristic temperature T_m through a first-order phase transition; if it manages to get below T_m without crystallizing, it is known as a super-cooled liquid. Upon further cooling the viscosity will increase until the liquid becomes so viscous that the time taken to find the equilibrium state at that temperature becomes very much longer than the time of the experiment — thus on any practical time-scale the structure is frozen and we call it a glass.

A good glass-former is a substance that displays this behaviour — it can be cooled below its melting temperature without crystallizing. One can distinguish two different types of glass-formers: *strong* and *fragile*. Experimentally, this classification differentiates the behaviour of the viscosity as the temperature is lowered. In the strong case, the viscosity η follows an Arrhenius law $\eta = Ae^{B/T}$, whilst for fragile glasses the increase of viscosity as the temperature is decreased is much more dramatic and one observes behaviour which can be described by a Vogel–Fulcher law $\eta = A\, e^{B/(T-T_o)}$ (see Figure 1.1 for examples). Loosely speaking, one might associate strong glasses with directional forces, such as those found in covalently bonded systems (e.g. silica), and fragile glasses with non-directional, van der Waals forces (e.g. argon). A glass transition temperature, T_g, can be defined but this does not refer to a thermodynamic phase transition, but instead to the point at which the experimental time-scale and the time-scale for relaxation within the glass-former cross — as such, T_g is different for different cooling rates, and the change is not a sharp event but occurs over a range of temperatures. Perhaps the most startling thing about the glass transition is that the relaxation time increases dramatically

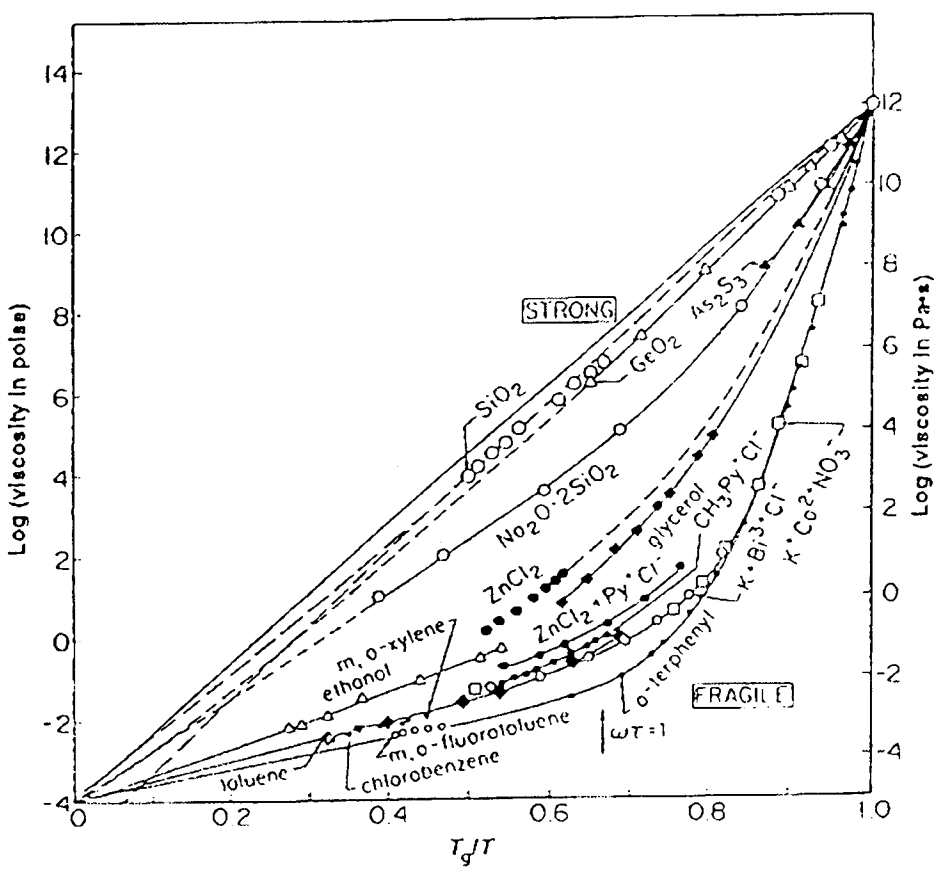

Figure 1.1: The logarithm of the viscosity against T_g/T for various materials, showing the strong and fragile glass classification. *Figure obtained from [2].*

— by more than twelve decades — without a significant change to the structural properties of the system. Understanding this feature is a considerable challenge.

A natural way to study a glass computationally is to build a model of a fluid; the beauty of computer simulations is that one can completely remove the tendency to crystallise (by, for example, carefully choosing the parameters in a binary system). In addition to this, any system and any observable can be investigated and one can reach states not readily accessible in the laboratory. The bulk of the numerical studies have taken place on amorphous silica, hard-sphere systems or binary Lennard–Jones models, all of which involve a number of parameters than can be chosen to suit the study. These have been the subject of intensive investigation within the context of Mode-coupling Theory, the predominant theory of the glass transition within the field today. In Chapter 2 we discuss a topological froth model which displays glassy behaviour despite its apparent simplicity, and thus it is natural to consider whether this model also satisfies some of the predictions of Mode-coupling Theory; thus we shall now move to a discussion of this theory.

1.1.1 Mode-coupling Theory

Mode-coupling Theory (MCT) encapsulates the idea that non-linear feedback mechanisms within the microscopic dynamics are responsible for the structural freezing that we observe. This theory has its roots in work that was undertaken in the 1970's to try and find a quantitative description of the dynamics of some dense

liquids. Its initial success was in a semi-quantitative description of the behaviour of simple liquids near the triple point and in a correct qualitative description of the 'cage effect' in dense liquids: this is the name given to the trapping of a particle by its neighbours such that it takes the particle some time to become mobile. The basic idea was to use mode-coupling approximations to derive equations of motion for density correlation functions. However, the theory was given a further thrust into the limelight in the 1980's when Bengtzelius, Götze and Sjölander argued that these equations could be simplified by neglecting some terms as irrelevant at low temperatures and in addition approximating the structure factor [3] (also proposed independently by Leutheusser [4]), which became known as the *ideal glass* scenario. In their paper they showed that the solutions to the equations contained a discontinuity in the time-dependence if the temperature were reduced below a critical value T_c, with a related divergence of the relaxation time, which naturally led to speculation that T_c could be associated with the glass transition. In particular, within the approximations of the ideal glass scenario, if the nonlinear feedback mechanism within the equations increases beyond a certain level, density fluctuations which are present initially will not decay to zero even at infinite times, with the result that the system is no longer ergodic. The idealized version of MCT is believed to give a good description of the short-time behaviour, i.e. when the particle is still in the cage, and the very long-time behaviour, i.e. when the cage has broken down and the particle is displaying diffusive behaviour.

The terms which had been neglected were later found to have some importance at very low temperatures: with these included the singularity disappears and even at very low temperatures the correlation functions will decay to zero eventually [5,6]. This comes about because the idealized version of MCT ignores *hopping processes*, i.e. when a particle escapes from its cage through activation. These terms tend to be treated in a fairly crude fashion because they considerably complicate the mode-coupling equations; MCT with the hopping effect taken into account is known as the *extended version.*

The advantage MCT possesses over other theories of the glass transition is that whilst the equations are extremely complex, they provide a great many predictions which can be tested by comparison with computer simulations and experimental results. There are many excellent articles which review this area of the field; we direct the reader towards [7] for a brief review, and [8,9] for longer overviews, but there are many more. Here, we shall only mention the features of MCT which will later be referred to in Chapter 2.

As mentioned previously, the ideal glass version of MCT predicts the existence of a critical temperature T_c, close to which the relaxation times τ of the correlation functions behave as a power law:

$$\tau \propto \frac{1}{(T - T_c)^\gamma} \tag{1.1.1}$$

with γ larger than 1.5, and T_c defined through this equation. We should make

it clear here exactly which relaxation time we are referring to, since at low temperatures one observes two-step relaxation in the correlation functions of glassy materials. The *β-relaxation regime* extends from the approach to the intermediate plateau until the initial stages of the departure from it, whereas the decay to equilibrium following the β-relaxation regime is called the *α-relaxation regime.* The relaxation time τ in the above equation refers to the long-time behaviour, i.e. the α-relaxation time. Lennard–Jones models do indeed display the behaviour encapsulated by this equation, but the exponent γ depends on whether one measures the self-diffusion constant or the relaxation times of the correlation functions, whereas the theory would predict γ to be independent of the quantity investigated [7]. Although the extended version of MCT concludes that the system is always ergodic, if the hopping processes are not too strong there will be a region within which the predictions of the idealized version hold. Thus one can identify a temperature T_c even in the presence of hopping, although the power law will not hold all the way down to T_c. Similarly, other predictions of the ideal glass scenario can be expected to hold if the temperature is not too close to T_c.

In the late β-relaxation regime, i.e. during the intermediate plateau and the early stages of the departure from it, MCT predicts that at low temperatures the equilibrium correlation functions $C(t)$ be governed by a von Schweidler law:

$$C(t) = f - B\left(\frac{t}{\tau(T)}\right)^b \tag{1.1.2}$$

where f is the plateau height and both B and b are constants [10]. All three parameters are expected to be independent of temperature and in addition b should be independent of the choice of correlator. Note that in the α-relaxation regime MCT predicts that after rescaling time to t/τ the correlation functions should lie upon each other — this is the *time-temperature superposition principle* — and that this master curve should be well fitted by a stretched exponential form $Ae^{-(t/\tau)^\beta}$, which is often known as the Kohlrausch–Williams–Watts (KWW) function (β in this function is a fitting parameter rather than inverse temperature). The parameters b in the von Schweidler law and β in the stretched exponential are generally not identical so the von Schweidler law is not simply a short-time expansion of the stretched exponential. Binary Lennard–Jones models have been observed to satisfy MCT predictions in both the late β and the α-relaxation regime.

MCT also predicts a relationship between the exponents γ and b; they are linked by:

$$\gamma = \frac{1}{2a} + \frac{1}{2b} \tag{1.1.3}$$

where

$$\frac{\Gamma(1+b)^2}{\Gamma(1+2b)} = \frac{\Gamma(1-b)^2}{\Gamma(1-2b)}. \tag{1.1.4}$$

The parameter a is related to the β-regime relaxation time. Thus MCT states that one can deduce the behaviour within the β-relaxation regime through measurements

of the α-relaxation regime and vice versa.

Given that the relaxation times of strong glasses follow an Arrhenius law, it is not immediately obvious that a critical temperature T_c can be defined and thus whether or not there is a temperature regime within which MCT can be applied. However, the dynamics of glycerol, which is a somewhat strong glass-forming liquid, can be described by MCT [11–13], and recent simulational results for viscous silica (a very strong glass-former) also show that MCT can be applied in that case [14,15].

1.1.2 The Fluctuation-Dissipation Theorem in Equilibrium

For systems within the glassy regime, one finds that measurements of two-time quantities (e.g. correlation functions) depend on both times, rather than just on the relative time as observed in equilibrium. This is a phenomenon known as aging — the system is not in equilibrium, and thus is slowly evolving in time, with the result that measurements performed on the sample will yield different results at different times. A clear indication of the presence of aging is the violation of the Fluctuation-Dissipation Theorem (FDT), which we shall review here for the equilibrium case before moving to a discussion of out of equilibrium generalisations to this theorem.

We shall derive the Fluctuation-Dissipation Theorem in a general form without specifying the exact dynamics of the system. Let us consider instead a system which is prepared so that it is in equilibrium at time s with Hamiltonian H. We then apply a small conjugate field h at time s, so that the new Hamiltonian governing the evolution is $H - hA$ (this is a zero-field cooled derivation, shown diagrammatically in Figure 1.2). The system will respond to the field and over time will relax to a new equilibrium average $\langle A \rangle_h$:

$$\langle A \rangle_h = \int dz\, A\mathcal{P}_h(z) \tag{1.1.5}$$

where $\mathcal{P}_h(z)$ is the Gibbs distribution with the field in place, and the integration over z is meant to express a sum over all configurations (i.e. the classical trace). In equilibrium it will not matter at what time we take this average, the result will always be the same. However, at time s, when the field is first applied, the average of A is:

$$\bar{A}(s) = \int dz\, A(s;z)\mathcal{P}(z) \tag{1.1.6}$$

where $A(s;z)$ means the value of A at time s and phase space point z, and $\mathcal{P}(z)$ is the Gibbs distribution *without the field present.*[2] At time $t > s$ this average will be:

$$\bar{A}(t) = \int dz\, A(t;z)\mathcal{P}(z) \tag{1.1.7}$$

where $A(t)$ has evolved from $A(s)$ according to the Hamiltonian $H - hA$. $A(t;z)$ is the value of A at time t given the initial phase space point z; we shall move to the

[2] We follow this argument for deterministic dynamics, for which $A(s;z)$ is uniquely defined, but it is equally applicable to stochastic processes if one allows that $A(s;z)$ is governed by a probability distribution which one must average over.

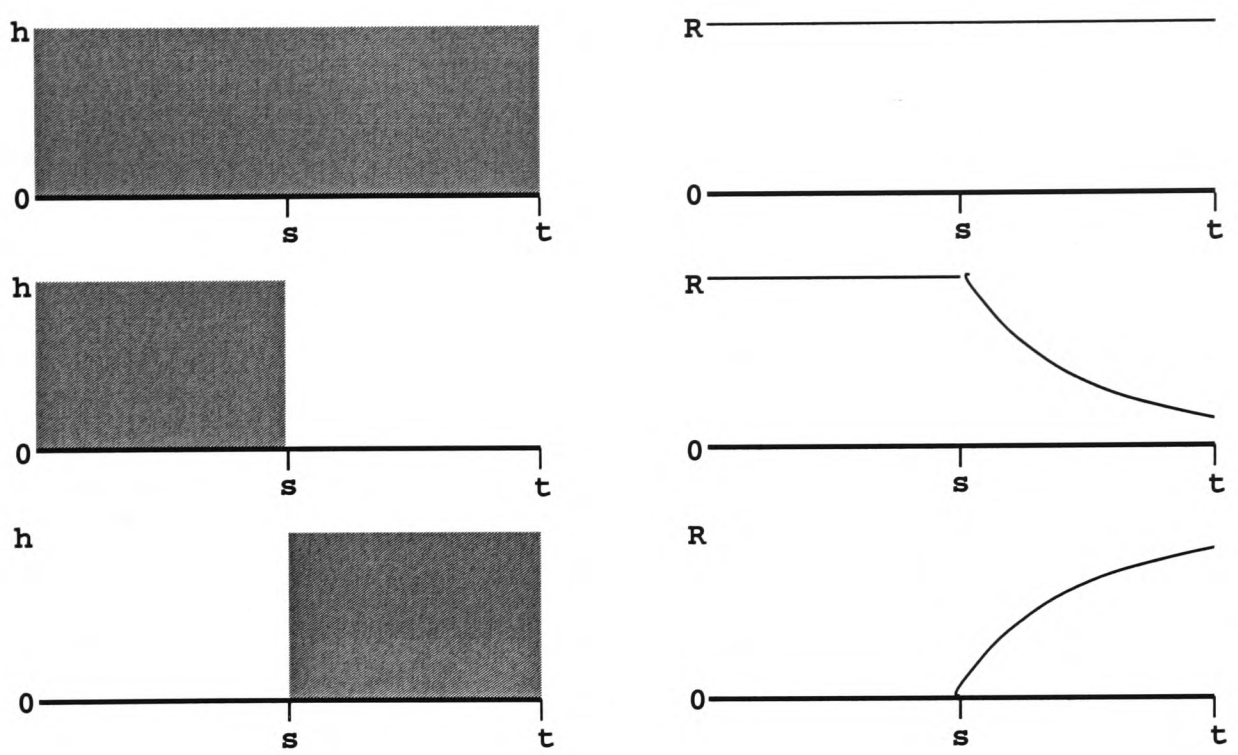

Figure 1.2: The applied field h and associated response R. On the top row, the field is on for all time, and thus one has a constant response. The second row shows a field switched off at time s, and the corresponding decrease of the response. Zero-field cooling is shown in the bottom row, where the field is switched on at time s; this is the situation considered in this derivation.

less cumbersome notation $A(t) = A(t;z)$. Note that the distribution which enters the above expression is $\mathcal{P}(z)$, in keeping with the fact that $A(t)$ implicitly depends on the initial conditions at time s. Let us now express $\mathcal{P}(z)$ in terms of $\mathcal{P}_h(z)$, using Tr to represent the usual sum over all configurations:

$$\begin{aligned}\mathcal{P}(z) &= \frac{\mathrm{e}^{-\beta H}}{\mathrm{Tr}(\mathrm{e}^{-\beta H})} \\ &= \frac{\mathrm{e}^{-\beta(H-hA)}\mathrm{e}^{-\beta hA}}{\mathrm{Tr}\left[\mathrm{e}^{-\beta(H-hA)}\mathrm{e}^{-\beta hA}\right]}\end{aligned}$$

where β is the inverse temperature. We stipulated that h be small — this allows us to expand each trace as a power series in h, from which we shall keep terms linear in h only:

$$\begin{aligned}\mathcal{P}(z) &\simeq \frac{\mathrm{e}^{-\beta(H-hA)}(1-\beta hA+\cdots)}{\mathrm{Tr}\left[\mathrm{e}^{-\beta(H-hA)}(1-\beta hA+\cdots)\right]} \\ &\simeq \frac{\mathrm{e}^{-\beta(H-hA)}(1-\beta hA)}{\mathrm{Tr}\left[\mathrm{e}^{-\beta(H-hA)}(1-\frac{\mathrm{Tr}(\beta hA\mathrm{e}^{-\beta(H-hA)})}{\mathrm{Tr}(\mathrm{e}^{-\beta(H-hA)})})\right]}\end{aligned}$$

Thus we find the following relationship between the distributions with and without

the field (to first order in h):

$$\mathcal{P}(z) = \mathcal{P}_h(z)\big[1 - \beta h A(s) + \beta h \langle A\rangle_h\big]. \tag{1.1.8}$$

We can then use the above equation to find $\bar{A}(t)$:

$$\bar{A}(t) = \langle A\rangle_h - \beta h\langle A(t)A(s)\rangle_h + \beta h\langle A\rangle_h^2. \tag{1.1.9}$$

At this point we must be very careful. $\bar{A}(t)$ is the average value of A at time t, given that the field that was switched on at time s. The averages on the right-hand side of the above equation are averages assuming the field has been on since $-\infty$. In fact we want to compare $\bar{A}(t)$ against the average of A without any field present, $\langle A\rangle$. We can expand $\langle A\rangle_h$ following the same procedure before, except the expansion is at time t rather than s, so we find:

$$\langle A\rangle_h \simeq \langle A\rangle + \beta h\big[\langle A(t)A(t)\rangle - \langle A(t)\rangle^2\big].$$

(We do not need to do the same procedure on the other terms as we are only keeping terms linear in h, so we can simply say $\langle A(t)A(s)\rangle_h \simeq \langle A(t)A(s)\rangle$ etc.) Notice that $\langle A(t)A(s)\rangle - \langle A\rangle^2$ is the connected correlation function $C_A(t,s)$; thus we have found that the change incurred in $A(t)$ due to switching on a small field at time s is:

$$\Delta A(t,s) = \bar{A}(t) - \langle A\rangle = \beta h\big[C_A(t,t) - C_A(t,s)\big] \tag{1.1.10}$$

This is the Fluctuation-Dissipation Theorem. It states that a plot of the integrated response (i.e. the response at time t due to the continuing presence of the field since time s) parametrically against the correlation function $C_A(t,s)$ will yield a straight line of slope $-\beta h$. One can also find an expression for the instantaneous response $G_A(t,s)$, which is the response at time t due to the presence of the field at time s. As we are in the linear regime we can easily define:

$$\Delta A(t,s) = \int_{-\infty}^{t} ds'\; h(s')G_A(t,s') = h\int_{s}^{t} ds'\; G_A(t,s'). \tag{1.1.11}$$

Differentiating both sides yields what might, to the reader, be a more familiar form of the Fluctuation-Dissipation Theorem:

$$G_A(t,s) = \beta\frac{\partial C_A(t,s)}{\partial s}. \tag{1.1.12}$$

In equilibrium one finds time-translational invariance and two-time quantities only depend on the difference between the two times e.g. $C_A(t,s) = C_A(t-s)$. Care must be taken if one chooses to change variable to, for example, $r = t - s$ as the sign in the above equation becomes negative in moving from $\partial/\partial s$ to $\partial/\partial r$.

1.1.3 Out of Equilibrium Generalisations of the Fluctuation-Dissipation Theorem

It is useful to consider what might happen in the non-equilibrium case. Equation (1.1.10) must be generalised as the response and correlation functions are now two-time quantities, therefore $C_A(t,s) \neq C_A(t-s)$. Following the procedure of Cugliandolo and Kurchan, one may propose the following form [16]:

$$G_A(t,s) = \beta X(t,s) \frac{\partial C_A(t,s)}{\partial s} \tag{1.1.13}$$

with $X(t,s)$ defined by this above equation. If $X(t,s) = 1$, Equation (1.1.13) reverts to the equilibrium case. For many systems it has been noted that for t and s both large, $X(t,s)$ depends on t,s only through the correlator i.e.

$$X(t,s) = x(C_A(t,s)). \tag{1.1.14}$$

In this manner a function of two times has been reduced to a function of a single variable. If that is indeed the case, one finds that the integrated response is:

$$\Delta A(t,s) = \beta h \int_{C_A(t,s)}^{C_A(t,t)} x(C_A(t,s))\, dC_A(t,s) \tag{1.1.15}$$

Thus if $x(C_A(t,s))$ is a constant:

$$\Delta A(t,s) = \beta h x(C_A)[C_A(t,t) - C_A(t,s)] \tag{1.1.16}$$

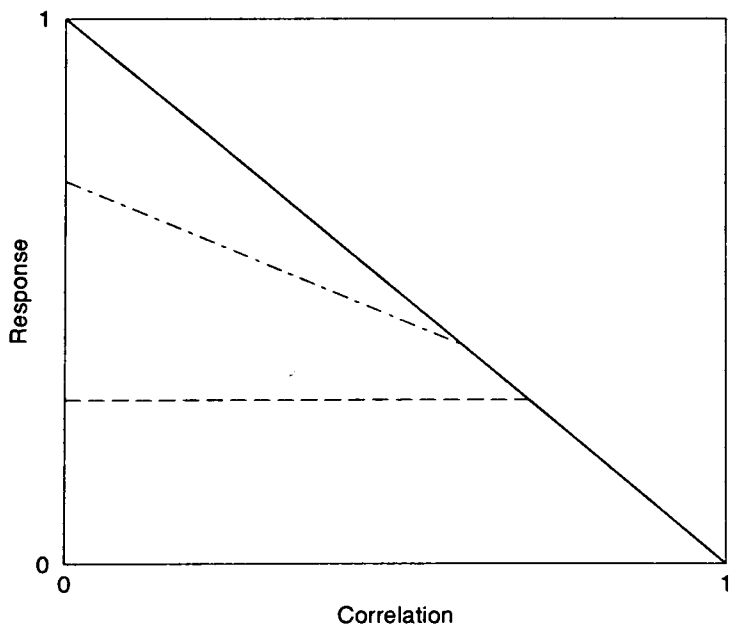

Figure 1.3: A stylised parametric plot of $(\beta h)^{-1}\Delta A(t,s)$ against the correlation function. For equilibrium, one finds the straight line with slope -1. For out of equilibrium systems one sees that the equilibrium relationship holds for some time, and then is broken. Coarsening systems then display a flat response, shown by the dashed line. Lennard–Jones models and the ACIC (shown by the dot-dashed line) break FDT to show a straight line of slope $-m$, where $0 < m < 1$.

and if $x(C_A(t,s)) = 1$ we recover the equilibrium FDT relationship of Equation (1.1.10). If $X(t,s)$ can indeed be reduced to a function of the correlator, a parametric plot of $(\beta h)^{-1}\Delta A(t,s)$ against $C_A(t,s)$ effectively allows us to see how $x(C_A)$ behaves. This is an interesting quantity which displays markedly different behaviour for different classes of systems [17]. Figure 1.3 shows a stylised plot of the type of behaviour typically observed: typically the correlation is normalised such that $C_A(t,t) = 1$, and these plots should be 'read' from right to left, with time increasing with decreasing correlation. We show the equilibrium case, with slope -1. We also show the results for coarsening systems, in which one finds a two-valued function: $x(C_A) = 1$ until some value of the correlator, at which point the response sticks at a certain value such that $x(C_A) = 0$. For Lennard–Jones binary glasses and the asymmetrically-constrained Ising chain (which will be covered in Section 1.2.2), after FDT is broken the response follows a straight line, but with a slope $-m$, where $0 < m < 1$. The situation is rather more complex for the symmetrically-constrained Ising chain (see Section 1.2.1) and the Backgammon model [18–20] amongst others [21,22], as one finds non-monotonicity of the response.

Within the field there has been much talk recently on the topic of 'effective temperatures', both with regards to their validity and usefulness [23–25]. The concept arises naturally through observations of FDT plots with results of the ACIC/Lennard–Jones type. In that case one might consider the system to be in equilibrium, but at some effective temperature T_{eff}, where T_{eff} is related to the true temperature and the observed slope m through $T_{eff} = T/m$. This concept does not seem to be physical in the coarsening case, as that would imply an infinite effective temperature, nor in the models where one finds non-monotonic response, as then one cannot extract a well-defined effective temperature (and in any case, at times any such quantity would appear to be negative). For the concept to be of any use, the effective temperature identified must be robust to the method used to obtain it. In our approach to FDT plots on the work throughout this thesis, we will try to establish how the models we investigate fit into this general picture, and whether one can draw some conclusions about FDT plots in general from our results.

1.2 Kinetically-constrained Ising models

The term *kinetically-constrained* as used in the title of this section refers to a class of models in which the Hamiltonian appropriate to the system may or may not contain disorder, but the dynamical rules introduce strong local constraints. These models were first introduced by Fredrikson and Anderson [26] in the 1980's as a simple tool for investigating the dynamical transition predicted by Mode-coupling Theory (MCT). In this introduction we shall focus on two models which have recently received a great deal of attention, and which we shall refer to for comparison at various points throughout this thesis. These are the 1d asymmetrically and symmetrically-constrained Ising models. In these models the Hamiltonian does not contain disorder; instead glassiness is introduced through the dynamics in a manner

$$101101 \xrightarrow{+1} 100101 \xrightarrow{-1} 110101 \xrightarrow{+1} 110001 \xrightarrow{-1} 111001 \xrightarrow{-1} 111101$$

Figure 1.4: Examples of activation within the SCIC. The system cannot relax further locally without first creating more down-spins, which incurs an energy penalty. The values above the arrows show the energy change involved in each move.

which is consistent with detailed balance and the Boltzmann–Gibbs distribution. One can of course find other models in the same vein — for example, the Backgammon model [18, 19] and the two-dimensional short-range spin model introduced by Newman and Moore [22, 27].

1.2.1 Symmetrically-constrained Ising chain (SCIC)

This model consists of N spins on a 1d line with periodic boundary conditions, where the allowed values of the spins v_i are 1 (spin up) or 0 (spin down). The energy is given by:

$$E = -\sum_{i=1}^{N} v_i \tag{1.2.1}$$

This favours $v_i = 1\,\forall i$; thus the model is equivalent to a paramagnet in the presence of a field. Glauber dynamics are employed, with a spin v_i chosen at random and flipped or not according to the following probability:

$$P(v_i \to 1 - v_i) = \big(1 - (av_{i+1} + bv_{i-1})\big)\min[1, \mathrm{e}^{-\beta\Delta E}] \tag{1.2.2}$$

where a, b are positive real numbers in the range $[0, 1]$. With the exception of $v_i = 1\,\forall i$, every configuration can be achieved from any other by applying this rule a sufficiently large number of times, thus ergodicity is ensured and detailed balance satisfied.

The symmetrically-constrained case [26] corresponds to $a = b = 1/2$; i.e. a spin may flip if either of its two neighbours are pointing down, with a probability that is linearly dependent on the number of down-pointing neighbours. In one dimension at zero temperature some exact results are known [28] but otherwise the dynamics has not been solved exactly.

This model displays activation as once the system has relaxed to a configuration where the majority of the spins are pointing up, with a few isolated down-spins, it cannot relax any further without creating more down-spins and thus incurring an energy penalty (see Figure 1.4). The presence of activation results in the decay of the energy with time displaying an intermediate plateau; because the energy barriers are constant, there is only one temperature-dependent time-scale which must be overcome and thus we see only one plateau before equilibrium is reached (see Figure 1.5). One can also track the average length of a spin-up domain, which grows like $t^{1/2}$.[3] We will later, in Chapter 4, present some work on the out of equilibrium FDT

[3] This is because the process can be described by the reaction scheme $A + A \to A$, which has

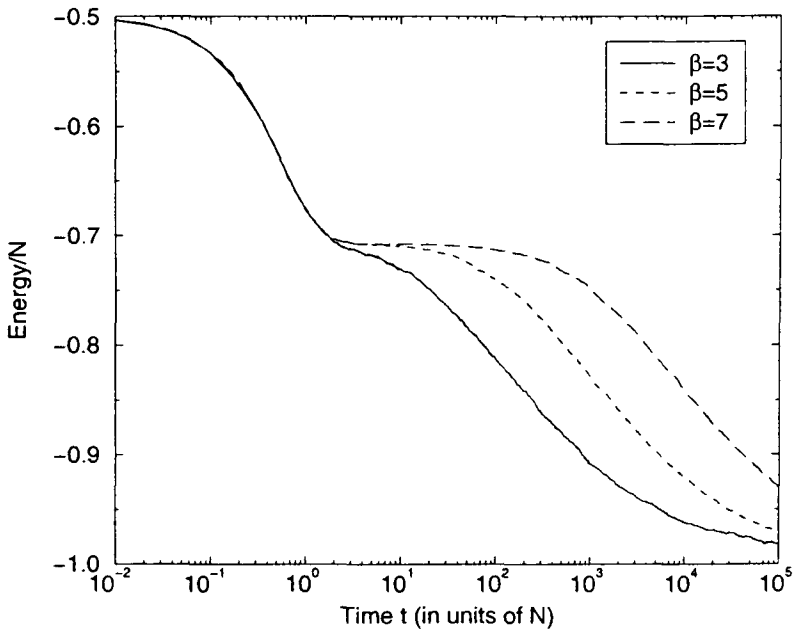

Figure 1.5: The behaviour of the energy with time in the SCIC.

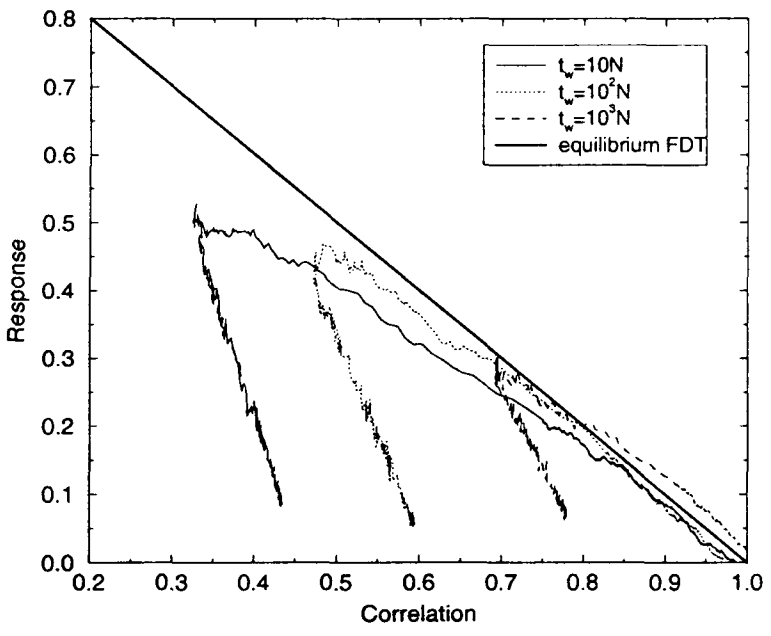

Figure 1.6: FDT plots for the SCIC. $\beta = 3$, $N = 10^4$, and the results are averaged over 10 realisations of the charge distribution.

plots for both this model and the asymmetrically-constrained model and thus we display the standard results here. It is conventional, for convenience, to transform from spin variables $v_i = \{0, 1\}$ to Ising spins $\sigma_i = 2v_i - 1$, and then use the disconnected two-time correlation function $C(s,t)$:

$$C(s,t) = \frac{1}{N}\sum_{i=1}^{N} \sigma_i(s)\sigma_i(t).$$

This is the procedure adopted by Crisanti et al [20], and we shall do the same, although we must point out that one should in fact use connected rather than disconnected correlation functions in FDT investogations, so this choice of function

---

the asymptotic density behaviour of $t^{-1/2}$; see Section 1.3 for details of reaction-diffusion models.

is not ideal.

A random field of intensity $h\epsilon_i$ is applied to the system at time s, where the charge ϵ_i is randomly assigned to be ± 1, such that the perturbation introduced to the Hamiltonian is:

$$\Delta H = -h \sum_{i=1}^{N} \epsilon_i v_i(t) \simeq -\frac{h}{2} \sum_{i=1}^{N} \epsilon_i \sigma_i(t), \quad \text{for } t \geqslant s,$$

and for $t < s$, there is no field and no perturbation. The integrated response function is then $R(t,s)$:

$$R(t,s) = \frac{2}{Nh} \sum_{i=1}^{N} \epsilon_i \sigma_i(t).$$

Parametric plots of this response against the correlation function give FDT graphs with distinctive humps, as shown in Figure 1.6. The non-monotonicity is ascribed the same origin as the two-step relaxation of the energy, namely the presence of two different time-scales within this model [20, 28]. For further details, there is a great deal of literature on this model; see, amongst others, [20, 26, 28–31].

1.2.2 Asymmetrically-constrained Ising chain (ACIC)

The asymmetrically-constrained Ising chain model introduced by Jäckle and Eisinger [32] is constructed in the same manner to the symmetric one, but with the parameter a of Equation (1.2.2) set to either 0 or 1. We shall take $a = 0$, thus a spin may only flip if its left neighbour points downwards; this model is more constrained than in the previous case. For details of these kinetically-constrained Ising models with $a \neq b$ and $a, b > 0$ see [31].

In this case the energy barriers are no longer constant but grow with the size of the domains: a defect a distance $2^{n-1} < d < 2^n$ to the left of the nearest defect has to surmount an energy barrier of size n. This is because relaxation can proceed through flipping down a spin in the centre of the domain, and using that as an anchor to relax the spin 2^{n-1} to the right of it, as shown in Figure 1.7. Thus the relaxation time for a domain of size d is $\sim \mathrm{e}^{(\beta \frac{\ln d}{\ln 2})} = d^{\frac{\beta}{\ln 2}}$, and the typical domain size at time t is given by $t^{\frac{\ln 2}{\beta}}$. Given that in equilibrium the typical domain size is e^{β}, one can then deduce that the time for equilibrium to occur behaves as $\mathrm{e}^{\frac{\beta^2}{\ln 2}}$ [33]. This form is a popular alternative to the Vogel–Fulcher law for fitting the relaxation time of fragile glasses, and it is generally very difficult to distinguish between the two types of behaviour.

One finds that the energy decay with time displays a series of plateaux, as shown in Figure 1.8, due to the step-wise nature of the energy barriers with domain size. We also display the FDT plots in Figure 1.9, obtained from exactly the same procedure and correlation and response functions as employed in the previous section. These are very different to the SCIC — the typical ACIC FDT plots are very similar to those obtained from models such as the Lennard–Jones binary fluid, and lend further support to the idea of an effective temperature as introduced in

$$\overbrace{0111110}^{E} \rightarrow \cdots \rightarrow \overbrace{0000110}^{E+3} \rightarrow \cdots \rightarrow \overbrace{0110110}^{E+1} \rightarrow \cdots \rightarrow \overbrace{0111111}^{E-1}$$

Figure 1.7: Examples of the energy barriers within the ACIC. In order to relax the underlined spin, the central spin is flipped down and it then facilitates the relaxation. During this relaxation path, the energy reaches a value 3 units larger than the energy of the original configuration; thus the energy barrier is 3 units.

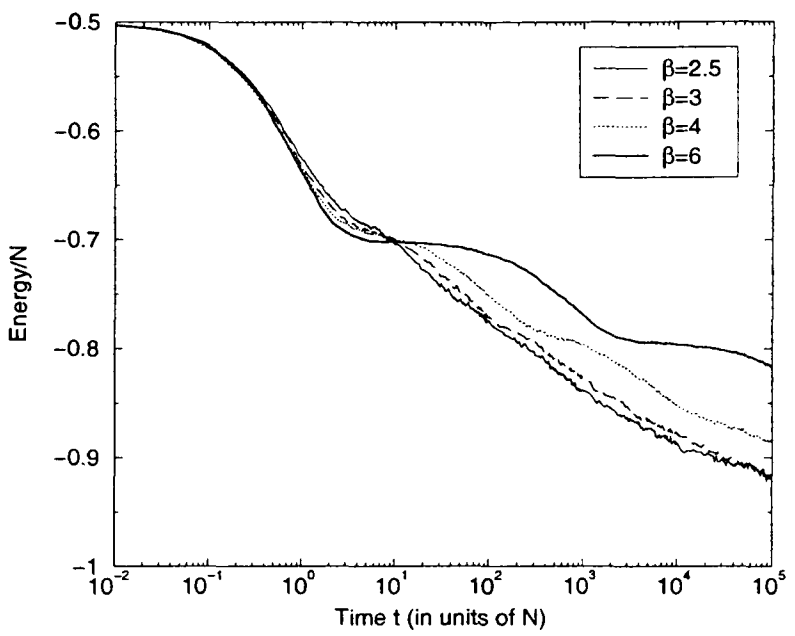

Figure 1.8: The behaviour of the energy with time in the ACIC.

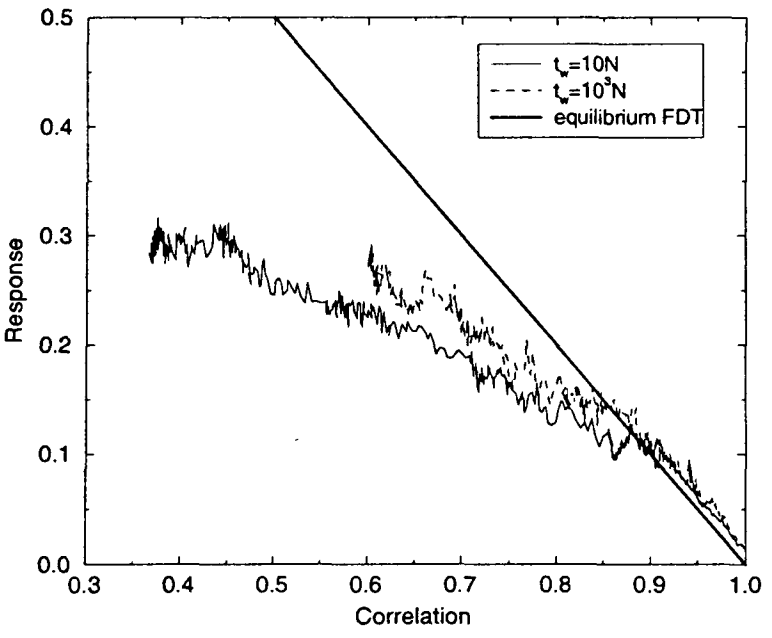

Figure 1.9: FDT plots for the ACIC. $\beta = 2.5$, $N = 10^4$, and the results are averaged over 10 realisations of the charge distribution.

Section 1.1.3.

1.3 Reaction-diffusion models

Reaction-diffusion processes are stochastic models in which particles are mainly transported by diffusion, with any number of reactions such as coagulation, annihilation, creation, transmutation, offspring production or induced absorption also present. Whilst these models are immediately reminiscent of chemical reactions and are commonly used to describe these, they have a wider applicability to pattern formation, epidemic processes and to the kinetically-constrained Ising models described in the previous section. The reaction-diffusion models are simplifications of what may be a very involved process, in which the reacting entities are replaced by single particles which are defined to be of species $A, B, C \ldots$ These carry no charge or mass but simply behave according to a well-defined rule-set, with rates attached to each reaction. These sorts of problems have attracted much interest as the problems themselves tend to be easy to state and to understand, but lead to complex and interesting physics.

The particles are allowed to diffuse either isotropically or anisotropically, with certain rates. If the diffusive move becomes more frequent than the reaction over long times, the processes are described as *diffusion-limited*; if the reverse is true, they are *reaction-limited*. The common unary and binary reactions are listed below:

$A \to \emptyset$	self-destruction
$A + A \to \emptyset$	annihilation
$\emptyset \to A + A$	creation
$A \to B$	transmutation
$A + B \to \emptyset$	two-species annihilation
$A + B \to B$	induced absorption
$B \to A + B$	induced creation
$A \to 2A$	offspring production
$2A \to A$	coagulation

Throughout this thesis we will be focusing on diffusion and annihilation processes (induced and spontaneous), thus in this introduction we shall neglect creation processes of all types, and will concentrate instead on processes which we will refer to in later chapters of this thesis. For a more complete review see [34].

1.3.1 Mean-field theory approach for $A + A \to \emptyset$

In many cases, the critical dimension of the corresponding mean-field theory for the relevant process is low enough for the results to be predicted by this theory. Effectively, the mean-field approach ignores any correlations or inhomogeneous distributions and assumes the diffusion is strong enough to mix all particles to give a homogeneous system. This becomes more exact in higher dimensions, when the diffusive processes do indeed become more efficient at mixing.

Generally it is the behaviour of the density of the particles with time that is the observable of interest. One obtains the mean-field equations by applying what is known in chemistry as 'the law of mass action'. The rate of each reaction is assumed to be directly proportional to the concentration of the reacting particles. With this in mind, one can transform the reaction lists into the relevant equations by ignoring diffusion and considering the positive and negative contributions to the particle concentration from these reactions. To take a simple but relevant example, for the reaction $A + A \rightarrow \emptyset$, with rate κ, one would write:

$$\frac{\partial \rho_A(t)}{\partial t} = -2\kappa \rho_A(t)^2$$

where ρ_A is the concentration of A particles. This is easily solved to give the mean-field result:

$$\rho_A(t) = \frac{\rho_A(0)}{1 + 2\kappa \rho_A(0) t}. \tag{1.3.1}$$

In this mean-field approach we have entirely neglected the effects of fluctuations and spatial correlations, which can, particularly in low dimensions, completely alter the physical behaviour of the system. It is vital that we know when these fluctuations become important, and for this we must write the full Langevin equation, as shown below for $A + A \rightarrow \emptyset$:

$$\frac{\partial \rho_A(\boldsymbol{x}, t)}{\partial t} = -2\kappa \rho_A(\boldsymbol{x}, t)^2 + D\nabla^2 \rho_A(\boldsymbol{x}, t) + \xi(\boldsymbol{x}, t) \tag{1.3.2}$$

where $\xi(\boldsymbol{x}, t)$ is a noise term which takes into account the fluctuations in particle density at position $\boldsymbol{x}$ with time. By the Central Limit Theorem the noise is assumed to take a Gaussian form:

$$\left.\begin{aligned} \langle \xi(\boldsymbol{x}, t) \rangle &= 0 \\ \langle \xi(\boldsymbol{x}, t) \xi(\boldsymbol{x}', t') \rangle &= \Gamma \rho_A(\boldsymbol{x}, t)^2 \delta^d(\boldsymbol{x} - \boldsymbol{x}') \delta(t - t') \end{aligned}\right\} \tag{1.3.3}$$

where d is the spatial dimension and Γ is the amplitude. This can be justified in the following way: without any particles present there will be no fluctuations, and with particles present the fluctuations will depend on the density field $\rho_A(\boldsymbol{x}, t)$. In addition the particle number may only fluctuate when two particles annihilate, and thus $\langle \xi(\boldsymbol{x}, t) \xi(\boldsymbol{x}', t') \rangle$ must depend on $\rho_A(\boldsymbol{x}, t)^2$.

One can then analyse the effect of the noise by applying a scaling transformation. We are interested in what happens to the amplitude of the noise as one approaches the fixed points of the system. We apply a length transformation

$$\boldsymbol{x} \rightarrow \Lambda \boldsymbol{x}$$

which leads to a similar time and density transformation:

$$t \to \Lambda^{\alpha} t$$
$$\rho_A(\boldsymbol{x}, t) \to \Lambda^{\beta} \rho_A(\Lambda \boldsymbol{x}, \Lambda^{\alpha} t)$$

where α and β are exponents to be determined. Notice that if one could assume homogeneity then the density would scale as one intuitively expects i.e. $\beta = -d$. However, whilst we do not know the effect of fluctuations we cannot make that assumption and thus the exponents are identified by putting the scaled variables into Equations (1.3.2) and (1.3.3). From this rescaling we find $\alpha = 2$ and $\beta = -2$, and we can identify that Γ scales as $\Lambda^{2-d}\Gamma$. So for $d > 2$ the fluctuations are irrelevant and we expect mean-field behaviour. The critical dimension of this $A + A \to \emptyset$ reaction scheme is $d_c = 2$, and so in two dimensions one expects marginal behaviour, which typically manifests itself in logarithmic corrections. Below the critical dimension, fluctuations are important and one must look for exact solutions, improved mean-field techniques or field-theoretic approaches. As this thesis is not concerned with field-theoretic calculations in any way, we shall merely state the results here (see [35] for details of these techniques). For $A+A \to \emptyset$ one finds in the asymptotic limit [35]:

$$\rho_A \propto \frac{1}{t^{d/2}} \quad (d < d_c). \tag{1.3.4}$$

Besides $A + A \to \emptyset$, there are several other processes which will be relevant to this thesis. We shall now review the long-time behaviour for these, both above and below the critical dimension.

1.3.2 $A + B \to \emptyset$

For convenience, we will consider a system with particles A, B which have equal diffusivities and we shall begin with equal concentrations homogeneously distributed. The reaction $A + B \to \emptyset$ proceeds with rate κ. The simplest mean-field equations (ignoring the diffusive term) are easy to write and solve:

$$\frac{\partial \rho_A}{\partial t} = -\kappa \rho_A \rho_B$$
$$\frac{\partial \rho_B}{\partial t} = -\kappa \rho_A \rho_B$$

giving:

$$\rho_A = \rho_B \propto \frac{\rho_A(0)}{1 + \rho_A(0)\kappa t}.$$

However, the critical dimension in this case is $d_c = 4$, and thus one must look to field theory for the behaviour in lower dimensions. Applying such techniques [35,36] shows that whilst one has the global constraint that $|\rho_A - \rho_B| = 0$ there is local segregation i.e. locally either $\rho_A \ll \rho_B$ or vice versa. One finds then that the density

behaves as: [4]

$$\rho_A \propto \frac{1}{t^{d/4}}. \tag{1.3.5}$$

1.3.3 $A + B \rightarrow B$

In this case we shall consider particles A diffusing through a background containing randomly-placed static 'traps' (the B particles). Particles A are absorbed onto the traps with a certain rate such that the reaction scheme is that of induced absorption, namely $A+B \rightarrow B$. The mean-field reaction-diffusion equation for this process takes the form:

$$\frac{\partial \rho_A(\boldsymbol{x},t)}{\partial t} = D\nabla^2 \rho_A(\boldsymbol{x},t) - k\rho_A(\boldsymbol{x},t)$$

which predicts an exponential decay of the density ρ_A with time for a homogeneous distribution of B particles. However, the distribution of traps will in general not be homogeneous and in the asymptotic limit one expects particles to only exist in trap-free regions, so the decay will be slower than exponential. It has been shown that one actually obtains an asymptotic result of [38,39]:

$$\rho_A \propto \mathrm{e}^{-Ct^{d/(d+2)}} \tag{1.3.6}$$

where C is a dimensionally-dependent constant.

1.3.4 $A + A + A \rightarrow \emptyset$

For this model the critical dimension is $d_c = 1$, so the mean-field result which is easily shown to be:

$$\rho_A \propto \frac{1}{t^{1/2}} \tag{1.3.7}$$

is applicable in 2 and 3 dimensions. One-dimensional systems are marginal and for those one would expect logarithmic corrections. In fact, for $d = 1$ one finds [40–44]:

$$\rho_A \propto \left(\frac{\ln t}{t}\right)^{1/2}. \tag{1.3.8}$$

It has also been shown that $kA \rightarrow lA$, with $k > l$, displays the same asymptotic time-dependence as $kA \rightarrow \emptyset$, but with a change in amplitude [43].

[4] This result holds only for $\rho_A(0) = \rho_B(0)$; see [37] for details of the behaviour for unequal starting concentrations.

Chapter 2

2d Topological Tiling Model

2.1 Introduction

It is well known that in many covalently-bonded solids the natural quasi-stable state appears to be an amorphous one, despite the existence of a crystalline ground state. One example of this is silicon, a well-known glass-former. It consists of tetrahedral covalent bonds for which the energetically favourable configuration is a crystalline structure. However, if silicon is cooled rapidly it cannot reach the crystal structure and remains trapped in an amorphous state, with the covalent bonds arranged such that there is no periodic structure, but also very few dangling bonds. A three-dimensional model which approximates amorphous silicon was developed by Wooten, Wiran and Weaire [45]; this employs a simple bond-switching move (see Figure 2.1) in conjunction with Monte Carlo methods and has proved to be a most useful tool for studying glassy behaviour.

In two dimensions, the hexagonal tiling is the best partition of the plane into equal cells, having minimal interfacial extension. Cellular structures are common in nature, but one finds many 2d cellular structures that in practice never achieve this ground state as some disorder is always present and relevant — examples of these include human epidermis, cucumber skin, soap froths and vegetable leaves [46–49]. In general, the structure is dynamically changing and the system cannot be described as being in equilibrium, and therefore to model the behaviour of such systems an understanding of non-equilibrium dynamics is required. Soap froths have proved to be an excellent system to study as they coarsen on laboratory time-scales, but the models developed to mimic the soap froth behaviour are generally very complex, driven by the surface tension (with possible inclusion of viscous dissipation due to the flow of the liquid if the foam to be modelled is wet). However, one finds that all vertices are three-fold and the average bubble is six-sided, features which can easily be translated into a simpler, more abstract model, and the rearrangements that take place both within natural foams and cell biology can be broken down into two processes, known as T1 and T2 moves. T1 moves involve the exchange of neighbours: two adjacent cells become next-nearest neighbours, each losing a side

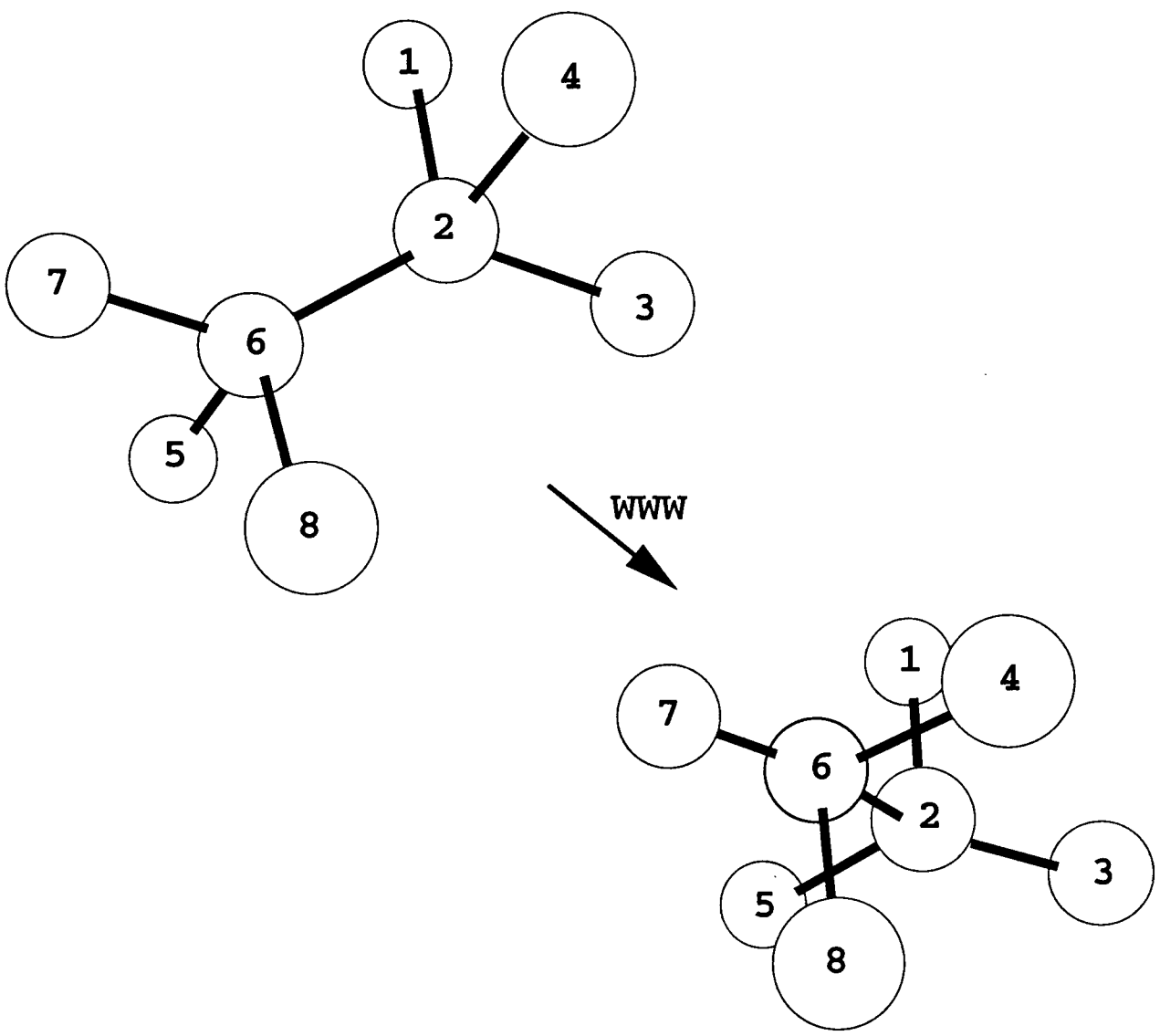

Figure 2.1: The WWW bond-switching move. In this case the parallel bonds 2 - 4 and 5 - 6 are switched; parallel bonds are chosen to avoid excessive bond distortion or twisting. Before the move, the structure is that of diamond, with tetrahedral bonds. The structure has been allowed to relax after the WWW move.

in the process, whilst two next-nearest neighbours become adjacent, each gaining a side in the process (Figure 2.2(a)). These are the 2d equivalent of the 3d WWW move — one can view it as the switching of two parallel bonds. T2 moves involve the generation or disappearance of triangular cells as shown in Figure 2.2(b). Cell division and cell coalescence (Figure 2.2(c)) are combinations of T1 and T2 moves; an example of this is shown in Figure 2.2(d).

As stated in Chapter 1, we wish to investigate a model with as few parameters as possible, in order to establish the extent to which the same features and behaviour can be reproduced. To that end we have chosen to follow the lead of Aste and Sherrington [50] in which they studied a purely topological cellular model that retained the basic features of a soap froth, namely three-fold vertices and an average cell-size of 6 sides. We have also limited ourselves to T1 moves only for further simplicity as these conserve the total number of cells, and we do not particularly wish to ensure the system coarsens, as it would do if T2 moves were included (see [51] for details of simulation results using T1 moves compared to those using both T1 and T2 moves). The purely topological nature of this model makes it

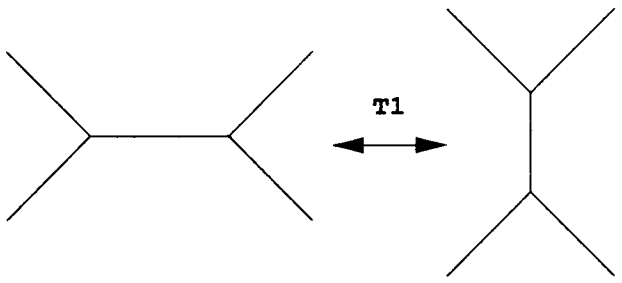

(a) A T1 move, in which adjacent cells become nearest neighbours, and vice versa.

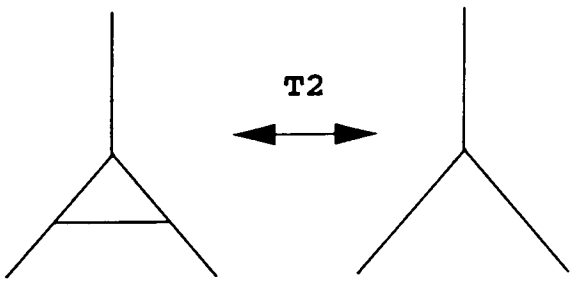

(b) A T2 move, in which a triangular cell is removed/created.

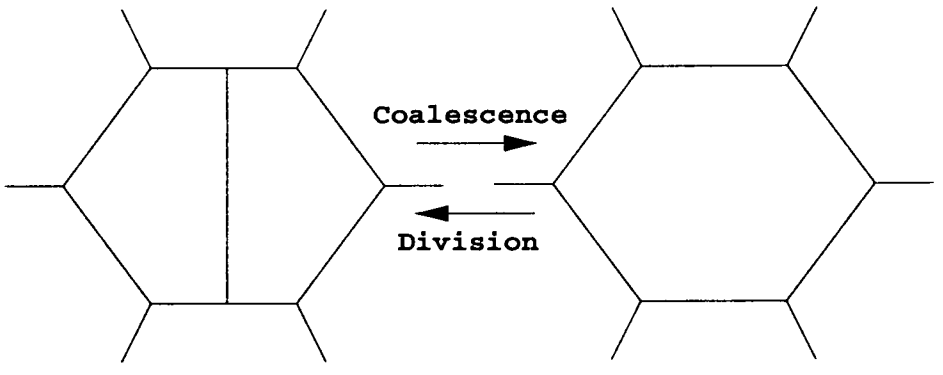

(c) The coalescence/division processes.

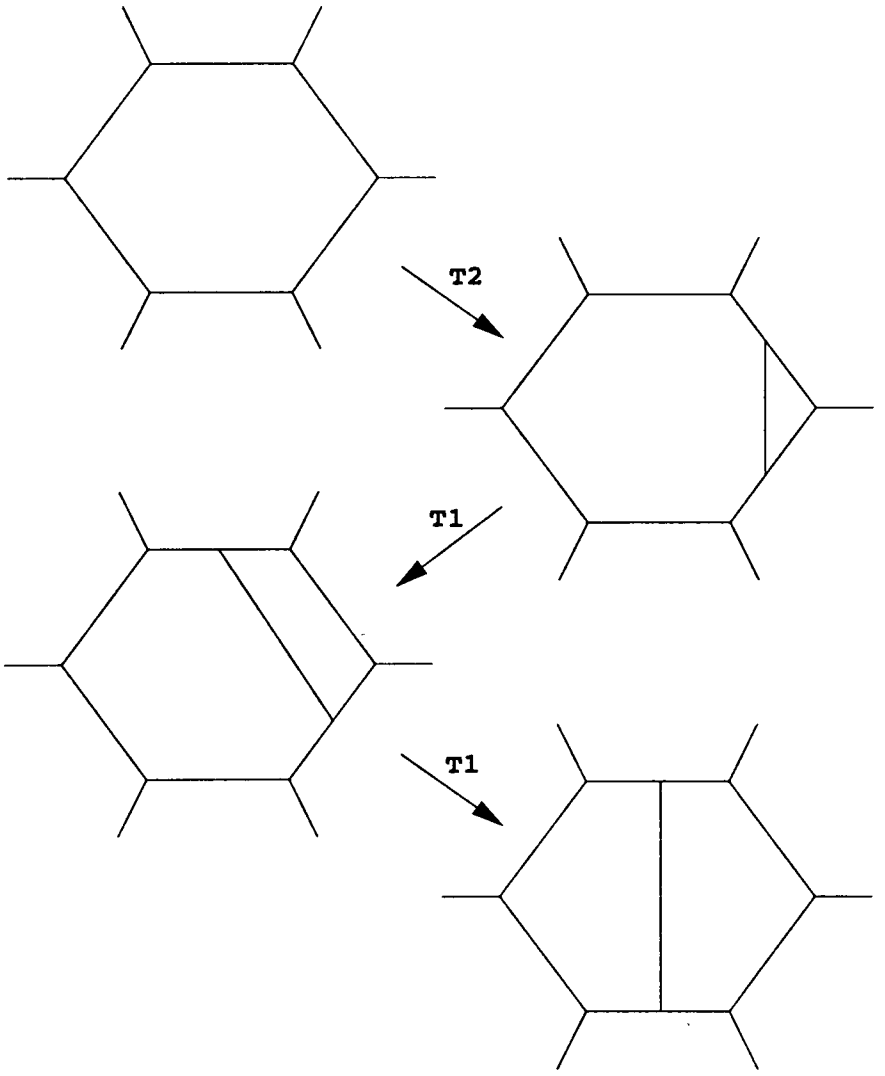

(d) The division move broken down into a sequence of T1 and T2 moves.

Figure 2.2: The move-sets found in cell biology and natural foams.

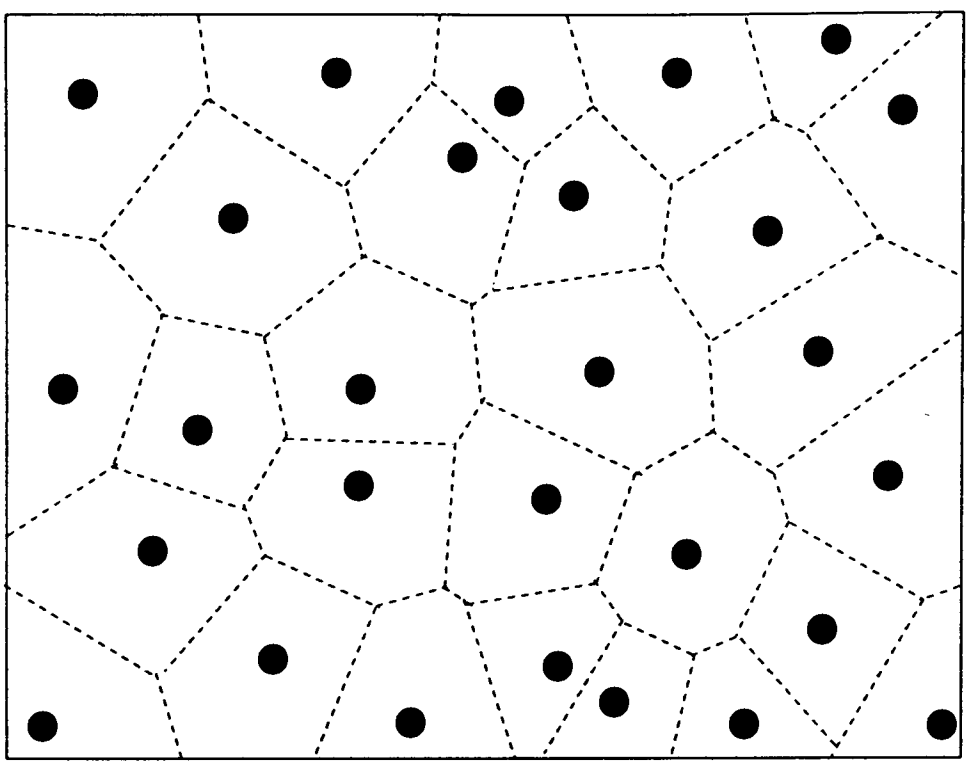

Figure 2.3: A Voronoi tessellation. All the space within each cell is closest to the atom it contains.

particularly attractive as there is no length scale involved at all. There is also the added advantage that the system shows no tendency to crystallise.

The bulk of the numerical studies on the nature of the glass transition have taken place on binary Lennard–Jones models, hard sphere systems or amorphous silica, all of which involve a number of parameters that can be chosen to suit the study e.g. to emulate experimental systems, or to avoid crystallisation etc. Despite the simplicity of our model, it can be related to a 2d atomic model such as those mentioned although one should bear in mind that the driving force is not the same in our case, and there is no true phase transition. To see the connection, one can take a 2d distribution of atoms and subject it to a Voronoi construct by partitioning the plane such that each atom is at the centre of a cell, and all the spatial points inside each cell are closer to the contained atom than to any other atom — see Figure 2.3 for an example. One sees that the resulting tessellation gives a cellular pattern in which vertices are generally three-fold; thus our simple model is in a sense the dual of an atomic model.

It is clear that the model with which we are concerned throughout this chapter links many different classes of glass-formers — foams, covalently-bonded solids and binary liquids. Much work has taken place on the behaviour of supercooled liquids, both experimentally and through computer simulations, particularly involving testing the predictions of Mode-coupling Theory (see Section 1.1.1), which has proved thus far to reliably describe many key aspects of the dynamics of glass-formers. However, many questions remain, particularly with regard to the extent to which one might expect a certain system to satisfy the predictions of MCT. We shall investigate how closely the MCT description fits the behaviour of this system.

2.2 The Model

The model we use is that introduced by Aste and Sherrington in [50]: it is an amorphous two-dimensional tiling of cells, with 3 edges incident on a vertex and 2 cells incident on an edge. The average number of sides of the cells is constrained to be 6 by the Euler Theorem [52,53]. These tilings are topologically stable.

If n_i is the number of sides of cell i, the topological charge $q_i = 6 - n_i$ measures the deviation from the hexagonal configuration i.e. q_i is a measure of inhomogeneity.

We define the energy as the second moment of the topological charge:

$$E = \sum_{i=1}^{N} (6 - n_i)^2 \tag{2.2.1}$$

where N is the total number of cells in the system. This quantity is naturally associated with the degree of inhomogeneity in the configuration: the ground state (a perfect hexagonal tiling) possesses zero energy. We shall often also refer to the energy density, by which we mean E/N.

The system is only allowed to evolve through T1 moves, as introduced in the previous section. Note that these moves cannot create or destroy topological charge, but merely exchange it between the four cells involved in the local rearrangement. The energy change associated with such a move on 4 cells v, w, x, y (as shown in Figure 2.4) with sides n_v, n_w, n_x and n_y is:

$$\Delta E(n_w, n_y; n_v, n_x) = 2(2 + n_w + n_y - n_v - n_x) \tag{2.2.2}$$

We use Glauber–Kawasaki dynamics, which allows evolution of the system even at zero temperature provided the move decreases the energy or leaves it unchanged. The probability P of performing a T1 move is given by:

$$P(n_w, n_y; n_v, n_x) = \frac{1}{1 + \exp\left(\beta \Delta E(n_w, n_y; n_v, n_x)\right)} (1 - \delta_{n_v,3})(1 - \delta_{n_x,3})(1 - \delta_{w,y}) \tag{2.2.3}$$

where β is the inverse temperature. The first two δ-functions forbid the production

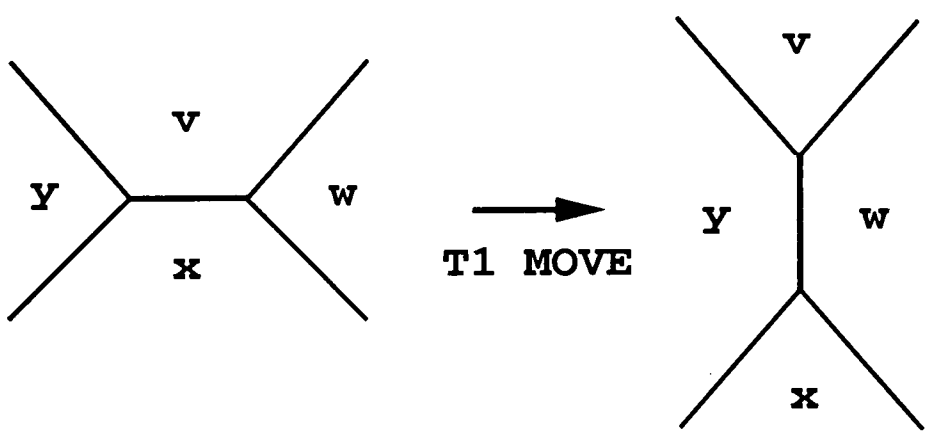

Figure 2.4: A T1 move: cells w and y gain a side, whilst v and x lose a side.

of two-sided cells, whilst the last δ-function forbids the production of tadpoles (i.e. self-neighbouring cells, which would arise if cell y was actually the same cell as cell w); unless these forbidden formations are present at the start, they will never appear.

In the following simulations the system consists of $N = 9900$ cells, with periodic boundary conditions. We exhibit results of simulations starting from configurations obtained by randomly performing 10^4N T1 moves on a perfect hexagonal tiling. This is equivalent to running the system at $\beta = 0$, and results in an extremely disordered network, with a value for E/N of approximately 13. Time is measured in units of N attempted moves.

2.3 Equilibrium Results

It is a practically impossible task to exactly evaluate the partition function. We know that certain values of n_i are forbidden — two-sided cells are forbidden, thus $n_i > 2$, and the ban on self-neighbouring cells implies $n_i < N$ — but there may be other sets of $\{n_i\}$ which are also forbidden. However, Aste and Sherrington made progress by using the following approximation to the partition function [50]:

$$Z(\beta, \lambda, N) \simeq \prod_{j=1}^{N} \sum_{n_j=3}^{N-1} \exp\left[-\beta \sum_{i=1}^{N} (6 - n_i)^2 - \lambda \sum_{i=1}^{N} (6 - n_i)\right] \tag{2.3.1}$$

where λ is a Lagrange multiplier inserted to ensure that $\langle n \rangle = 6$, and may be positive or negative. Thus one finds that the probability of a cell having n sides is given by:

$$\left.\begin{aligned} p(n) &\simeq \frac{\exp\left[-\beta(6-n)^2 - \lambda(6-n)\right]}{Z(\beta,\lambda,N)} \\ &= p(6)\exp\left[-\beta(6-n)^2 - \lambda(6-n)\right] \end{aligned}\right\} \tag{2.3.2}$$

and E/N is approximated by:

$$\frac{E}{N} = \sum_{n=3}^{N-1} (6 - n)^2 p(n). \tag{2.3.3}$$

Let us consider what happens at $\beta = 0$ in the thermodynamic limit $N \to \infty$. Then $p(n) = p(6)\mathrm{e}^{-\lambda(6-n)} = Ax^n$, where $x = \mathrm{e}^{\lambda}$. One can then use the following relationships:

$$\sum_{n=3}^{\infty} p(n) = 1, \quad \sum_{n=3}^{\infty} np(n) = 6$$

to solve for both x and A. One finds that $x = 3/4$ and $A = 16/27$; thus for $\beta = 0$ in the thermodynamic limit we expect:

$$p(n) = \tfrac{16}{27}\left(\tfrac{3}{4}\right)^n, \quad E/N = 12. \tag{2.3.4}$$

In fact, if $10^4 N$ T1 moves are performed on a perfect hexagonal tiling (equiv-

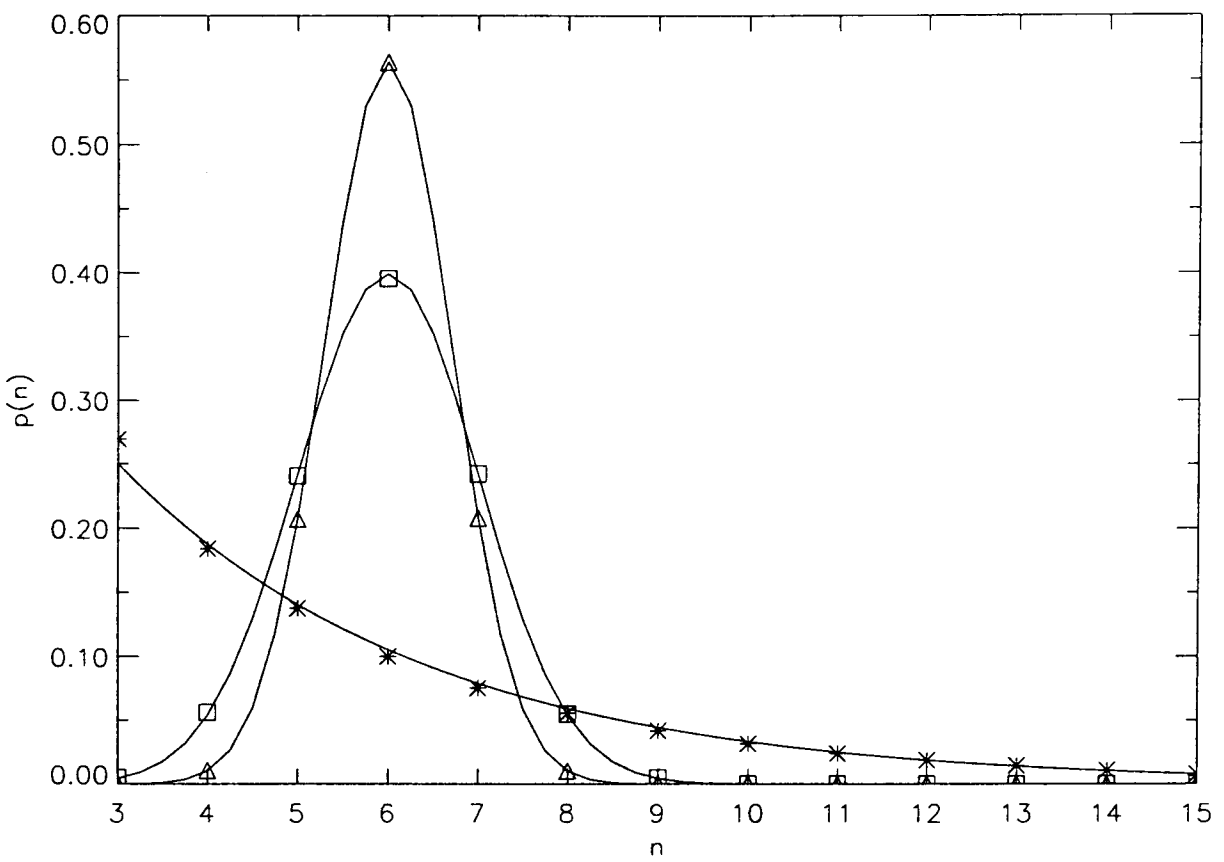

Figure 2.5: The distribution $p(n)$ of the number of sides of the cells. The symbols correspond to equilibrium results at the following temperatures: $\beta = 0$ ($\star$), $\beta = 0.5$ ($\Box$), $\beta = 1$ ($\triangle$).

alent to running the system at $\beta = 0$), the resultant configuration is an extremely disordered network with a value for E/N of approximately 13. This deviation from the predicted value of 12 no doubt reflects the approximations made in calculating the partition function.

Figure 2.5 shows the distribution of the number of sides of the cells at various temperatures in equilibrium conditions, along with the theoretical predictions — the procedure by which one ensures that the system is in equilibrium will be discussed in the next section. Apart from exactly at $\beta = 0$, λ must be calculated numerically. It is clear that the simulation results are in good agreement with the theoretical predictions. Notice that for $\beta \gg 0$, $p(n)$ is apparently symmetrical about $n = 6$, reflecting the fact that the energy cost for a non-hexagonal cell is dependent on the square of the topological charge i.e. the penalty for 5-sided and 7-sided cells is identical[1].

2.4 Relaxation Dynamics

We study the temporal dependence of the energy of the system by quenching from a disordered network to $T = 2.0$ and allowing the system to equilibrate at that

[1]The distribution will not be exactly symmetrical, because cells with less than three sides are forbidden, whereas it is possible to produce cells with more than nine sides.

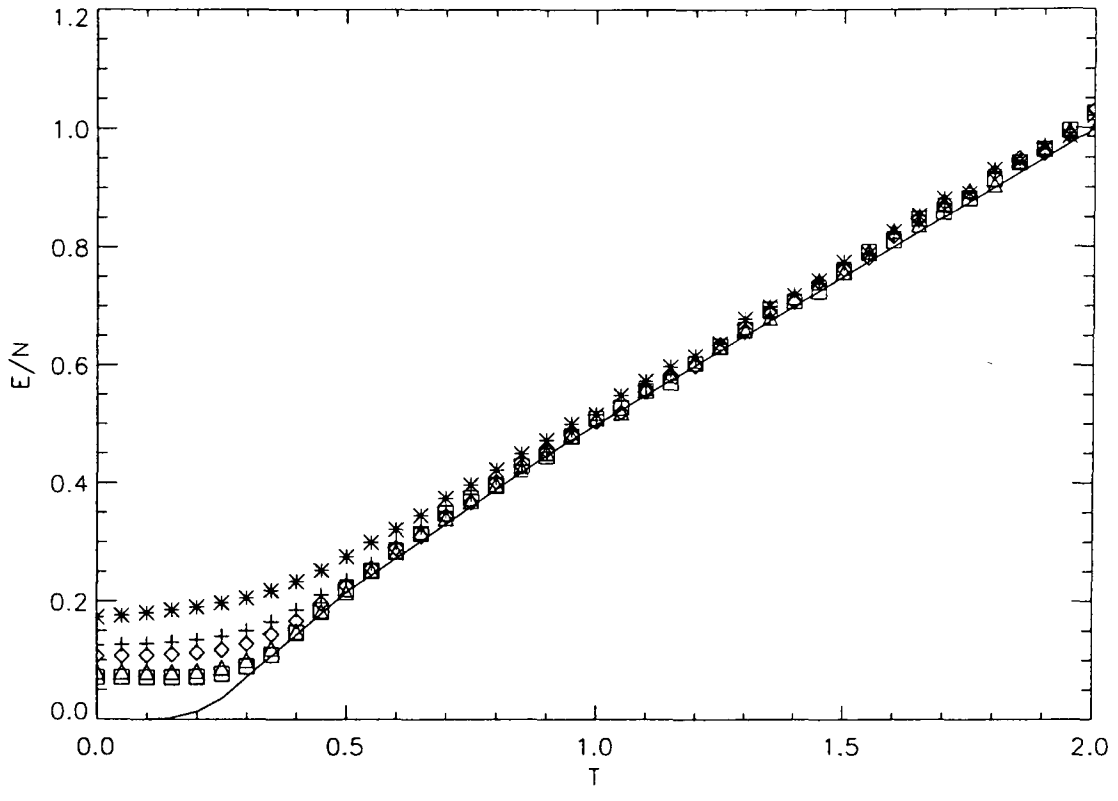

Figure 2.6: The behaviour of the energy density with temperature. The symbols correspond to the following waiting times at each temperature decrement of $\delta T = 0.05$: $10N$ ($\star$), $50N$ ($+$), $100N$ ($\diamond$), $500N$ ($\triangle$), $1000N$ ($\square$).

temperature for $10^4 N$ attempted moves. Cooling is then carried out by waiting a time $t = \gamma N$ at each temperature decrement of $\delta T = 0.05$. The results (averaged over 3 runs) are shown in Figure 2.6; the solid line superimposed on the graph is the equilibrium curve. We can clearly see characteristic glassy behaviour: the system fails to reach equilibrium even at slow cooling rates for temperatures less than $T \sim 0.3$, and displays the typical strong dependence of the energy on the cooling rate, as found at low temperatures in glasses.

The behaviour of the energy density with time for different temperatures, subsequent to a quench from $\beta = 0$, shows some extremely interesting features (see Figure 2.7(a); the curves are averaged over 3 runs). The initial decay is independent of temperature, which fits with the observation that the extremely disordered starting configuration will allow many moves to be made which reduce the energy, and thus are extremely favourable whatever the temperature. The curves for $\beta = 2$ and 3 decay to their equilibrium values, but for $\beta > 3$ we do not see equilibrium achieved on the time-scale investigated. This is about the same temperature at which the system failed to reach equilibrium in even the slowest cooling rate simulation as shown in Figure 2.6. In the region $\beta > 3$ there is clear evidence of two-step relaxation, with an intermediate plateau forming. The length of time spent on that plateau is temperature-dependent, increasing with increasing β. This suggests there are activated processes present within this model — one can hypothesise the presence of an energy barrier whose height is dependent on temperature to explain why it takes longer for the energy to decay at lower temperatures (higher β). This figure

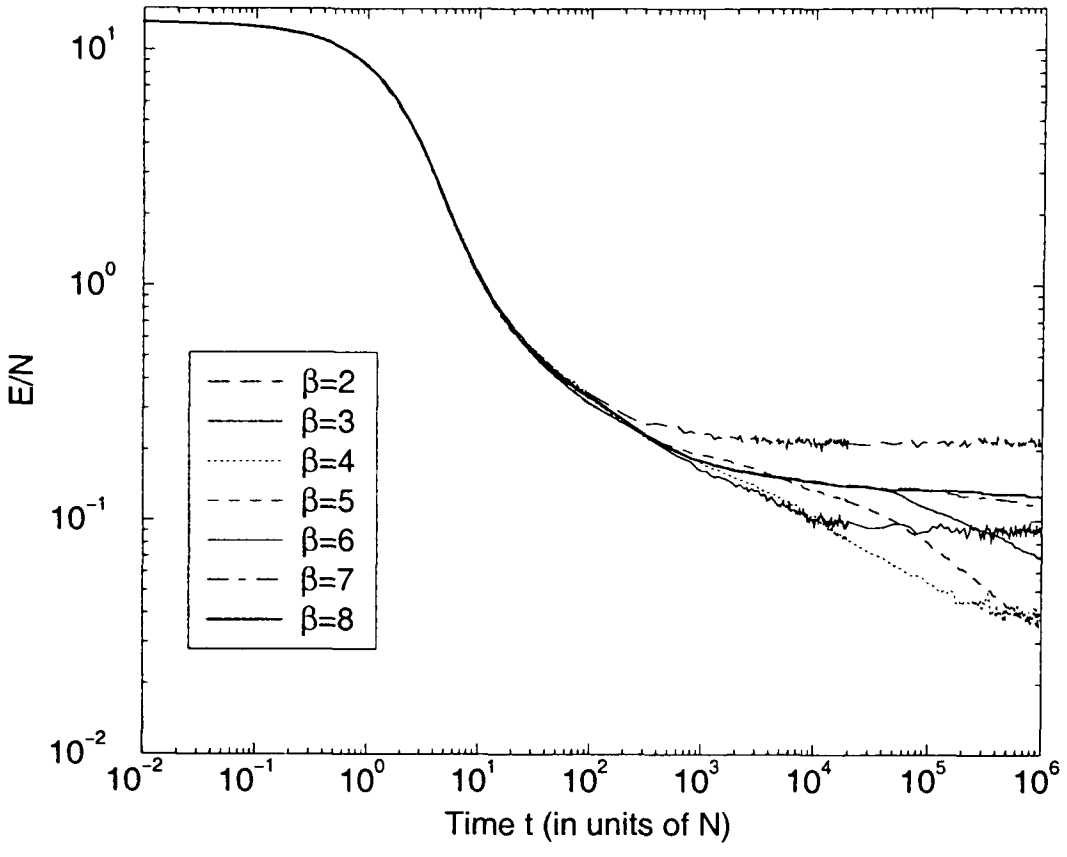

(a) E/N at various temperatures. The curves for $\beta \leq 3$ equilibrate within the simulation time-scale, whereas those for $\beta > 3$ do not.

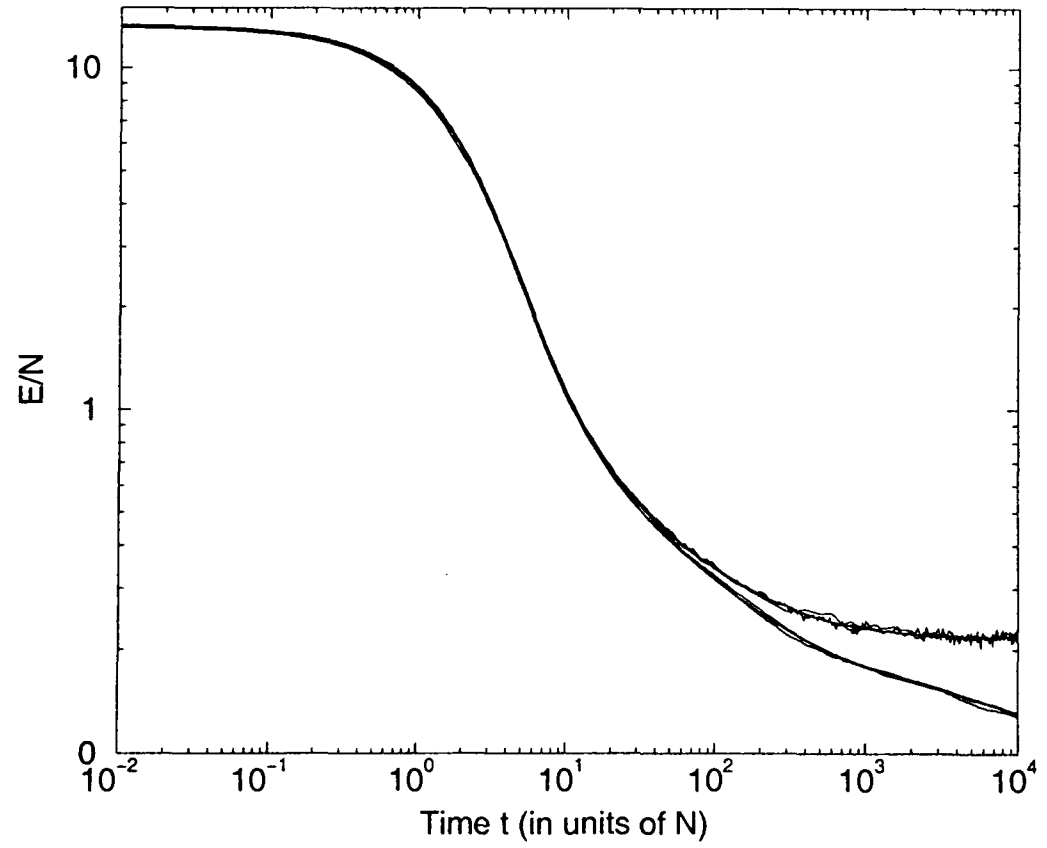

(b) The upper curves correspond to $\beta = 2$, the lower ones to $\beta = 5$. The system sizes are: 50 x 49, 100 x 99, 200 x 199 and 300 x 299. One can see no discernible finite-size effects at these sizes, beyond the fact that the smallest system size clearly introduces more noise.

Figure 2.7: The behaviour of E/N with time, subsequent to a quench from infinite temperature.

provides evidence to suggest there are two time-scales within this model, one fast and temperature-independent, and the other much slower, and dependent on the temperature. To reassure the reader that there is no dependence on the system size N in this data, we include Figure 2.7(b), showing quenches from infinite temperature to $\beta = 2$ and $\beta = 5$; the system sizes range from 50×49 to 300×299. It is clear from the figure that there is no advantage to using such large system sizes as the latter (in fact, there is a decided disadvantage in terms of computing time).

It is possible that for the duration of the plateau, the system is effectively at equilibrium, but that equilibrium corresponds to a temperature which is higher than that of the heat-bath i.e. one can postulate the existence of a T_{eff}, where $T_{eff} > T$. If the distribution $p(n)$ is studied at various times subsequent to the quench, one sees in Figures 2.8(a) and 2.8(b) that although the early distributions clearly could not map onto any equilibrium distribution, as time goes on and the system is reduced to only 5, 6 and 7-sided cells, it becomes impossible to tell from this simple function whether or not the system is in equilibrium. The function $p(n)$ becomes symmetrical about $n = 6$ and one could easily believe it was the equilibrium distribution for some effective temperature. In order to identify whether or not a system is in equilibrium, one must look at correlations: either two-time correlation functions, or cell-cell correlation functions. It would be extremely computer intensive to study an observable such as the neighbour cell-size distribution as a function of the size of the central cell, and so instead we shall now turn our attention to the two-time correlation functions.

The choice of correlation function for this particular system is by no means obvious. In previous work on this topological model, a persistence function has been studied, which measures the fraction of the total cells which have NOT been involved in a T1 move [50]. However, this provides only limited information about the system: by the very definition of the function, information about a cell is thrown away once it has been involved in a move. If the system was in a metastable state in which it performed then undid many T1 moves, this would not be revealed.

Instead we have chosen to use self-correlation functions: thus we study the behaviour of

$$C(t+\tau,\tau) = \frac{\sum_{i=1}^{N} \left(n_i(\tau) - 6\right)\left(n_i(t+\tau) - 6\right)}{\sum_{i=1}^{N} \left(n_i(\tau) - 6\right)^2}. \tag{2.4.1}$$

We add in passing that the results for this particular function differ negligibly in a qualitative sense from those for an energy-energy self-correlation function such as that used in conjunction with the backgammon model [18, 19].

We shall first present the results in equilibrium, where the correlation functions are stationary and possess no τ dependence. Thus the correlator $C(t+\tau,\tau)$ becomes $C(t)$, a function of t only. In order to obtain stationarity, the system was allowed to equilibrate for $60,000\,N$ at each temperature before measurements were taken, and for $200,000\,N$ at $\beta = 4$. The energy was found to have equilibrated in each case and no τ dependence was found. For $\beta > 4$ it became impossible to achieve equilibrium within any practical timescale; even if the correlation curves appeared

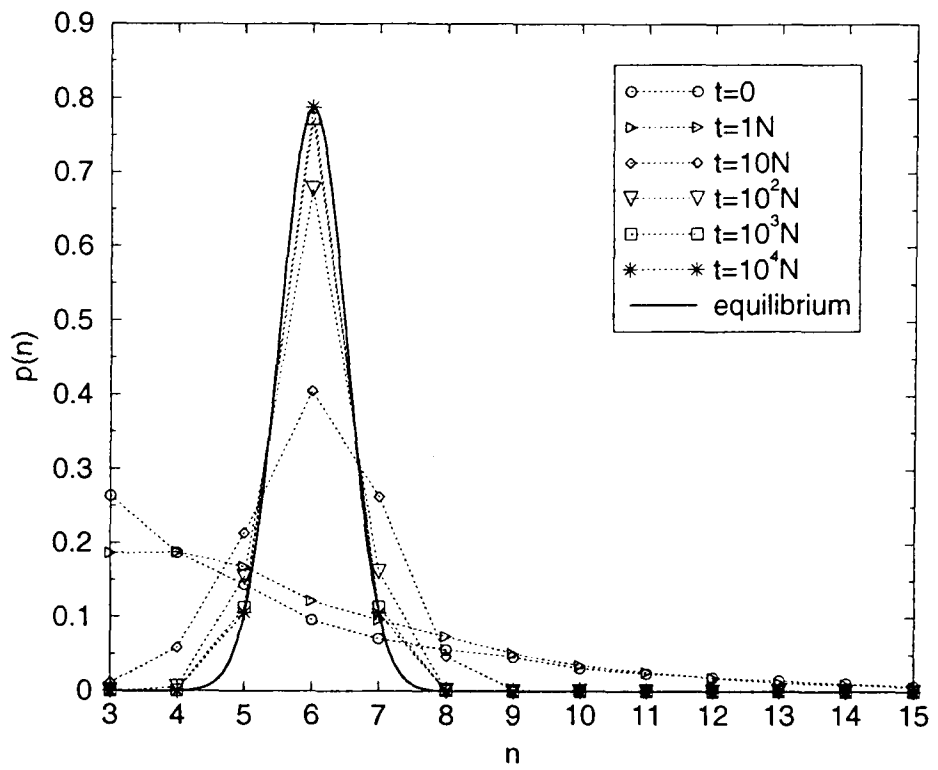

(a) $\beta = 2$. Equilibrium has been achieved by $t = 10^4 N$.

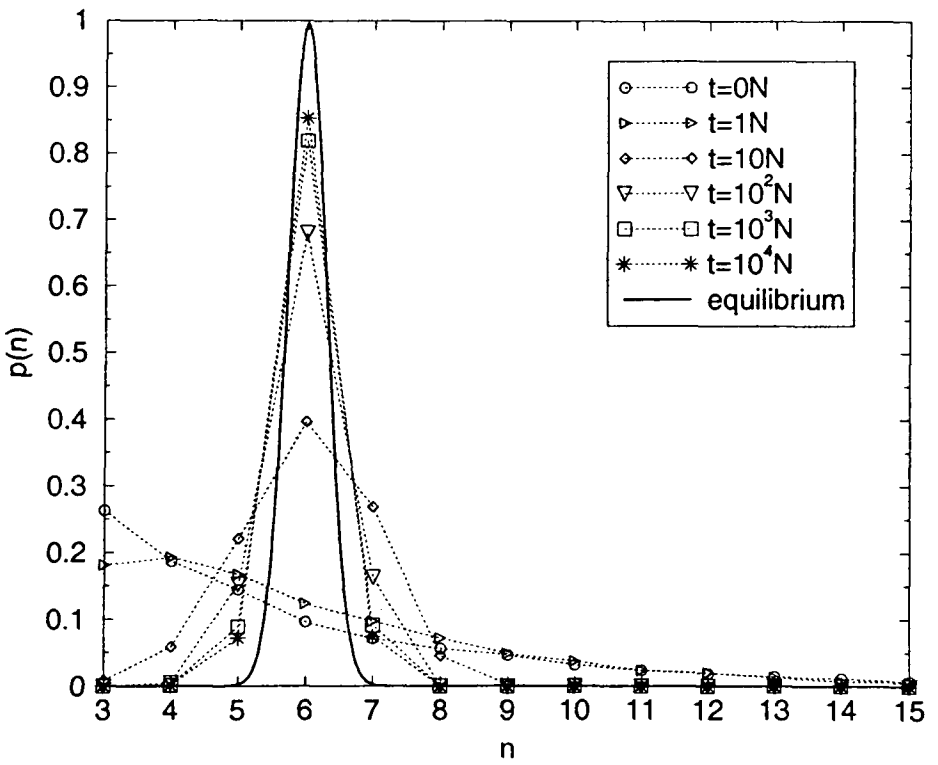

(b) $\beta = 6$. At this temperature equilibrium is not reached during the time-scale of this simulation.

Figure 2.8: The distribution of the number of sides of the cells, subsequent to a quench from infinite temperature. The simulation results are shown by symbols with lines directly joining the points, whereas the theoretical equilibrium distribution is shown as a smooth curve.

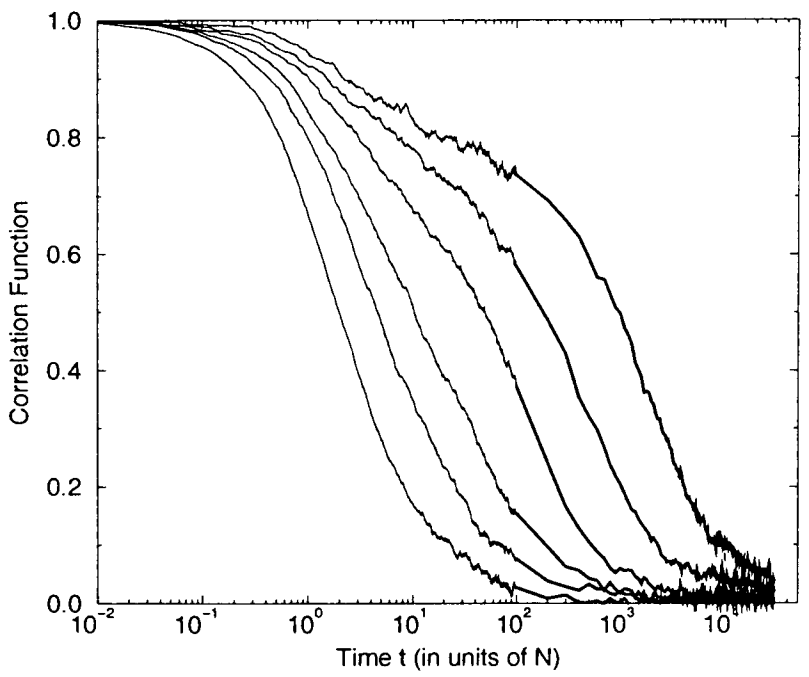

(a) $C(t)$ for $\beta = 1.0, 2.0, 2.5, 3.0, 3.5, 4.0$ (from left to right). These are equilibrium results.

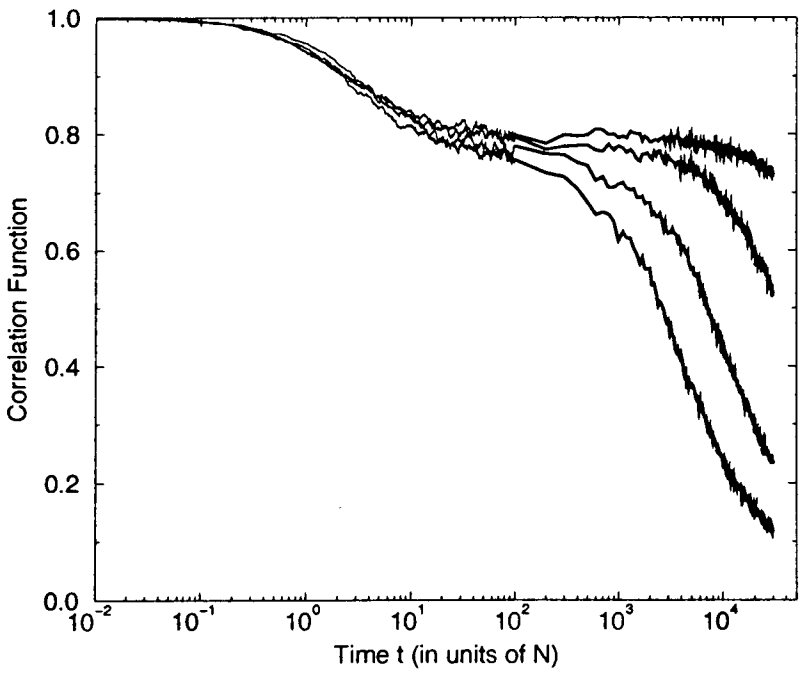

(b) $C(t+\tau, \tau)$ for (from left to right) β =4.5, 5.0, 6.0, 7.0. $\tau = 60,000\,N$. These are non-equilibrium results.

Figure 2.9: Correlation functions both in and out of equilibrium (each averaged over 3 runs).

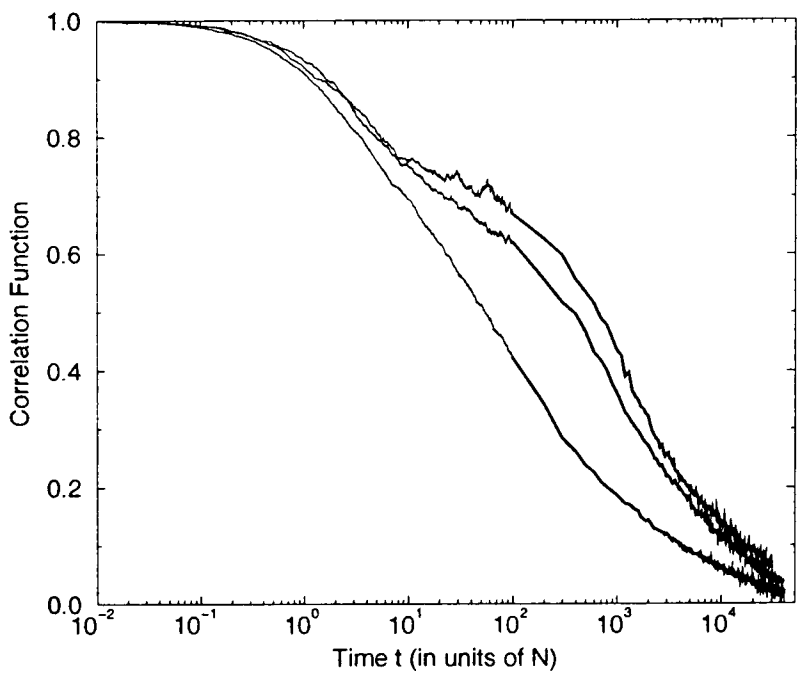

(c) $C(t+\tau,\tau)$ for $\beta = 4.0$. From left to right, the curves correspond to $\tau = 10^2N, 10^3N$ and 10^4N.

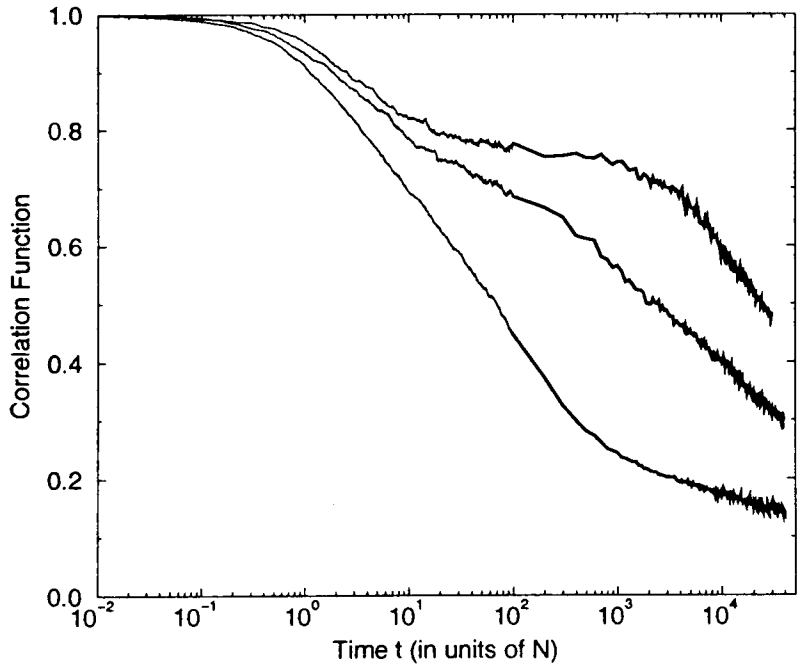

(d) $C(t+\tau,\tau)$ for $\beta = 6.0$. From left to right, the curves correspond to $\tau = 10^2N, 10^3N$ and 10^4N.

Figure 2.9: Correlation functions both in and out of equilibrium (each averaged over 3 runs).

stationary, the energy had not equilibrated.

Figure 2.9(a) shows the correlation functions for a range of temperatures. At low values of β (high temperatures) the correlator decays directly to zero. As the value of β is increased, we see a shoulder develop, again indicating that two-step relaxation is taking place. If we were able to attain stationarity at higher values of beta we would see this shoulder broaden to a plateau. The plateau can be seen more clearly in Figure 2.9(b), which shows the correlation function for higher values of β, with the waiting time of $60,000\,N$; however, one must keep in mind that this figure shows non-equilibrium results. Figures 2.9(c) and 2.9(d) show the strong τ dependence that exists out of equilibrium. Thus one can establish from the non-stationary nature of the correlation function during the plateau in the energy density that the system does not correspond to an equilibrium system at some effective temperature.

We study the correlation function within the stationary regime. As mentioned in Section 1.1.1, Mode-coupling Theory predicts the behaviour of conventional correlation functions in the late part of the β-relaxation regime to be governed by the von Schweidler law:

$$C(t) = f - B\left(t/t_r(T)\right)^b \tag{2.4.2}$$

where f is the plateau height (also known as the non-ergodicity parameter), and both B and b are positive constants. All three should be temperature-independent, and in addition b should be independent of the choice of correlator. However, this theory is based on atoms interacting via a two-body potential and studies conventional correlation functions with explicit position dependence, such as the density-density correlator (for a recent review see [8]). Thus it is interesting to plot our rather unusual correlation function against rescaled time t/t_r to investigate the predictions of MCT in our case.

Following the procedure of Kob [54], we define the relaxation time t_r in Equation (2.4.2) as the time at which $C(t)$ first drops below e^{-1}. Figure 2.10 shows the correlation functions for a range of beta against rescaled time. All the functions collapse onto a master curve in the region after the plateau or shoulder, and in the late β-relaxation regime this curve can be fitted by a von Schweidler law with $f = 0.86$, $B = 0.483$ and $b = 0.42$ as shown on Figure 2.10. The data fits well to this law, although because of the noise the margin of error on the fitting parameters is large.

Figure 2.11(a) shows the relaxation time against inverse temperature. This can be fitted extremely well by the following offset Arrhenius function:

$$t_r = A + B\mathrm{e}^{C/T} \tag{2.4.3}$$

where A, B, C are constants. This is plotted on Figure 2.11(a), with $A = 3.13, B = 0.0195$ and $C = 2.85$. Thus at very low temperatures (high inverse temperature) the system is displaying Arrhenius behaviour, which is characteristic of strong glass-formers (see Section 1.1). In the high temperature regime, one can fit the Vogel–

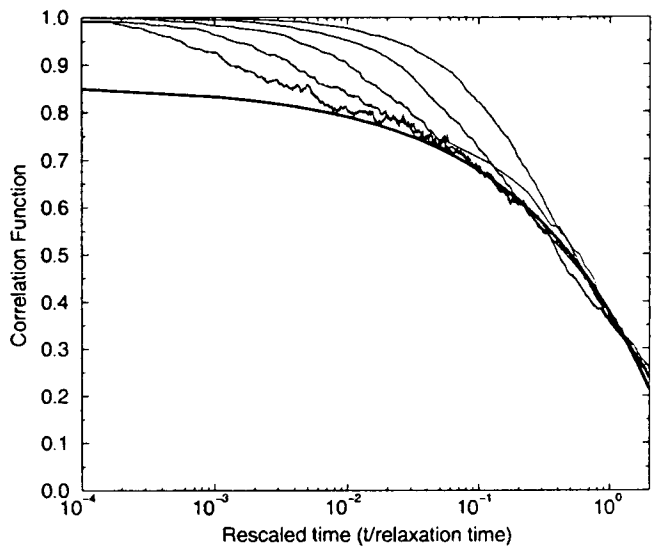

Figure 2.10: $C(t)$ for $\beta = 1.0, 2.0, 2.5, 3.0, 3.5, 4.0$ (from right to left) against rescaled time. The solid curve is a von Schweidler fit as in Equation (2.4.2) with $f = 0.86$, $B = 0.483$ and $b = 0.42$.

Fulcher law typical of fragile glass-formers i.e. $t_r = A\, e^{C/(T - T_o)}$ with $T_o = 0.202$ (see Figure 2.11(b)), but it does not suit the data as well as the offset Arrhenius curve, leading us to conclude that this system is indeed strong.

In Section 1.1.1 we stated that MCT predicts that the relaxation time should behave as:

$$t_r \propto (T - T_c)^{-\gamma} \tag{2.4.4}$$

close to a critical mode-coupling temperature T_c, with T_c defined through this equation. By performing such a fit on our data, we find that $T_c = 0.218$, as shown on Figure 2.11(c), with $\gamma = 2.86$. Neither this law nor the Vogel–Fulcher law fit the data well very close to T_c, although they both fit reasonably well slightly above T_c. However, it would seem that whilst one can fit both of these functions in certain regions, the best description at all temperatures is provided by the offset Arrhenius law. This suggests that either the relaxation-time behaviour for this model is not well described by MCT, or perhaps the somewhat arbitrary definition of t_r is inadequate.

By employing Equations 1.1.3 and 1.1.4 we use our value of $b = 0.42$ to find a value for γ of 3.12, which can be compared with the power law fit of $\gamma = 2.86$. These two results agree to within 10%, which is reasonable given that the noise of the data makes it is very difficult to fit either exponent accurately.

2.5 The Dominant Processes

We shall now discuss the processes by which the system evolves. At low temperatures, out of equilibrium, moves which increase the energy occur very rarely; we can consider the system to evolve by a combination of zero-energy moves and

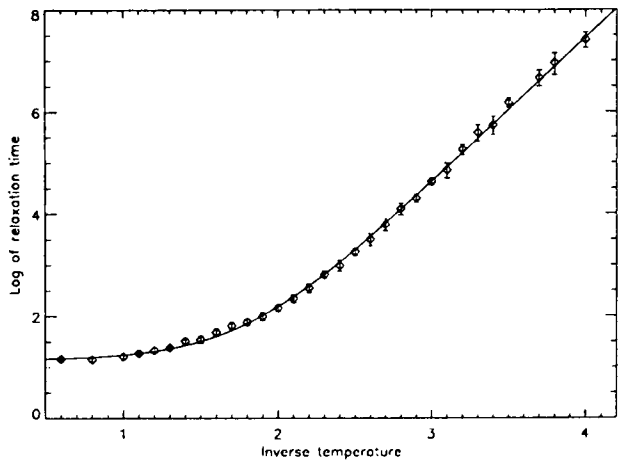

(a) **The logarithm of t_r against inverse temperature.** The solid curve is an offset Arrhenius fit i.e. $t_r = 0.0195\exp(2.85\beta) + 3.13$

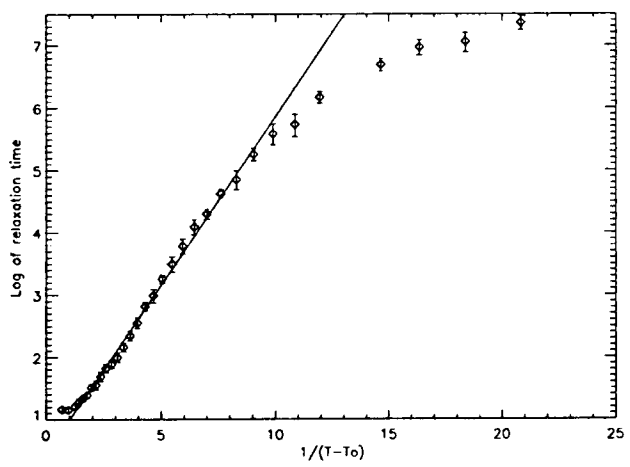

(b) **The logarithm of t_r against $(T - T_o)^{-1}$.** The straight line is a best-fit Vogel–Fulcher law with $T_o = 0.202$.

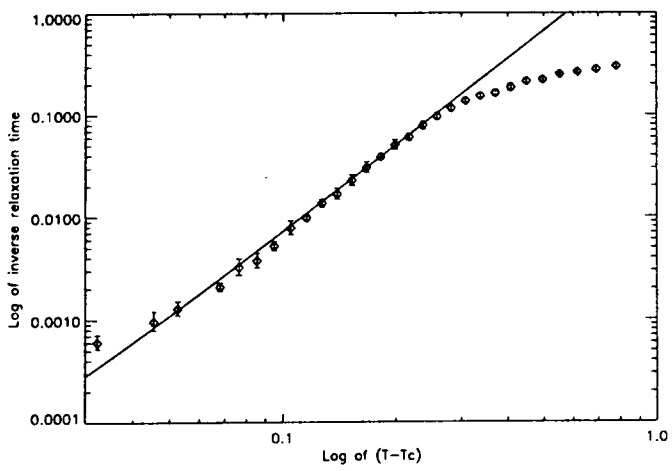

(c) **The logarithm of the inverse relaxation time against the logarithm of $(T - T_c)$.** The straight line is a best-fit power law with $T_c = 0.218$.

Figure 2.11: The behaviour of the relaxation time with temperature.

moves which reduce the energy. Subsequent to a quench from infinite temperature ($\beta = 0$), after a short time ($\sim 10^3 N$) the system consists almost entirely of 5, 6 and 7-sided cells (see Figures 2.8(a) and 2.8(b) for confirmation). Under these conditions the possible moves are as shown in Figure 2.12(a) and 2.12(b). The moves in Figure 2.12(c) are considered very unlikely due to the low probability of finding four non-hexagons clustered together; this is corroborated by the extreme rarity of finding octagons and rectangles present. We see from Figure 2.12(a) that in certain topological arrangements, pentagons and heptagons can effectively diffuse freely through the system; in particular, pentagons and heptagons can 'pair up' to move through the system together with no energy cost. We shall refer to these 5-7 pairs as 'dimers'. To reduce the energy, one must annihilate two or more 'defects' (i.e. non-hexagons) as in Figure 2.12(b); this requires the absorption of a dimer by an isolated pentagon or heptagon, or the annihilation of two dimers. Once the dimers have almost all been absorbed, the isolated pentagons and heptagons must overcome energy barriers in order to pair up and move off together as dimers — this happens over a long time-scale as the isolated defects can only move by creating a 5-7 pair. This process has an energy barrier of 2 units, and thus takes place over a time-scale of $\sim e^{2\beta}$. This brings us to a conceptual picture containing both fast and slow dynamics: the fast dynamics is due to the rapid diffusion and absorption/annihilation of dimers moving freely through the system, whereas the slow dynamics is due to the pairing and subsequent annihilation of isolated defects. Of course, in equilibrium an equal number of dimers are created as annihilated/absorbed, but in the relaxation to equilibrium, annihilation/absorption has the upper hand as the system starts from a configuration in which there are more dimers present.

This neatly explains the behaviour of the energy density subsequent to a quench from infinite temperature (Figure 2.7(a)). The initial time-independent decay is due to the system performing moves which reduce the energy and thus are extremely favourable regardless of temperature. One then reaches a level where the dimers have reduced to their equilibrium density and activated processes become important — the system must overcome the energy barriers in order for the energy density to reduce further. These activated processes introduce the temperature dependence which can be clearly seen in the Figure. One can also apply this picture to the correlation functions, keeping in mind that the correlation function we use depends only the defects — cells which were 6-sided at time τ or are 6-sided at time t do not contribute at all. One sees a fast initial decay to a plateau as the moves which cost no energy or reduce the energy are quickly carried out; these are defect diffusion (in dimers) and absorption. To further reduce the correlation function, the activated processes must come into play.

2.6 Response Functions

One can look for violation of the Fluctuation-Dissipation Theorem, which was briefly reviewed in Sections 1.1.2 and 1.1.3 as an indicator of the presence of aging. In

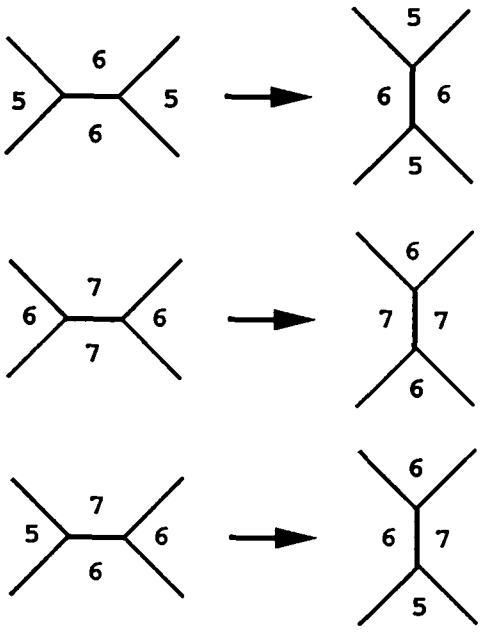

(a) Zero energy T1 moves.

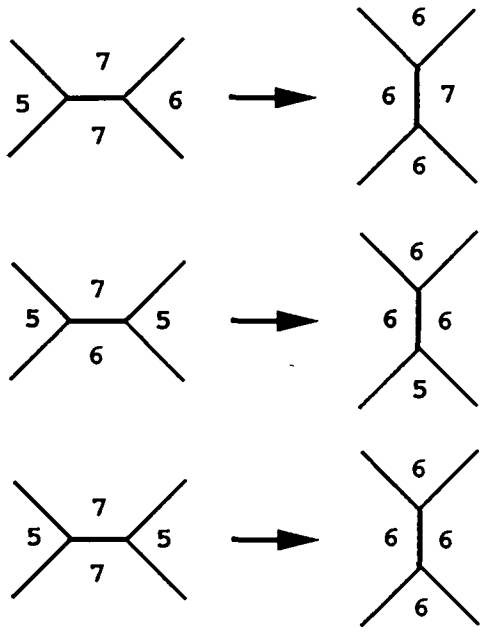

(b) T1 moves which reduce the energy.

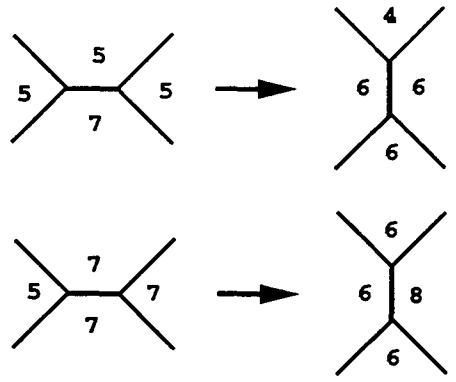

(c) Unlikely zero energy T1 moves.

Figure 2.12: The possible T1 moves at low temperatures.

this particular case, we apply a perturbation $+h\sum_{i=1}^{N}\epsilon_i(n_i-6)$ at time τ; this perturbation is left switched on. The parameter ϵ_i is randomly assigned to be $+1$ or -1 as we are interested in the self-correlation functions, and this choice ensures that cross-site correlation functions average to zero. The parameter h is chosen carefully to ensure linear response whilst also obtaining a reasonable signal-to-noise ratio. We follow the integrated response $\sum_{i=1}^{N}\epsilon_i(6-n_i(t+\tau))$. It is easy to see that the appropriate correlation function for this observable is of the form of that given in Equation (2.4.1), although one must be careful with normalisation factors, which we will discuss below. It should also be noted that this response contains the same feature as the correlation function: 6-sided cells make no contribution whatsoever, and thus at low temperatures the majority of the system has no input to the response function. The data is in general very noisy and it is necessary to average over at least 8-10 different field configurations to be able to reach any

conclusions.

It is usual to normalise $C(t+\tau,\tau)$ such that it is equal to 1 at $t=0$, as has been done in Equation (2.4.1). The response then has to be divided by the same normalising factor. If one then parametrically plots the normalised response against the normalised correlation function in equilibrium, the result will be a straight line (within experimental limits) of slope -1 i.e. the relationship reproduced is that of equilibrium FDT. However, for systems out of equilibrium care must be taken. Let us denote the 'pure' un-normalised response by $R_p(t+\tau,\tau)$ and the 'pure' un-normalised correlation function by $C_p(t+\tau,\tau)$. Equation (1.1.15) can then be applied to the current situation to find:

$$R_p(t+\tau,\tau) = \beta \int_{C_p(t+\tau,\tau)}^{C_p(t+\tau,t+\tau)} X(t+\tau,\tau)\, dC_p(t+\tau,\tau) \tag{2.6.1}$$

If we normalise by the usual factor i.e. $\sum_{i=1}^{N}(n_i(\tau)-6)^2 = C_p(\tau,\tau)$ and then parametrically plot the normalised response against the normalised correlation function we find a graph which can give a great deal of insight into the nature of the system, *but which gives no information about the value of* $X(t+\tau,\tau)$. This is because the upper limit of the integral has NOT become unity through this normalisation — for a constant $X(t+\tau,\tau)$ with this normalisation we would find the equation:

$$R(t+\tau,\tau) = \beta X(t+\tau,\tau)\Big[\frac{C_p(t+\tau,t+\tau)}{C_p(\tau,\tau)} - C(t+\tau,\tau)\Big] \tag{2.6.2}$$

where $R(t+\tau,\tau)$ and $C(t+\tau,\tau)$ are now the normalised functions. However, in order to test FDT we need to obtain $\beta X(t+\tau,\tau)\,[1-C((t+\tau,\tau)]$ on the right-hand side of the above equation. In equilibrium $C_p(t+\tau,t+\tau) = C_p(\tau,\tau)$ and thus normalising by $C_p(\tau,\tau)$ is fine, but out of equilibrium $C_p(t+\tau,t+\tau)$ evolves with time; in fact, it is exactly equal to the energy $E(t+\tau)$. Thus while a parametric plot of the response and correlation function with this normalisation may be a useful tool in its own right, it cannot tell us about $X(t+\tau,\tau)$ because the equation contains a coupling to the energy in the first term inside the bracket. To investigate $X(t+\tau,\tau)$ we must in fact normalise by $C_p(t+\tau,t+\tau)$. This subtle point is avoided in most models, where the correlation function is chosen such that $C(t+\tau,t+\tau)$ is 1 for all times. Normalising by a quantity such as $C_p(t+\tau,t+\tau)$ might alarm the reader as one generally does not want to introduce any quantity that is related to the energy of the system, but we would argue that in this instance this process *removes* the coupling to the energy. In fact we shall present results for normalising by both $C_p(t+\tau,t+\tau) = E(t+\tau)$ and $C_p(\tau,\tau) = E(\tau)$, although we stress that in the latter case we are in no way attempting to draw conclusions about $X(t+\tau,\tau)$ from these plots; we simply wish to show that there are some valuable insights to be gained from these plots for this system.

Figure 2.13 shows the results for $\beta = 5$ and 6, normalised by $E(\tau)$, where we have absorbed the factor of β into the response and therefore the quantity plotted

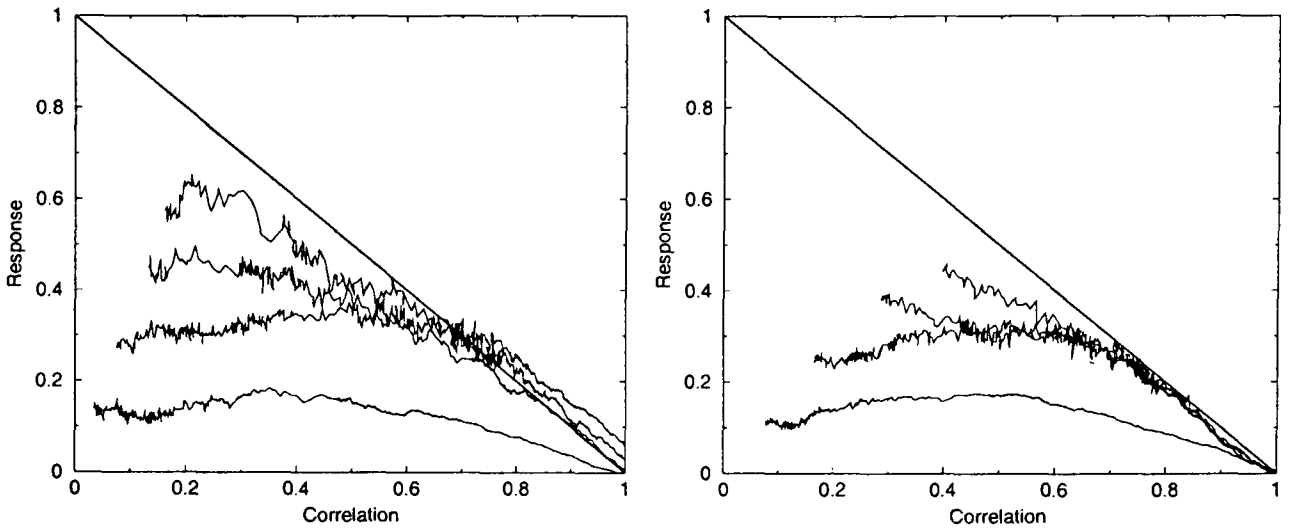

(a) $\beta = 5$. From lower curve to upper curve, $\tau = 10N, 10^2N, 10^3N, 10^4N$.

(b) $\beta = 6$. From lower curve to upper curve, $\tau = 10N, 10^2N, 10^3N, 10^4N$.

Figure 2.13: The response plotted parametrically against the correlation function, both normalised by $C_p(\tau, \tau) = E(\tau)$.

on the y-axis is actually $TR(t+\tau, \tau)$. These are non-equilibrium results in all cases, as the waiting times are not long enough for the system to have equilibrated. The superimposed straight lines have slope -1, but are not best fits; they are there to give the eye a comparative reference. These plots should be examined from right to left i.e. short times are on the right, where the correlator is close to 1, and long times are on the left. Although the value of the response at time τ fluctuates about zero due to the randomness of the charge distribution, one finds an initial section with slope -1 for all curves, although this is less clear in the case of the very shortest waiting times ($\tau = 10N$) as deviations from linearity occur so quickly. The striking feature is clearly the non-monotonicity. This can be understood with reference to the processes dominating the evolution of the system, as discussed in the previous section. The effect of the field is to try and 'pin' defects onto the appropriate cell i.e pentagons try to settle on sites with $\epsilon_i = +1$ and heptagons on $\epsilon_i = -1$. Thus with the field switched on, the diffusion processes move the defects around until they are on the appropriate sites, and in this way increase the value of the response. However, annihilation/absorption processes remove defects from the system entirely, thus reducing the response and also reducing $C(t+\tau, \tau)$. We have competition between the annihilation/absorption processes and the diffusive processes; when annihilation/absorption dominates, the slope on the parametric plot becomes positive, as seen particularly clearly for small values of $C(t+\tau, \tau)$ in Figure 2.13(b).

However, had we normalised by $E(t+\tau)$ rather than $E(\tau)$ the picture would look very different. Figure 2.14 shows those results for $\beta = 6$; these plots do give us some information about the nature of $X(t+\tau, \tau)$. Again, the straight lines have slope -1, and are there purely as a reference. One finds that $X(t+\tau, \tau) = 1$ for

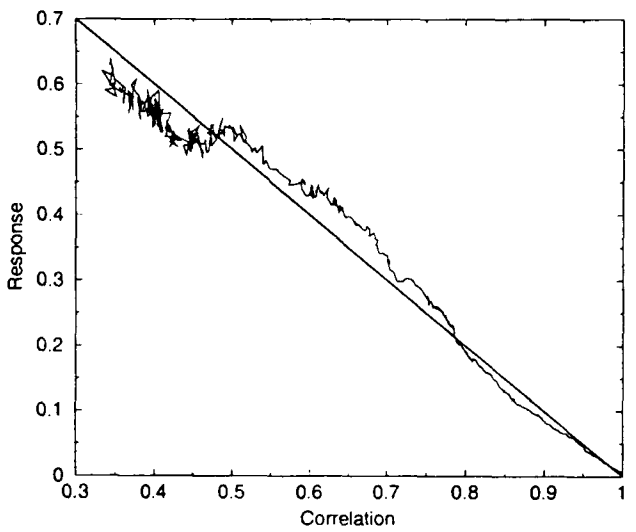

(a) $\tau = 10N$

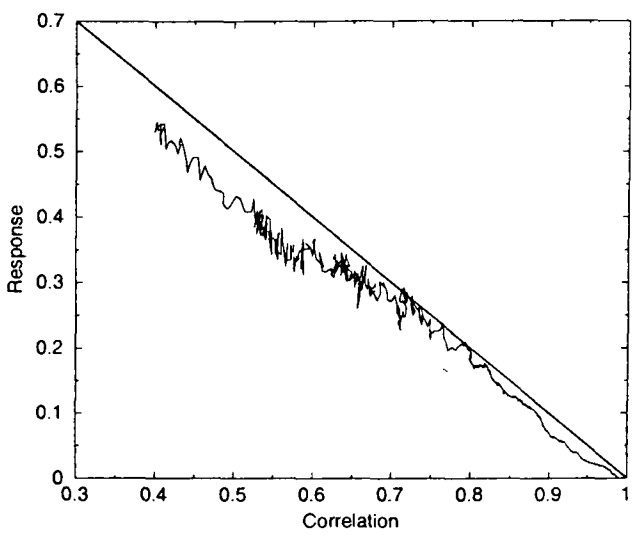

(b) $\tau = 10^2 N$

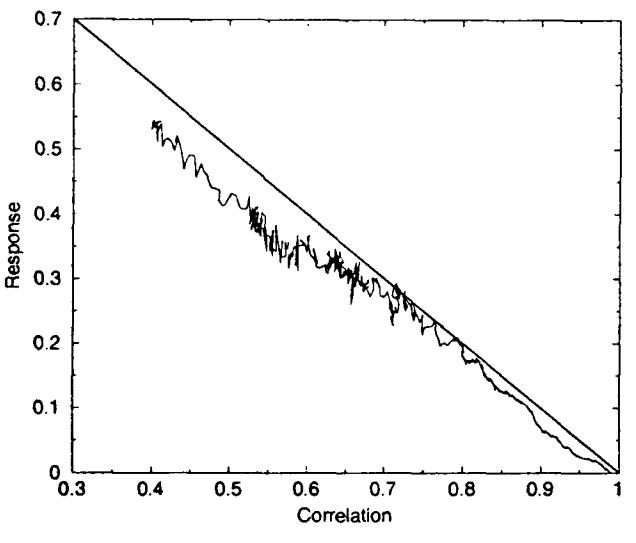

(c) $\tau = 10^3 N$

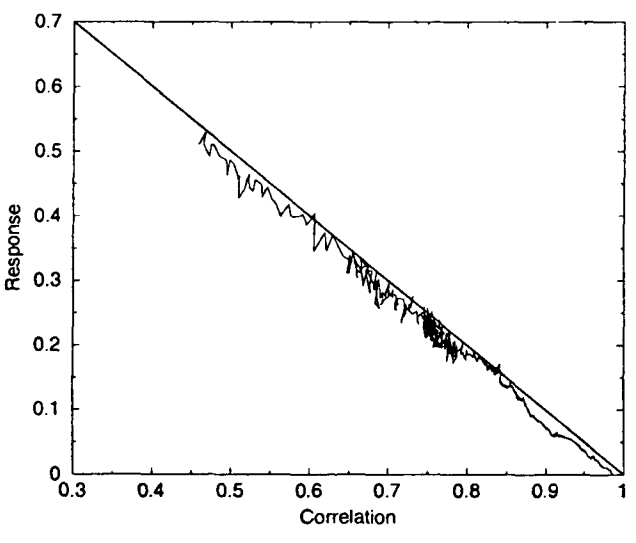

(d) $\tau = 10^4 N$

Figure 2.14: The response against the correlation function at $\beta = 6$, for various waiting times τ. Both functions are normalised by $C_p(t+\tau, t+\tau) = E(t+\tau)$.

long waiting times ($\tau > 10^3 N$, as in Figure 2.14(d)), showing that the equilibrium FDT is upheld, despite the fact that the energy density has not equilibrated (see Figure 2.7(a)). For shorter waiting times one sees a drift away from the slope of -1 at intermediate times, with a return to that slope at long times. This behaviour does not fit into the patterns commonly observed in other models, but is best understood by considering the behaviour of $E(t+\tau)$ during each of these simulations (recall that this is the quantity by which we have normalised). Figure 2.15 shows the behaviour of the energy density for each of the waiting times τ; note that for $\tau = 10N, 10^2 N$ one begins measuring the response and correlation function well before the intermediate plateau has been reached. Thus it seems that the deviations away from linearity occur for shorter waiting times τ in which the fast processes are still ongoing. If we wait for these processes to be finished, as in Figure 2.14(d) the equilibrium FDT expression is upheld. This does NOT mean the system is equilib-

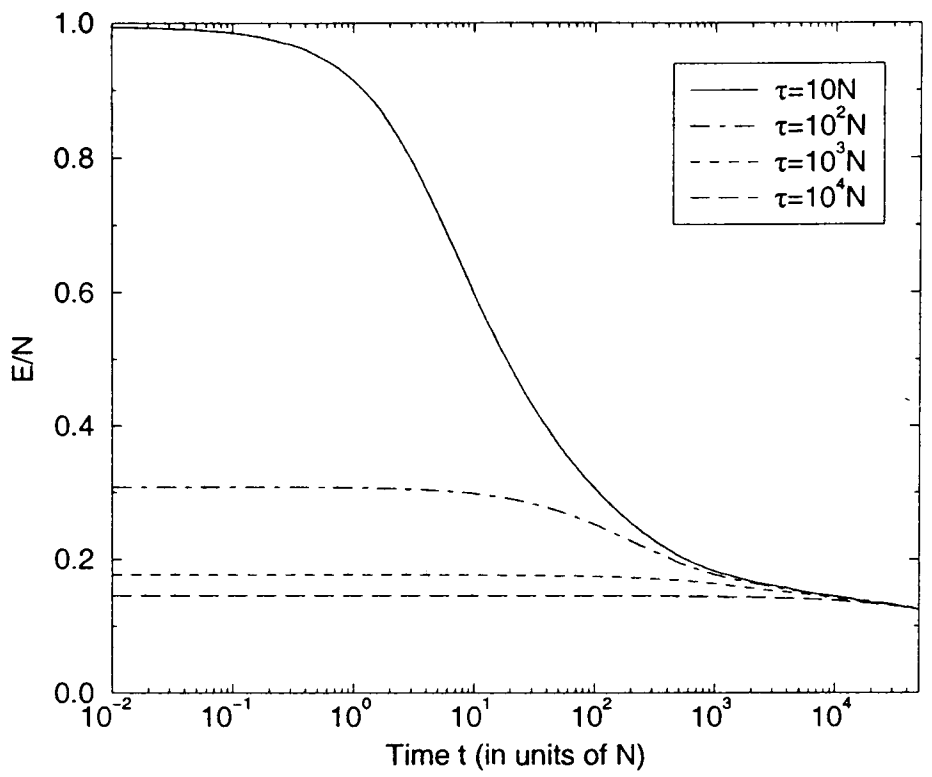

Figure 2.15: The behaviour of E/N throughout the response simulations.

rium; an equilibrium system must satisfy the equilibrium Fluctuation-Dissipation Theorem, but a system satisfying that theorem is not necessarily in equilibrium. Thus whilst the plots in which the functions are normalised by $E(\tau)$ give some intuition as to the behaviour of the system — one can clearly see the effects of the competing processes of energy decay (defect removal) and response increase (defect pinning) — the correctly normalised FDT plots show that the response per defect behaves in a manner which is consistent with equilibrium behaviour for that current temperature. The point we would wish to make here is that *neither* sort of plot is fully unrelated to the energy; we have to deal with this energy-dependence either explicitly or implicitly, as so far we have not succeeded in devising a sensible observable that is unrelated to the energy. We would like to point out that this is also the case in many other models — for example in the ACIC and SCIC models (introduced in Section 1.2) one generally works with spins $s_i = \{0, 1\}$. However, for purposes of investigating the off-equilibrium Fluctuation-Dissipation behaviour, a transformation to spins $\sigma_i = \{-1, 1\}$ is used [20,28], as then a correlation function is obtained for which $C(t,t)$ is unity at all times (although, as mentioned in Section 1.2.1, there is the disadvantage that this correlation function is disconnected). Nonetheless, this does not remove the energy coupling as the proportion of 1's and -1's is of course directly related to the energy, and thus one cannot claim to have an observable entirely independent of the energy of the system in those cases either. This will be discussed further in the next two chapters.

2.7 Concluding Remarks

In summary, we have studied a simple two-dimensional topological glassy model, testing some of the predictions of Mode-coupling Theory for this system. We find that this theory can indeed be used to describe some features of the behaviour of the system in so far as we have investigated, although it fails for others. The correlation functions follow a von Schweidler law as predicted in the late β-relaxation regime, and the exponent of this roughly agrees with the exponent of the power law fitted to the relaxation time data. However, the relaxation times fit better to an offset Arrhenius law in all temperature investigated, and thus attempts to define a critical temperature in keeping with MCT are not convincing. Due to the difficulty in obtaining stationarity over a large range of temperatures in this model, one cannot find conclusive evidence that MCT is the best description of this system for the temperature range studied.

Investigation of the fluctuation-dissipation ratio in off-equilibrium conditions reveals some interesting features, and raises some questions as to the validity of such investigations given that one can rarely obtain an observable that is not directly or indirectly related to the energy of the system. This is a question that will be returned to in later chapters.

Chapter 3

2d Spin Models on a Hexagonal Lattice

In Chapter 2 we focussed on a purely topological tiling model which exhibited glassy dynamical behaviour. This was driven by a desire to investigate the behaviour of supercooled liquids in a model which contained as few parameters as possible, but still displayed the relevant physics. In this chapter we continue the minimalistic approach, and consider systems which are conceptually similar to the topological model, but have the major advantage of involving variables (spins) based on a fixed lattice.

The conceptual framework of two different processes (dimer diffusion and defect pairing) leading to both fast and slow dynamics is directly applicable to the lattice-based spin model with which this chapter is concerned, and thus one might expect it to yield qualitatively similar results to the topological model. Given that this spin model is computationally simpler and more tractable, one might hope to be able to probe more deeply, and to investigate to what extent one obtains the same features displayed by other kinetically constrained models (for examples see [20,22, 26,32,33,55,56]). In fact, as we show below, these expectations are borne out and it is possible to provide a physical understanding of the features observed. It is also both possible and instructive to consider a generalization with a very different (highly degenerate) ground state, which will be covered in Section 3.3.

3.1 The Model

The model we use comprises a perfect hexagonal tiling of the plane, with a variable (spin) associated with each hexagon. The spin in cell i, denoted by s_i, is restricted to the values 0, ± 1. This is analogous to a topological froth in which the cells are all pentagons, hexagons or heptagons, so that the topological charge $q_i = (6 - n_i)$ of each cell is restricted to the values 0, ± 1, as was observed at low temperatures in the froth of the previous chapter. However, the topological froth model has a

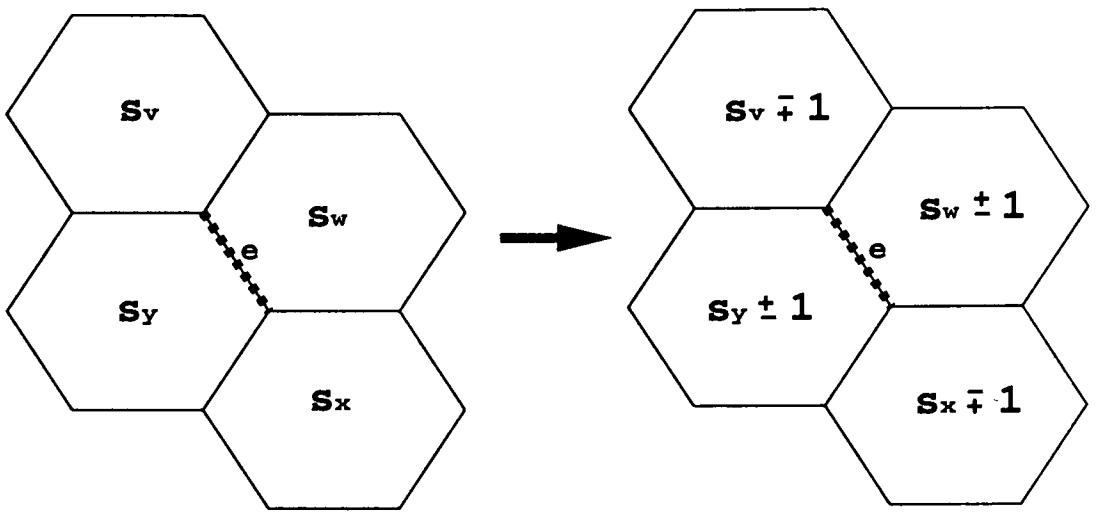

Figure 3.1: The spin-flip rules for the 3-state spin model: the total spin is conserved and the choice of whether to attempt the upper or lower signs is made randomly at each time-step. The quadruplet of cells is identified uniquely by the dashed edge e.

non-periodic and dynamically changing cell structure, whereas this model is firmly fixed on a perfect hexagonal tiling.

We define the energy as follows:

$$E = D\sum_{i=1}^{N} s_i^2 \tag{3.1.1}$$

where N is the total number of cells/spins in the system, and D may be positive or negative. The case of $D > 0$ emulates the original topological model of Chapter 2 where hexagonal order is energetically preferable, but $D < 0$ is also of interest, as we shall show. The dynamics conserve the total spin of the system and we choose our starting configuration such that the total spin is always zero i.e.

$$\sum_{i=1}^{N} s_i = 0 \tag{3.1.2}$$

in analogy with the Euler rule $\sum_i^N (6 - n_i) = 0$ which applies to a froth [52, 53]. Therefore the ground state for $D > 0$ consists of $s_i = 0$ for all spins, whereas for $D < 0$ the ground state is degenerate, with half the spins taking the value $+1$ and half taking the value -1.

The system is allowed to evolve through local spin-flips which are similar to the T1 moves introduced in Chapter 2. In that case two adjacent cells had their topological charges decreased by 1, and their two common neighbours had their topological charges increased by 1: see Figure 2.4. As a direct analogy, in the present model the allowed move-sets consist of choosing a pair of neighbouring cells and either increasing their spins by 1 unit, and decreasing those of their common neighbours by 1 unit, or vice versa, as shown in Figure 3.1; both possibilities need to be allowed to ensure detailed balance is satisfied.

The actual dynamical process is as follows: at each time step an edge is chosen

randomly on the hexagonal lattice; this defines a set of four cells as shown in Figure 3.1. A choice is then made randomly of whether to consider increasing the spins of the adjacent cells y and w (and thus decreasing v, x) or vice versa, with equal probabilities for both cases. The probability of actually performing the move is dependent on the energy change that would be incurred, and is given by a temperature-dependent Metropolis–Kawasaki algorithm. We choose to use the Metropolis algorithm rather than Glauber dynamics as in the previous chapter because the qualitative features of the results show no dependence on which of these algorithms we choose, and Metropolis is the faster of these two. The reference to Kawasaki is included to emphasise the fact that although more than one spin is flipped at once, the total spin is conserved. Specifically, assuming w and y have been chosen as candidates for an increase in spin, the energy change associated with these spin-flips on spins s_v, s_w, s_x, s_y is:

$$\Delta E(s_w, s_y; s_v, s_x) = 2D(2 + s_w + s_y - s_v - s_x) \tag{3.1.3}$$

and the probability P of actually performing this move is:

$$P(s_w, s_y; s_v, s_x) = (1 - \delta_{s_w,1})(1 - \delta_{s_y,1})(1 - \delta_{s_v,-1})(1 - \delta_{s_x,-1})\ \mathrm{Min}[1, \exp(-\beta \Delta E(s_w, s_y; s_v, s_x))] \tag{3.1.4}$$

where β is the inverse temperature. The δ-functions ensure that the spins are forbidden to take values other than ± 1 or 0.

The simple form of Equation (3.1.1), with no interaction between the cells, shows that this system is thermodynamically trivial in equilibrium and all the static equilibrium properties are readily calculable. However, the microscopic dynamics are constrained and non-trivial, involving several spins simultaneously; this leads to glassy macro-dynamics.

Most of the data results from simulations on a system of size N=9900 although in order to perform more accurate fits, in certain cases the system size was increased to 160,000. However, unless otherwise stated, one should assume the former system size is in use. Periodic boundary conditions are enforced in all cases.

This chapter is structured in the following manner: first we present results for $D > 0$, including a discussion on the processes involved in relaxation of the system and the form of the energy density and correlation functions; this is followed with results for $D < 0$. There is then a section on the results of investigations into the non-equilibrium Fluctuation-Dissipation Theorem for both $D > 0$ and $D < 0$, and we conclude with some general remarks.

3.2 $D > 0$

3.2.1 Relaxation Dynamics

We shall turn our attention first of all to the case where D is positive. Setting $D = 1$, it is a simple matter to calculate the equilibrium behaviour of $\frac{E}{N}$, for which one finds:

$$\frac{E}{N} = \frac{2e^{-\beta}}{1 + 2e^{-\beta}}. \tag{3.2.1}$$

One has instant access to equilibrium states, as one can randomly place the appropriate number of ± 1's throughout the system to access a particular temperature. Of course, there is always the very remote possibility of constructing an extremely strange configuration, with some unusual correlations within it, but if one then runs the system for some time ($\sim 10^2 N$ or $10^3 N$) at the temperature in question before taking measurements, the likelihood of obtaining a pathological configuration becomes negligible. Using this feature, we may study the behaviour of the energy with temperature at a number of different cooling rates, starting from equilibrium at any chosen temperature. Above $T = 1$ the system equilibrates very rapidly at even the fastest cooling rate, so we have chosen a starting configuration of $T = 1$, and then cooling is carried out by waiting a time $t_w = \gamma N$ at each temperature decrement of $\delta T = 0.05$. The results (averaged over 3 runs), with the equilibrium curve, are shown in Figure 3.2(a); the system exhibits strong dependence of the energy upon the cooling rate. This is characteristic of glassy systems, and qualitatively similar to the results found for the purely topological froth.

It is instructive to study also the behaviour of the system when subjected to a rapid quench from an infinite temperature ($\beta = 0$) configuration to a temperature at which it is allowed to evolve for a time t_w. Figure 3.2(b) shows the energy density results from such a quench for a range of different temperatures. For longer values of t_w we see a minimum develop — this strongly suggests activation is present: at very low temperatures the system cannot overcome the energy barriers and thus cannot access lower energy states. The temperature at which this minimum occurs is dependent on the waiting time t_w. At very low temperatures, even at the largest waiting times employed ($t_w = 10^5 N$) the system is unable to reach energy densities below $\frac{E}{N} \sim 0.09$.

The significance of this value can be seen if we turn to the temporal behaviour of the energy density. Figure 3.3(a) is a plot of $\frac{E}{N}$ against time, quenched from a fully disordered starting configuration corresponding to $\beta = 0$ to the temperature in question. The initial decay of the energy is fast and independent of temperature until $\frac{E}{N} \sim 0.09$, at which point one sees the existence of a plateau; the time spent on this plateau is clearly dependent on temperature. Upon departure from the plateau, the energy density relaxes directly to the appropriate equilibrium value; on the graph shown, the curve for $\beta = 4$ equilibrates within the time-scale of the simulation, whereas those for $\beta > 4$ do not. This two-time behaviour, with one time-scale temperature-independent and the other increasing with inverse tempera-

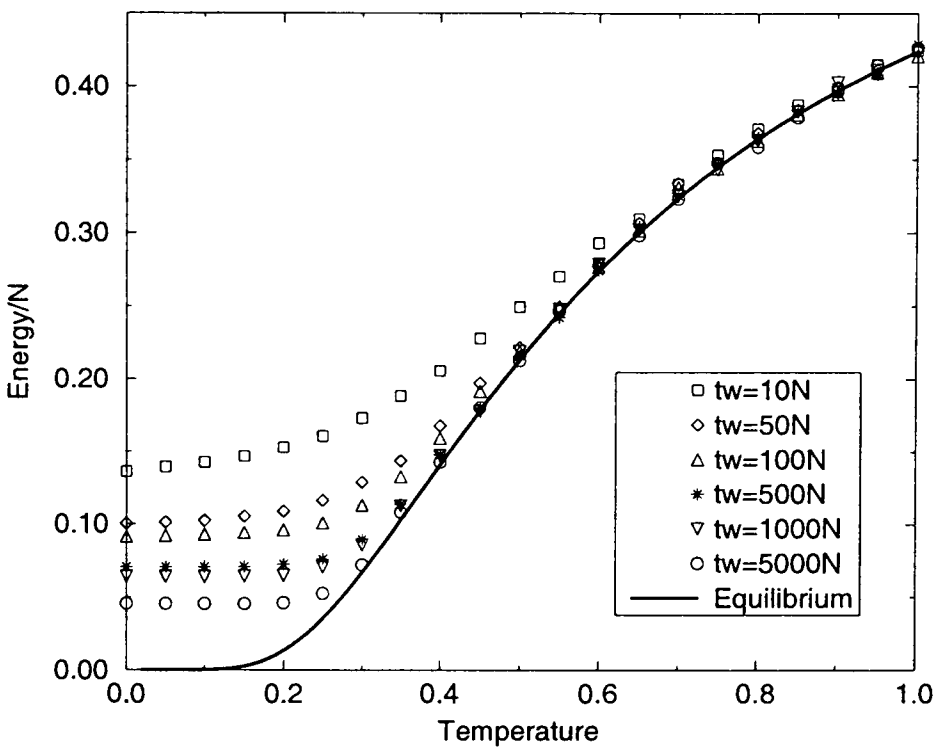

(a) The behaviour of the energy with temperature under slow cooling ($D > 0$). The values of t_w are the waiting times at each point.

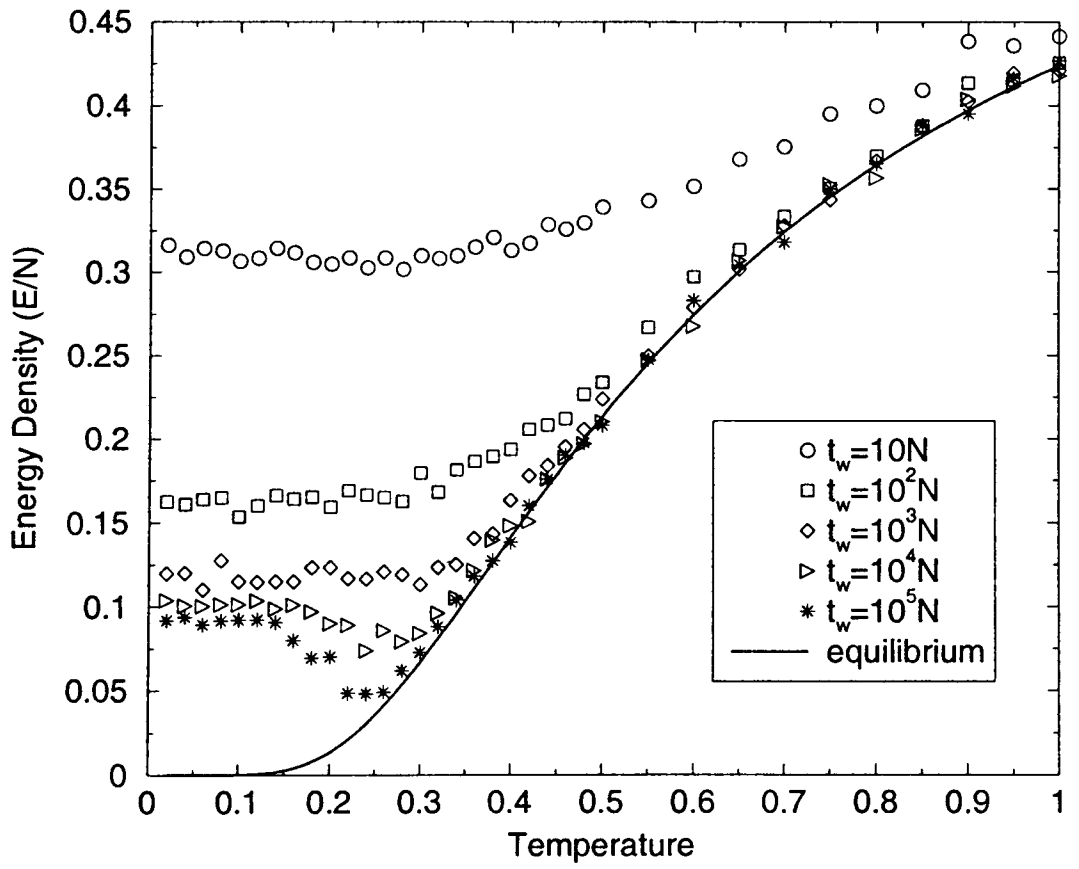

(b) The behaviour of the energy with temperature after a rapid quench ($D > 0$). The values of t_w are the times, subsequent to the quench, at which the energy is measured.

Figure 3.2: Energy against temperature for slow cooling and rapid quench.

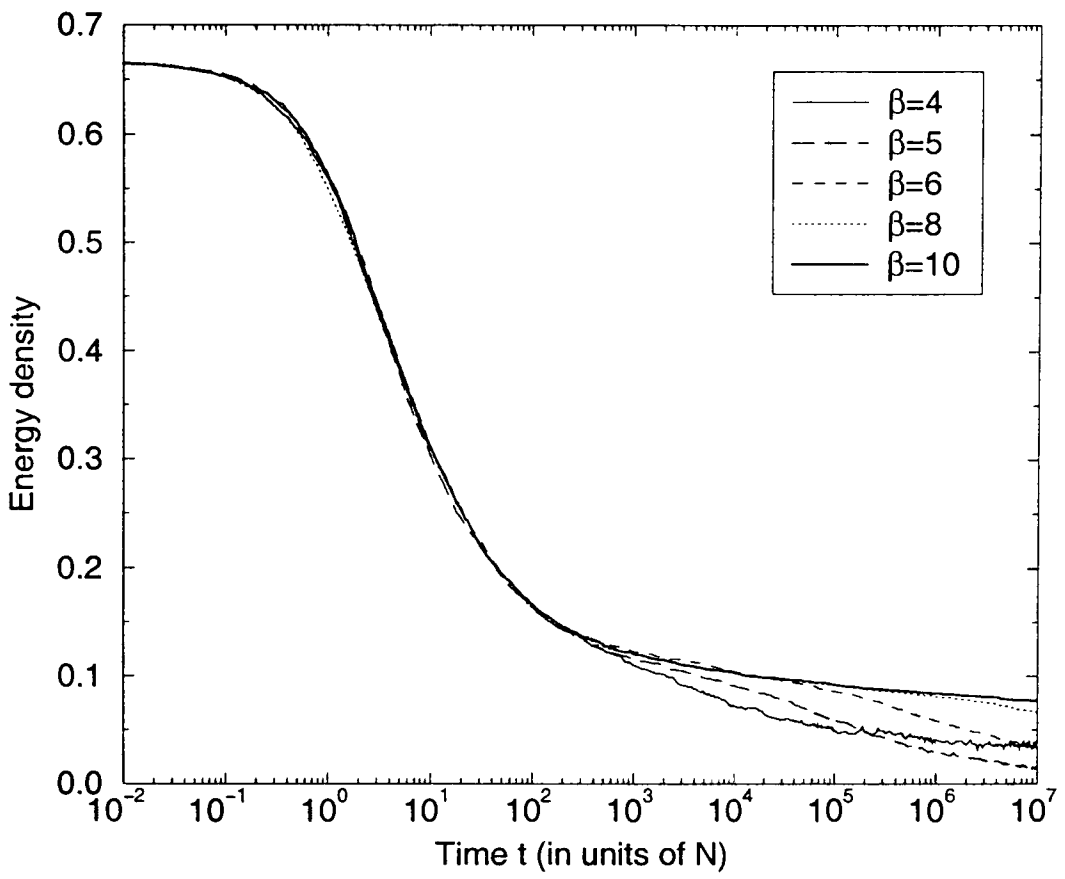

(a) Energy density against time. The curve for $\beta = 4$ reaches the equilibrium value, whereas the others do not.

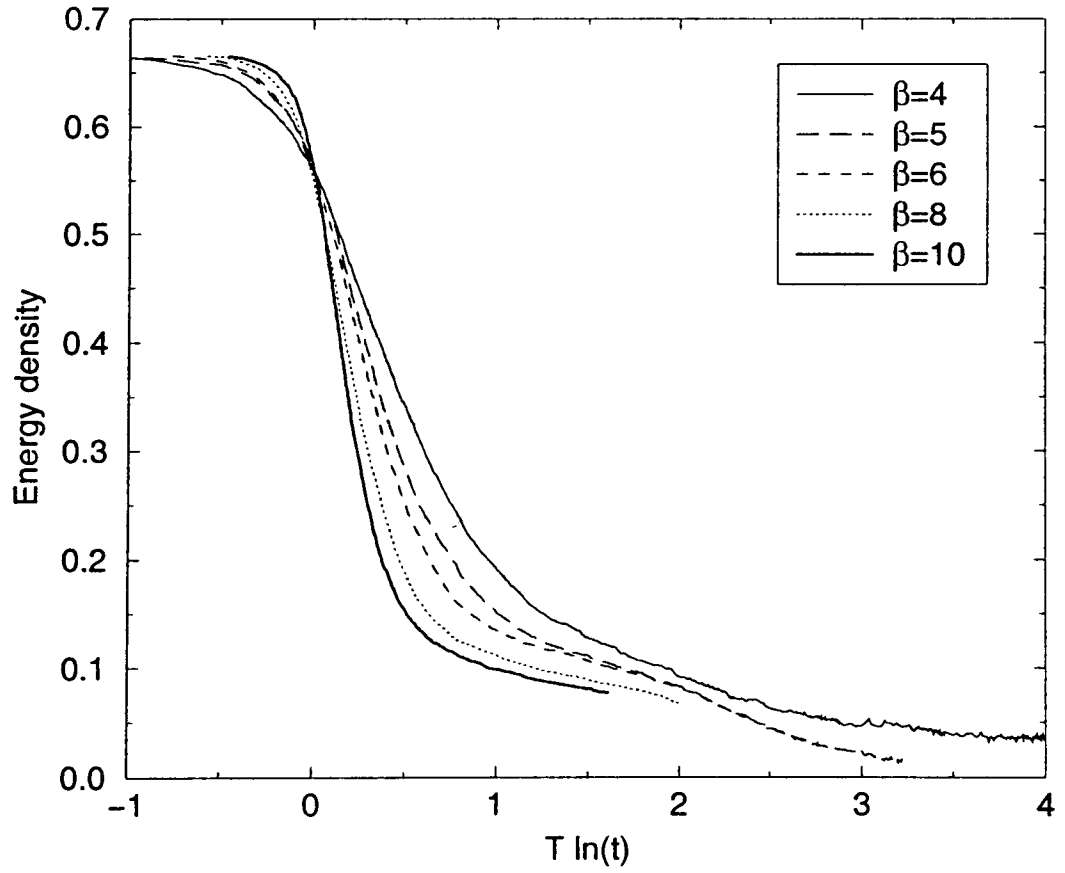

(b) Energy density against $T \ln t$ (where t is measured in units of N).

Figure 3.3: The behaviour of the energy with time.

ture, can be understood in the same way as in the previous chapter. The mechanism for lowering the energy is equivalent to that in the topological froth — the annihilation/absorption of pairs of adjacent $+1$ and -1 spins (we shall refer to a $+1, -1$ pair as a 'dimer'; a dimer in this model is the equivalent of the 5-7 pair of the previous chapter). This occurs in two ways: (i) two neighbouring conjugate dimers can destroy each other to leave four zero spins as shown in Figure 3.4(a), with a reduction in energy of 4 units, or (ii) a ± 1 can absorb a dimer, thus shifting its position and reducing the energy by 2 units as in Figure 3.4(b); note that the ± 1 can be part of a dimer at a different orientation. Any such local arrangements present in the starting configuration will be eliminated quickly without need of any thermal excitation. Furthermore, dimers can move freely though a background of zero spins (just like the 5-7 pairs could move freely though the hexagonal background) as shown in Figure 3.4(c) until they reach a local environment which favours annihilation/absorption, such as those previously mentioned. This diffusion occurs on a time-scale of 2 steps per spin, as one can alter the configuration on the left of the arrow in Figure 3.4(c) in 2 ways, one of which will be possible and one of which will be forbidden through the δ-functions in Equation (3.1.4). Consequently, the initial fast decay of the energy is temperature-independent, and of a diffusive character with an underlying time-scale of 2. This fast, diffusive process describes the behaviour of the energy until the plateau is reached. To describe it further, one has to consider isolated defects i.e. isolated spins of ± 1. To completely remove these defects, they must be paired up with a conjugate isolated defect to form a dimer which can then diffuse freely as in Figure 3.4(c), and eventually annihilate as in Figure 3.4(a) and 3.4(b). An isolated defect can move through fortuitous collisions with existing dimers, but after the initial fast decay these dimers become rare. Alternatively, a defect can move by creating a new dimer (reversing the arrow in Figure 3.4(b)), at an activation energy cost of 2 units and with a probability that scales as $e^{-2\beta}$. As is clear from this figure, one can interpret the resulting configuration as a dimer-plus-defect in two ways; either of these two possible dimers can diffuse away freely if adjacent to two zero spins, or annihilate if adjacent to another dimer. This factor of 2 will cancel that introduced by the diffusive time-scale of the dimers. Thus again one has a diffusive process leading to a final reduction in energy, in this case with a time-scale of $e^{2\beta}$ (since the time-scale for annihilation of the dimer is negligible compared to that to produce the dimer for $e^{2\beta} \gg 1$). Therefore $E(t)/N$ is expected to consist of two diffusive processes: a fast process of time-scale 2 decaying to a state of isolated defects, and a slow process of time-scale $e^{2\beta}$ decaying to the equilibrium configuration. We shall leave a discussion of the exact form of the energy density until Section 3.2.4.

The plateau in $E(t)/N$ can be seen more clearly if the time axis is rescaled to $T \ln t$ as in Figure 3.3(b); as the temperature is decreased (β increased) the curves tend to a sharp staircase form. This is reminiscent of the results found under such rescaling for other kinetically constrained models [20, 22, 26, 32, 33, 55, 56]; in these other models one observes several plateaux corresponding to several characteristic

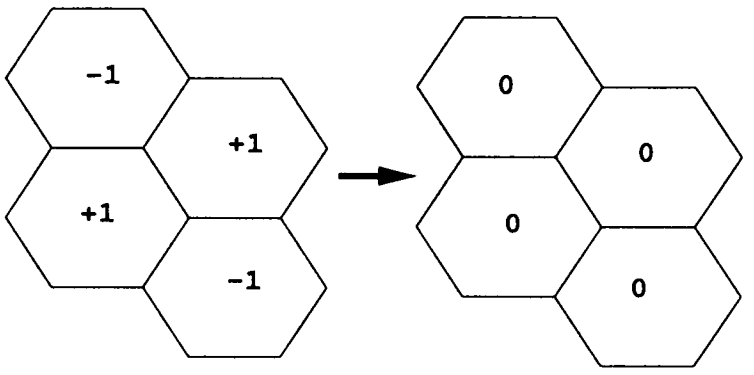

(a) Annihilation of two (conjugate) dimers. This is also possible if each spin is multiplied by -1.

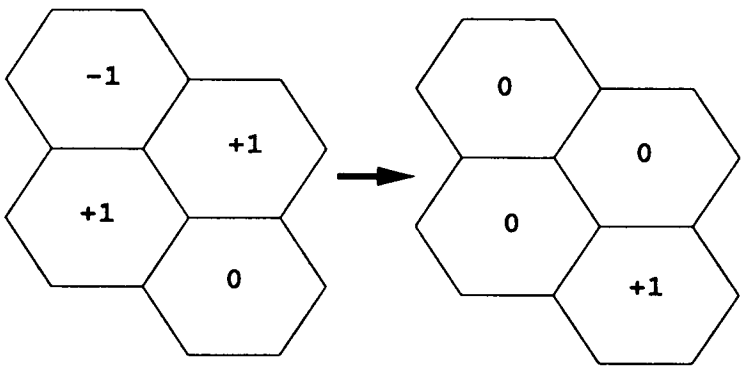

(b) Absorption of a dimer by a defect. The defect is shifted in position.

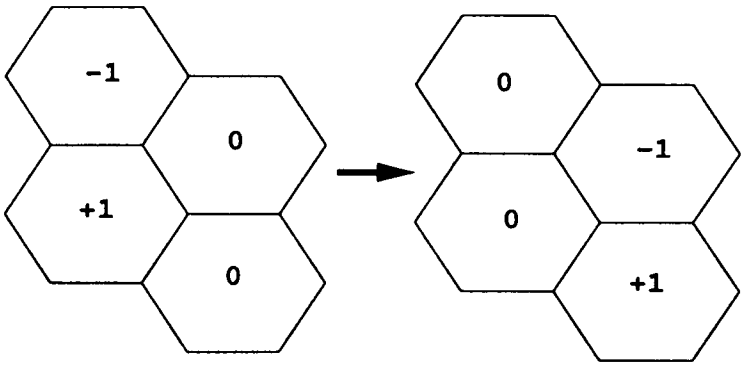

(c) Free diffusion of a dimer in a background of zero spins.

Figure 3.4: The dominant moves through which this model evolves.

activation energies, but in this particular case the situation is simpler as there is only one dominant characteristic activation energy.

With this particular model, due to the simple relationship between equilibrium temperature and energy density in Equation (3.2.1) it is always possible to associate an energy density with a particular temperature. Therefore one might be tempted to assume that for the duration of the plateau the system is in equilibrium at some effective temperature ($\beta_{eff} \sim 3.1$) corresponding to that energy density ($E/N \sim 0.085$). However this idea is not valid as there are correlations present in non-equilibrium configurations which clearly distinguish them from equilibrium

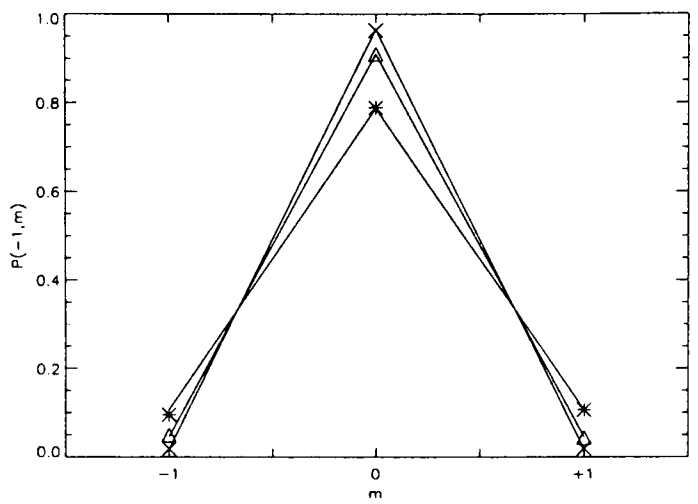

Figure 3.5: The equilibrium pair distribution $p(-1, m)$ at $\beta = 2$ ($\star$), $\beta = 3$ ($\Box$) and $\beta = 4$ ($\triangle$). The straight lines link the theoretically predicted points (no symbols are shown on those points to avoid confusion).

configurations. This is immediately apparent if one considers the correlations between a central spin and its neighbours. Let us look at the pair distribution $p(n, m)$ of spins of value m that are neighbours to a spin of value n:

$$p(n,m) = \frac{\sum_{i=1}^{N} \sum_{j=1}^{6} \delta_{s_i,n} \delta_{s_j,m}}{6 \sum_{i=1}^{N} \delta_{s_i,n}}. \tag{3.2.2}$$

Notice that the following relationship must hold (where $n, m \in \{-1, 0, +1\}$):

$$\sum_{m} p(n,m) = 1. \tag{3.2.3}$$

First let us consider what we might expect in equilibrium. In that case we can easily calculate the concentration of non-zero spins, and assuming no correlations are present, we can predict the values of $p(n, m)$. Figure 3.5 shows the predictions and simulation results for $p(-1, m)$ for various temperatures in equilibrium (these results are averaged over 10 configurations, and the results for $p(0, m)$ and $p(1, m)$ are effectively identical). We see that the simulation results are in good agreement with the predicted values, thus supporting our assumption that there are no correlations present in equilibrium. However, Figure 3.6 shows the simulation results for $\beta = 8$ at various times subsequent to a quench from $\beta = 0$. Although $p(0, m)$, shown in Figure 3.6(c), remains symmetrical, with the probability of $p(0, 0)$ increasing at the expense of $p(0,\pm1)$, we see a clear asymmetry quickly developing in $p(\pm1, m)$, shown in Figures 3.6(a), 3.6(b), with defects more likely to be alongside a defect of the same value rather than alongside an opposite one as is the case in a dimer pair. This is because dimers can freely diffuse and are quickly absorbed, or they annihilate with another dimer. If we compare the energy density curve for $\beta = 8$ in Figure 3.3(a) with the pair distribution data, we see that the dimer distribution is very close to the equilibrium after $t \sim 10^2 N$; this is very close to the time at which

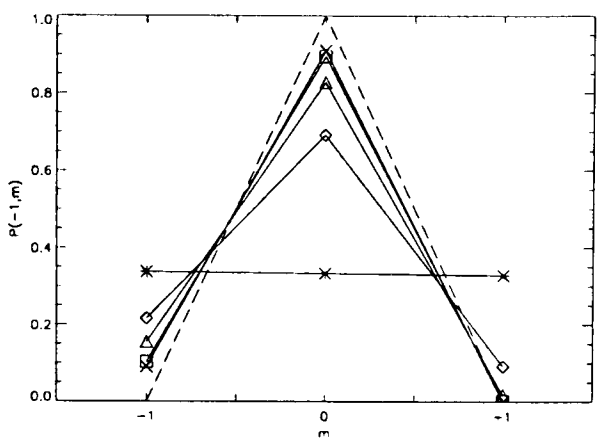

(a) The out of equilibrium pair distribution $p(-1, m)$.

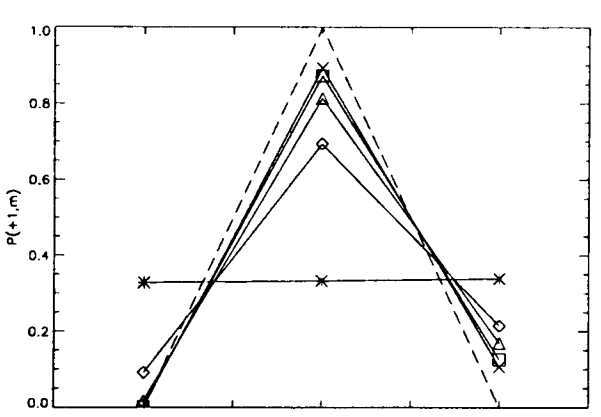

(b) The out of equilibrium pair distribution $p(+1, m)$.

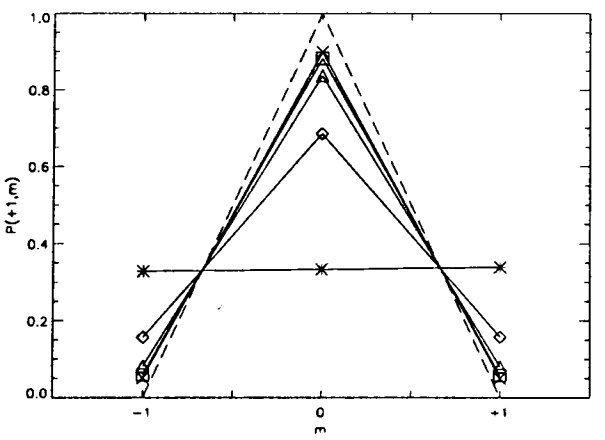

(c) The out of equilibrium pair distribution $p(0, m)$.

Figure 3.6: The pair distributions $p(n, m)$ out of equilibrium, for $\beta = 8$, at the following waiting times after a quench from $\beta = 0$: 0 ($\star$), $10N$ ($\diamond$), 10^2N ($\triangle$), 10^3N ($\square$), 10^4N ($\times$). The equilibrium distribution is shown by the dashed line. Note that (a) and (b) are mirror images of one another.

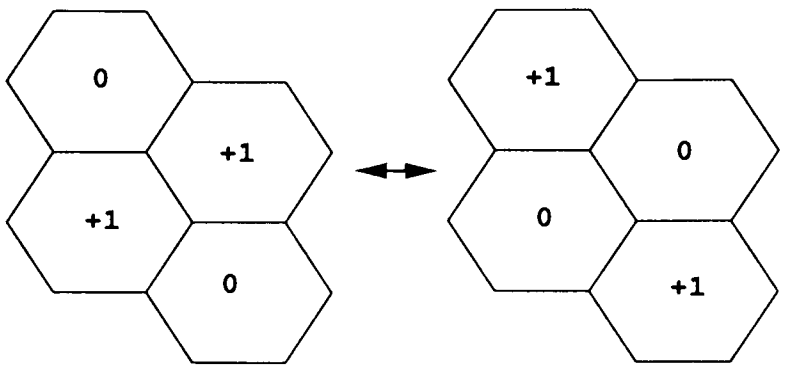

Figure 3.7: Zero-energy moves for oscillating +1 like-pairs. An identical configuration exists for −1 like-pairs.

the plateau begins, providing more evidence that the initial energy density decay is due to the absorption and annihilation of dimers. Like-pairs, on the other hand, can oscillate with no energy cost as in Figure 3.7 but are still effectively localized until they either absorb or create a dimer, which takes place over the long time-scale of $e^{2\beta}$. Thus the dimers quickly reduce to the equilibrium level, whilst the like-pairs linger causing the asymmetric pair distributions observed. This means that one can readily see whether a system is in equilibrium by studying the pair distribution, and one cannot identify a non-equilibrium configuration at a certain temperature with an equilibrium configuration at an effective temperature because the former will have a pair distribution that is asymmetric for $p(\pm 1, m)$ and thus cannot be mapped onto that of any equilibrium system.

We probe further the typical distribution of the defects by investigating the number of like neighbours each defect has at various times through the evolution of

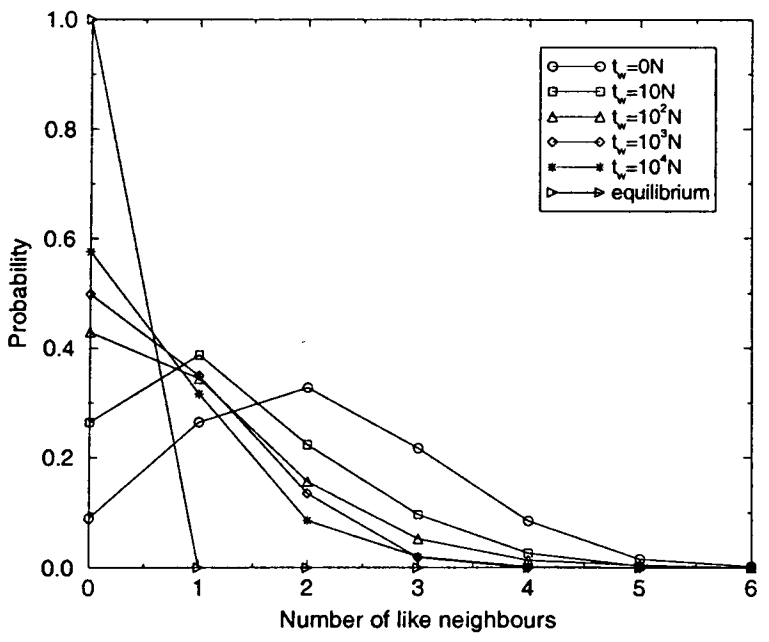

Figure 3.8: The distribution of the number of like neighbours of a defect. The data is for $\beta = 8$, measured at the times shown in the key subsequent to a quench from an infinite temperature configuration. For this low temperature, virtually all defects are isolated in equilibrium; for $\beta \leqslant 5$ there is a non-negligible probability of a defect having like neighbours in equilibrium.

the system. Figure 3.8 shows the probability that a defect will have n neighbours of the same sign, where $n \in \{0, 1, 2 \ldots 6\}$, measured at times t_w subsequent to a quench to $\beta = 8$ from an infinite temperature configuration (one finds similar results for all temperatures in the range $\beta > 5$, thus we show only one temperature here). Whilst our pair distribution observations lead us to expect many defects to have one like neighbour even at long times such as $t_w = 10^4 N$, we observe that a considerable proportion have two or even three like neighbours. Thus the vision of the system as consisting of mainly isolated defects after the onset of the plateau is not entirely accurate — in fact, although the majority will be isolated, with the exact proportion increasing with time, there are many clusters of two, three or even four like defects present. Clusters are more difficult to eradicate than lone defects, and thus are likely to slow down the dynamics somewhat.

We have also investigated the behaviour of the energy if one quenches to $T = 0$ from an initial equilibrium configuration corresponding to a finite temperature T_I, which is in some sense an investigation of the inherent structures of the system. This concept was introduced by Stillinger and Weber in the early 1980's [57, 58] in an attempt to ascribe some order to essentially disordered states, and has been subject to extensive study since (see [59–62] amongst others). The approach involves identifying the minima on the potential energy hypersurface. In a conventional glass the potential energy hypersurface is assumed to have a complex topology involving many deep valleys connected by saddles, and the evolution of the system to be composed of inter-valley motion and intra-valley motion. At low temperatures these two motions become well separated in time, and thus if each configuration is referred to the minimum for the basin of attraction it lies in, the intra-valley motion, which is essentially a temperature-dependent vibrational motion, is removed to leave

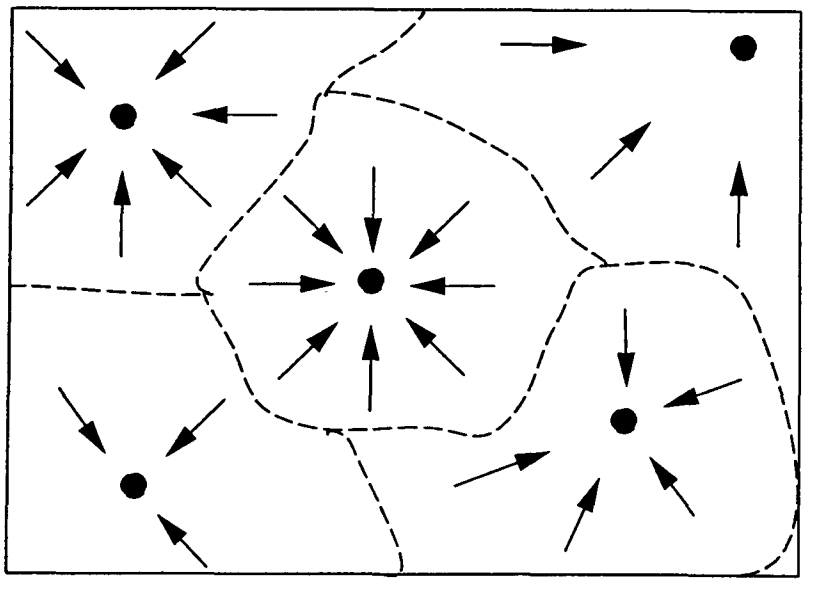

Figure 3.9: A pictorial representation of the inherent structures concept: the dark circles represent the local minima in the potential energy hypersurface, and each minimum lies within a basin of attraction marked out by dashed lines. Each configuration lying within a basin of attraction is mapped to the minima of that basin.

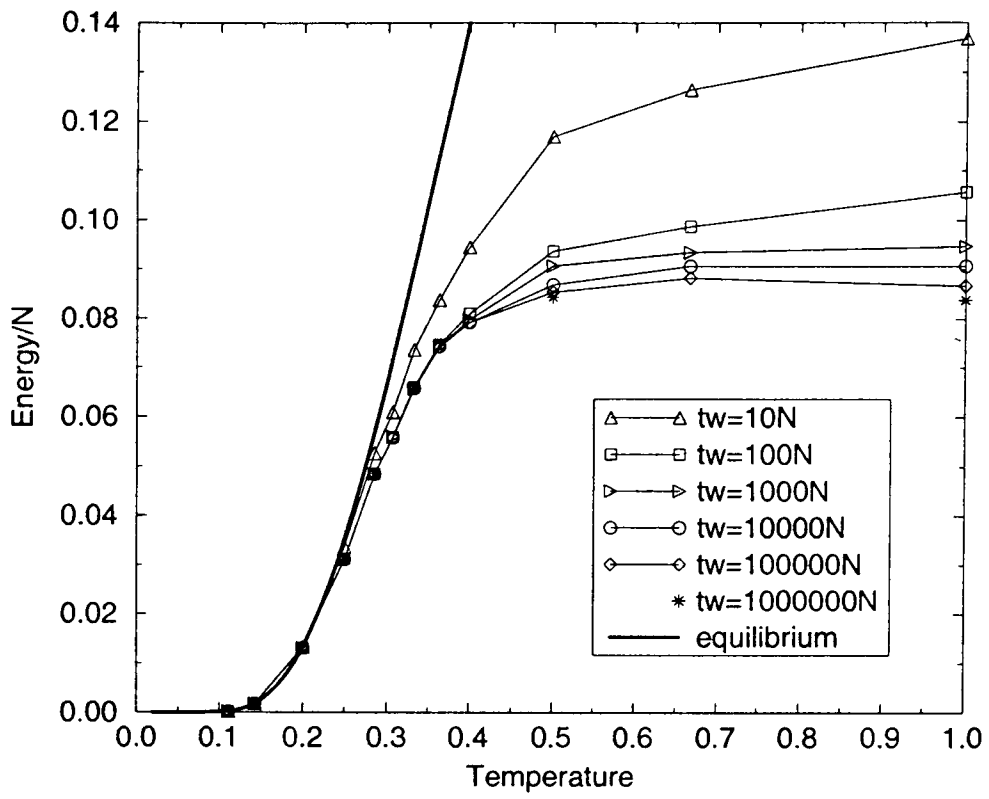

Figure 3.10: The behaviour of E/N after a $T = 0$ quench from equilibrium.

the underlying inter-valley motion (see Figure 3.9 for a pictorial representation). The term *inherent structures* was introduced by Stillinger and Weber to mean the potential energy minima reached by a steepest descent energy minimization process (e.g. a $T = 0$ quench). One could then proceed to define a thermodynamics based on the inherent structures by replacing the partition function with a sum over the inherent structures; the dynamics on time-scales longer than the typical time spent inside each basin should then be described by the inherent structures dynamics, an assumption which is supported by simulation results on Lennard–Jones liquids [61,63–65].

At very low temperatures, the equilibrium state for T_I consists mainly of isolated defects, thus when quenched to $T = 0$ the system very quickly settles. However, at higher initial temperatures this takes an extremely long time to happen. Thus we show in Figure 3.10 the energy measured at waiting time t_w after a quench from the equilibrium configuration to $T = 0$. At low T_I the energy stays on the equilibrium curve, as there are no energetically favourable moves to be made. However, for higher T_I the energy tends towards a constant value given by the plateau in Figure 3.3. Thus we see that if one quenches from an equilibrium configuration with energy above the plateau, the lowest energy one can reach is that of the plateau — to decrease energy further would require activated processes, which one cannot perform at $T = 0$. If one quenches from an equilibrium start-point with energy below that of the plateau, one cannot decrease the energy by much as there are very few energetically favourable moves to be made, and so the curves in Figure 3.10 do

not deviate far from the equilibrium curve. The temperature at which a crossover is seen between these two types of behaviour is $T \sim 0.35$: this is the temperature at which activated processes become important.

3.2.2 Correlation Functions and Relaxation Time

We investigate the temporal correlations in the system through a two-time single-site spin correlation function of the form

$$C(t + t_w, t_w) = \frac{\sum_{i=1}^{N} s_i(t + t_w) s_i(t_w)}{\sum_{i=1}^{N} s_i^2(t_w)}. \tag{3.2.4}$$

Under equilibrium conditions this becomes a function of the relative time t only. The equilibrium correlation functions (averaged over 5 runs) for a range of temperatures are shown in Figure 3.11(a). As β increases, plateaux develop, revealing that again two-step relaxation is taking place. We also show examples of typical non-equilibrium correlation functions in Figure 3.11(b), where the system has been rapidly quenched from infinite temperature to the temperature in question, and then evolved at that temperature for a time t_w before measurement of the correlation function commences. We observe aging behaviour, with the correlation function showing dependence on the waiting time t_w.

Following the procedure in [54,66], we may define a relaxation time τ_r as the time at which the equilibrium correlation function decays to e^{-1}. This is plotted on Figure 3.12 against inverse temperature; the data can be reasonably fitted by an offset Arrhenius curve of the form:

$$\tau_r = A + B\, e^{C/T} \tag{3.2.5}$$

where A, B, C are constants. The solid line superimposed on Figure 3.12 corresponds to $A = 2.172, B = 0.0088, C = 2.67$. This indicates that this model displays strong glassy behaviour, in agreement with the results from the topological model, where an offset Arrhenius law fitted the data considerably better than either a power law, or a Vogel–Fulcher law (see Chapter 2). The anomalous upturn in the curve at very low β is due to the restriction that the spins may only take the values ± 1 or 0; when the density of non-zero spins is very high, it becomes likely that some defects will sit next to each other, in locally 'stuck' configurations which slow the decay of the correlation function (see Figure 3.13).

However, if we look closely at Figure 3.12, we see that at high inverse temperature the data seems to be drifting below the curve. If we consider more carefully the expected form of $C(t)$ it becomes clear that the above definition of τ_r is not the most appropriate one, since again, as in the topological model, there are two decay processes. The fast processes move the system away from the starting configuration to the plateau, and are temperature-independent; however, the position of the plateau and the subsequent departure from it is dependent on temperature. In

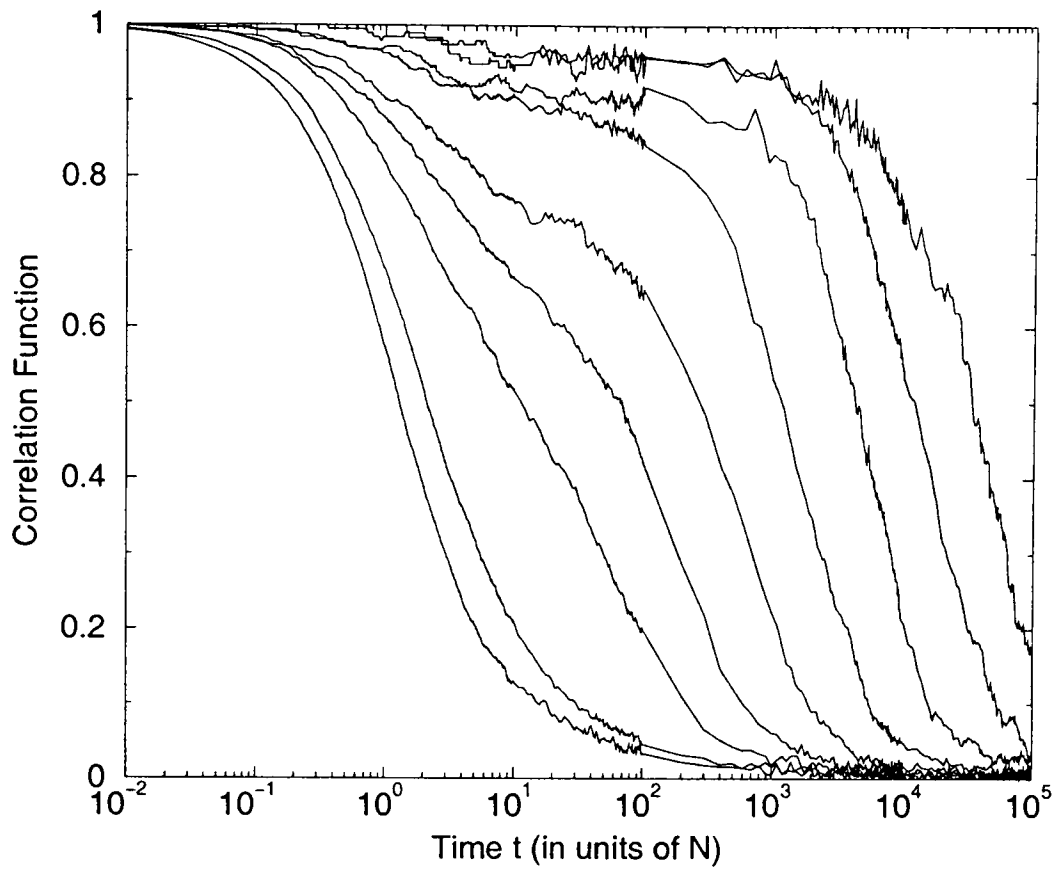

(a) Equilibrium correlation functions $C(t)$ for (from left to right) $\beta = 1, 2, 3, 3.5, 4, 4.5, 5, 5.5, 6$.

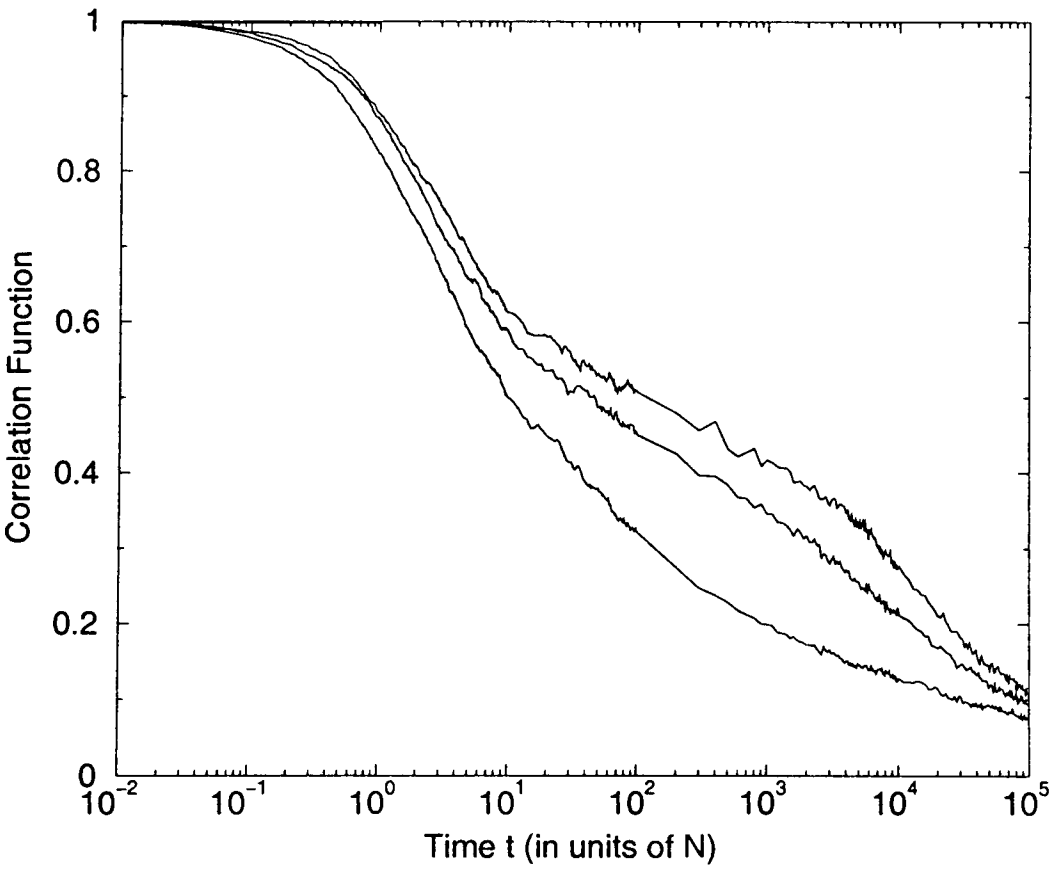

(b) Out of equilibrium correlation functions $C(t+t_w, t_w)$ for $\beta = 6$ for (from left to right) $t_w = 10^2 N, 10^3 N, 10^4 N$.

Figure 3.11: Correlation functions both in and out of equilibrium.

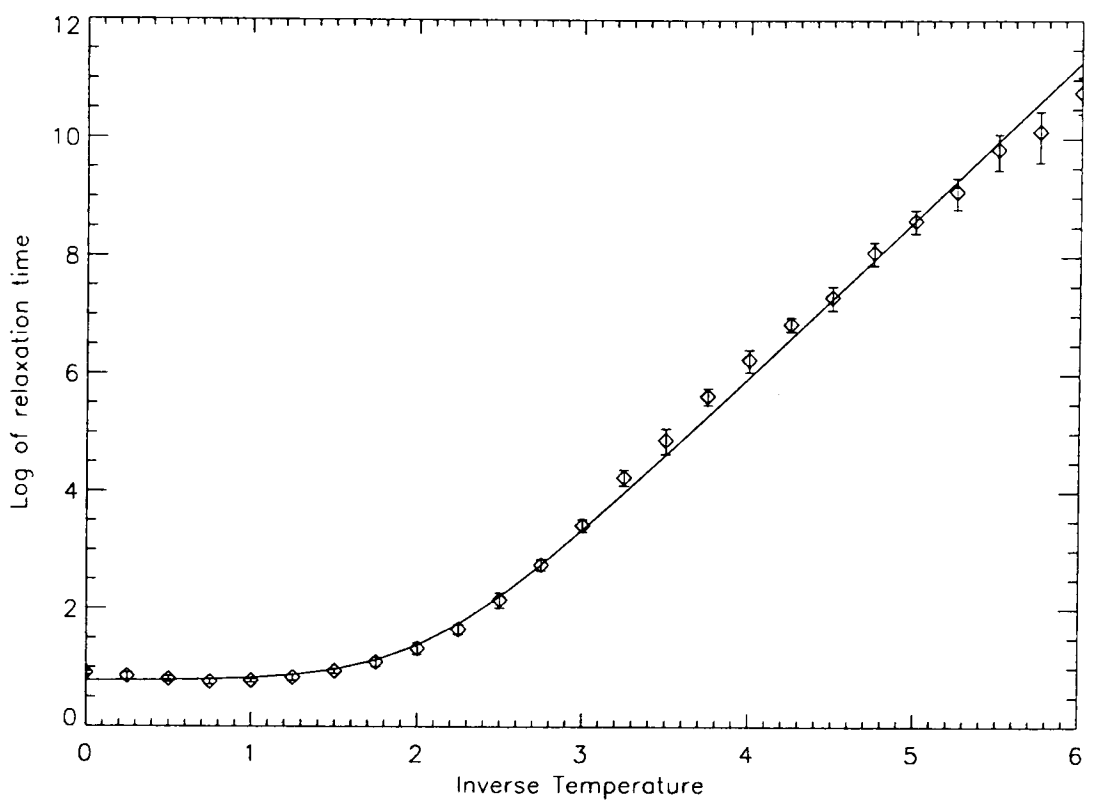

Figure 3.12: The logarithm of τ_r against inverse temperature. The solid line is an offset Arrhenius law of the form $\tau_r = 2.172 + 0.0088 e^{2.67/T}$.

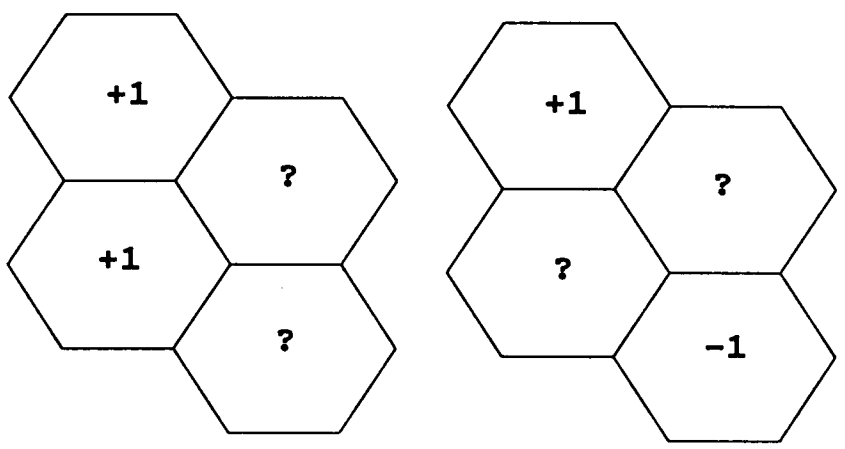

Figure 3.13: 'Stuck' configurations. On the left, one sees that two spins of $+1$ adjacent to each other are unable to be flipped within the isolated cluster, regardless of what values the other two spins take (and similarly for two adjacent spins of -1). On the right, we see that two next-to-nearest neighbours of opposite spin cannot be flipped, regardless of the values of the other two spins. A favourable configuration external to the cluster can provide an opportunity to 'unstick' these cells.

particular, the depth of the drop to the plateau from the initial $C(t = 0) = 1$ is determined by the equilibrium concentration of spins of ± 1 in local configurations that are free to move with no change to the energy (these local configurations include the dimers). One can therefore suggest that $C(t)$ might be a sum of two functions in the following way:

$$C(t) = \alpha\, f(t, \tau_1) + (1 - \alpha)\, g(t, \tau_2) \tag{3.2.6}$$

where α and τ_2 are functions of T, but τ_1 is a constant, and $(1 - \alpha)$ is the height at which one would expect to find a plateau. The functions f and g are to be determined, but they must be monotonically decreasing functions of t, satisfying $f(0, \tau_1) = g(0, \tau_2) = 1$ and $f(\infty, \tau_1) = g(\infty, \tau_2) = 0$.

We tried to fit Equation (3.2.6) to the data using exponentials for both f and g such that $C(t)$ is of the following form:

$$C(t) = \alpha\, \mathrm{e}^{-t/\tau_1} + (1 - \alpha)\, \mathrm{e}^{-t/\tau_2}. \tag{3.2.7}$$

The results are shown in Figure 3.14; in order to fit more accurately, the system size has been increased to $N = 160,000$. The fit is extremely good at high values of β (low temperature), although at lower values there is some deviation. We also note that the fitted form drifts below the data at very low values of $C(t)$; the tails would appear to follow some power law behaviour that we shall not attempt to fit[1]. We do not claim that this form is exactly correct; nevertheless, it is a useful approximation that may allow us to separate out the two time-scales. Previously we stated that we expect τ_1 to be independent of temperature — Figure 3.15(a) shows that this seems to be the case at low β, although as β increases it becomes harder and harder to fit τ_1 accurately due to the extremely high position of the plateau. We have shown the error bars on a few of the points to give some idea of the difficulty in accurately performing this fit at high β; one can see that it is impossible to say anything sensible about the functional form of $\tau_1(\beta)$ for $\beta > 4.5$. However, the naïve theory as discussed earlier in connection with $E(t)$ gives $\tau_1 = 2$ and the data is in general accord.

We turn now to τ_2 and consider the dominant processes involved in relaxation in the β-relaxation regime. These are, as previously mentioned, absorption and creation of dimers. Creating a dimer costs 2 units of energy. Each dimer will rapidly diffuse freely through the system until it is absorbed by a defect; this happens quickly as it is an energetically favourable process. Therefore we have energy barriers of 2 units in this regime, leading to a time-scale of $\sim \mathrm{e}^{2\beta}$. Absorption of pre-existing dimers also has a characteristic time-scale of $\sim \mathrm{e}^{2\beta}$ as the fraction of cells occupied by dimers scales as $\mathrm{e}^{-2\beta}$. This is reflected in the behaviour of the second time-scale τ_2 as shown in Figure 3.15(b): τ_2 exhibits the Arrhenius behaviour

[1] We believe the tails to be due to defects returning to sites where a defect was initially present, as one does not observe such tails when persistence functions are measured instead; however, the tails are not the focus of our attention so we do not pursue this line here.

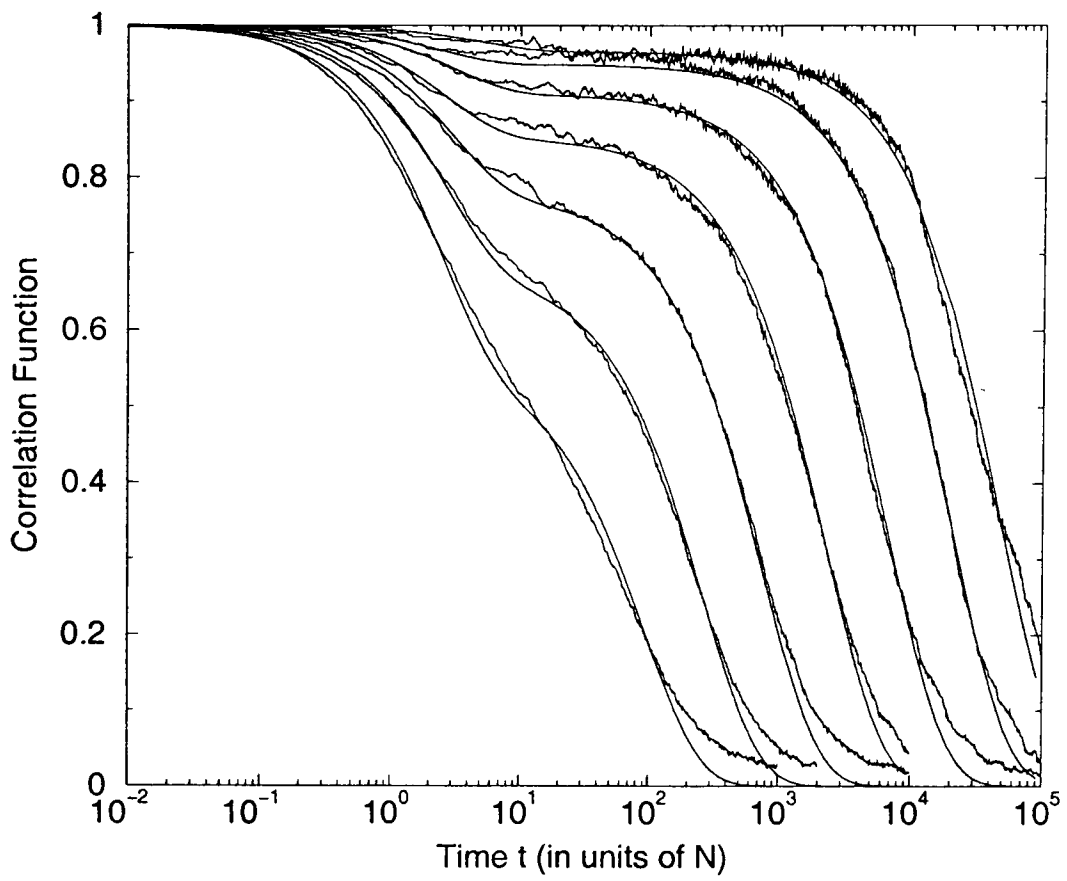

Figure 3.14: Correlation functions for, from left to right, $\beta = 3, 3.5, 4, 4.5, 5, 5.5, 6$. The solid lines superimposed are the best fits of the form $C(t) = \alpha\, e^{-t/\tau_1} + (1 - \alpha)\, e^{-t/\tau_2}$. *Data courtesy of A. Buhot; fits by author.*

of $\tau_2 = Ae^{B\beta}$, with $B = 2.12$. We have shown error bars on a few of the points; these tend to suggest that the value of B is not exactly 2; however, it is encouraging for the value to be so close given that this is a very crude theory.

The plateau parameter α, is somewhat more complicated. As noted earlier, the initial fast decay of the correlation function is dominated by all the local configurations that can move freely, without any energy costs. Thus we expect the plateau height to occur roughly at a value of 1 minus the fraction of total spins which can move freely in equilibrium conditions. This fraction contains the dimers, but also certain configurations of like-pairs (i.e. $+1, +1$ and $-1, -1$) which can oscillate, as shown in Figure 3.7, although they cannot delocalise without interacting with dimers. In equilibrium the probability that a given defect is part of a $+1, -1$ dimer is:

$$6p(1)p(0)^2 = \frac{6e^{-\beta}}{(1 + 2e^{-\beta})^3} \tag{3.2.8}$$

where $p(s)$ is the probability of a spin of value s (the factor 6 comes from the fact that the second defect may be situated on any of the 6 nearest neighbours to the original defect). The probability that any given defect is part of an oscillating like-pair is given by $12p(1)p(0)^2$ (the factor 12 is because there are 12 positions at which the second defect may be situated to make up an oscillating like-pair). However, subsequent to $t = 0$ one supposes that at any instant in time half of the oscillating like-pairs will be in exactly the same position as at time $t = 0$, and the other half

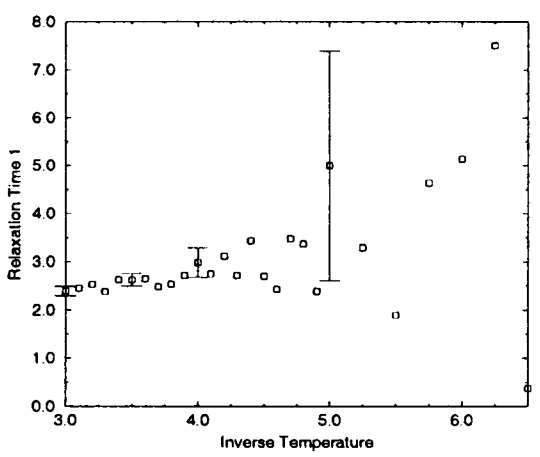

(a) τ_1 against inverse temperature.

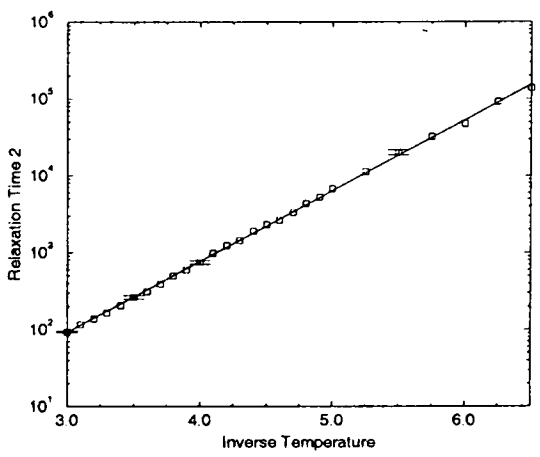

(b) τ_2 against inverse temperature; the superimposed line is $y = Ae^{B\beta}$, where $B = 2.12$.

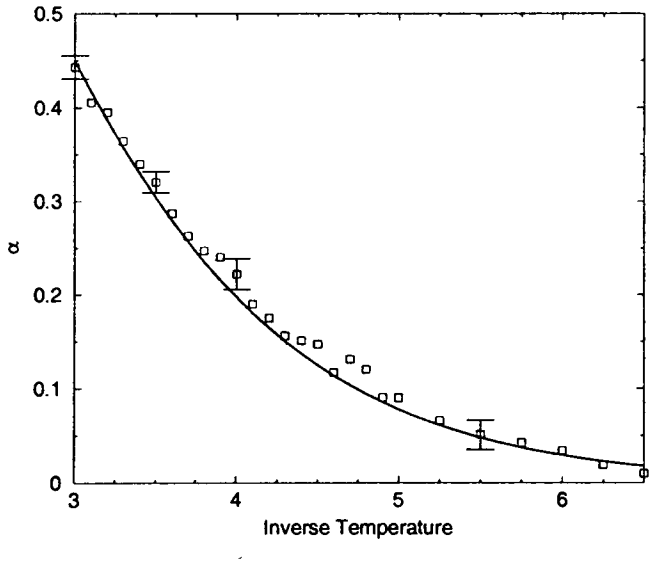

(c) α against inverse temperature; the superimposed curve is $y = \frac{12e^{-\beta}}{(1+2e^{-\beta})^3}$

Figure 3.15: The behaviour of the fitting parameters τ_1, τ_2 and α with temperature; obtained by fitting $C(t) = \alpha\, e^{-t/\tau_1} + (1-\alpha)\, e^{-t/\tau_2}$. *Data courtesy of A. Buhot.*

will be in the alternative position. All processes which reduce energy involve at least 3 defects, and thus are suppressed in comparison by factors of e^{β} or $e^{2\beta}$. As we are investigating the region of $\beta > 2.5$, we neglect those, and simply suggest:

$$\alpha(\beta) = \frac{12e^{-\beta}}{(1+2e^{-\beta})^3} \tag{3.2.9}$$

Figure 3.15(c) shows this predicted curve of α against the simulation results for fitting with a sum of two exponentials, from which good agreement can be seen. Therefore for all three parameters (τ_1, τ_2, α) the results of the simulations provide some support to the theory of the dominant processes involved in the evolution of this system.

Note that the relaxation behaviour of the equilibrium correlation function $C(t)$ differs from that of $E(t)$ in two important respects. One is that for $C(t)$ the system is always in macroscopic equilibrium so that the macroscopic distribution of non-zero spins fluctuates around a constant value throughout the the dynamics, and all the observed results are due to re-arrangements of the location of these non-zero spins i.e. annihilations/absorptions are balanced by creations on a macroscopic level. The second is that one has merely to move a non-zero spin in order to affect $C(t)$, whilst for $E(t)$ to decay from the infinite temperature starting configuration one must actually remove ± 1 spins overall.

3.2.3 Overlap Functions

We continue to probe this simple model with the introduction of overlap functions. In order to distinguish between different types of aging, Barrat, Burioni and Mezard suggested the study of the overlap $Q_{t_w}(t)$ between two replicas [67]. These replicas are identical configurations at time t_w, but are subsequently evolved according to different stochastic thermal noise (but of the same characteristic temperature), with $Q_{t_w}(t)$ of the form:

$$Q_{t_w}(t) = \frac{\sum_{i=1}^{N} \sigma_i^1(t+t_w)\sigma_i^2(t+t_w)}{\sum_{i=1}^{N} \left(\sigma_i^1(t_w)\right)^2} \tag{3.2.10}$$

where σ is some order parameter of the system and the superscripts 1,2 refer to replicas 1,2. Barrat et al classify systems as either Type I or Type II models: for the former, the appropriate $Q_{t_w}(t)$ (normalised to 1 at time $t = 0$) decays to a finite, non-zero value in the double limit $\lim_{t_w \to \infty} \lim_{t \to \infty} Q_{t_w}(t)$; this class includes models which are dominated by coarsening (for a review of coarsening see [68]). For the class of Type II, $Q_{t_w}(t)$ decays to zero in this limit; this class includes glassy systems [20]. In equilibrium (i.e. t_w greater than the equilibration time of the system) there is no t_w dependence so $Q_{t_w} = Q(t)$; one also finds that $Q(t) = C(2t)$ (for details see Appendix).

For this model, the overlap we use is as given in Equation (3.2.10) with $\sigma_i = s_i$. We start from non-equilibrium conditions, where the system is quenched at

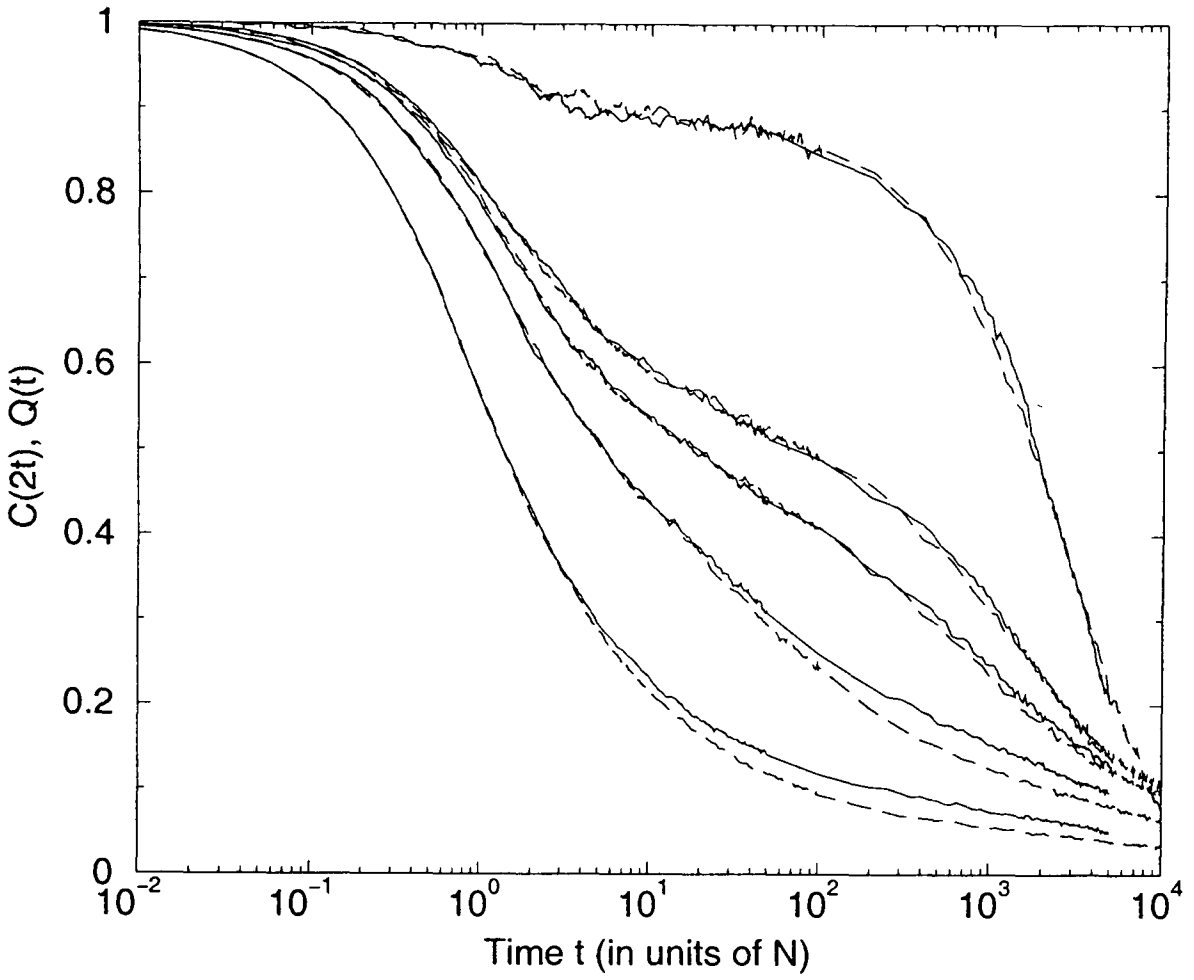

Figure 3.16: The behaviour of $C(2t+t_w, t_w)$, $Q_{t_w}(t)$ with time for β=5. $Q_{t_w}(t)$ is given by the dashed curves and $C(2t+t_w, t_w)$ by the solid curves. From lower curve pair to upper curve pair, $t_w = 10N, 10^2N, 10^3N, 10^4N$. The uppermost pair is that of equilibrium, with $Q(t) = C(2t)$.

$t = 0$ from $\beta = 1$ to the temperature in question, and then allowed to run at that temperature until time t_w when measurements commence. In Figure 3.16 we show the overlap and $C(2t+t_w, t_w)$ against time for $\beta = 5$; initially Q is almost identical to $C(2t+t_w, t_w)$, but it drops below $C(2t+t_w, t_w)$ at longer times. For larger values of t_w this takes longer to happen since these systems start off closer to equilibrium. We also show the equilibrium curves, for which $Q(t) = C(2t)$.

Given that $Q(t) = C(2t)$ in equilibrium, we can check our proposed functional form for the equilibrium correlation function through a parametric plot of the overlap against $C(t)$. If $C(t)$ is indeed of the form given in Equation (3.2.7) then one expects:

$$Q(t) = C(2t) = \alpha\, \mathrm{e}^{-2t/\tau_1} + (1-\alpha)\, \mathrm{e}^{-2t/\tau_2} \tag{3.2.11}$$

Thus for long times one would expect to find:

$$Q(t) \sim (1-\alpha)\, \mathrm{e}^{-2t/\tau_2} \sim \frac{C(t)^2}{(1-\alpha)} \tag{3.2.12}$$

and for short times:

$$Q(t) \sim \alpha\, \mathrm{e}^{-2t/\tau_1} + (1-\alpha) \sim \frac{(C(t)+\alpha-1)^2}{\alpha} + (1-\alpha) \tag{3.2.13}$$

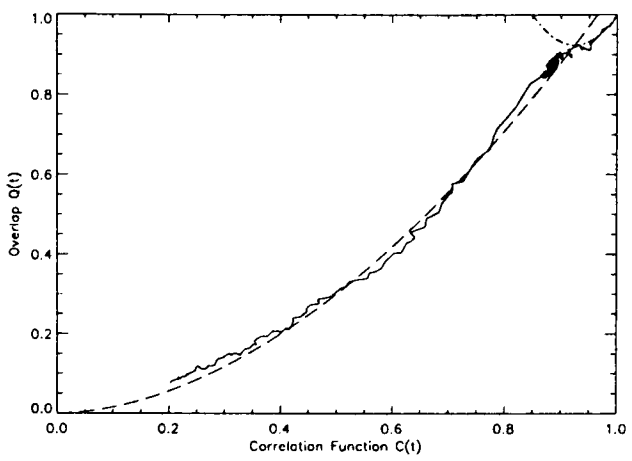

(a) $\beta = 5$, $a = 0.0899$

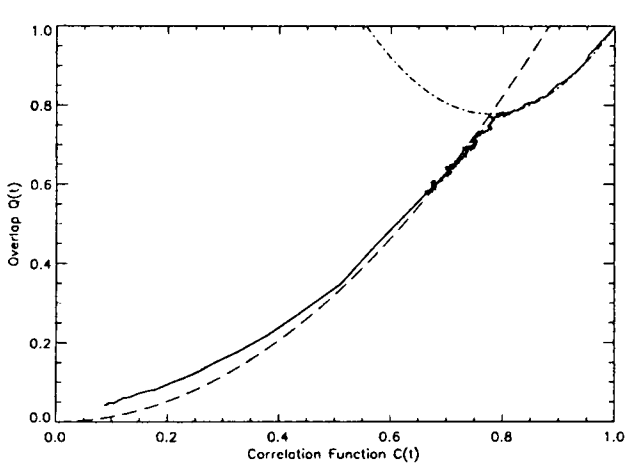

(b) $\beta = 4$, $a = 0.222$

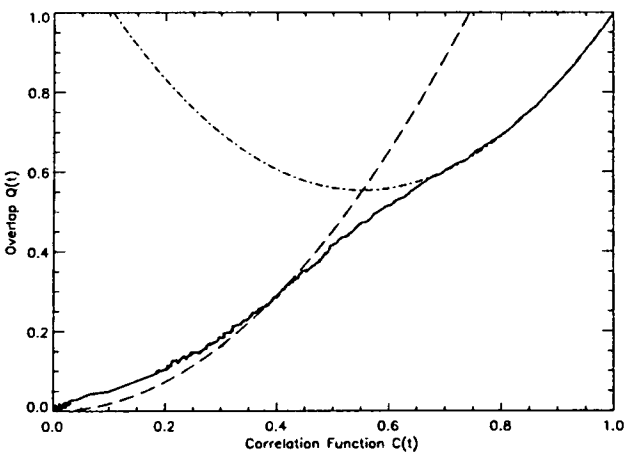

(c) $\beta = 3$, $a = 0.447$

Figure 3.17: The overlap function $Q(t)$ against the correlation function $C(t)$. In each case the dot-dashed curve is the expected short time behaviour and the dashed curve is the expected long time behaviour, if Equation (3.2.7) holds. The values of α are those fitted in the previous section.

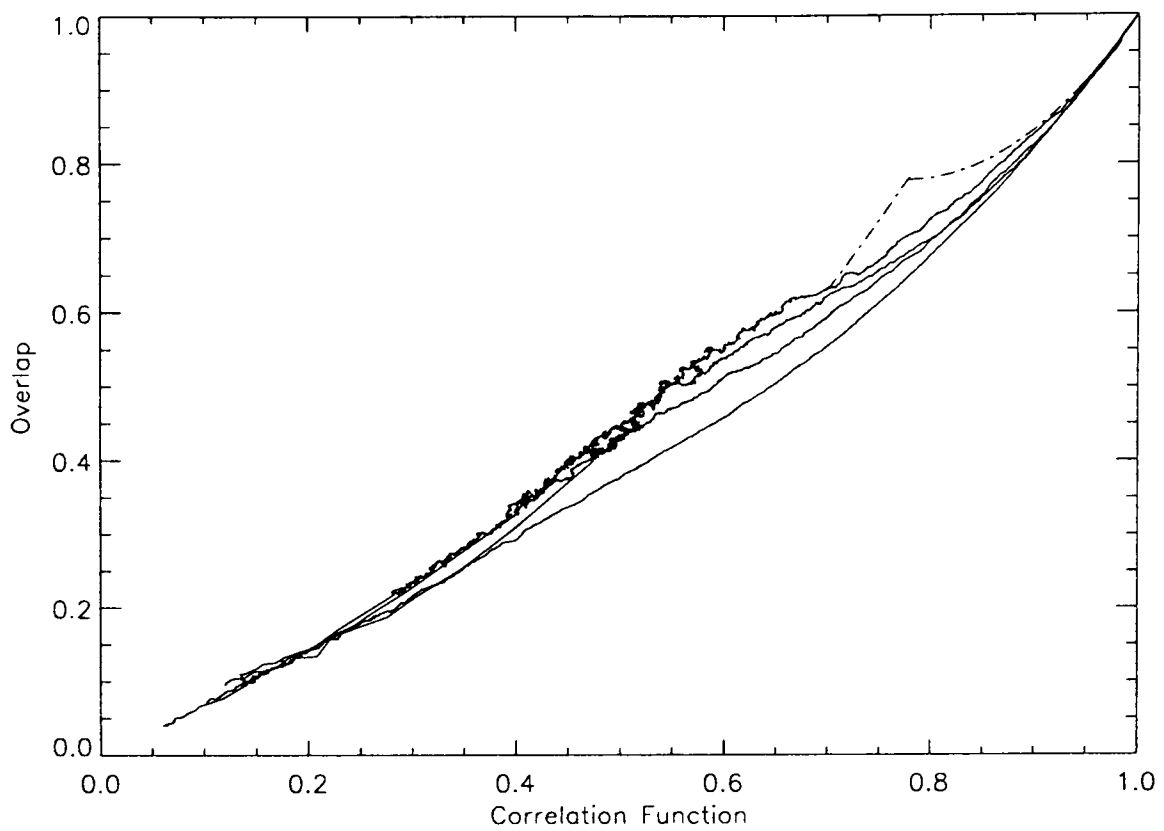

Figure 3.18: $Q_{t_w}(t+t_w)$ against $C(t+t_w, t_w)$ for $\beta = 4$. From lower to upper curve, $t_w = 10N, 10^2N, 10^3N, 10^4N$. The dotted curve is that of expected behaviour for $Q(t)$ against $C(t)$ in equilibrium, shown only for $C(t) > 0.7$.

Figure 3.17 shows parametric plots of the overlap $Q(t)$ against the correlation function $C(t)$ (in equilibrium) for different values of β. These plots should be 'read' from the top right corner i.e. $t = 0$ occurs when $Q(t) = C(t) = 1$, and long times correspond to low values of $Q(t), C(t)$. We have plotted on each the expected short time and long time behaviour as given in Equations (3.2.12) and (3.2.13), where the values of α are those fitted in the previous section. One sees that the short time expression fits the data extremely well, supporting our hypothesis that the initial decay of the correlator, from 1 down to the plateau, is exponential. The longer time behaviour initially fits very well for both $\beta = 4$ and 5 (Figures 3.17(a), 3.17(b)), although as time goes on the theoretical curve drops below the data. This tends to suggest that at long time-scales there is some correction to this fitted form which we have not taken into account; the second relaxation may be some kind of modified exponential rather than pure exponential. For the case of $\beta = 3$ (Figure 3.17(c)) the values of τ_1, τ_2 are much closer together and thus the two time-scales are not so well separated. Therefore one does not see a well-defined plateau in the equilibrium correlation function (see Figure 3.11(a)), and the cusp in this parametric plot is also not as clear. The cusp in these plots is a direct result of the existence of the plateau; since $Q(t) = C(2t)$ in equilibrium, the overlap function $Q(t)$ reaches the plateau before the correlator $C(t)$. Thus there is a time period for which $Q(t)$ is effectively stationary whilst $C(t)$ is still dropping fast. This is followed by a time period for which the plateaux in both functions overlap, and therefore both are stationary,

and then there is a regime in which $Q(t)$ drops away from the plateau whilst $C(t)$ is still stationary. This tells us that whilst the dominant process is diffusion of the dimers, the two copies of the system are restricted to a narrow area of phase space; this is because the isolated defects have not yet moved in either copy, and thus the overlap will be high. It is only once the activated processes become dominant that the two copies can move well apart from each other.

Figure 3.18 shows a parametric plot of the overlap against the correlator for the non-equilibrium case i.e. $Q_{t_w}(t)$ against $C(t + t_w, t_w)$. The initial behaviour is independent of t_w and in fact follows the short time behaviour we both expect and observe in equilibrium. However, as $C(t + t_w, t_w)$ drops below 0.9, the curves fall below the equilibrium behaviour and we see evidence of dependence on t_w. The cusp that develops is sharper for larger t_w, with the behaviour tending towards that of equilibrium. For the smaller values of t_w there is no channeling in phase space because the starting configuration is well away from equilibrium, and thus there are many different energetically favourable routes to be taken. It is clear from these figures that our model falls into the class of Type II, as the overlap decays to zero rather than a finite value as it would do for Type I systems; this is as expected as we believe our model to be glassy rather than dominated by coarsening.

3.2.4 Discussion: The Form of $E(t)$

In order to have some intuition as to exactly how we expect the energy density to behave over time, we must have some understanding of the class of problems this model falls into. We can easily break down the processes into a list of the available moves; these are shown below, written in the form $\{s_y, s_w; s_v, s_x\} \longmapsto \{s_y - 1, s_w - 1; s_v + 1, s_x + 1\}$ where we will not bother to list pairs such as $\{+1, +1; -1, 0\}$ and $\{+1, +1; 0, -1\}$ separately as they involve the same energy change:

1. $\{+1, +1; -1, -1\} \rightarrow \{0, 0; 0, 0\}$, $\Delta E = -4$
2. $\{+1, +1; -1, 0\} \rightarrow \{0, 0; 0, +1\}$, $\Delta E = -2$
3. $\{+1, 0; -1, -1\} \rightarrow \{0, -1; 0, 0\}$, $\Delta E = -2$
4. $\{+1, 0; -1, 0\} \rightarrow \{0, -1; 0, +1\}$, $\Delta E = 0$
5. $\{+1, +1; 0, 0\} \rightarrow \{0, 0; +1, +1\}$, $\Delta E = 0$
6. $\{0, 0; -1, -1\} \rightarrow \{-1, -1; 0, 0\}$, $\Delta E = 0$
7. $\{+1, 0; 0, 0\} \rightarrow \{0, -1; +1, +1\}$, $\Delta E = +2$
8. $\{0, 0; -1, 0\} \rightarrow \{-1, -1; 0, +1\}$, $\Delta E = +2$
9. $\{0, 0; 0, 0\} \rightarrow \{+1, +1; -1, -1\}$, $\Delta E = +4$

First, let us consider the initial temperature-independent energy decay, so we shall ignore moves 7–9 as they increase energy and are very unlikely at this stage. Moves 5 and 6 do not reduce the energy, and the defects concerned remain localised even after these moves, so we shall not consider them explicitly at this stage; move 4 on the other hand is the mechanism by which free diffusion of dimers takes place. With regards to energy-reducing processes, if move 1 dominates, perhaps we can

describe this model as an annihilation-diffusion process of the form $A + B \rightarrow \emptyset$, in which A and B are two conjugate dimers which diffuse quasi-isotropically throughout the system[2], as shown in Figure 3.4(a). This would lead us to expect the initial part of the energy decay to behave as $t^{-0.5}$ (see Section 1.3.2). However, if moves 2 and 3 dominate, the picture will be very different; thus it is imperative that we identify which move-sets dominate in the early stages of the energy decay.

To this end we ran the system at $T = 0$, starting from an infinite temperature configuration, and noted the number of accepted moves involving $\Delta E \in \{0, -2, -4\}$ taking place over each time interval of $1N$; the results are shown in Figure 3.19(a). Note that as this simulation was performed at $T = 0$ no positive energy moves were allowed. Without a doubt, the moves involving an energy reduction of 2 units are far more prevalent than those involving an energy reduction of 4 units, even for short time-scales, as Figure 3.19(b) emphasises. The reason for the low frequency of $\Delta E = -4$ events is that for in order for them to happen, two conjugate dimers must meet each other with exactly the right orientation — given that there are 3 different orientations of dimers, and those dimers can be $\{+1, -1\}$ or $\{-1, +1\}$, it becomes improbable that many meeting of dimers will lead to an allowed move and an energy reduction.

In that case one might view the system as a member of the class of $A + B \rightarrow B$, where A is a dimer and B is a lone defect, or alternatively one might find that the dimer concept is not useful to formulate the system in terms of annihilation-diffusion models, and that a three particle interaction of the form $A + A + B \rightarrow B$ is needed, where A and B are defects of opposite sign.

Given that the $\Delta E = -4$ are much less prevalent in comparison to the $\Delta E = -2$ moves, we shall ignore these and concentrate on formulating a (simplified) description of the behaviour with $\Delta E = -2$ moves only. We can reduce moves 2 and 3 to a three-particle interaction by ignoring the zero-spin on the left-hand side — it is valid to do so as before too long it becomes overwhelmingly probable that the fourth spin will be zero in any case. Thus we can classify these moves as:

$$\left.\begin{array}{l} A + A + B \rightarrow A \\ A + B + B \rightarrow B \end{array}\right\} \qquad (3.2.14)$$

where A and B are defects of opposite sign. As we know, the A's and B's cannot actually diffuse freely, but instead must do so in an AB pair (i.e. as a dimer). However, in the early stages of the energy decay subsequent to a quench from infinite temperature, almost all defects should effectively be mobile, as they are likely to have at least one neighbour of the opposite sign. In addition, defects do not stay fixed within a dimer pair, but can 'switch partners' so the A's and B's effectively diffuse by themselves, although the actual movement has to be facilitated by a partner of the opposite sign. At all times the concentration of A's and B's are equal as we have the restriction that $\sum_{i=1}^{N} s_i = 0$, a detail which reduces the reaction

[2] The term quasi-isotropically is used because dimer diffusion in fact involves zig-zags at 30° to the axis perpendicular to the common edge between the two cells constituting the dimer.

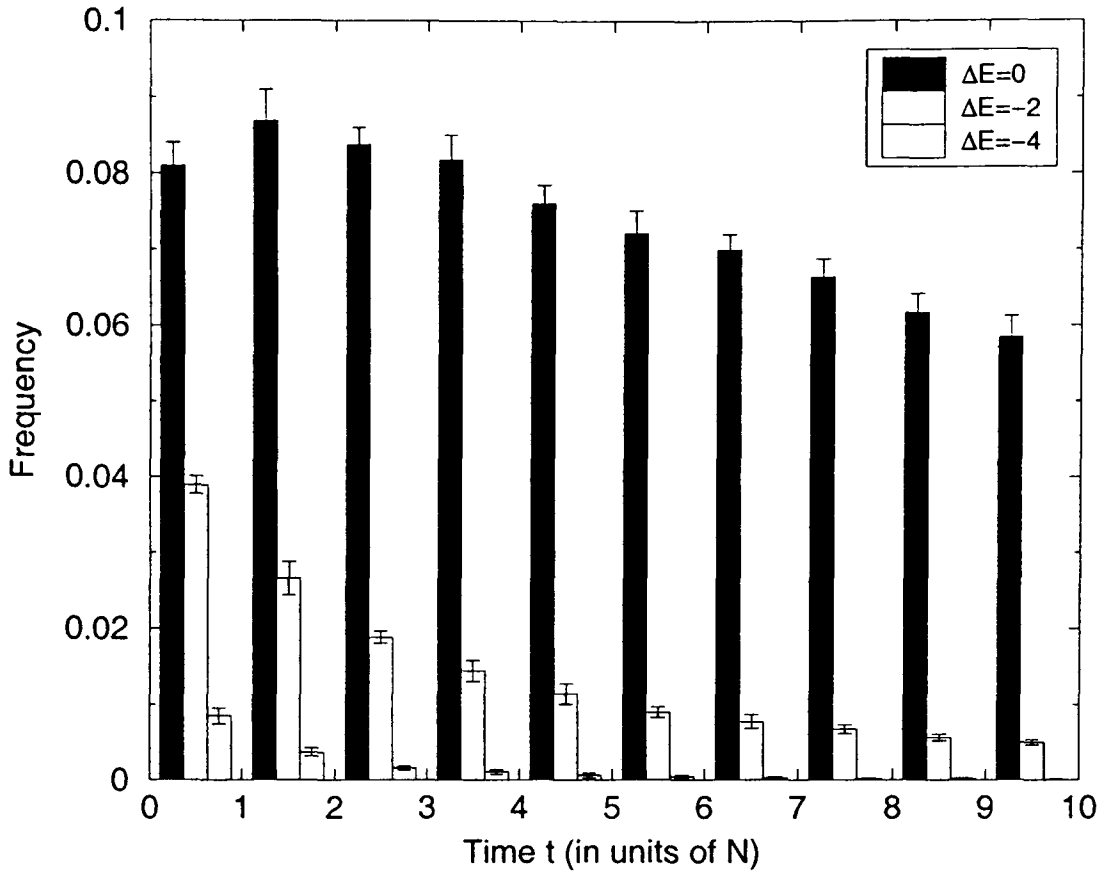

(a) The frequency of accepted moves involving $\Delta E \in \{-4, -2, 0\}$, measured over time-intervals of $t = 1N$.

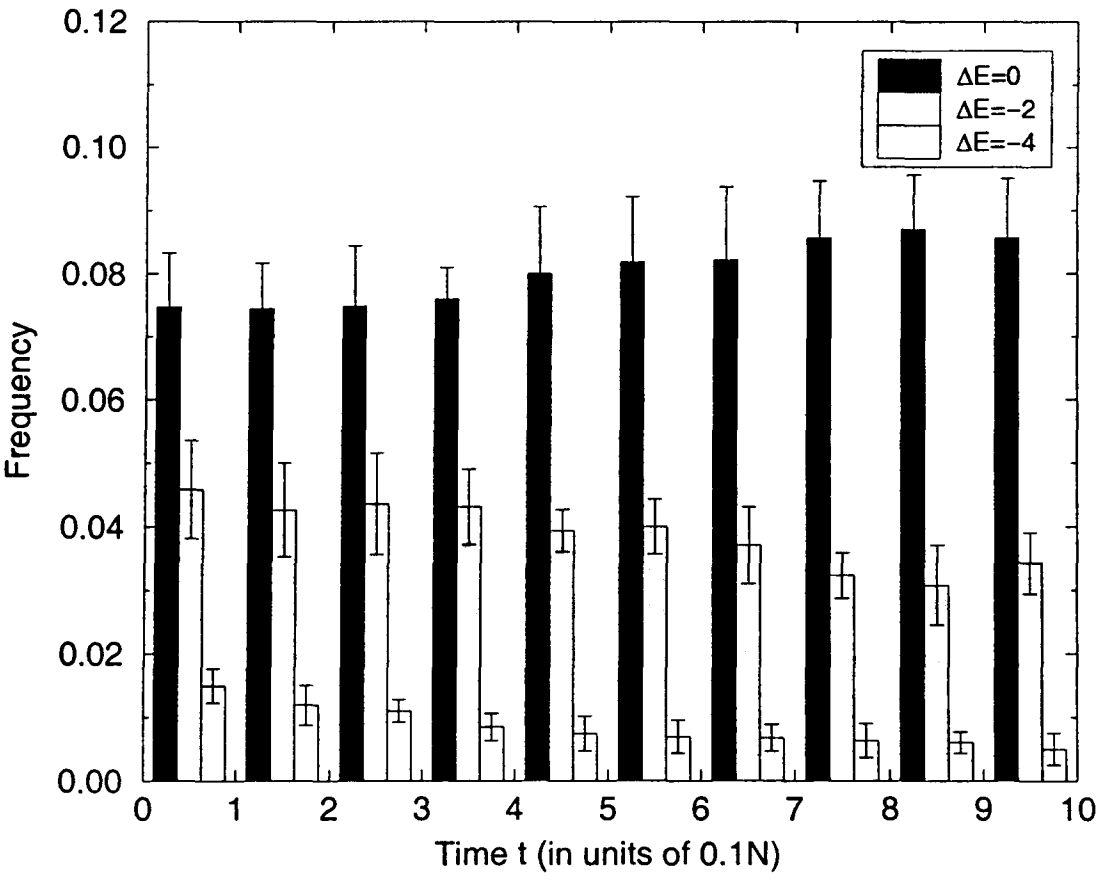

(b) The frequency of accepted moves involving $\Delta E \in \{-4, -2, 0\}$, measured over time-intervals of $t = 0.1N$.

Figure 3.19: Comparative rates for moves involving $\Delta E \in \{-4, -2, 0\}$ at $T = 0$.

schemes of Equation (3.2.14) to $A+A+A \to A$. As described in Section 1.3.4, this behaves like $A + A + A \to \emptyset$, with only a change in amplitude; if this is indeed the correct description we would expect the first decay of the energy density to behave as $t^{-1/2}$. This is a mean-field result as the critical dimension is 1, thus we can test this hypothesis in 2d, as we shall do shortly, but also in 3d, which we shall do in the next chapter.

The slow, temperature-dependent decay is due to isolated defects and clusters of like defects slowly pairing with defects of opposite sign to make a dimer which is then absorbed/annihilated; the defects can only move by creating/absorbing a dimer, both of which happen over a time-scale of $e^{2\beta}$. This time-scale is considerably longer than the subsequent absorption/annihilation and thus we need only consider the pairing. This can be classed as an $A + B \to \emptyset$ process (see Section 1.3.2), for which the standard asymptotic behaviour is $t^{-d/4}$, where d is the dimensionality. Therefore we suggest the same asymptotic $(t/\tau)^{-0.5}$ behaviour for both the slow and the fast process, and fit the following form to the energy density:

$$\frac{E(t)}{N} = \left(\frac{2}{3} - a\right)\left(1 + \frac{t}{2}\right)^{-b} + (a - e_{eq})\left(1 + \frac{t}{e^{2\beta}}\right)^{-c} + e_{eq} \qquad (3.2.15)$$

where a is the plateau value, e_{eq} is the energy per spin in equilibrium, and we expect both b and c to be approximately 0.5. The results are shown in Figure 3.20; it is clear that these fits are good. One can also fit with free parameters multiplying t in each power law, but one obtains results of almost exactly $1/2$ and $e^{-2\beta}$ in any case, and therefore we fix them both; further investigation of the characteristic time-scales has already been given in connection with the correlation function. Note that we do not attempt to fit the data very close to equilibrium, as the description we wish to test applies only to the non-equilibrium regime. We see that the exponent of the first power law, b, does indeed result in a value very close to 0.5, as predicted, which lends support to our hypothesis that this part of the decay can be described by an $A + A + A \to A$ reaction scheme. We note only that, as required, a is less than $\frac{2}{9}$, which is the maximum energy for a $T = 0$ frozen state (see Figure 3.21).

The exponent of the second power law is less conclusive, as the decay is somewhat slower than the predicted exponent of $c = 0.5$. One reason for this may be the clusters of like defects, identified in Figure 3.8), which are considerably more difficult to shift than lone defects. It is difficult to quantify exactly how this effect will modify the expected behaviour, but it is clear that persistent clusters will indeed slow down the energy decay: if defects cluster in like-groups, then in general a defect will have to travel further to find one of an opposite sign with which to pair. This distance will be dependent on the energy density, but not linearly since a cluster will not in general still remain after the removal of one defect. Therefore we understand the origin of this slower-than-anticipated second decay, but are unable to comment any further.

To summarise our findings so far, we have shown that the $D > 0$ model does indeed give results that are quantitatively similar to those of the topological model for

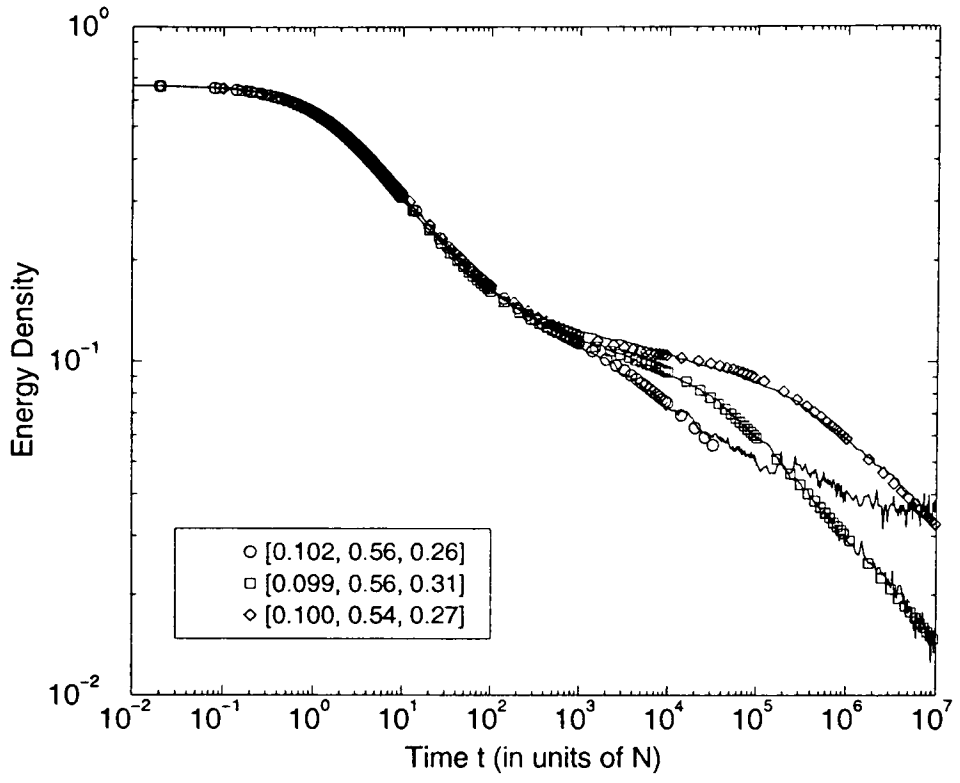

Figure 3.20: The energy for $\beta = 4, 5$ and 6 fitted with Equation (3.2.15), using the values shown in the key.

the energy, correlation and response functions, whilst having the advantage of being simpler, computationally faster and more suited to analytic study. The conceptual picture of fast and slow dynamics developed in relation to the topological froth model has been extended in this case, and many of the features of this model can be described in terms of this picture. We find good agreement between theoretical predictions and data for the behaviour of the correlation function, overlap function

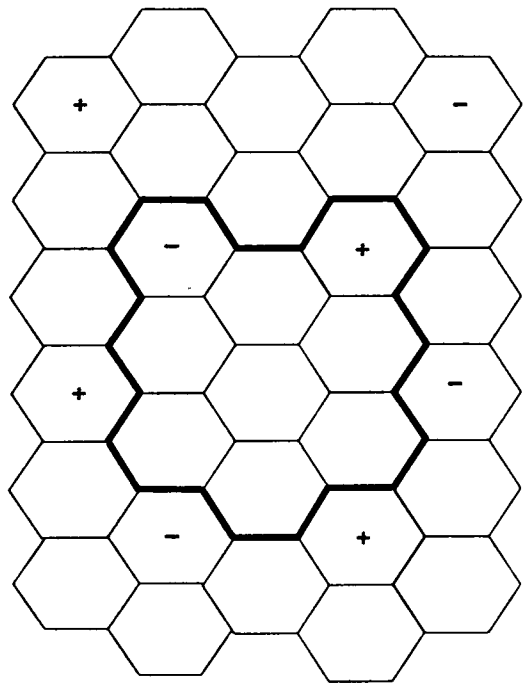

Figure 3.21: The highest energy $T = 0$ frozen configuration. This can be formed by tiling the configuration-space with the 9-cell unit heavily outlined, so the energy of this configuration is 2/9.

and energy; in particular, the initial decay of the energy density is appropriate to $A + A + A \rightarrow \emptyset$ processes occurring on a fast time-scale, and the data is not in disagreement with the hypothesis of $A + B \rightarrow \emptyset$ processes occurring on the slow, temperature-dependent time-scale, although further study is needed on this point.

3.3 $D < 0$

3.3.1 Relaxation dynamics and correlation functions

We shall now turn our attention to the model with $D < 0$, setting $D = -1$. Unlike the previous case, this model does not have a unique absorbing ground state; instead, there are a great many degenerate ground states, although some of these are not accessible using our dynamical rules. This raises the possibility that in preparing an 'equilibrium' system by randomly placing throughout the lattice the correct number of ± 1's for that temperature, one might pick out a configuration that is inaccessible from any other state under these dynamics. However, the probability of this occurring is so small as to be negligible, and we have checked that the results obtained by this method do not differ from those obtained through waiting long enough for equilibration to occur. Thus when we refer to an equilibrated system, we mean one that has been prepared through a random allocation of the correct number of non-zero spins.

We expect the $D < 0$ model to also show glassy behaviour with two different time-scales, but as the system now favours $s_i = \pm 1$ rather than $s_i = 0$, the equivalent of the free-moving dimers will be fast-moving pairs of spin zero, and the analogue of the slow-moving energetically-trapped defects will be isolated zero-spins (we no longer have an equivalent of the like-pairs of $D > 0$, as a like-pair in this case is a dimer and is free to diffuse). With the correct choice of observables, one expects to see all the same features as with the $D > 0$ model. However, although one expects similar qualitative behaviour,[3] the quantitative behaviour should be different, both because we only have one type of defect present in this model (zero-spins only rather than ± 1's) and because the zero-spin dimers cannot move quite so easily through the disordered ± 1 background. As shown earlier in Figure 3.13, there are certain configurations that simply cannot move.

Simulations were again performed for $N = 9900$. Figure 3.22(a) confirms that we do see glassy behaviour when the system is cooled at different cooling rates. A plot of the energies attained after running for a variety of times t_w at various temperatures T from a starting configuration corresponding to infinite temperature are shown in Figure 3.22(b); the presence of activated processes is indicated by the clear minima and by the plateau at $\frac{E}{N} \sim -0.94$ below which the system cannot penetrate at low temperatures, even after the longest waiting times. Again one can see this plateau clearly in a plot of energy against time subsequent to a quench from infinite temperature (see Figure 3.23(a)); upon re-scaling the time axis to $T \ln t$ we

[3] except in pathological cases

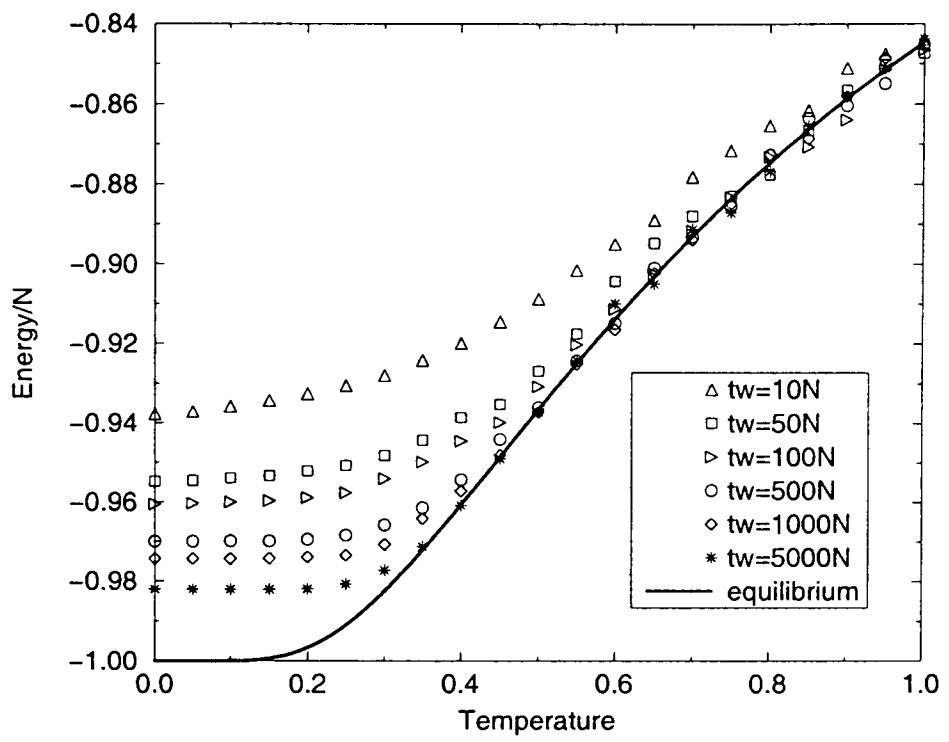

(a) The behaviour of the energy under cooling ($D < 0$). The values of t_w are the waiting times at each point.

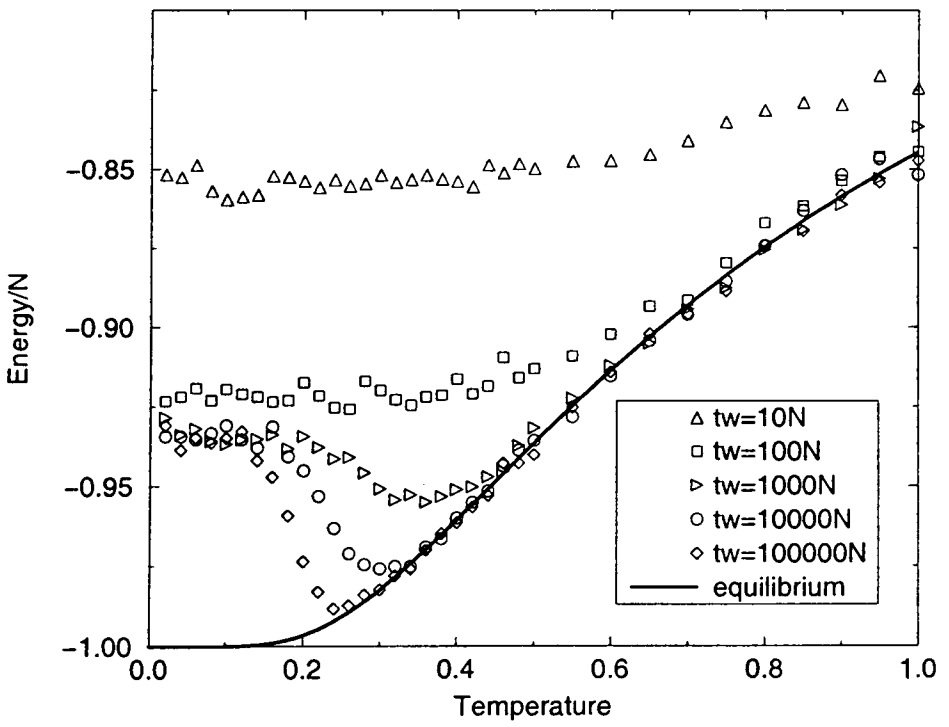

(b) The behaviour of the energy after a rapid quench ($D < 0$). The values of t_w are the times, subsequent to the quench, at which the energy is measured.

Figure 3.22: Energy against temperature for slow cooling and rapid quench.

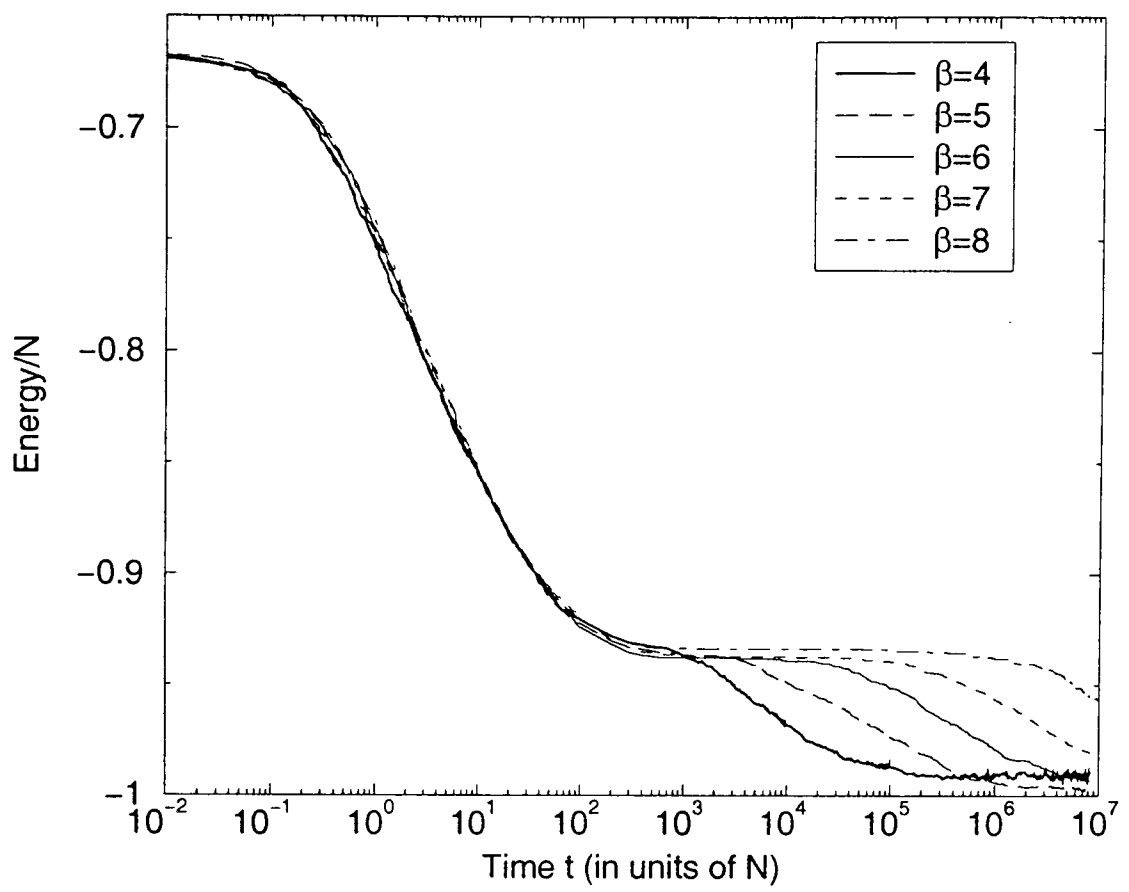

(a) Energy against time.

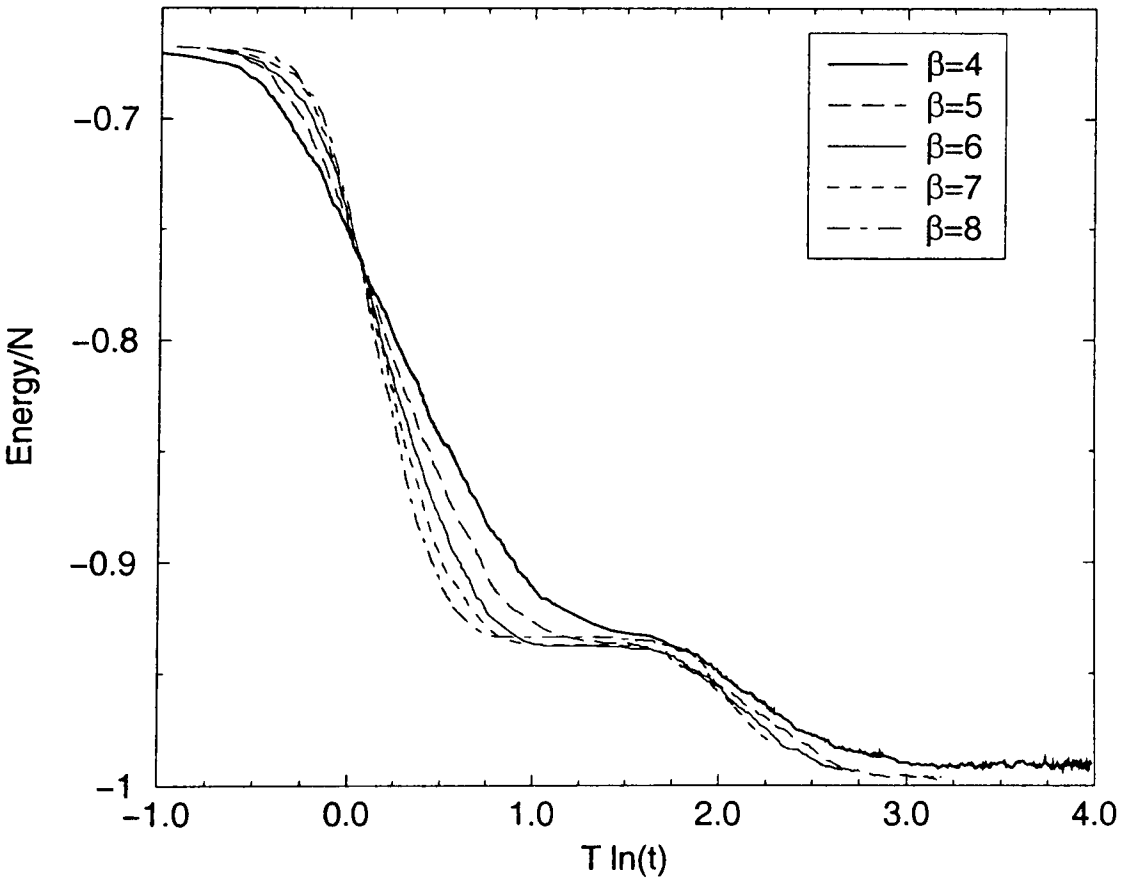

(b) Energy against $T \ln t$, where t is measured in units of N.

Figure 3.23: The behaviour of the energy with time.

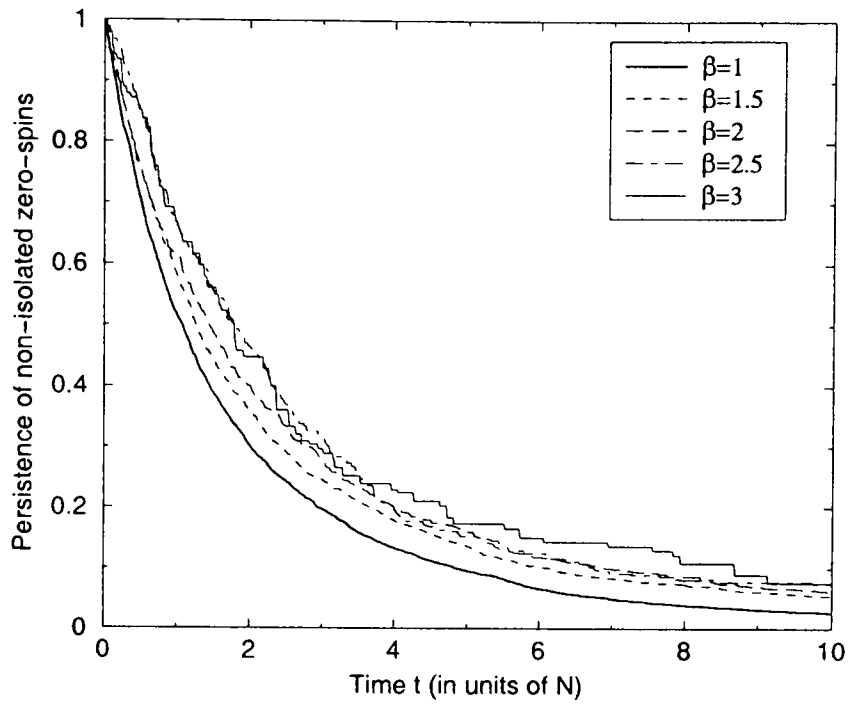

(a) The persistence of non-isolated zero-spins for $D < 0$.

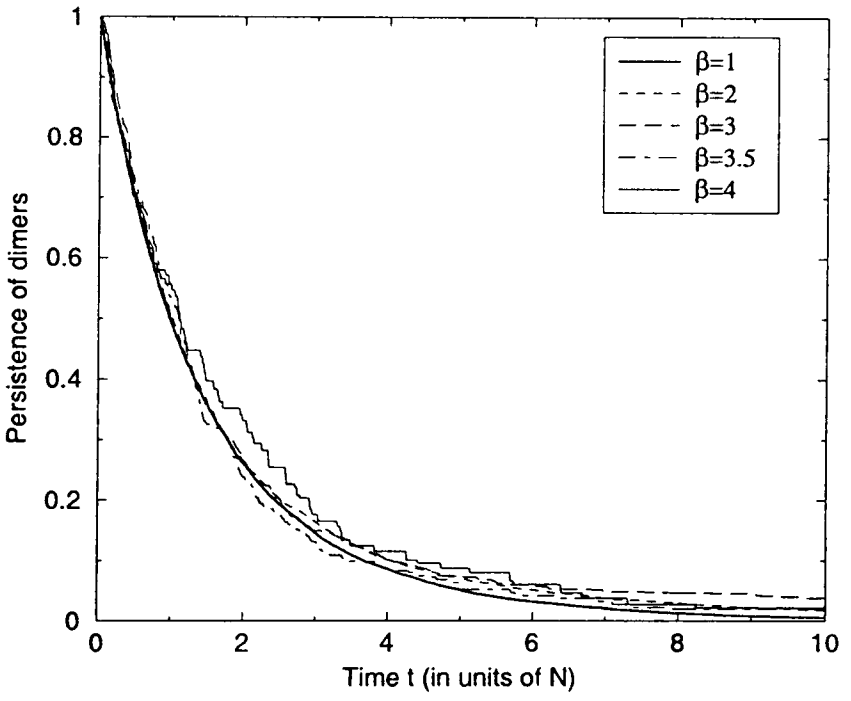

(b) The persistence of non-zero spins with at least one opposite neighbour for $D > 0$.

Figure 3.24: Persistence functions for both $D < 0$ and $D > 0$.

see the staircase shape appear (Figure 3.23(b)).

Because the background does not necessarily allow the dimers to move freely, one must consider the possibility that the dimer diffusion may be dependent upon the density of non-zero spins. In equilibrium, this density is dependent upon the temperature; therefore we have investigated the persistence of non-isolated zero-spins under equilibrium conditions. In order to do this, one can identify all zero-spins that

have at least one neighbouring spin which is also zero in the starting equilibrium configuration; as the system evolves, one can measure the fraction of these that have *not* been involved in a move. Figure 3.24(a) shows these results for $D < 0$; one can see that the persistence is weakly temperature-dependent. One cannot sensibly investigate the effect at lower temperatures because there are so few zero-spins present in equilibrium conditions. For comparison, we also show the results for the $D > 0$ model, where the persistence is defined as the fraction of non-zero spins with at least one neighbour of the opposite sign that have NOT undergone a move. The results are shown in Figure 3.24(b) and show no temperature-dependence. This result has implications for the form of both the correlation function and the energy.

In order to produce a fit for the energy relaxation from a starting configuration corresponding to infinite temperature, one must think very clearly about the processes involved. We shall assume that, as in the $D > 0$ case, $\Delta E = -4$ moves occur extremely rarely and thus can be neglected. In that case the dominant energy-reducing process in the early stages of the energy decay will be that of three zero-spins interacting with a ± 1, resulting in an energy reduction of 2 units. We can classify this under the reaction scheme $A + A + A \rightarrow A$, and hence, as in the $D > 0$ case, we expect an asymptotic behaviour of $(1 + m_1 t)^{-0.5}$ (assuming that the density-dependence of the dimer diffusion has little influence at this point). For the slow decay from the plateau to equilibrium, the density-dependence of the dimer diffusion will have a substantial effect because there are far more ± 1 spins present as the system flows closer to equilibrium. This slow process involves the pairing of isolated zero-spins through the mechanism of dimer creation and absorption; this can be classified as an $A + A \rightarrow \emptyset$ process, but it is unlikely to behave exactly as such given that the dimers cannot diffuse freely to facilitate it[4]. One can fit this latter part to the energy density separately, and one finds it takes the form $a_1(1 + te^{-2\beta})^{-\kappa}$; the factor of two in the exponential was fitted as a free parameter and a result of almost exactly 2 was obtained for every temperature. This is in keeping with the energy barrier of 2 involved in creating a dimer. The parameter a_1 is naturally associated with the plateau value and clearly takes a value ~ -0.94. The value of κ is approximately 0.6; this is substantially slower than the behaviour one would find asymptotically with a pure $A + A \rightarrow \emptyset$ process and is due to the inhibited movement of the dimers.

Having fitted the latter part, we attempted a fit of the full dataset of the form:

$$\frac{E}{N} = \left(-\frac{2}{3} - a_1\right)(1 + m_1 t)^{-\kappa_1} + a_1\left(1 + te^{-2\beta}\right)^{-\kappa_2} \qquad (3.3.1)$$

where a_1, m_1, κ_1 and κ_2 are all parameters to be determined. This fits the data very well in all regions except during the final approach to the intermediate plateau, where the energy relaxes faster than the fits we have obtained. We shall discuss the reasons for this shortly, but will focus on the values of the fitting parameters for the

[4]Note that in this case we do not have cluster of like defects, as was found in the $D > 0$ case, because we now only have one type of defect, the zero-spin, and any two zero-spins can partner up and diffuse as a dimer.

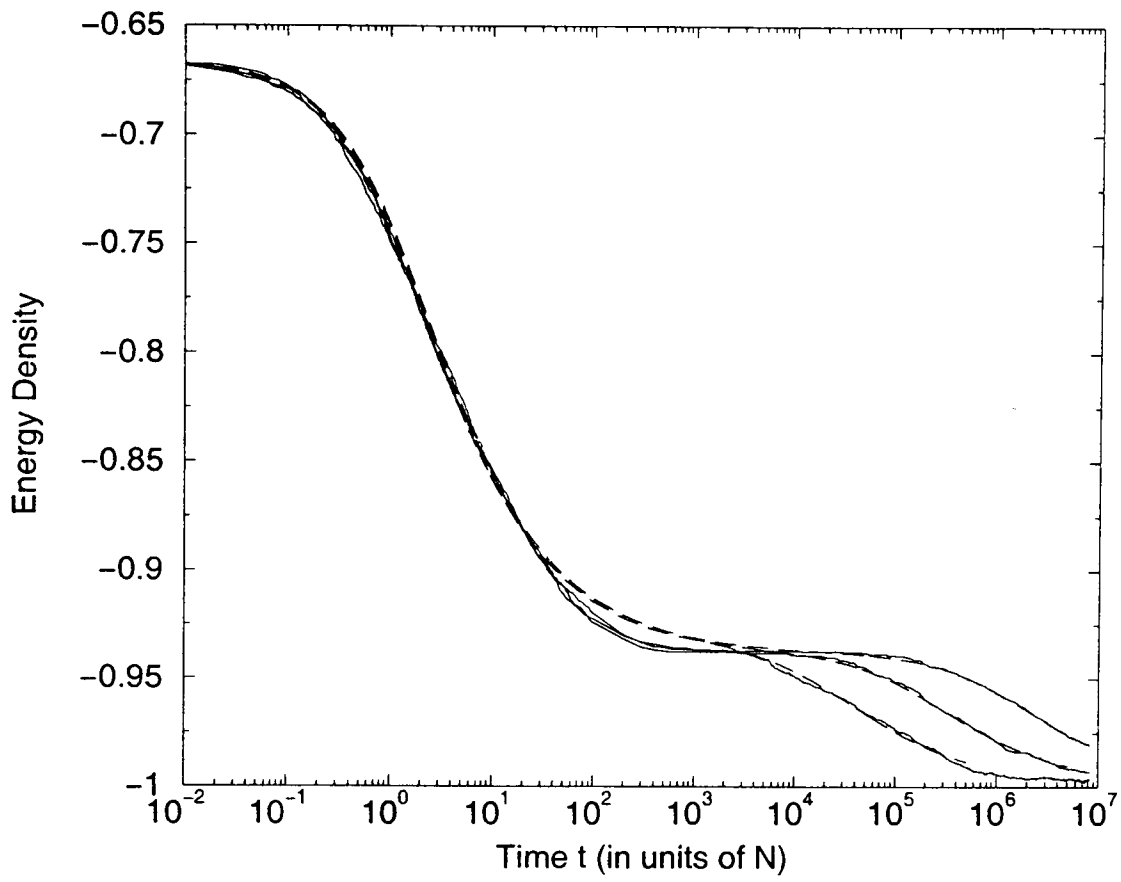

Figure 3.25: The energy density for, from left to right, $\beta = 5, 6, 7$ (solid lines). The dashed lines are fits of the form of Equation (3.3.1). The parameters $[a_1, m_1, \kappa_1, \kappa_2]$ are, for $\beta = 5, 6, 7$ respectively: $[-0.94, 0.87, 0.54, 0.54]$, $[-0.94, 0.80, 0.55, 0.54]$ and $[-0.94, 0.81, 0.53, 0.57]$.

moment. As expected, κ_1 is very close to 0.5, further reinforcing the $A+A+A \rightarrow A$ hypothesis (where each A particle is a zero-spin defect). The parameter m_1 should be of the order of 1, but without a rigorous theory one cannot say much more than that, and thus the observed value of ~ 0.8 is satisfactory. With regard to κ_2, fitting the full dataset gives results of ~ 0.55 rather than 1.0; as previously mentioned, we believe this slowing-down to be due to the disordered background hindering the movement of the dimers.

Returning now to the poor fit close to the plateau, we must look closely at the assumptions made in our $A + A + A \rightarrow A$ classification. In ascribing an asymptotic behaviour of $t^{-0.5}$ we are implicitly assuming that all A particles may diffuse and are not trapped (although we are aware that the diffusion is 'facilitated', in that each A may only diffuse in tandem with another A). For very short times (i.e. $t < 1N$) this is certainly a valid assumption; however, it may not be quite correct at longer times. Then, as the system evolves towards more and more ± 1's and fewer zero-spins, it becomes likely that some zero-spins may become completely trapped. It also becomes more likely that the defects within a dimer pair will stick with their partner. In that case, the system may tend to behave in a manner appropriate to dimer absorption by static traps; in the reaction-diffusion scheme formalism, this would be $A + B \rightarrow B$, where the B's are fixed, unmoving zero-spins and the A's are diffusing dimers. This implies a crossover from the $t^{-0.5}$ behaviour towards a

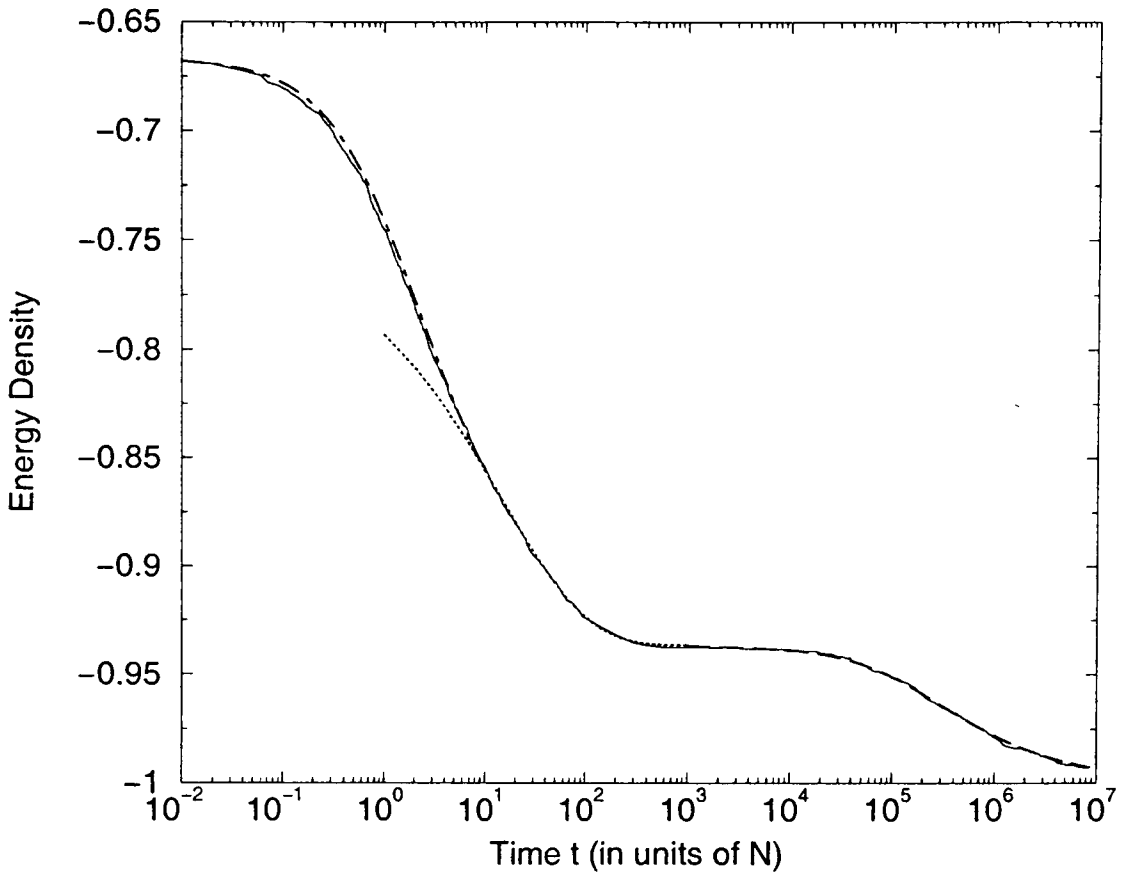

Figure 3.26: The energy density for $\beta = 6$ fitted in three separate sections. The first part (up to $t = 10N$) is a power law of the form $(1 + 0.8t)^{-0.54}$ (dot-dashed line). The second part ($10N < t < 10^3 N$) is stretched exponential behaviour of the form $e^{-(0.07t)^{0.501}}$ (dotted line). The final part ($t > 10^3$) is a power law of the form $(1 + te^{-2\beta})^{-0.54}$ (dashed line).

stretched exponential form (see Section 1.3.3), which could be responsible for the poor fit in the latter stages of the initial temperature-independent decay of the energy. If we try to fit the energy density in three separate sections, as shown in Figure 3.26, we see that there is clear evidence for stretched exponential behaviour, with the power within the exponent almost exactly 0.5, which is the theoretically predicted value for two-dimensional systems displaying this behaviour.

The reader will have realised that the argument leading to the investigation of this stretched exponential behaviour also applies in the $D > 0$ case. However, in that case the background is not disordered and thus it is less likely that defects will become completely stuck such that they can be described as static traps — hence this behaviour does not dominate for any region and can be neglected to a first approximation.

With regards to the correlation function, in order to study the $D > 0$ model we chose a function which focussed on the defects. We do the same in this case, and thus the correlation function we measure is:

$$C(t + t_w, t_w) = \frac{1}{1 - p_{eq}(0)} \left(\frac{\sum_{i=1}^{N} \delta_{s(t_w),0} \delta_{s(t+t_w),0}}{\sum_{i=1}^{N} \delta_{s(t_w),0}} - p_{eq}(0) \right) \qquad (3.3.2)$$

where $p_{eq}(0)$ is the equilibrium density of zero spins at the temperature of interest.

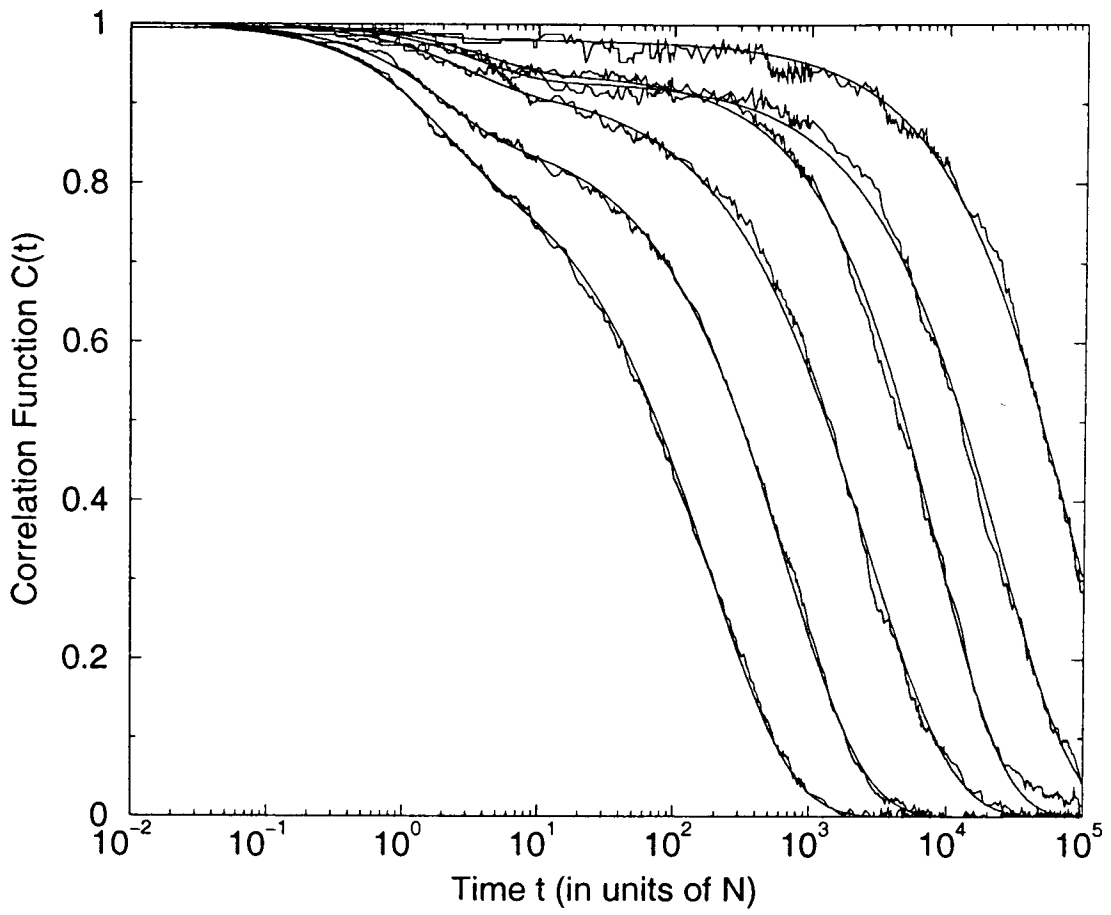

Figure 3.27: Correlation functions in equilibrium conditions. From left to right, $\beta = 2.5, 3, 3.5, 4, 4.5, 5$. The superimposed fits are of the form: $C(t) = \alpha\, \mathrm{e}^{-t/\tau_1} + (1-\alpha)\, \mathrm{e}^{-(t/\tau_2)^\gamma}$.

This form may look somewhat unusual at first glance but the reader will notice that in equilibrium conditions this is the connected correlation function, normalised to run between 0 and 1; we shall only be considering the equilibrium correlation functions for this model. Figure 3.27 shows that this function does indeed produce similar results to those of the $D > 0$ model: again, we can see clear evidence of two-step relaxation. The fits superimposed upon the data are of the following form:

$$C(t) = \alpha\, \mathrm{e}^{-t/\tau_1} + (1-\alpha)\, \mathrm{e}^{-(t/\tau_2)^\gamma} \tag{3.3.3}$$

It will be noted that these fits are extremely good, and also that the relaxation in the long-time region follows a stretched exponential rather than an exponential as in the $D > 0$ case. Debye relaxation (conventional pure exponential decay) is associated with a single relevant relaxation time τ, such that one can write for a relaxing quantity $c(t)$:

$$c(t) = c_0 \mathrm{e}^{-t/\tau}.$$

If instead one has a range of relaxation times then one might naturally write:

$$c(t) = \int_0^\infty w(\tau)\, \mathrm{e}^{-t/\tau} d\tau$$

and thus one can explain an observed behaviour of $c(t)$ by a suitable choice of $w(\tau)$.

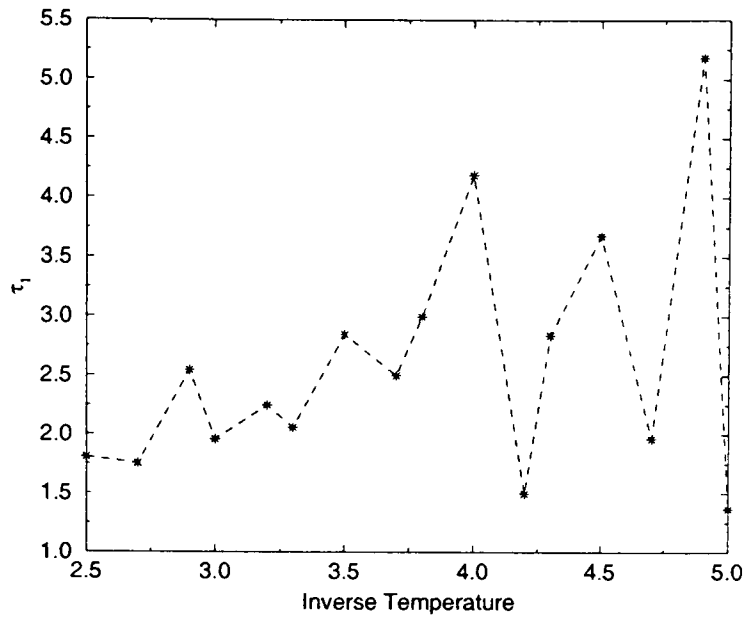

(a) τ_1 against inverse temperature

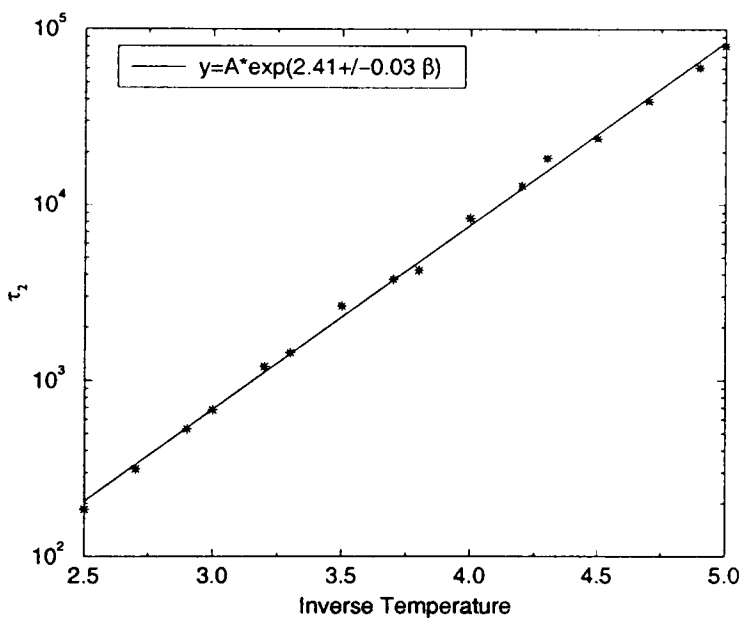

(b) τ_2 against inverse temperature

Figure 3.28: The behaviour of the fitting parameters α, τ_1, τ_2 and γ with temperature. The data was obtained by fitting the form $C(t) = \alpha\, e^{-t/\tau_1} + (1 - \alpha)\, e^{-(t/\tau_2)^\gamma}$ to the equilibrium correlation functions.

In particular, Palmer et al [69] observed in 1984 that a stretched exponential form can be obtained from a picture of 'hierarchically constrained' dynamics, in which different degrees of freedom relax on different time-scales, but *sequentially*. For example, one might consider an atomic model in which certain clusters of atoms may only move once other, faster, atoms have moved in just the right manner to give the cluster freedom to relax, which might then in turn free other atoms to move, and so forth. With the disordered ±1 background of this model, it is easy to imagine that many defects are jammed, and unable to move in any way until certain move-sets or combination of move-sets have occurred in order to 'unjam' them. From

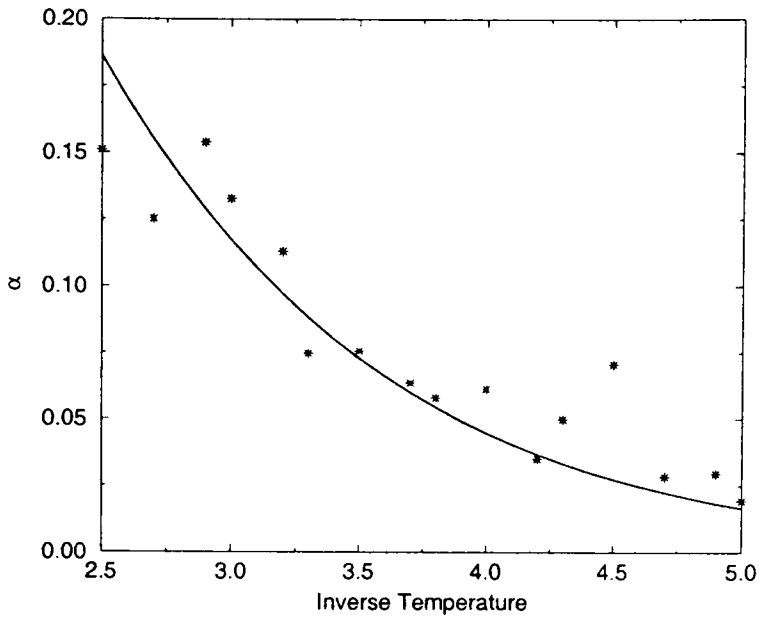

(c) α against inverse temperature; the superimposed line is $y = \frac{12e^{\beta}}{(1+2e^{\beta})^2} - \frac{e^{-\beta}}{2}$

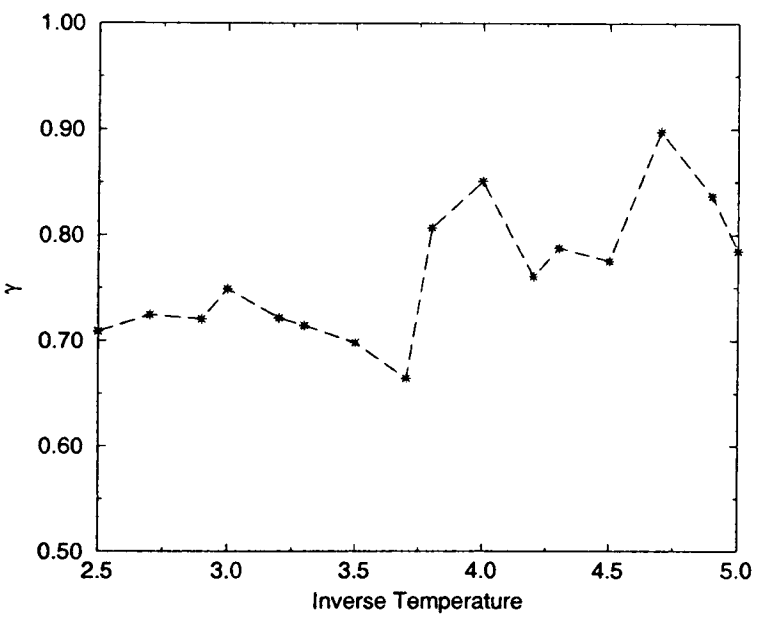

(d) γ against inverse temperature

these arguments one expects that the exponent γ (shown in Figure 3.28(d)) should be less than one in all cases, but we do not have a full theory of the behaviour and therefore cannot comment further.

One might naïvely expect the predicted value of τ_1 to be altered by the fact that the zero-spin dimers are not necessarily free to move through the ± 1 background. In fact this is not the case: τ_1 is the time-scale for the dimers that are *free to move* only, and we can still expect those free dimers to move with a time-scale of 2, independent of temperature, exactly as in the $D > 0$ case. Figure 3.28(a) shows the values of τ_1 against inverse temperature obtained from fitting the correlation functions with Equation (3.3.3) — this data is in keeping with a temperature-

independent value of $\tau_1 = 2$. Those dimers that are not free to move do not contribute to the initial fast decay of the correlation function. The parameter that the extra jamming *does* alter is α: one expects the correlation function to decay to a plateau value which is one minus the density of free zero-spins (although one must remember to normalise correctly as in Equation (3.3.2)). Thus we have to calculate the probability of obtaining a zero-spin dimer which can move (shown in Figure 3.4(c), but one should now think of the ±1's as being the background and the zero-spins as being the dimer), and also of obtaining a zero-spin pair which can oscillate (as in Figure 3.7). This gives a probability of $24p(0)p(1)^2$; thus after normalisation, we expect α to behave as:

$$\alpha = \frac{12e^{\beta}}{(1+2e^{\beta})^2} - \frac{e^{-\beta}}{2} \tag{3.3.4}$$

Figure 3.28(c) shows this curve superimposed upon the fitted values of α against temperature; the data shows reasonable agreement with the theory.

One can see from Figure 3.28(b) that we again observe Arrhenius behaviour for τ_2. In this case, however, the best-fit Arrhenius law is $\tau_2 \sim e^{2.4\beta}$, whereas the energy barrier argument would suggest $\tau_2 \sim e^{2\beta}$. As mentioned earlier, we lack a full understanding of the behaviour in this region, and can only say that this discrepancy is probably also due to the fact that the ±1 background does not allow the zero-spin dimers to diffuse freely.

3.3.2 Overlap functions

We continue our study of the $D < 0$ model by turning now to the overlap function, defined in this case as:

$$Q_{t_w}(t) = \frac{\sum_{i=1}^{N} \delta^1_{s_i,0}(t+t_w)\delta^2_{s_i,0}(t+t_w)}{\sum_{i=1}^{N} \delta^1_{s_i,0}(t_w)}. \tag{3.3.5}$$

Recalling that in equilibrium one finds $Q(t) = C(2t)$, we can use the equilibrium overlap to test our proposed form of $C(t)$, as given in Equation (3.3.3). If this equation holds we expect to find that for short times:

$$Q(t) \sim \left(\alpha e^{-2t/\tau_1} + (1-\alpha)\right) \sim \left(\frac{(C(t)+\alpha-1)^2}{\alpha} + (1-\alpha)\right) \tag{3.3.6}$$

and for long times:

$$Q(t) \sim (1-\alpha)\, e^{(-2t/\tau_2)^{\gamma}} \sim \frac{C(t)^{2\gamma}}{(1-\alpha)^{2\gamma}}. \tag{3.3.7}$$

Figure 3.29 shows the equilibrium results for $\beta = 2.5$ and 3.5; the superimposed curves are the expected short and long time behaviour using the values of α, γ obtained from fitting the correlation functions with Equation (3.3.3). The theoretical

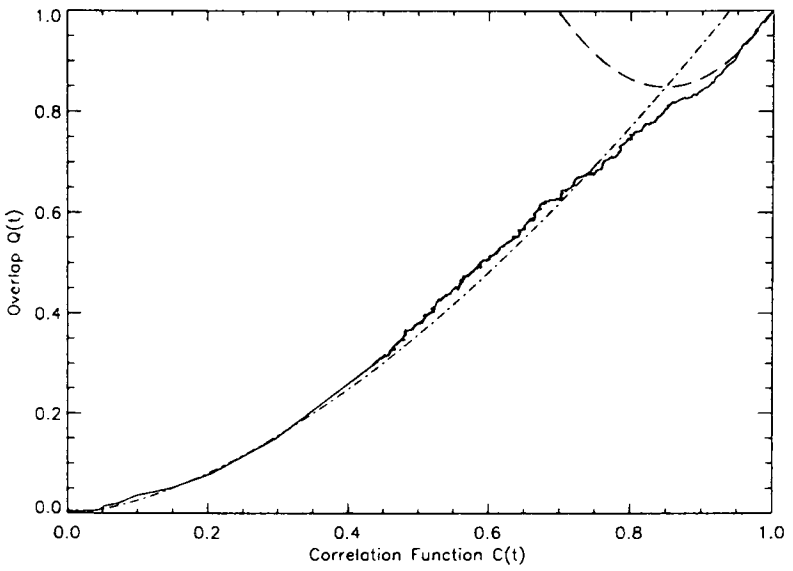

(a) $\beta = 2.5$

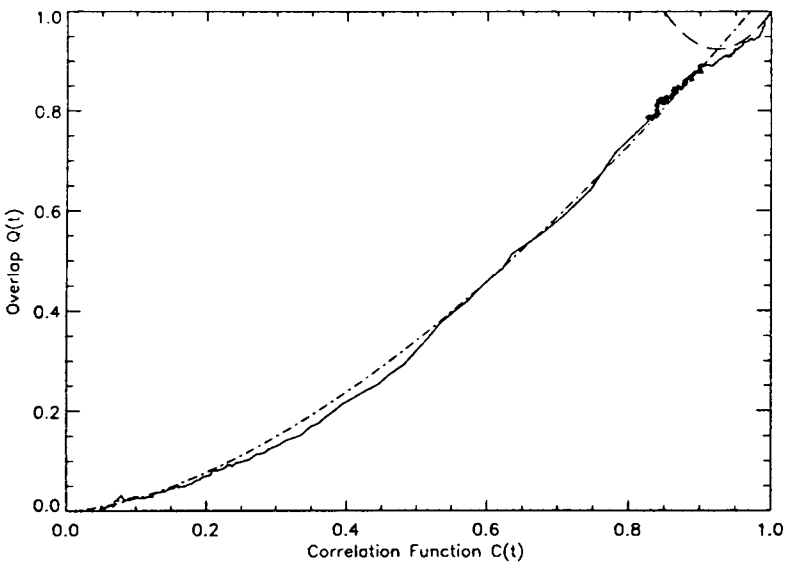

(b) $\beta = 3.5$

Figure 3.29: Overlap $Q(t)$ against $C(t)$ in equilibrium. In each case the dashed line is the expected short-time behaviour and the dot-dashed line is the expected long-time behaviour, if Equation (3.3.3) holds. The values of α, γ are those fitted in the previous section.

behaviour clearly fits the data very well, lending further support to Equation (3.3.3) as a description of the behaviour of the equilibrium correlation functions. We also see that $Q(t)$ decays to zero, thus placing the $D < 0$ model in the Type II class along with the $D > 0$ model.

3.4 Response Functions: $D > 0$ and $D < 0$

We continue to show that the simple spin model with $D > 0$ behaves in the same fashion as the topological froth by studying response functions in relation to the fluctuation-dissipation ratio. Again we concentrate on the single-site (averaged) case, for which we require the linear response at a site to an infinitesimal perturbation field at the same site. The system is quenched from $\beta = 0$ to the temperature required, and then allowed to evolve at that temperature until time t_w when a field of magnitude h and random sign $\epsilon_i = \pm 1$ is applied. Therefore the perturbation to the energy introduced by the field/charge interaction is:

$$\Delta E(t) = h \sum_{i=1}^{N} \epsilon_i s_i(t)\, \theta(t - t_w) \tag{3.4.1}$$

where $\theta(t - t_w)$ is the Heaviside function: $\theta(t - t_w) = 1 \,\forall\, t \geqslant t_w$; 0 otherwise. As before, h is a carefully chosen compromise which gives both linear response and a reasonable signal-to-noise ratio. In keeping with the procedure in the previous chapter, the pure, un-normalised linear response function $R_p(t + t_w, t_w)$ is given by:

$$R_p(t + t_w, t_w) = \frac{1}{h} \sum_{i=1}^{N} -\epsilon_i s_i(t + t_w) \tag{3.4.2}$$

This is multiplied by the temperature and plotted parametrically against the correlation function. As before, in order to investigate FDT, we must normalise by $E(t + t_w)$, but it is also instructive to show plots where the normalisation is with respect to $E(t_w)$, and we shall present those results first.

Figure 3.30 shows the results with the $E(t_w)$ normalisation at various temperatures. One observes the same features as the topological froth, namely a reduction in the magnitude and an eventual change in sign of the slope as t increases and the correlation function decreases, when t_w is too short for equilibration to have occurred. As we noted in the case of the topological froth, the non-monotonicity is a consequence of the existence of an absorbing equilibrium state: competition exists between the field, which encourages the non-zero spins to settle on energetically favourable sites and thus increases the response, and the natural relaxation to equilibrium, which removes non-zero spins altogether thus reducing the response (one should recall that spins of value 0 make no contribution whatsoever to the response). These processes occur on different time-scales, as a defect generally only has to move once to find a favourable site, whereas many more moves are required to completely remove the same defect. These plots highlight the competition between the influence of the field and the natural relaxation, and the two different time-scales leading to the non-monotonic curves; this would not be underlined if one only investigated correlation and response functions with the normalisation of $E(t + t_w)$, which we shall now discuss.

Figure 3.31 shows the FDT plots with this normalisation at $\beta = 7$, for different

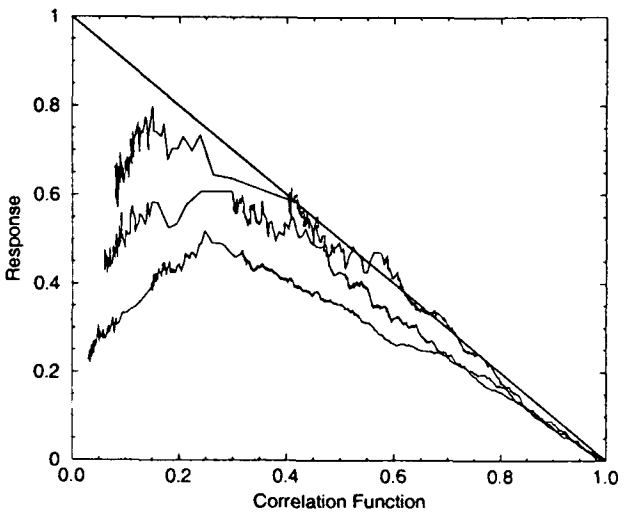

(a) $\beta = 4$. From lower curve to upper curve, $t_w = 10N, 10^2N, 10^3N$. The straight line of slope -1 is shown for comparison.

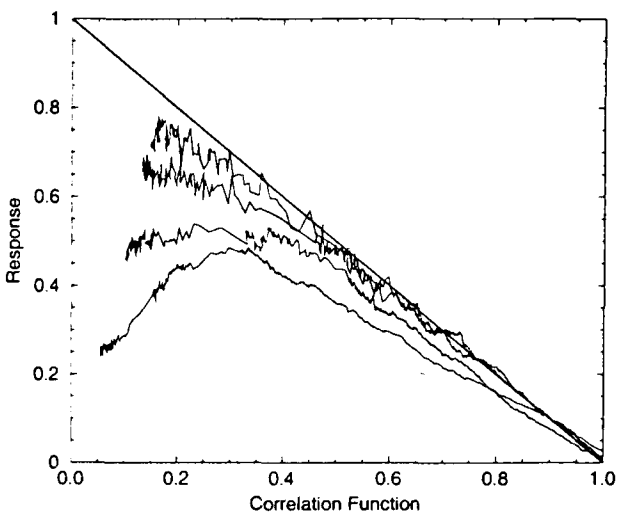

(b) $\beta = 5$. From lower curve to upper curve, $t_w = 10N, 10^2N, 10^3N$ and 10^4N. The straight line of slope -1 is shown for comparison.

Figure 3.30: Parametric plots of the response function against the correlation function, with both functions normalised by $E(t_w)$. The data is averaged over 10 realisations of the charge distribution.

values of t_w. As with the topological froth model, it would appear that FDT is broken for short waiting times t_w and short measurement times t, but the curves subsequently return to the linear FDT behaviour (see Figures 3.31(a) and 3.31(b)). From these results one might be tempted to postulate that there is a time t_f, such that for $t_w > t_f$ one finds FDT, and t_f is less than the equilibration time of the system. In fact, it is more likely that FDT is upheld, approximately, for all waiting times — the deviations are probably due to initial transients as the system settles from its initial configuration. These last only a short time ($\sim t \leqslant 10^2N$), but the response function and the correlator change extremely quickly during that time for short waiting times, and thus they appear to have a considerable effect. Figures 3.31(d), 3.31(e) and 3.31(f) show the correlation functions against time, with one minus the response function superimposed; if FDT is upheld these should lie roughly on top of each other, although one must allow some latitude as there can be an offset due to the response not being exactly zero when measurement commenced. These figures show that there is no convincing evidence to suggest that FDT is really broken for $D > 0$ in this system. If one looks again at the equivalent results for the topological froth (Figure 2.14), there is no convincing evidence for FDT breaking there either; the deviations observed there for short waiting-times are also likely to be due to initial transients. This upholding of equilibrium FDT is a somewhat unusual result as one expects systems out of equilibrium to exhibit some form of FDT-breaking. We note that the correlation functions and response functions only receive contributions from the defects, rather than from the zero-spin background, and that the normalising factor is the total number of these defects. Thus the normalisation factor carries the out of equilibrium information about the system,

whilst the defects themselves respond to the field as if they were in equilibrium.

We now move to a investigation of FDT in the $D < 0$ model. In this case, the applied field $h\epsilon_i$ must couple to the zero-spin defects, such that the perturbation introduced to the energy is $\Delta E(t) = h\sum_{i=1}^{N} \epsilon_i \delta_{s(t),0}\, \theta(t - t_w)$, where $\theta(t - t_w)$ is again the Heaviside function. The pure, un-normalised linear response function $R_p(t + t_w, t_w)$ is then:

$$R_p(t + t_w, t_w) = \frac{-1}{h(1 - p_{eq}(0))} \left(\frac{\sum_{i=1}^{N} \epsilon_i \delta_{s(t),0}}{\sum_{i=1}^{N} \delta_{s(t_w),0}} \right). \tag{3.4.3}$$

Given the normalisation of Equation (3.3.2), one has to think a little with regards to the normalisation of the response. The denominator in that equation, $\sum_{i=1}^{N} \delta_{s(t_w),0}$ is equal to $N + E(t_w)$. Thus, if we wish to compare the pure response against the pure correlation function, and simply normalise by a constant then we should use $(1 - p_{eq}(0)) \sum_{i=1}^{N} \delta_{s(t_w),0}$ as the normalising factor. If, on the other hand, we wish to investigate the FDT relationship then we must use $(1 - p_{eq}(0)) \sum_{i=1}^{N} \delta_{s(t+t_w),0}$. Let us denote these factors by $\widetilde{E}(t_w)$ and $\widetilde{E}(t + t_w)$ respectively.

Figure 3.32 shows such a parametric plot for a variety of temperatures and waiting times t_w, normalised by $\widetilde{E}(t_w)$; we remind the reader that with this normalisation one can extract no information at all about the behaviour of the system in relation to FDT. In Figure 3.32(a) we see similar results to the equivalent $D > 0$ plots, namely that the curves follow a straight line of slope -1 for a time which is dependent on the waiting time t_w (if t_w exceeds the equilibration time of the system, as is the case for $t_w = 10^4 N$ in this figure, then a straight line is obtained for all time). Subsequent to the departure from the straight line, we see non-monotonicity, with the response decreasing. This has the same origin as in the $D > 0$ case: at long times (i.e. low values of the correlator) the time-scale to increase the response is less than the time-scale to remove the defect, and this mismatch of time-scales for the two competing processes results in the non-monotonic behaviour. However, in Figures 3.32(b) and 3.32(c) we see, for short waiting times ($t_w \leqslant 10^2 N$), an additional hump earlier in the curve, besides the behaviour just discussed (although we cannot always run for long enough to see the final turnover at low values of the correlator). This suggests two different time-scales for the response and the energy during the initial regime where fast processes dominate. This is a consequence of the disordered background which prevents dimers from diffusing freely. In the $D > 0$ model, the fast processes tend to wipe out a great deal of the defects very quickly, but in doing so will leave many defects on favourable sites, thus increasing the response. The system then has to create dimers to further increase the response, and on a longer time-scale, reduce the energy. In the $D < 0$ model, dimers can become blocked, and thus persist for long enough to make a positive contribution to the response before being wiped out i.e. for the fast processes as well as the slow ones, the time-scale to increase the response is faster than the time-scale to eradicate defects. This effect is temperature-dependent because the dimer diffusion is temperature-dependent, as

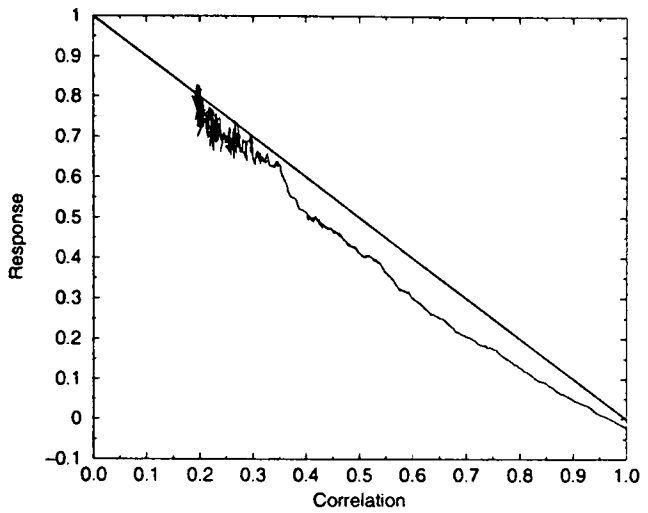

(a) $t_w = 10N$

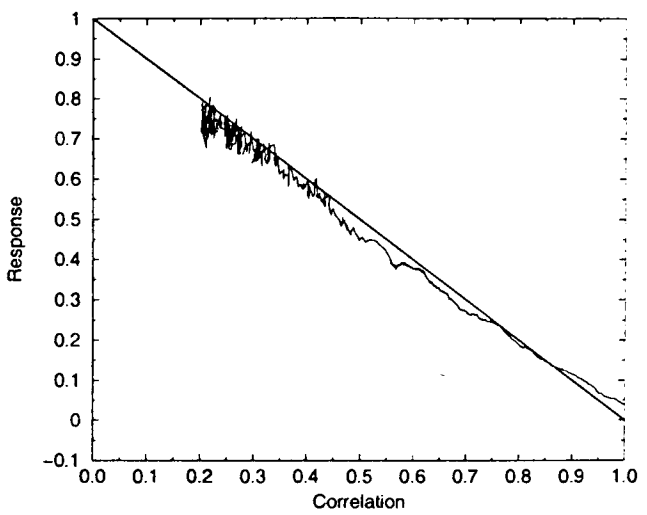

(b) $t_w = 10^2 N$

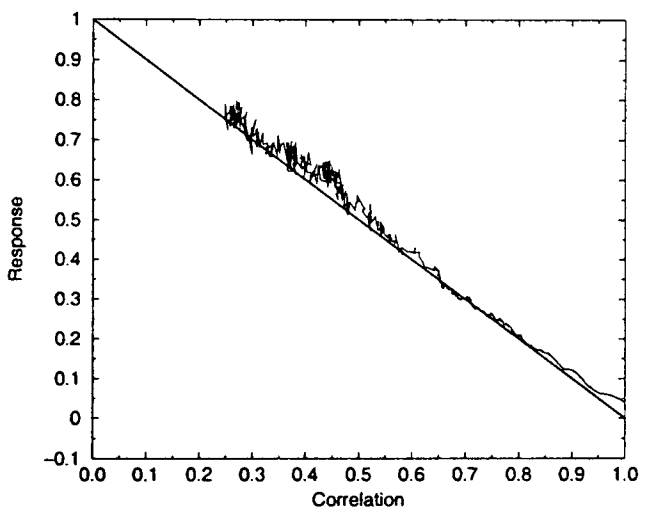

(c) $t_w = 10^4 N$

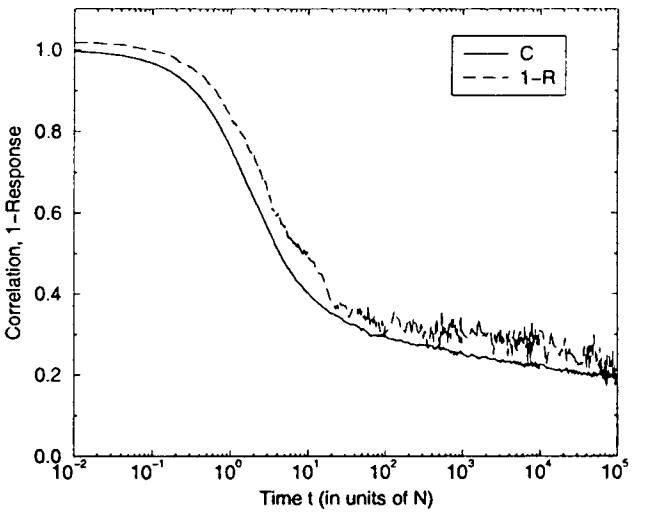

(d) $t_w = 10N$

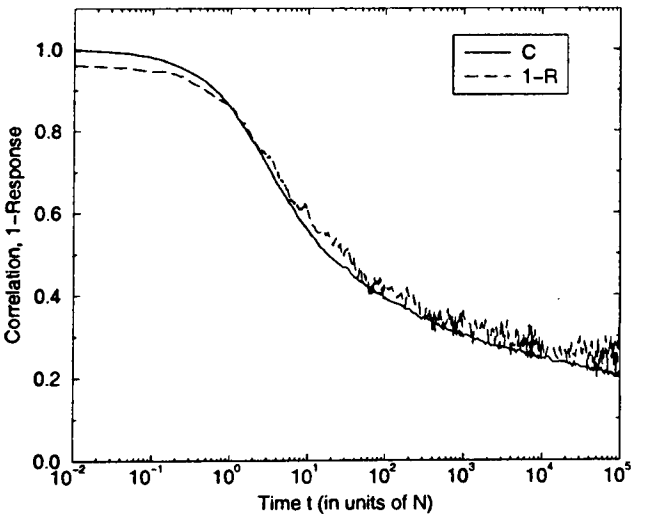

(e) $t_w = 10^2 N$

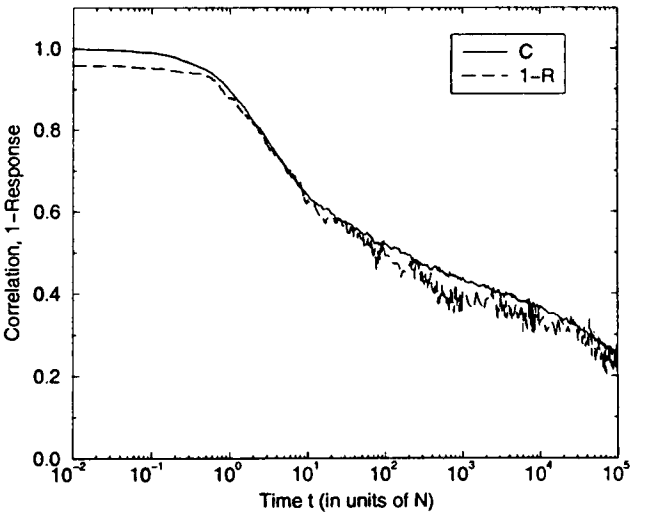

(f) $t_w = 10^4 N$

Figure 3.31: The response and the correlation functions for $\beta = 7$, normalised by $E(t + t_w)$, plotted both parametrically and against time. In the parametric plots, the straight line is the equilibrium FDT relationship. (Results are averaged over 10 realisations of the charge distribution).

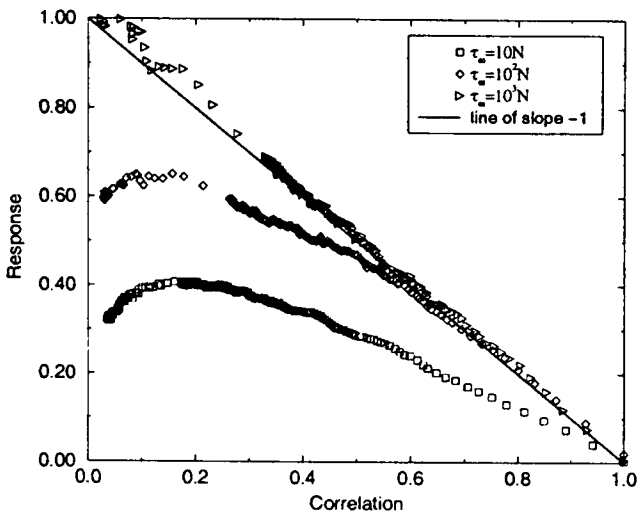

(a) $\beta = 2.5$

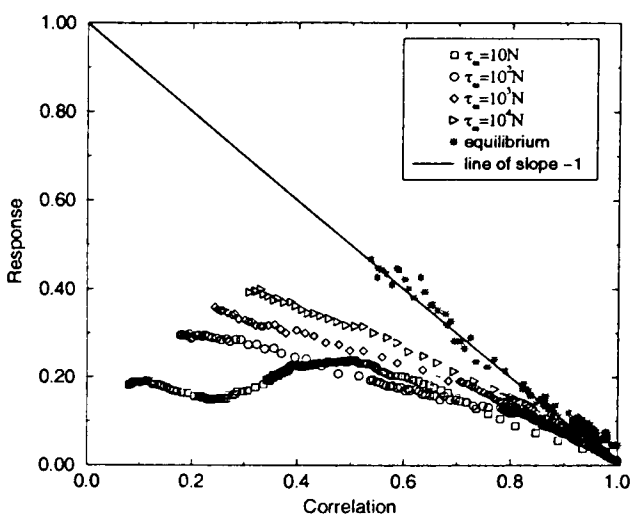

(b) $\beta = 4.5$

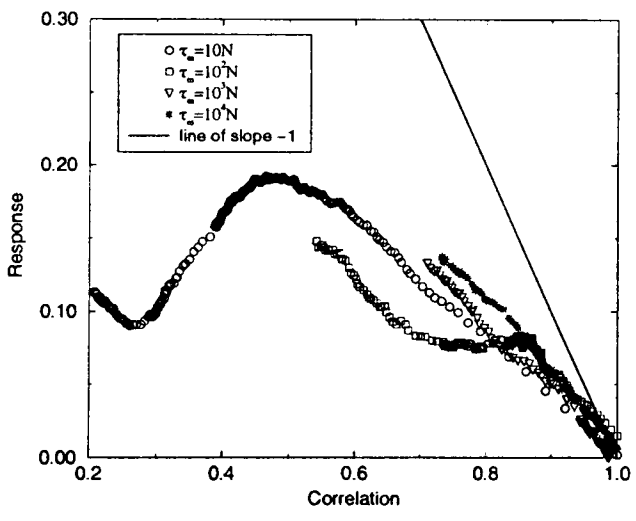

(c) $\beta = 6$

Figure 3.32: Parametric plots of the response against the correlation function, normalised by $\widetilde{E}(t_w)$. The straight lines have slope -1.

we showed earlier (Section 3.3). It is also not present at longer waiting times as then the system has reached a point where most dimers have been eradicated and the slow processes are dominant.

Moving now to a direct investigation of the FDT relation for the $D < 0$ model out of equilibrium, we exhibit results in Figure 3.33 where the normalisation factor is $\widetilde{E}(t+t_w)$. By cross-referencing the parametric plots with Figures 3.33(e) and 3.33(f) one can be left in no doubt that the equilibrium fluctuation-dissipation relation is broken for $t_w \leqslant 10^2 N$, and small times t. It would appear that there is an eventual return to the linear relationship for large t in all cases except $t_w = 10N$, where the correlation function decays to zero before any such return can be observed, although in the case of Figure 3.33(d) one would need to run for much longer times to establish with any certainty that this is the case. The early behaviour must have the same origin as the additional humps found in Figures 3.32(b) and 3.32(c); we

remind the reader that the crucial difference in these plots is that one can only decrease the response by moving defects from favourable to unfavourable sites — removing defects entirely only further increases the response. Initially dimers may have some freedom to move, and will rest on favourable sites — some of these may subsequently become blocked on these sites. Over time the blockade will be removed and these dimers will become free to travel, but will not necessarily be eradicated or find favourable sites, with the result that the response will temporarily decrease. Thus it would appear that this breaking of FDT is due to the disordered background which prevents the defects from moving freely in dimers — this is the main difference between the $D > 0$ and $D < 0$ models, and it clearly has a profound effect on the behaviour of the system. However, further investigation involving longer simulations would be required to produce more convincing evidence that there is a return to the equilibrium FDT relationship after the blocking has subsided.

Rather than choosing to use the correlation functions of Equations (3.2.4) and (3.3.2), and normalising correctly in order to investigate off-equilibrium FDT, we could instead map the spin variables $s_i = \pm 1, 0$ onto an Ising variable $\sigma = \pm 1$ such that the same-time correlator $C(t,t)$ is always unity. We shall do this by employing the following simple transformation:

$$\sigma_i = 1 - 2s_i^2 \tag{3.4.4}$$

Let us consider the $D > 0$ case. The above transformation treats all defects equivalently, regardless of their sign. We may then apply a field $h\epsilon_i$, with ϵ_i randomly ± 1, which introduces a perturbation to the energy $\Delta E(t) = h \sum_{i=1}^{N} \epsilon_i \sigma_i \ \theta(t - t_w)$. We shall follow the linear response:

$$R(t + t_w, t_w) = \frac{1}{hN} \sum_{i=1}^{N} -\epsilon_i \sigma_i (t + t_w) \tag{3.4.5}$$

and the corresponding correlation function

$$C(t + t_w, t_w) = \frac{1}{N} \sum_{i=1}^{N} \sigma_i (t + t_w) \sigma_i (t_w). \tag{3.4.6}$$

As desired, $C(t_w, t_w) = C(t + t_w, t + t_w) = 1$ at all times. Note, however, that this correlation function will not decay to zero, but to a value which is dependent on the initial conditions. In addition, this correlation function is of the disconnected form, rather than the connected form which one ideally uses in investigating FDT.

Figure 3.34 shows parametric plots of the response against the correlation function for various waiting times, using the above functions. We see a completely different shape to those in Figure 3.31; in these plots there is a dramatic turnover in the slope of the curves. This is reminiscent of the results for the SCIC (see Section 1.2.1), although in this case the slope before the turnover appears to have some waiting time dependence, as well as the point at which the turnover appears.

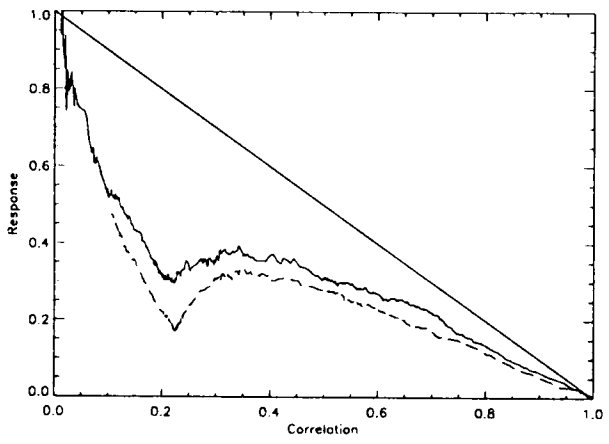

(a) $t_w = 10N$, $\beta = 4.5$ (solid curve) and $\beta = 6$ (dashed curve).

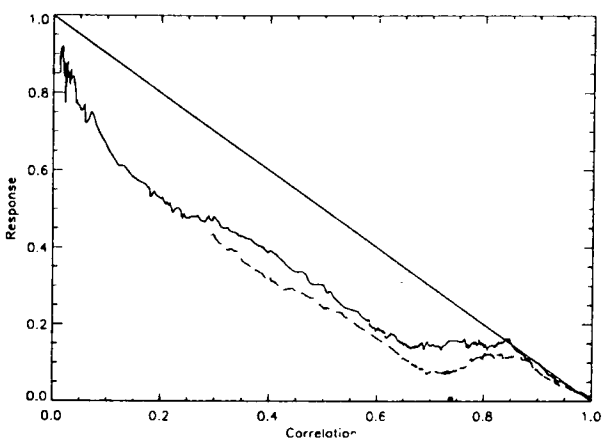

(b) $t_w = 10^2N$, $\beta = 4.5$ (solid curve) and $\beta = 6$ (dashed curve).

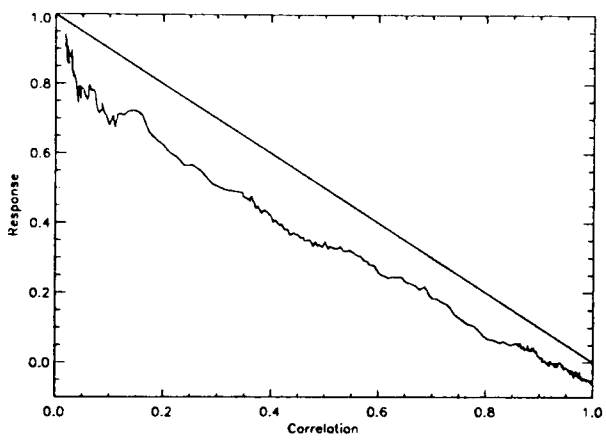

(c) $t_w = 10^4N$, $\beta = 4.5$

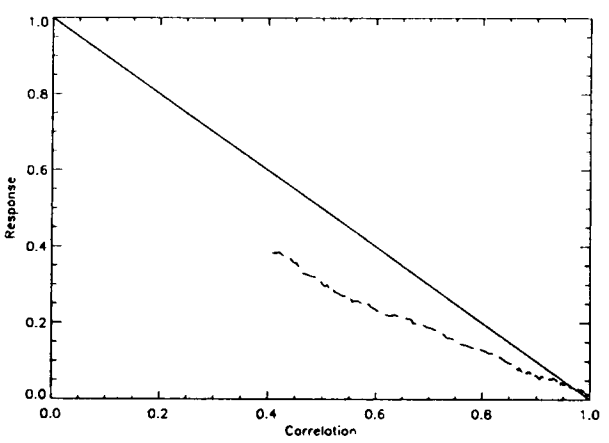

(d) $t_w = 10^4N$, $\beta = 6$

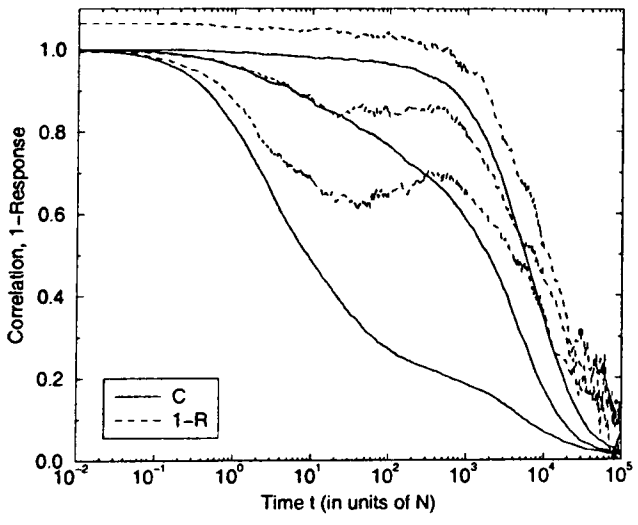

(e) $\beta = 4.5$. From left to right, $t_w = 10N$, 10^2N and 10^4N.

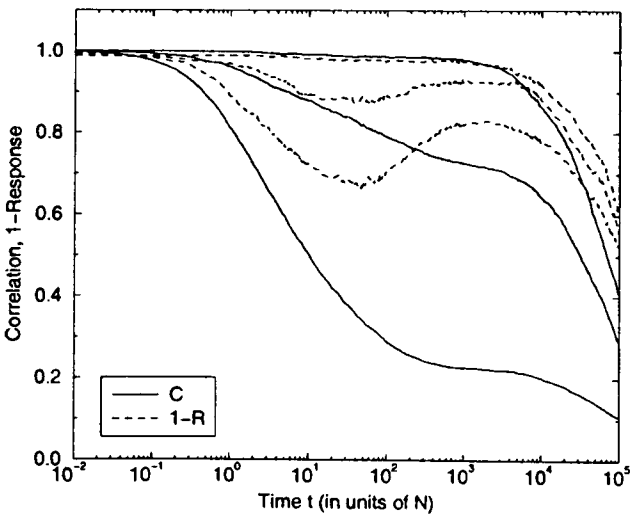

(f) $\beta = 6$.From left to right, $t_w = 10N$, 10^2N and 10^4N.

Figure 3.33: The response and correlation functions, normalised by $\widetilde{E}(t+t_w)$, plotted both parametrically and against time. In the parametric plots, the straight line has slope -1 and is there as a comparative device only.

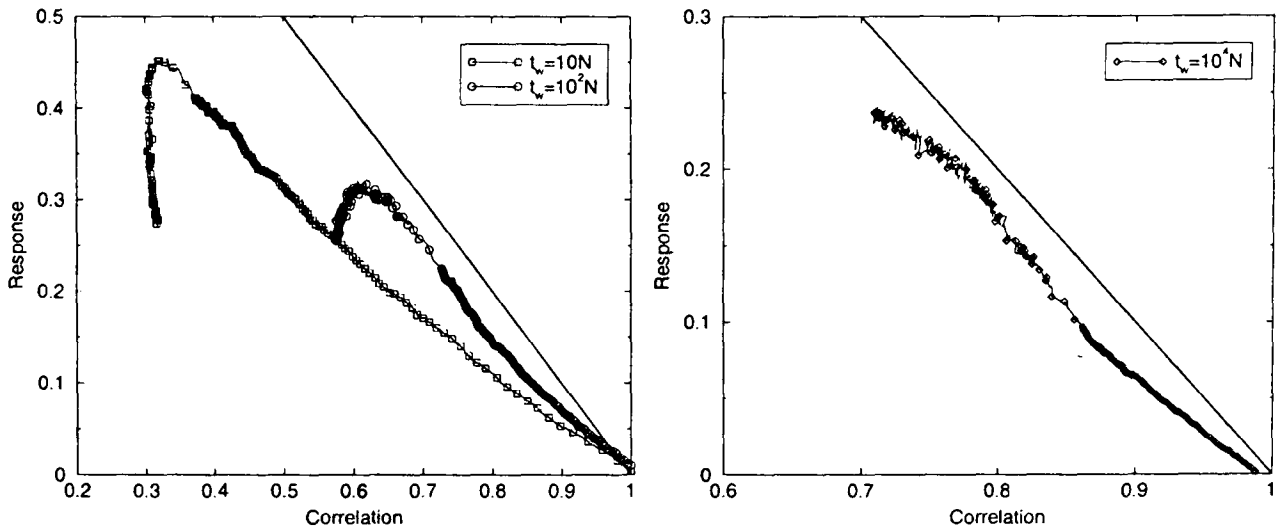

(a) (b)

Figure 3.34: The response against the correlation function, using the definitions in Equations (3.4.5) and (3.4.6), for $\beta = 7$. The straight line is the FDT equilibrium relationship.

The non-monotonicity is of course due to the decay in the energy — although we have succeeded in insisting that $C(t,t) = 1$ for all times, we have not removed the energy dependence, but simply transferred it. The ratio of $\sigma_i = 1$ to $\sigma_i = -1$ spins is now directly related to the energy, and the energy decay reduces the number of $\sigma_i = -1$ spins which forces some $\sigma_i = 1$ spins to occupy unfavourable sites, in turn reducing the response.

Figures 3.34 and 3.31 were both achieved by following perfectly valid procedures to investigate the out of equilibrium response, although again we must highlight the fact the the disconnected (rather than connected) correlation functions have been used, which is not ideal. The fact that Figures 3.34 and 3.31 are so dissimilar strongly suggests a sickness in this area of the field. To accord any respect to FDT results, one would wish to be assured that they were not observable-dependent; as shown in Section 1.1.3, the aim of these studies is to define a quantity $x(C)$ which in some way encapsulates the relevant physics of the non-equilibrium behaviour of the system. We have found obvious observable dependence. However, if would be premature to suggest that FDT plots are in general worthless. We have also found that by judicial choice of the perturbation (which then defines the most sensible response and correlation functions to use) one can recover equilibrium FDT — we have transferred the energy dependence to the normalisation factor and in doing so may have accessed instead the underlying behaviour. It would be instructive to investigate whether one can produce FDT plots with equilibrium FDT behaviour for different lattices, and also for different kinetically-constrained models, where we have already noted that the standard procedure is to transform variables into a convenient notation that preserves $C(t,t) = 1$. A full investigation is beyond the scope of this thesis, but some preliminary results will be presented at the end of the

next chapter.

3.5 Concluding remarks

We have studied a simple lattice-based spin model which has a non-interacting Hamiltonian, but constrained dynamics, and find it exhibits both glassy behaviour and behaviour typical of diffusion-limited reaction models. A single parameter D distinguishes two types of ground state. By choosing $D > 0$, one can study a system with a unique ground state, evolving by way of annihilation-diffusion processes which are either fast temperature-independent or slow temperature-dependent diffusive processes, with the latter slower by a factor exponential in inverse temperature. The differences in these two time-scales allow us to observe two-step relaxation in both the energy density and the equilibrium correlation functions, and we can directly attribute each time-scale to the different processes. We can categorise the fast processes as: $A + A + B \to A$ and $A + B + B \to B$, with only facilitated diffusion allowed (A and B signify defects of opposite sign). This should have the same asymptotic behaviour (apart from an amplitudinal alteration) as $A + A + A \to A$, namely $t^{-0.5}$, and this is what we observe for the initial energy density decay. The slow processes involve pairing of defects of opposite sign: this can be classed as $A + B \to \emptyset$, which should have, in two dimensions, an asymptotic behaviour of $t^{-0.5}$. In fact we find a power law with an exponent of approximately 0.3; this slower behaviour is likely to be due to clusters of like defects, which are harder to eradicate than isolated defects.

For $D < 0$, the ground state is highly degenerate and the system evolves according to the fast annihilation-diffusion processes $A + A + A \to \emptyset$, where the A's now represent zero-spins. In this case the movement of A's are hindered by the background due to the ground state degeneracy, and even the fast processes have some temperature dependence. Nonetheless, the initial energy density decay also yields a power law with exponent close to -0.5. We find in this case that one needs to introduce stretched exponential behaviour to adequately describe the latter stages of the approach to the plateau — this behaviour is attributed to pinning of some isolated zero-spins, such that the dominant process becomes $A + B \to B$, where A now represents dimers, and B pinned isolated zero-spins. The subsequent departure from the plateau is described by a power law, although the decay is slower than might be anticipated by the $A + A \to \emptyset$ classification, because of the effect of the disordered background.

We have studied the correlation functions for D positive and negative; in both cases, a naïve theory gives a predicted form for these which fits the data extremely well. Studies of the overlap in equilibrium serve to reinforce these results, and also put the present model into the Type II (glassy) classification, for D both positive and negative.

Studies of the behaviour of the system in response to a small applied field yield some thought-provoking results. For both $D > 0$ and $D < 0$ one finds that the

FDT plots are dependent upon the method used to obtain them. One can recover equilibrium FDT in certain regions with careful choice of observable; this merits further investigation.

In this chapter we have employed a hexagonal basis for the cell edges. This was naturally motivated by analogy with the two-dimensional froth of Chapter 2. Extensions to different lattices and dimensions are clearly possible and desirable in order to further test our understanding of these systems: this will be the basis for study for the next chapter.

Chapter 4

2d Spin Model on a Square Lattice

In simplifying the two-dimensional froth of Chapter 2, the hexagonal lattice was the natural lattice upon which to base the spin model presented in Chapter 3. This lattice preserved two notable features of froth topology, namely three-fold vertices and cells which are hexagonal on average. However, it can be instructive to apply the same evolutionary rules to a different lattice in order to understand what rôle, if any, the geometry of the lattice plays. To this end, we now turn our attention to a two dimensional square lattice.

We shall first present the details of the model, and then move to a discussion of what we might expect to observe in comparison with the hexagonal model. The results for this model will follow, and then we shall move to a discussion of the FDT results, including some comparisons with the asymmetric and symmetric Ising chains introduced in Section 1.2.

4.1 The Model

We can view the shift from a hexagonal structure to a square lattice as a shrinking of the central bond involved in a T1 move, as shown in Figure 4.1. The three-

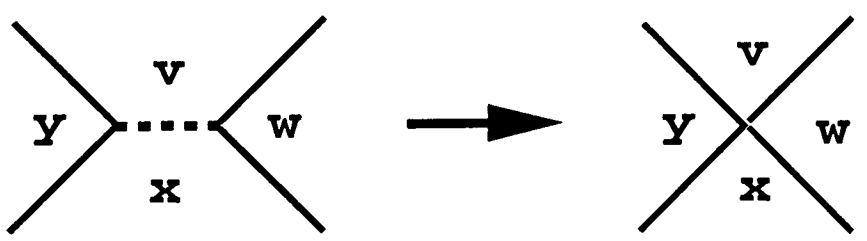

Figure 4.1: The square lattice (right) can be considered equivalent to a hexagonal lattice (left) in which the central bond, denoted by a dashed line, has been shrunk to a point.

state spin model considered in this section consists of a square lattice with a spin placed at the centre of every square. These may take the values $s_i \in \{\pm 1, 0\}$. As in the previous chapters, we use spin-conserving dynamics, choosing a plaquette of four cells in which one pair of diagonally-opposite cells are randomly chosen as candidates to have their spins increased by one unit, and the other pair to have their spins decreased by one unit. The plaquette is uniquely defined through the vertex common to all four cells. We use the same energy form as in chapters 2 and 3 i.e. $E = \sum_{i=1}^{N} s_i^2$, and again utilise the Metropolis algorithm; thus, assuming cells w and y on the right hand side of Figure 4.1 have been chosen as candidates for a spin increase, the probability of performing that move is exactly that given by Equation (3.1.4), namely:

$$P(s_w, s_y; s_v, s_x) = (1 - \delta_{s_w,1})(1 - \delta_{s_y,1})(1 - \delta_{s_v,-1})(1 - \delta_{s_x,-1})\ Min[1, \exp(-\beta \Delta E(s_w, s_y; s_v, s_x))] \tag{4.1.1}$$

Periodic boundary conditions are applied, and the system size is $N = 100^2$.

4.2 Discussion

We shall now consider what similarities and differences one might expect between this model and the 2d hexagonally-based lattice model. The probability of choosing cell z to be part of the plaquette for flipping is the same in each case: on the square

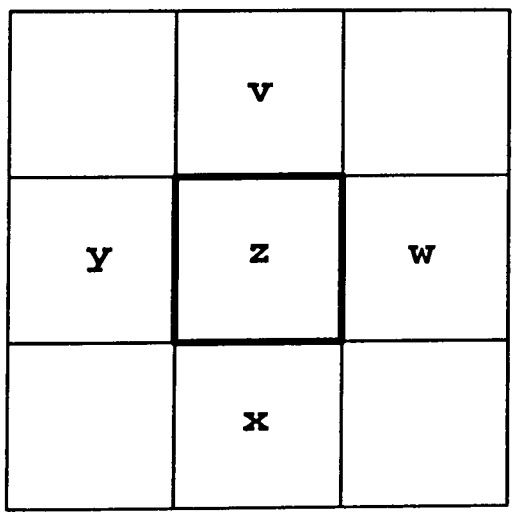

(a) The square tiling. Cell z has four first neighbours: v, w, x and y. The spin at z can be flipped by choosing any of the four vertices it has in common with its first neighbours.

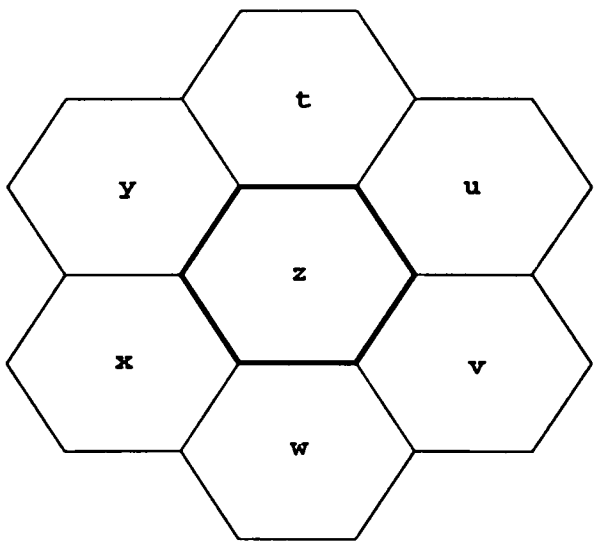

(b) The hexagonal tiling. Cell z has 6 first neighbours: t, u, v, w, x and y. The spin at z may be flipped by choosing any of the edges of z itself, and also any of the edges between two of z's first neighbours.

Figure 4.2: Features of the geometry of the square and hexagonal lattices.

lattice, there are 4 vertices out of a total of N that may be chosen to include z in the plaquette (see Figure 4.2(a)), and on the hexagonal lattice there are 12 edges out of a total of $3N$ that may be chosen to include z in the plaquette (Figure 4.2(b)). However, the square lattice is more prone to jamming as there are fewer routes by which z can have its value altered. This reduction makes it much easier for spins on the square-based system to become jammed: for example, in Figure 4.2(a) if y, z and w all take the same non-zero spin value, then z is completely unable to move until either y or w have been altered in value. In the hexagonal case, z cannot be completely locked until five of its six neighbours all have the same, non-zero spin. With this in mind we expect the plateau to appear at a higher energy density in the square lattice than in the case of the $D > 0$ model on the two-dimensional hexagonal lattice. Nevertheless, the same move-sets are possible in this model, and thus we expect to find the same two-step relaxation with the initial fast decay classed as $A + A + A \to A$, and the slow defect pairing as $A + B \to \emptyset$.

One should bear in mind that although dimers exist, and diffuse freely though a background of zero-spins, with this particular lattice geometry they may only move one-dimensionally (see Figure 4.3(a)). This is unlikely to affect the initial fast decay in any way, as the defects do not stay fixed within the dimer pair and can attach to a different defect to become a part of a dimer of the other orientation; thus the defects themselves move through the system isotropically, although the pair they move within must only move one-dimensionally, as shown in Figure 4.3(b). This feature should not affect the slow defect pairing either, as the defects may absorb/create dimers in any direction and thus also move isotropically.

There are some extra constraints within the square-based model due to the application of the spin-flip rules. One finds that the sum of the spins across each row, and down each column must *always* add up to zero if one wishes to be able to access the zero-energy ground state. This is because the four-spin rules locally conserve the sum of the spins in the rows and columns of the plaquette. Thus in preparing an equilibrium state at a finite temperature one must take care to ensure these constraints are satisfied — the easiest way to do that is to throw down the correct number of defects for that temperature in rectangles of random sizes as shown in Figure 4.3(c). This might appear to be a very contrived configuration, but we have thoroughly checked that this procedure gives the same results as would be obtained by heating to infinite temperature from the ground state and then achieving equilibrium by running for a sufficiently long time at the temperature one wishes to investigate. It is not clear whether these additional constraints might have some bearing on the results at very low temperatures and for long times, as then there are likely to be very few (often only two) defects per row/column, and thus the slow-moving defects are likely to meet a defect of opposite sign first. This might possibly have the effect of turning the $A + B \to \emptyset$ behaviour of the slow defect pairing into $A + A \to \emptyset$; although as like-pairs persist for a very long time, this cross-over could only occur after very long times and at very low temperatures.

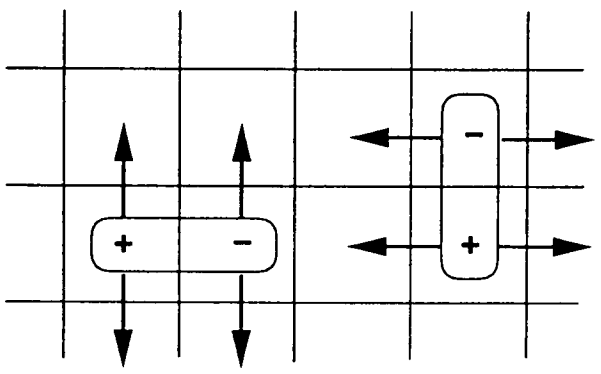

(a) On the square lattice, dimers can only move one-dimensionally though the spin-zero background. Sites without a central spin shown have spin zero.

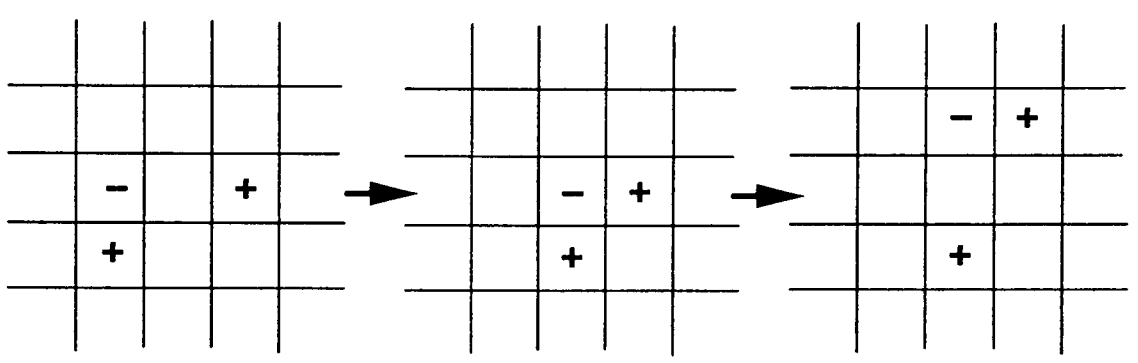

(b) Although the dimers are constrained to move one-dimensionally, the defects within them can move two-dimensionally by switching their dimer-partner, as shown in this sequence of events.

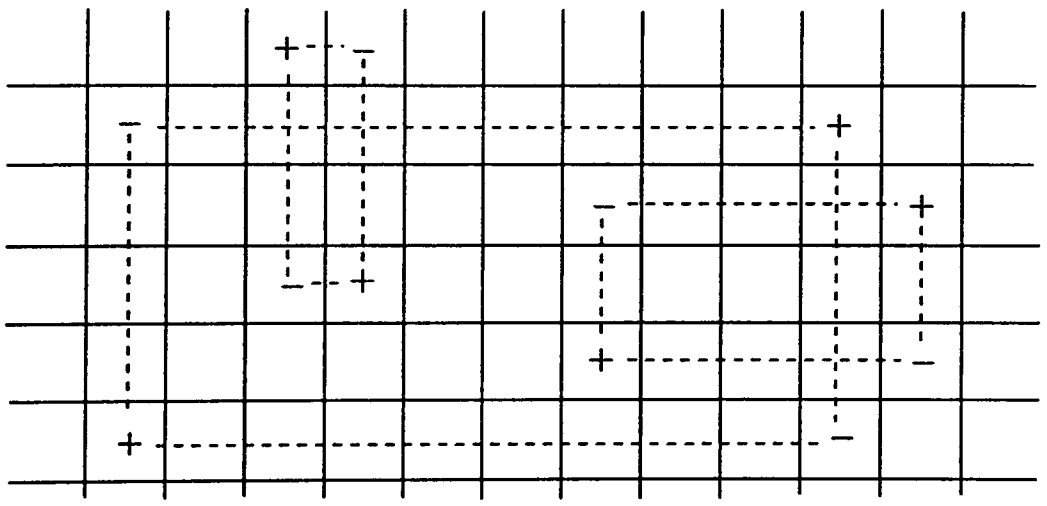

(c) To satisfy the constraints, configurations are prepared by laying the defects throughout the system in rectangles of random size and shape. Rectangles whose corners would lie on already-occupied sites are rejected.

Figure 4.3: Dimer movement and configuration preparation on the square lattice.

4.3 Dynamics

As anticipated, this model produces qualitatively similar results to those for the 2d hexagonally-based model for the energy density behaviour under slow cooling, and

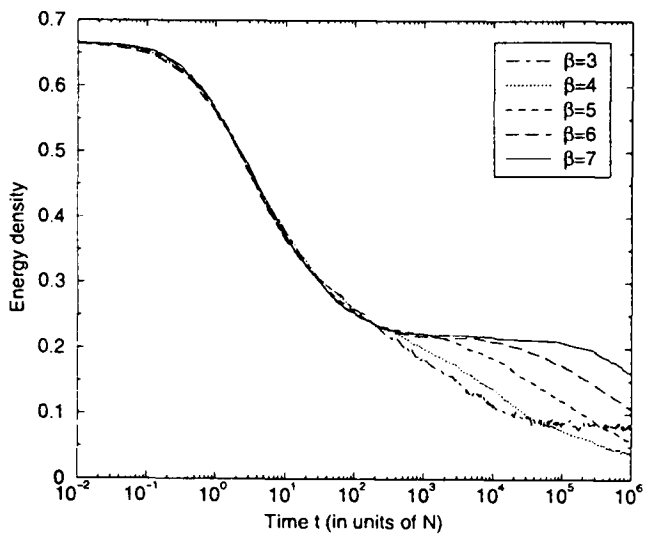

(a) The energy density at various temperatures from an infinite-temperature starting configuration. The curves for $\beta \leqslant 4$ attain equilibrium, whereas the others do not.

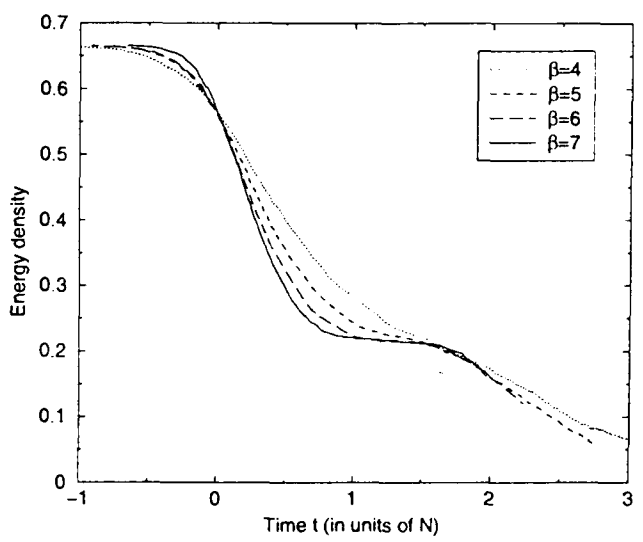

(b) The energy density against $T\ln t$, showing a sharp staircase shape due to the presence of energy barriers.

Figure 4.4: The energy density with time.

also at different times subsequent to a quench from infinite temperature; thus we do not show those results here as they do not require further discussion. Instead we shall proceed directly to the temporal behaviour of the energy after a quench from an infinite temperature configuration; these results are shown for various temperatures in Figure 4.4(a). As predicted, we see the familiar two-step relaxation, with the intermediate plateau height somewhat higher than in the 2d hexagonal lattice model. Again, plotting the energy density against $T\ln t$ shows a clear staircase shape.

Following the arguments of the previous chapter, we shall fit the energy density with the following form:

$$\frac{E}{N} = (\frac{2}{3} - a)(1 + mt)^{\kappa_1} + a(1 + te^{-2\beta})^{\kappa_2} \tag{4.3.1}$$

where we expect $\kappa_1 \sim -0.5$ as we believe the first part of the behaviour to be dominated by $A + A + A \rightarrow A$ processes. m should be approximately 0.5, and a is the plateau height, which is ~ 0.15. For the latter part of the curve, we are unclear as to exactly what to expect for κ_2, although it should be of order 1.

The results of such a fit are displayed in Figure 4.5; it will be observed that these fits are very good. Note that we do not try to fit the curves close to equilibrium, as we are interested in the out of equilibrium behaviour; also the fits lie above the data at the initial onset of the plateau, which is due to a crossover to stretched exponential behaviour as discussed in Section 3.3. We find that κ_1 is indeed very close to -0.5, providing support for the $A + A + A \rightarrow A$ hypothesis and showing that this part of the decay is not dependent on the lattice upon which the model is based. The plateau height, on the other hand, is influenced by the lattice geometry and we find a plateau height here that is over twice that of the hexagonally-based

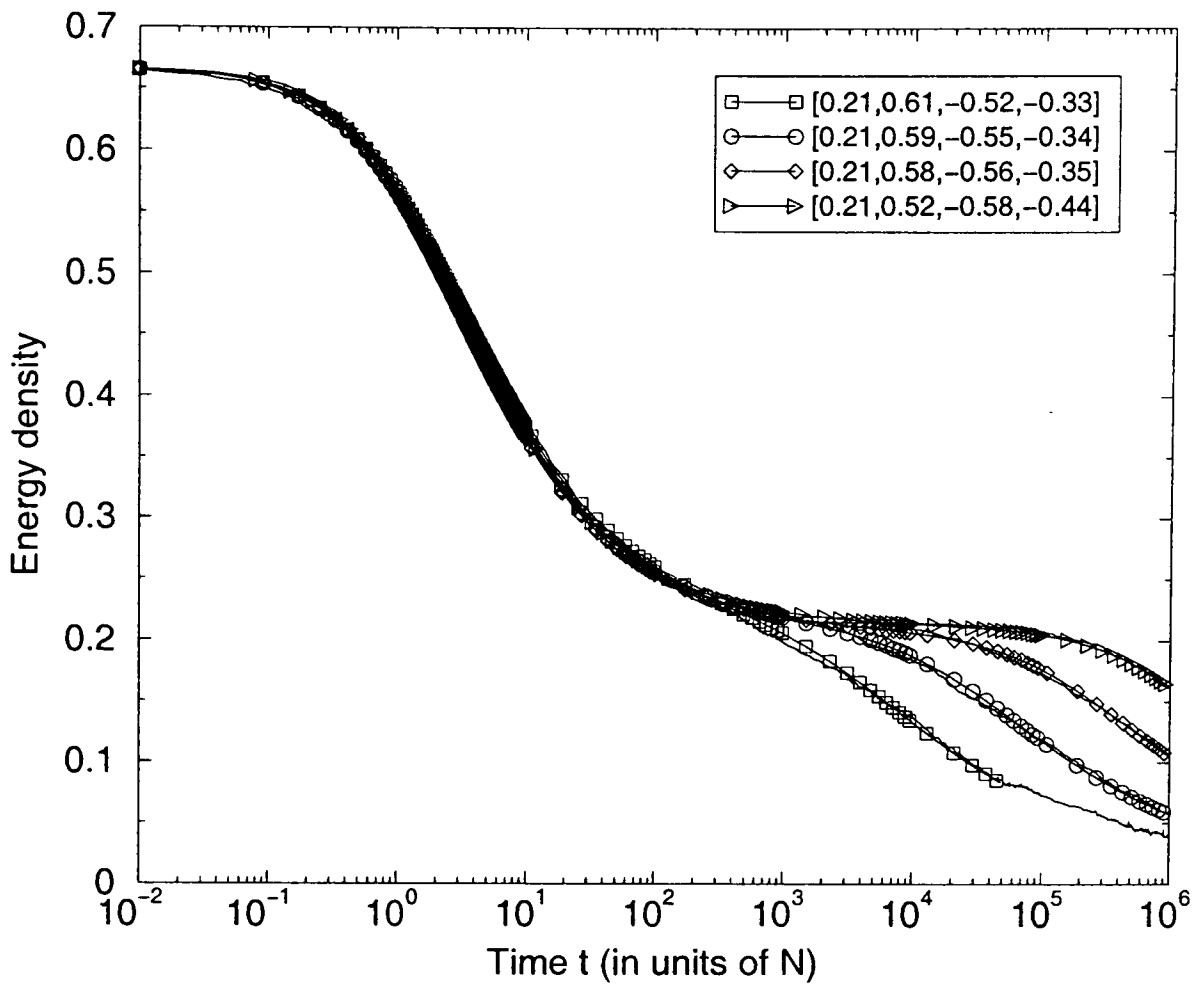

Figure 4.5: The energy density fitted with Equation (4.3.1) for, from left to right, $\beta = 4, 5, 6, 7$.

equivalent model, reflecting the fact that this lattice is more prone to jamming. The exponent κ_2 is found to be roughly -0.35, which is very similar to the value of approximately 0.3 found for this exponent in the $D > 0$ hexagonal model. Thus it appears that the square lattice geometry and the associated constraints do not affect this behaviour at these temperatures and over the time-scales probed in these simulations; it is an open question as to whether they have some influence on the behaviour at much longer times and lower temperatures. As in the hexagonal case, one ascribes the fact that the behaviour observed is slower than simple $A + B \to \emptyset$ to the clustering of like defects; Figure 4.6 shows snapshots of a section of the lattice at various times after a quench to $\beta = 6$ from infinite temperature. The clusters of like defects are easily observable.

We move now to an investigation of the single-site two-time correlation functions, as defined in Equation (3.2.4); the equilibrium functions are shown for a variety of temperatures in Figure 4.7, fitted with the sum of an exponential and a stretched exponential as in Equation (3.3.3). Again, we do not attempt to fit the slow tails. The stretched exponential has the same origin as in the hexagonal $D < 0$ case i.e. move-sets exist which must be carried out in sequence to free blocked cells, leading to hierarchical relaxation times and stretched exponential behaviour. That this occurs for $D > 0$ in the square lattice but not the hexagonal lattice is purely a result of the geometry — as mentioned in Section 4.2, situations very easily arise

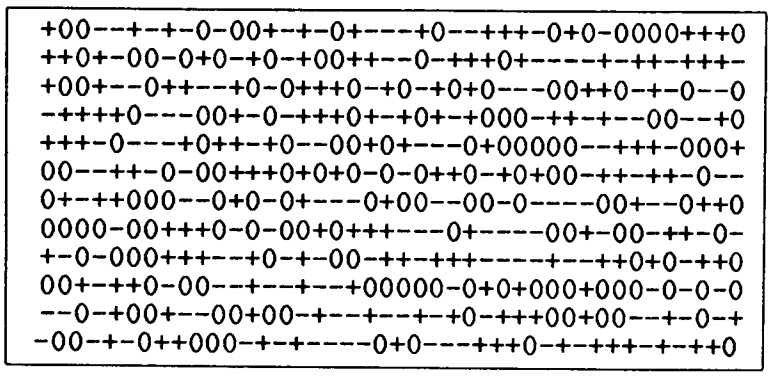

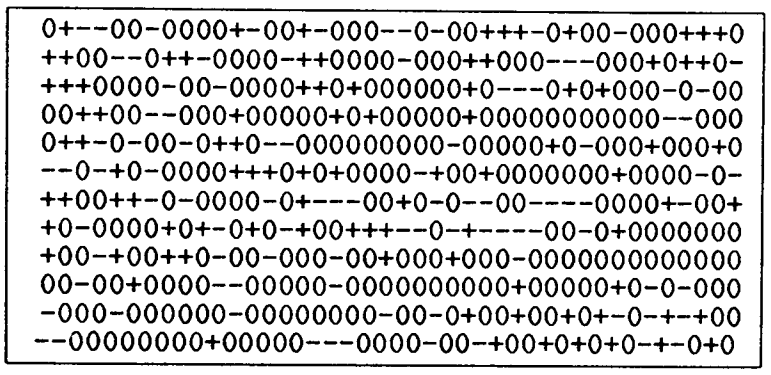

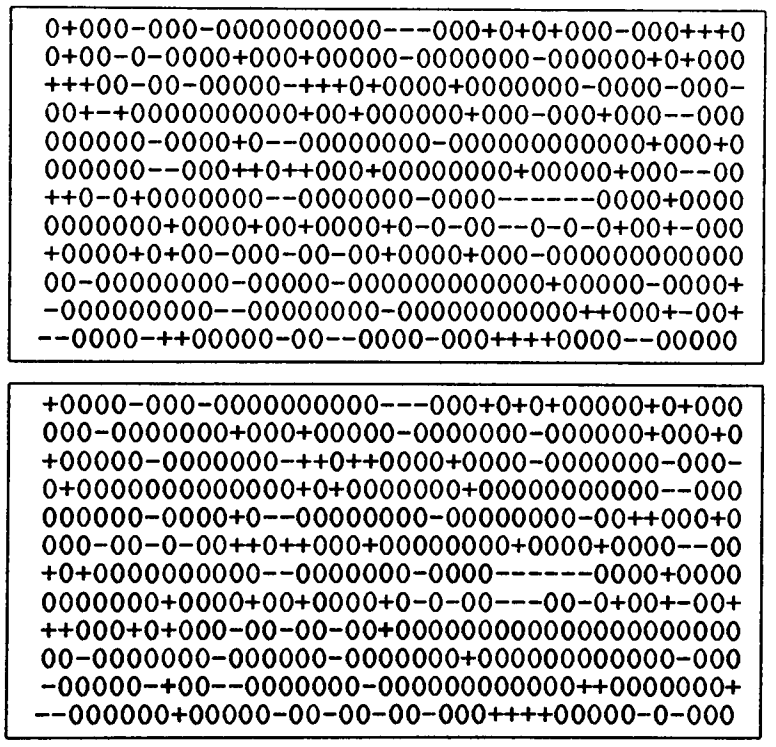

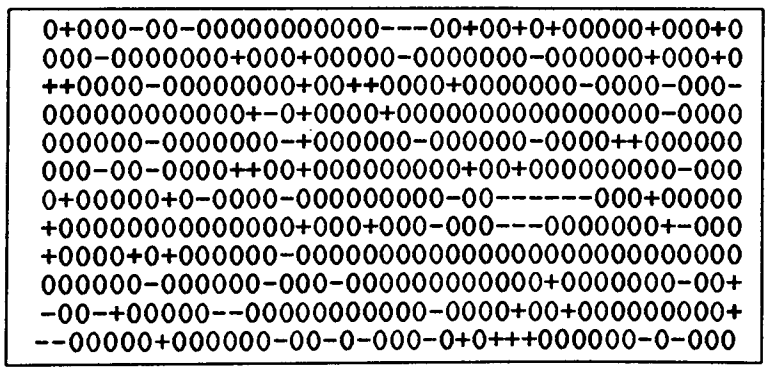

Figure 4.6: Snapshots of the spins subsequent to a quench from infinite temperature to $\beta = 6$. The configurations correspond to the following times after the quench (from top to bottom): $0N$ (i.e. the infinite temperature configuration), $10N$, 10^2N, 10^3N and 10^4N.

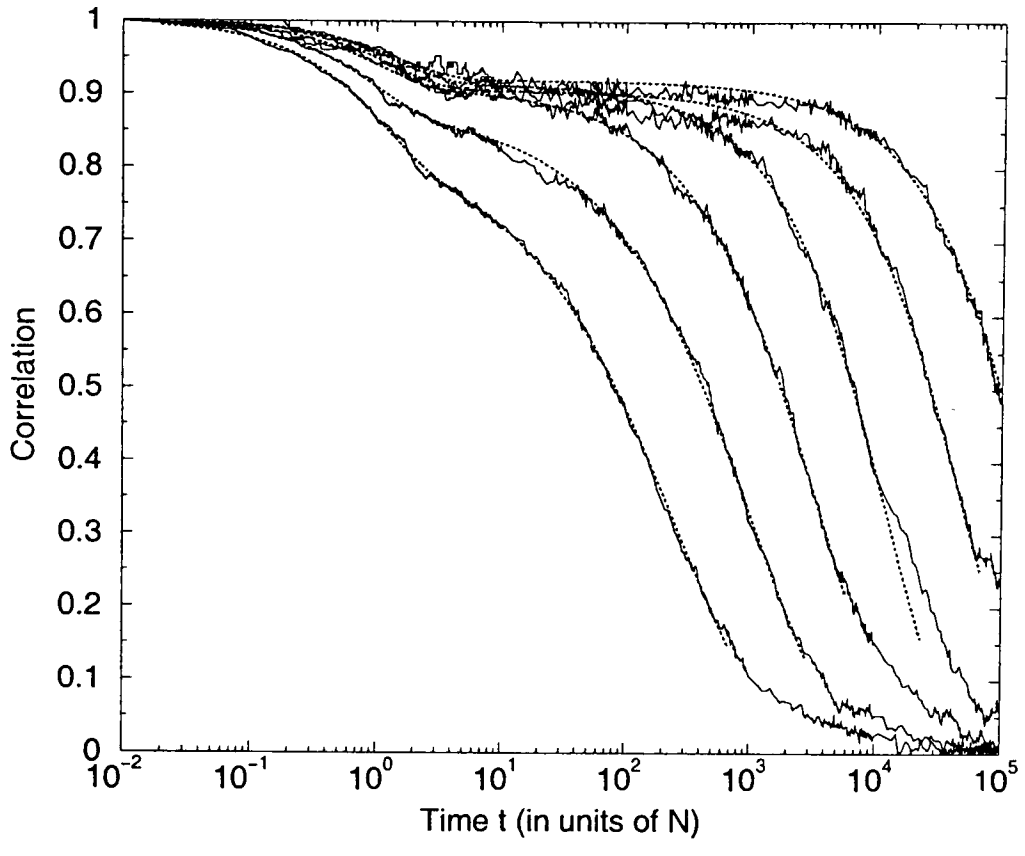

Figure 4.7: The equilibrium correlation functions for, from left to right, $\beta = 3, 3.5, 4, 4.5, 5, 5.5$ (averaged over 3 runs). The dotted lines are fits of the form $C(t) = \alpha\, e^{-t/\tau_1} + (1 - \alpha)\, e^{-(t/\tau_2)^\gamma}$.

in which a spin cannot be flipped until one or more of its neighbours have changed value, while no such complete locking occurs easily in the hexagonal lattice because of the many routes through which a spin can have its value altered. In particular, in this model, lines of like defects develop which can only be removed from the endpoints[1] (shown clearly in Figure 4.6). However, it must be emphasised that it is the *equilibrium* correlation functions that are under investigation, so for very low temperatures the starting configuration will have few defects, and thus very few of these persistent lines will be present. Therefore we expect the power within the stretched exponential, γ, to increase towards 1 as the temperature is decreased.

The parameters τ_1, τ_2, α and γ obtained from the fits are shown in Figure 4.8; the fitting form of Equation 3.3.3 is given in the caption for convenience. These are very similar to the results obtained in the hexagonal model in the $D < 0$ case — thus it seems that the predisposition to jamming, in this case imposed by the geometry of the lattice, gives similar results to the case where the lattice imposes no such predisposition, but the Hamiltonian is chosen such that the background is disordered and produces jamming. As in the latter case, we see that τ_1 is of the order of 1, and an Arrhenius law is obtained for τ_2, although the exponent is closer to 2.5β rather than the value of 2β expected from the energy barrier argument.

For α, we apply the argument used in the hexagonal case to the square geometry to predict that the fraction of defects which are free to move should behave as

[1] The lengths of these persistent lines are not temperature-dependent, although of course the time for which they persist is dependent on temperature.

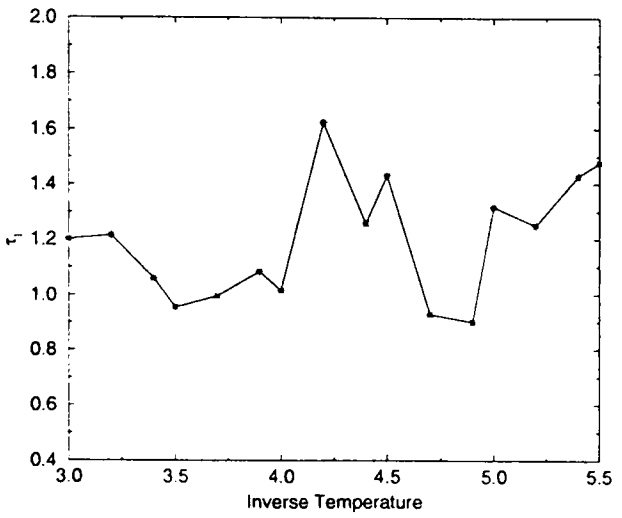

(a) τ_1 against inverse temperature.

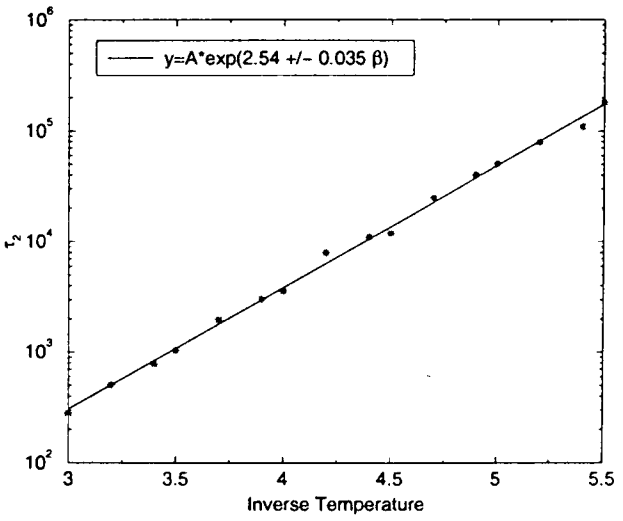

(b) τ_2 against inverse temperature.

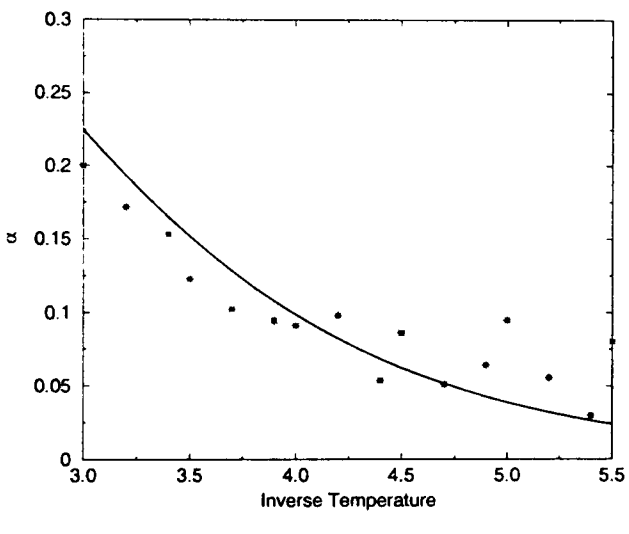

(c) α against inverse temperature. The solid curve is $y = \frac{6e^{-\beta}}{(1+2e^{-\beta})^3}$.

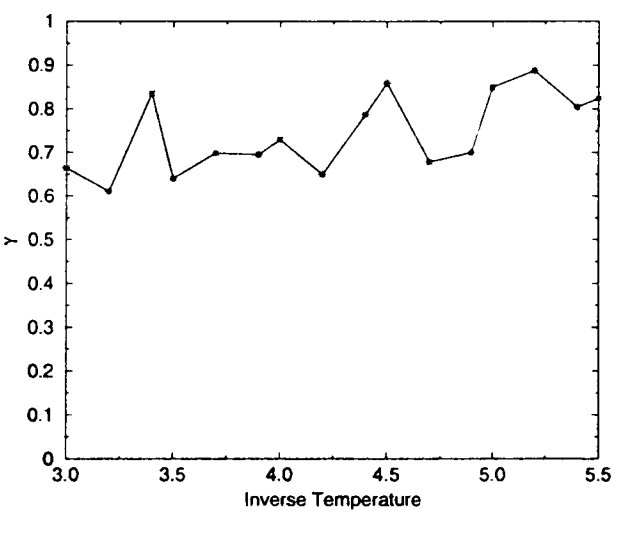

(d) γ against inverse temperature.

Figure 4.8: The behaviour of the fitting parameters $\tau_1, \tau_2, \alpha, \gamma$ with temperature. The parameter data was obtained by fitting the form $C(t) = \alpha\, e^{-t/\tau_1} + (1 - \alpha)\, e^{-(t/\tau_2)^\gamma}$ to the equilibrium correlation functions.

$6p(1)p(0)^2 = 6e^{-\beta}/(1 + 2e^{-\beta})^3$. As Figure 4.8(c) shows, the data is in reasonable agreement with the predicted curve, although the agreement is poorer at lower temperatures (higher β) where fitting is more difficult as the noise of the data is greater. The parameter γ, shown in Figure 4.8(d), increases towards 1 with increasing β as predicted.

4.4 Out of Equilibrium FDT Studies

We shall now present the results from investigations of the non-equilibrium response with regard to FDT, and show that here too there are many similarities to the $D < 0$ 2d hexagonal model. We continue to use the same procedure introduced in Section 3.4, and move directly to a comparison of the FDT plots obtained using

three-state spins $s_i \in \{\pm 1, 0\}$ and those obtained using Ising variables $\sigma_i = \pm 1$. In the former case, we apply the following perturbation to the Hamiltonian at time t_w:

$$\Delta H(t) = h \sum_{i=1}^{N} \epsilon_i s_i(t), \quad t \geqslant t_w$$

and employ these correlation functions and response:

$$C(t+t_w, t_w) = \frac{\sum_{i=1}^{N} s_i(t+t_w) s_i(t)}{\sum_{i=1}^{N} s_i(t+t_w)^2}, \quad R(t+t_w, t_w) = \frac{1}{h} \frac{\sum_{i=1}^{N} -\epsilon_i s_i(t+t_w)}{\sum_{i=1}^{N} s_i(t+t_w)^2} \tag{4.4.1}$$

for which the results are exhibited in Figure 4.9. We see that if the waiting-time is long enough equilibrium FDT is obtained, as shown in the inset of Figure 4.9(a) and in Figure 4.9(d). The waiting-time must be larger than some threshold value for this to occur, and that threshold value is seen to be larger for $\beta = 5$ than for $\beta = 4$ — the inset of Figure 4.9(a) shows equilibrium FDT for $t_w = 10^2 N$ at $\beta = 4$, but that is not obtained until $t_w = 10^4 N$ for $\beta = 5$. Note that, as in the previous two chapters, although the FDT line can be recovered in these cases, the system is not in equilibrium, as the waiting-times are not long enough for equilibration to occur.

Figures 4.9(a), 4.9(b) and 4.9(c) show deviations away from the equilibrium FDT line for short waiting-times, although it appears there is a return to the equilibrium line at long times (i.e. low values of the correlator). Figures 4.9(e) and 4.9(f) show that these deviations cannot be dismissed as the result of initial transients. The origin of the deviation away from the equilibrium relationship are the same as in the $D < 0$ hexagonal case: some dimers are localised (in this case due to the impact of the square geometry) and thus the time-scale upon which they become able to move freely throughout the system is longer than the time-scale upon which they are able to make a contribution to the response. Sometime after a dimer becomes able to move freely, it is likely to be eradicated, which increases the response, but in the meantime the response will be reduced as it will not necessarily rest on favourable sites; note that whilst the dimer has been blocked, the concentration of defects has decreased so it will take longer in any case for it to be removed. The length of time for which this effect can be seen is temperature-dependent because the process of removing the blocking spins is itself temperature-dependent — thus we see that the effect has died out by $t_w = 10^2 N$ for $\beta = 4$ but still persists at that waiting-time for $\beta = 5$.

To implement Ising variables rather than three-state spin variables, we employ the transformation given in Equation (3.4.4), and measure the response as given in Equations (3.4.5) to a perturbation of the form $\Delta E(t) = h \sum_{i=1}^{N} \epsilon_i \sigma_i \theta(t - t_w)$. The correlation function utilised is that given in Equation (3.4.6); again we must stress that this is a disconnected correlation function rather than a connected function. Figure 4.10 shows the FDT plots obtained in this manner. Again we see that there is a clear difference between the curves obtained using the two different procedures.

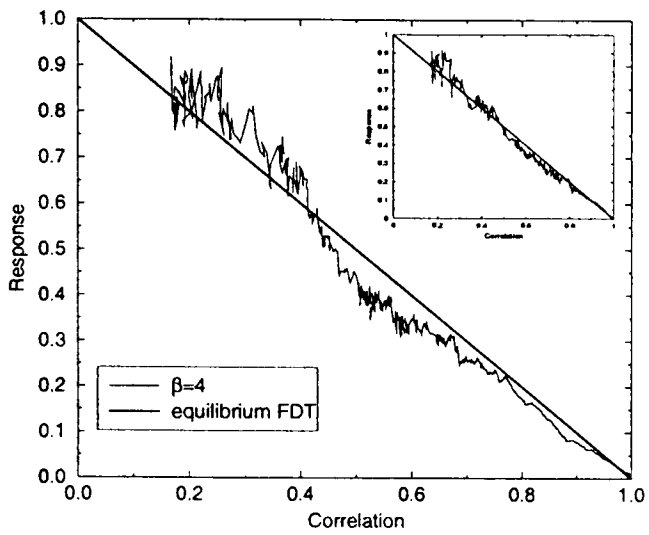

(a) $t_w = 10N$. Inset: $t_w = 10^2 N$.

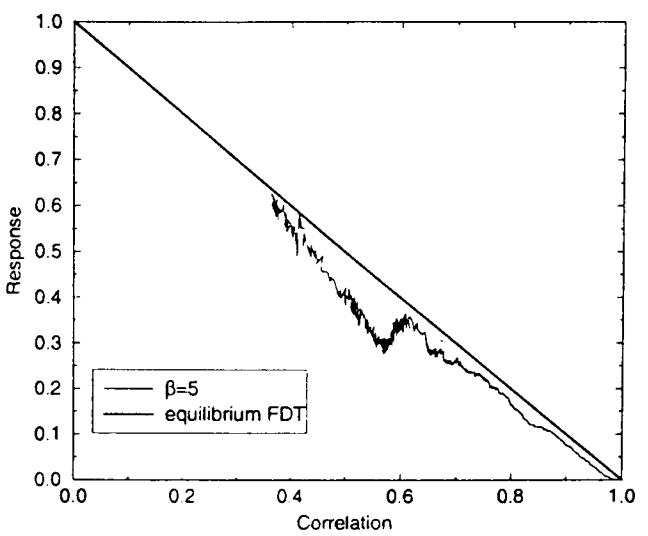

(b) $t_w = 10N$.

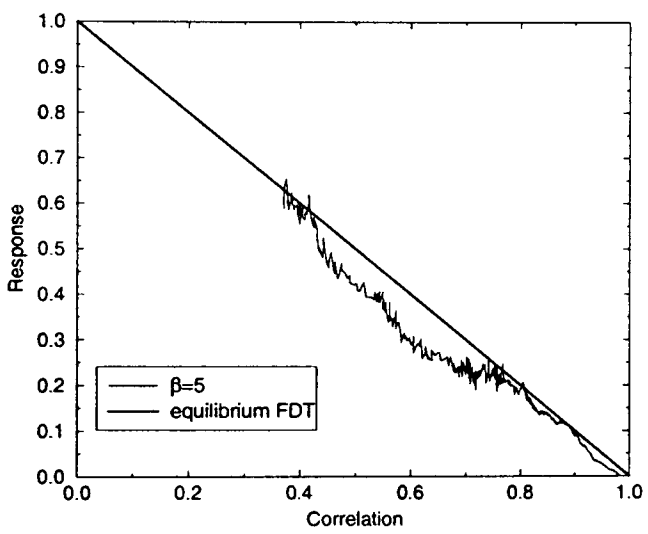

(c) $t_w = 10^2 N$.

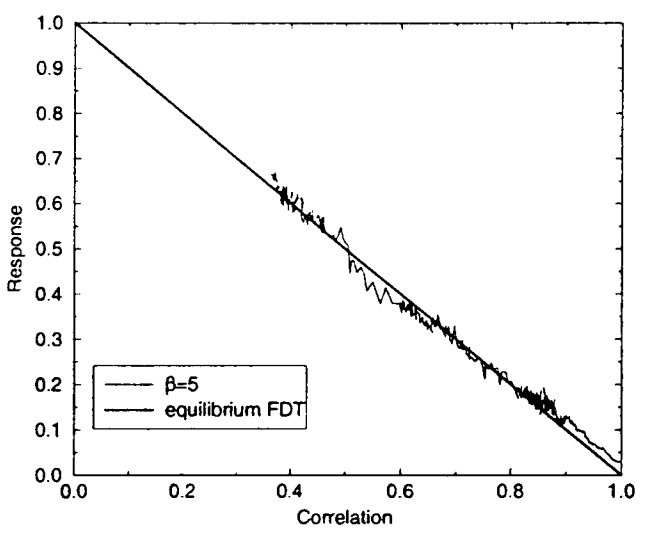

(d) $t_w = 10^4 N$.

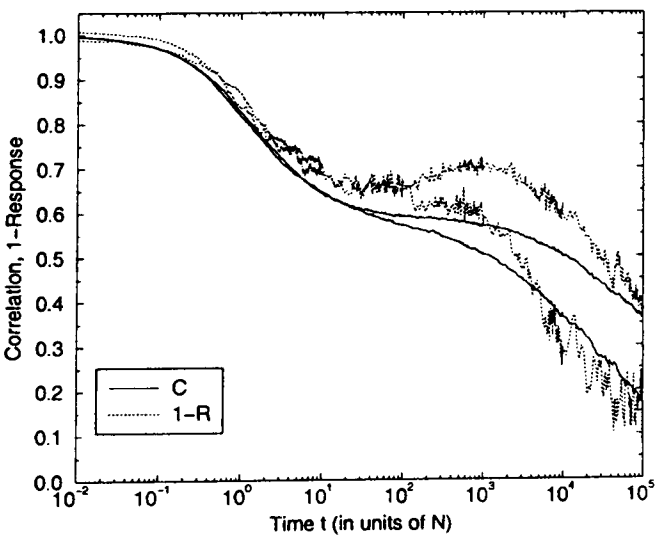

(e) $t_w = 10N$. The lower pair of curves are for $\beta = 4$, and the upper pair for $\beta = 5$.

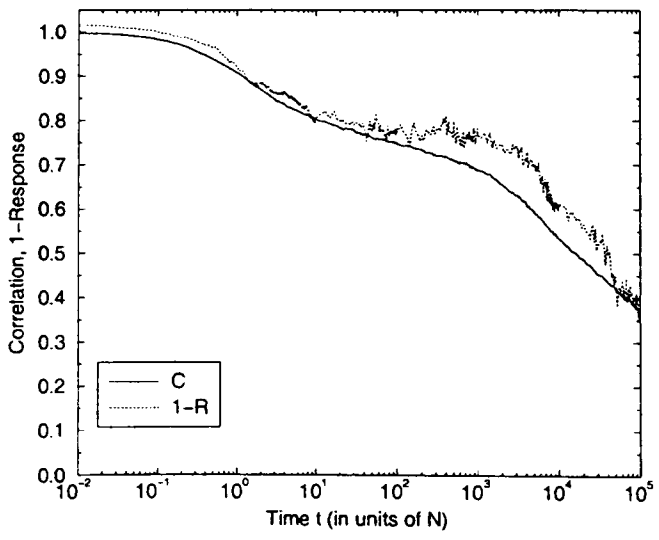

(f) $t_w = 10^2 N$, $\beta = 5$.

Figure 4.9: FDT plots produced using the definitions in Equation 4.4.1, which employ three-state spin variables.

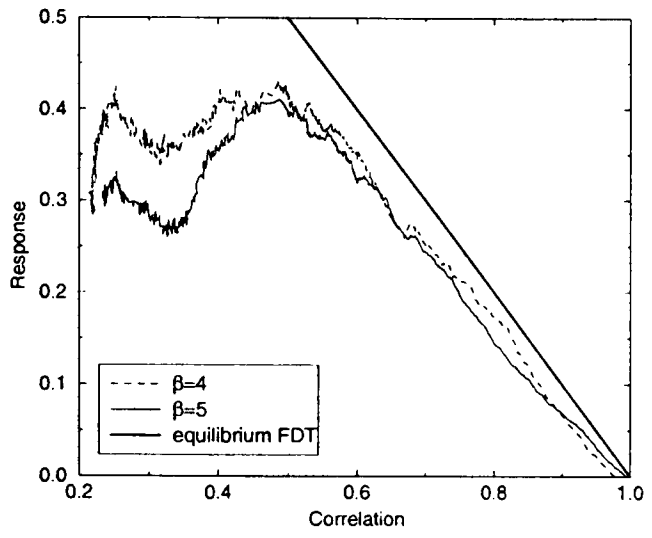

(a) $t_w = 10N$

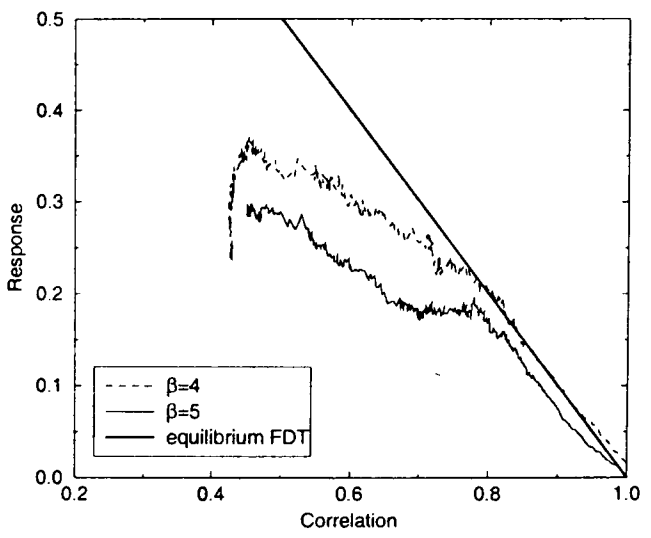

(b) $t_w = 10^2 N$

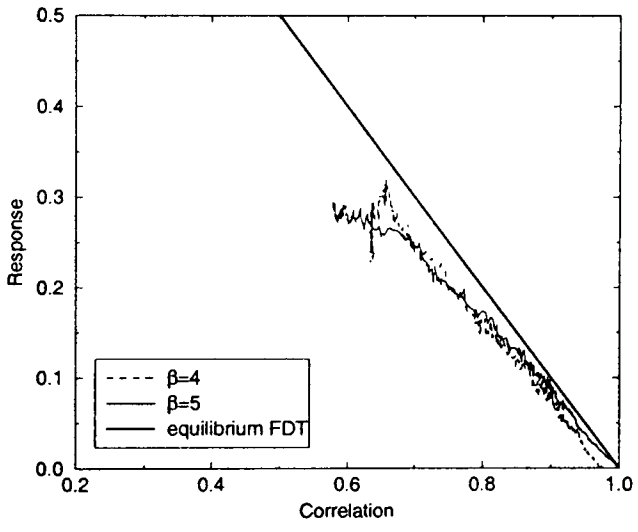

(c) $t_w = 10^4 N$

Figure 4.10: The response and the correlation function plotted parametrically, using Ising variables.

The two humps present in the curves for $t_w = 10N$ are easily related to the arguments presented above, although using this procedure the eradication of defects reduces the response, as well as the placement of defects on unfavourable sites. In both procedures we have seen a clear similarity to the behaviour of the $D < 0$ 2d hexagonal model, from which we deduce that one obtains qualitatively similar results for models of this sort regardless of whether jamming and blocking are introduced explicitly through the Hamiltonian, or implicitly through the geometry of the chosen lattice.

As for the two-dimensional hexagonal model (both D positive and negative), FDT plots obtained using three-state spin variables and a transformation to Ising variables produce entirely dissimilar results. With the three-state variables, one has normalised such that the decay of the energy will not result in a decrease of

the response (in fact, quite the contrary). Thus we can be sure that any non-monotonicity of the response is not simply a manifestation of the energy decay. This is not the case with the Ising variables, and thus the three-state spin variables are preferable for that purpose.

The FDT studies in this chapter and the previous chapters strongly suggests that an equilibrium FDT relationship can always be found for these models by judicial choice of perturbation and observables. The evidence is very convincing for the 2d $D > 0$ square and hexagonal tiling models, although perhaps less so for the $D < 0$ hexagonal model where we would like to perform longer simulations. It seems appropriate to turn our attention to some other kinetically-constrained models to see if we can recover equilibrium FDT in those cases too, and with that aim in mind, we shall now present some results for the SCIC and ACIC models introduced in Section 1.2.

In Section 1.2.1 it was noted that it is conventional with these models to transform from spin variables $v_i = \{0, 1\}$ to Ising spins $\sigma_i = \pm 1$. We shall not perform this transformation. We shall apply the same perturbation as in Section 1.2.1, namely $\Delta H = -h \sum_{i=1}^{N} \epsilon_i v_i(t)$, but we shall look at the following integrated response function and correlation function:

$$R(t + t_w, t_w) = \frac{-1 \sum_{i=1}^{N} \epsilon_i \left(1 - v_i(t + t_w)\right)}{\sum_{i=1}^{N} \left(1 - v_i(t + t_w)\right)^2} \tag{4.4.2}$$

$$C(t + t_w, t_w) = \frac{\sum_{i=1}^{N} \left(1 - v_i(t + t_w)\right) \left(1 - v_i(t_w)\right)}{\sum_{i=1}^{N} \left(1 - v_i(t + t_w)\right)^2} \tag{4.4.3}$$

Again we would like to point out that this is a disconnected rather than connected correlation function. Note also that instead of concentrating on the absorbing state of $v_i = 1$, these functions focus on the defect spins ($v_i = 0$), as we have been doing so far with the 2d hexagonal and square-based models. Up-spins make no contribution to either the response or the correlation function. We choose to focus on the defects because there are always enough favourably-charged sites for the defects to rest upon. If the majority spin (i.e. spin-up in this case) is used instead, the response can decrease as a direct manifestation of the energy relaxing towards equilibrium — as down-spins relax they will be unable to find any free favourable sites and thus will make a negative contribution to the response. We would like to avoid any such non-monotonicity occurring as a direct consequence of the energy relaxation.

The results of performing this procedure on the SCIC are shown in Figures 4.11(a) and 4.11(b); for comparison, we remind the reader that the standard plots are shown in Figure 1.6. It seems that equilibrium FDT is upheld for all the curves shown until low values of the correlator at which point a sudden dramatic increase is observed. This is because the correlation function settles at a non-zero whilst the response function is continuing to increase; this is likely to be a result of using the disconnected rather than connected form for the correlation function, and we suggest further work should be undertaken with the latter form. Nonetheless, it does appear

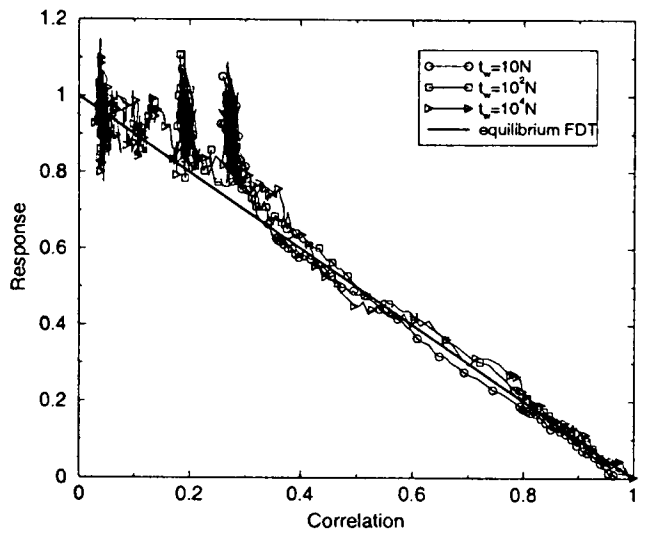

(a) SCIC: $\beta = 3$.

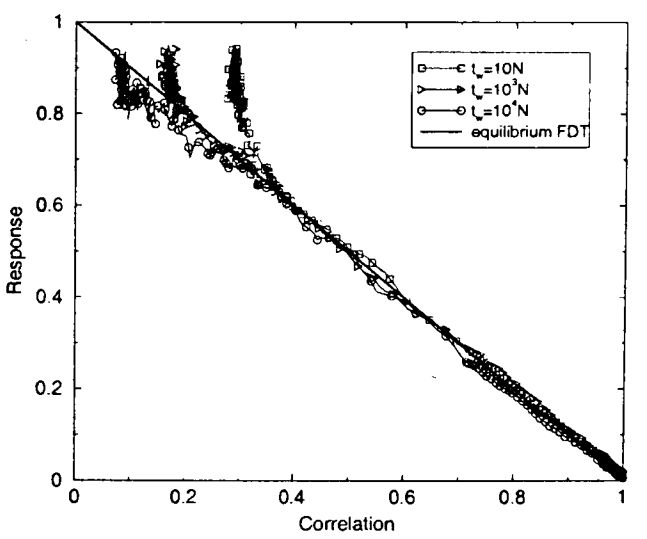

(b) SCIC: $\beta = 5$.

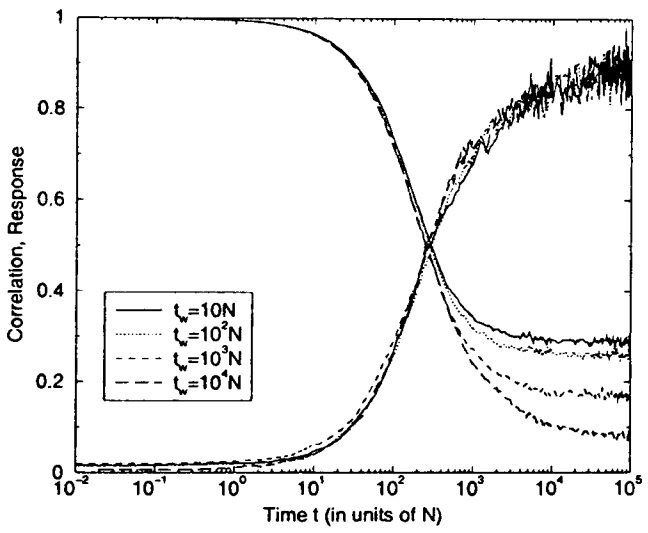

(c) SCIC: $\beta = 5$. The curves beginning at 1 on the y-axis are the correlation functions, and those beginning at 0 are the response functions.

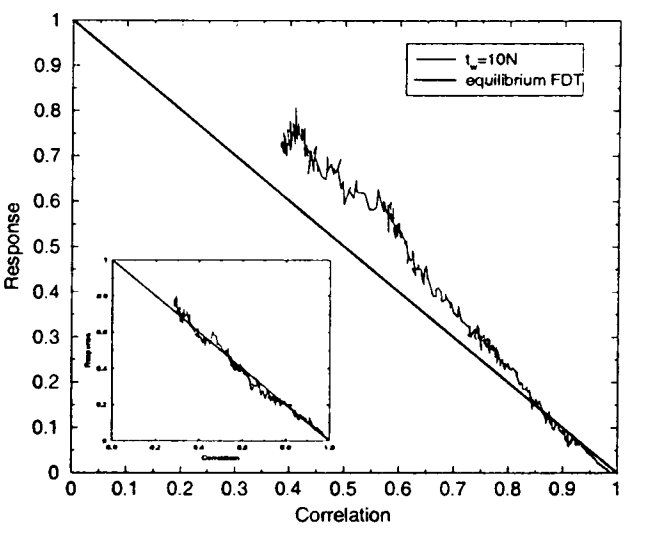

(d) ACIC: $\beta = 2.5$, $t_w = 10N$. Inset: $\beta = 2.5$, $t_w = 10^3 N$.

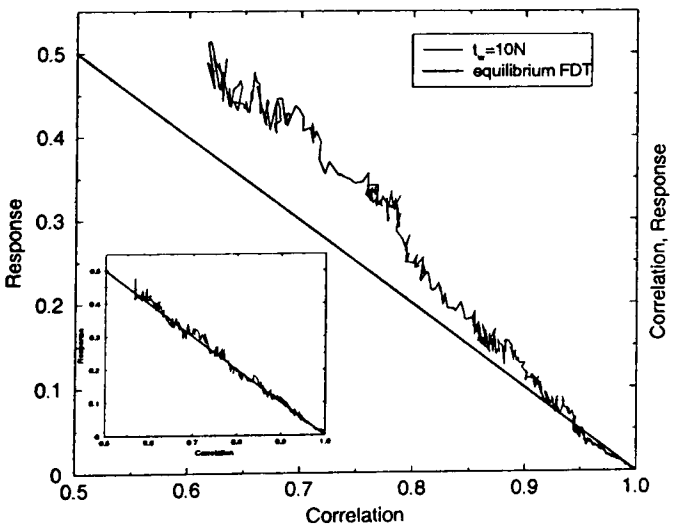

(e) ACIC: $\beta = 3$, $t_w = 10N$. Inset: $\beta = 3$, $t_w = 10^3 N$.

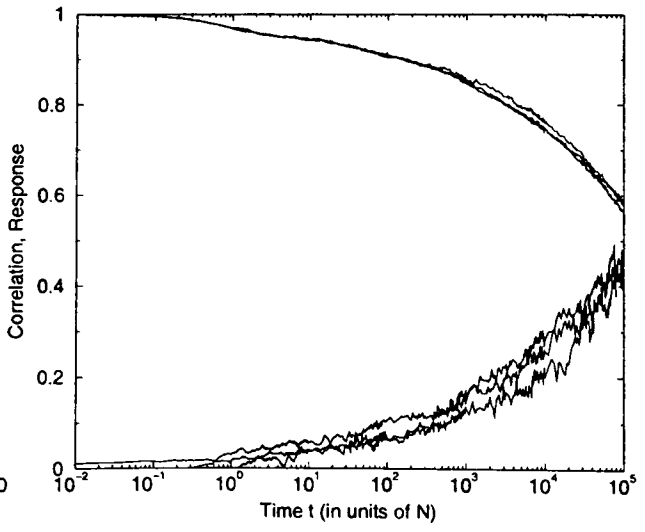

(g) ACIC: $\beta = 3$. The curves beginning at 1 on the y-axis are the correlators, whereas the response begins at 0. From bottom response curve to top, $t_w = 10^2 N, 10^3 N, 10^4 N$.

Figure 4.11: FDT studies on the SCIC and ACIC. In all cases the results are averaged over 10 realisations of the charge distribution.

that on the whole we are able to 'fix' the FDT plots such that equilibrium FDT is obtained initially, but for longer times, we see a significant departure. The actual point at which that departure occurs is dependent on the waiting-time, and occurs at lower values of the correlator for longer waiting-times. This can be seen clearly if we look at the correlation functions and the response against time, as shown in Figure 4.11(c); it becomes clear that this approach has completely removed any waiting-time dependence from the response function, and the correlation function only contains waiting-time dependence for $t > 10^3 N$, through the final value at which it settles. Thus it seems that only the correlation function carries information about the status of the system with regard to equilibrium; we feel that this is a result of incorrect choice of correlator, and that with the correct choice FDT will be upheld throughout, but further simulations will be necessary to provide more evidence for that.

The results for the asymmetrically-constrained chains are shown in Figures 4.11(d) and 4.11(e). For short t_w we see initial deviation from the equilibrium FDT line, but for $t_w \geqslant 10^3$ FDT is recovered. We would have liked to access longer times (i.e. lower values of the correlator) to ensure there is no subsequent deviation, and we suggest that further work is required on this point. Figure 4.11(g) shows the correlation and response functions against time: there does not appear to be any waiting-time dependence in the correlation functions, and for the response there is little difference between the curves for $t_w \geqslant 10^3 N$. Thus it appears that for the ACIC this approach has removed the waiting-time dependence in both the response and the correlation functions, provided the waiting-time exceeds a certain threshold value. However, we would like to stress that longer simulations must be undertaken, again with the correct choice of correlator, to ensure there is no subsequent departure from equilibrium FDT, as can be clearly seen in the SCIC case. In addition, the temperatures investigated for the asymmetric case are lower than those at which the clear staircase shape develops in the energy decay (see Figure 1.8) and thus we are not currently probing the deeply activated regime. To probe that regime would be highly computer-time intensive as the correlation and response functions relevant to our approach drop very slowly and therefore it would take an extremely long time to obtain adequate data on the parametric plot.

4.5 Conclusions

In this chapter we have tried to establish to what extent the geometry of the underlying lattice influences the behaviour observed. We have studied a model with the same Hamiltonian and equivalent dynamics to the $D > 0$ two-dimensional hexagonal model of Section 3.2.1, but based on a square lattice. It was found that although the behaviour of the energy decay is extremely similar to that of the $D > 0$ hexagonal model, the correlation functions and FDT plots are more in keeping with that of the $D < 0$ two-dimensional hexagonal model. From this we conclude that the geometry of the lattice can have a large impact on the behaviour of these models.

We have found that the energy decay can be well-fitted with the sum of two power laws, with the exponent of the first power law providing further support for the classification of this early behaviour into the reaction-diffusion description $A+A+A \rightarrow A$. The second power law is somewhat slower than would be predicted by an $A + B \rightarrow \emptyset$ behaviour; the exponent observed is extremely close to that obtained in the $D > 0$ hexagonal model — as in that case, the slower-than-predicted behaviour is due to clustering of like defects. In the square tiling model, the defects can easily become pinned into lines which persist for a long time; one can see these lines if the spin configurations are observed at various times throughout the simulations.

The correlation functions follow the same form as in the $D < 0$ hexagonal case, and the parameters obtained from such a fit can be explained using the same arguments. The FDT plots also take a similar form, and are subject to the same arguments in describing the results.

As with the two-dimensional hexagonal model (both D positive and negative), FDT plots obtained using three-state spin variables and a transformation to Ising variables produce entirely dissimilar results. With the three-state variables, one has normalised such that the decay of the energy will not result in a decrease of the response (in fact, quite the contrary). Thus we can be sure that any non-monotonicity of the response is not simply a manifestation of the energy decay. This is not the case with the Ising variables. As a result, FDT plots performed with three-state spin variables are in these models preferable as one wishes to see something other than the influence of the energy decay within the FDT plot.

We also extended our FDT investigations to two other kinetically-constrained models, the ACIC and SCIC introduced in Chapter 1. By choosing to apply a perturbation to the Hamiltonian that depends on the defect spins rather than on the majority spins, and measuring the appropriate correlation and response functions, we obtained different FDT plots to the standard results presented in Chapter 1. For the SCIC, equilibrium FDT was upheld until the point at which the correlation function settled at a finite, non-zero value, although this deviation might be removed by utilising a connected correlation function. For the ACIC, no deviations from equilibrium FDT were observed provided the waiting-time exceeded a certain threshold value, although much longer simulations must be undertaken to ensure there are no deviations at later times. These studies suggest that more thought must be devoted to the correct procedure with regard to out of equilibrium FDT investigations; in the meantime we suggest that FDT results be treated with some caution.

Chapter 5

3d Spin Model

It is not difficult to formulate a three-dimensional version of the 2d hexagonal spin model, as we shall show, but given that 3d simulations are generally more unwieldy and computer-intensive, we find that we are unable to extract any information about the slower time-scale through these simulations. Nonetheless, this still proves to be a useful exercise in consolidating our ideas, as we shall show.

The reader may wonder why we have not chosen to extend the work on the purely topological foam into three dimensions. Although the three dimensional equivalent to the T1 move is the WWW move (shown in Figure 2.1 and discussed in Section 2.1), one cannot see an obvious variable to track whilst maintaining the minimalistic ethos. One requires a fool-proof method of identifying faces or volumes in a non-ambiguous way, but even in a perfect diamond structure it can be difficult to do so. Those ambiguities are magnified once the structure is distorted by WWW moves, making a three-dimensional analogue to the 2d topological foam a very difficult enterprise.

5.1 The Model

The lattice we have chosen to use for this three dimensional extension is the underlying basis of the diamond lattice (see Figure 5.1), the face-centered cubic (fcc) lattice. This is most easily visualized in terms of close-packed spheres, as shown in Figure 5.2. Notice that any two adjacent cells together define three planes which contain both of these cells.

We take this structure and place a spin $s_i = \{\pm 1, 0\}$ at the centre of each sphere/cell. Thus any one plane is exactly equivalent to the two dimensional spin model — a network of spins has been obtained, each with six neighbours, arranged in a hexagonal lattice. Considering the 3d structure as a whole, any one cell has a total of 12 neighbours (see Figure 5.2: any cell A has 6 neighbouring A's in the horizontal plane it is part of, 3 neighbouring B's in the plane above and 3 neighbouring C's in the plane below). Once again we proceed by defining the energy of the system to be $E = D\sum_{i=1}^{N} s_i^2$ (we shall take $D = 1$). We choose a potential plaquette

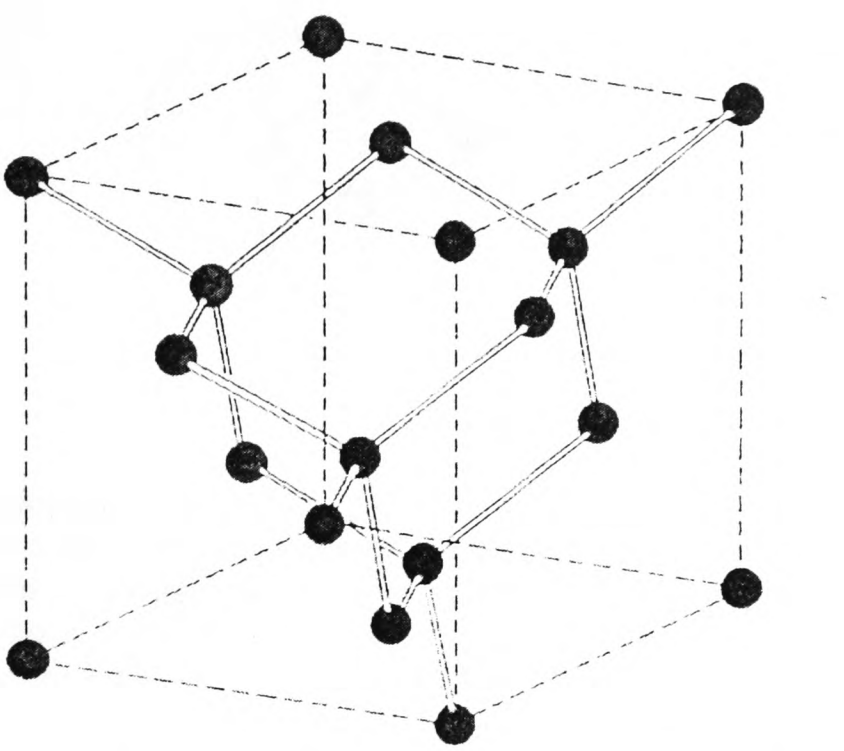

Figure 5.1: The crystal structure of diamond, showing the tetrahedral bonds between the carbon atoms. The space lattice of diamond is face-centered cubic, with a primitive basis of two identical atoms at $000;\frac{1}{4}\frac{1}{4}\frac{1}{4}$.

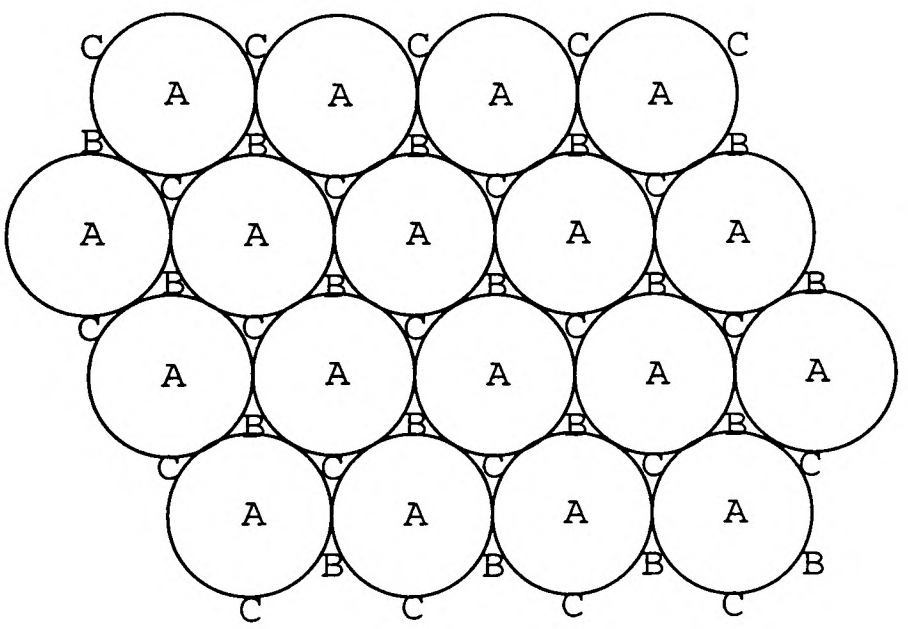

Figure 5.2: Close-packed layers of spheres in the face-centered cubic structure. The first layer have their centres marked with an A. Above that another layer is added with the centre of the spheres at points B. The third layer is laid above that, with the centres at C, and this process is repeated in sequence $ABCABCABCABCA...$

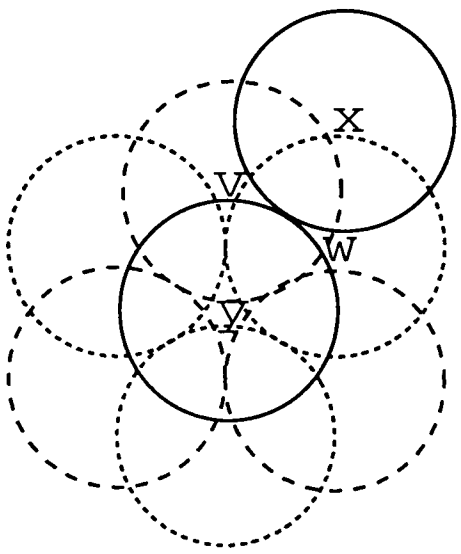

Figure 5.3: An example of choosing a plaquette as a candidate for spin-flipping. Cell y, shown with a solid line, is chosen randomly, and then two of its neighbours, v and w, are chosen. v happens to be in the layer above, where spheres are shown by dashed lines, and w is in the layer below, where spheres are denoted by dotted lines. x is the only cell which is both a neighbour of v and w and coplanar to y, v, w.

for spin-flipping as follows (see Figure 5.3 for clarification): a cell y is chosen at random, and then two of its neighbours (v and x) are randomly selected, with the only constraint being that the three cells cannot be colinear. The fourth cell w of the plaquette is then uniquely defined by enforcing the condition that it must be coplanar with all three cells, and a neighbour of both v and x — there is only one cell other than y that will satisfy this condition. We add in passing that the results differ negligibly if one does not enforce the condition that the 4 chosen cells be coplanar and instead chooses three coplanar cells which are all neighbours of each other, and then chooses as the fourth cell the only remaining cell which is also a neighbour to the other three (i.e. choosing a tetrahedral structure every time).

With the plaquette chosen, the procedure is then exactly the same as in the two-dimensional case. One chooses randomly to attempt to increase or decrease by one unit the spins s_w and s_y, with a corresponding decrease/increase to spins s_v, s_x. Choosing to increase s_w, s_y would give a potential energy change as given in Equation (3.1.3); the probability of actually carrying out this move is given by Equation (3.1.4).

The system size in these simulations is $N = 8400$, and periodic boundary conditions are exercised.

5.2 Dynamics

As one expects the three-dimensional system to be less jammed than either of the two-dimensional models (hexagonally-based or square-based) with $D > 0$, we do not proceed directly to an investigation of the temporal behaviour of the energy density, but first investigate the temperature region within which we might expect to find two-step relaxation. We do this initially by performing a cooling rate sim-

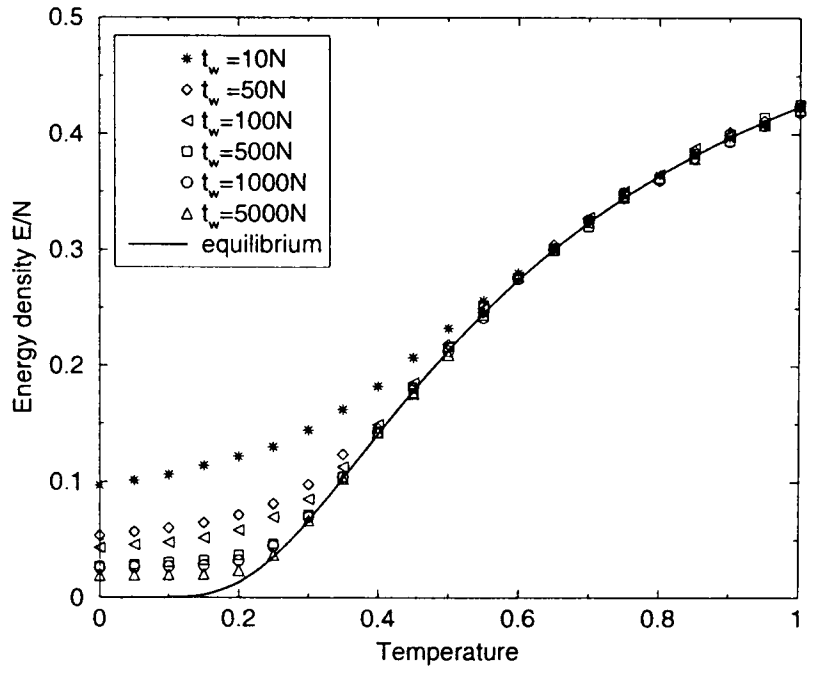

(a) The energy density with temperature. The system was in equilibrium at $\beta = 1$, and then cooled by waiting a time t_w after each temperature decrement of $\delta T = 0.05$.

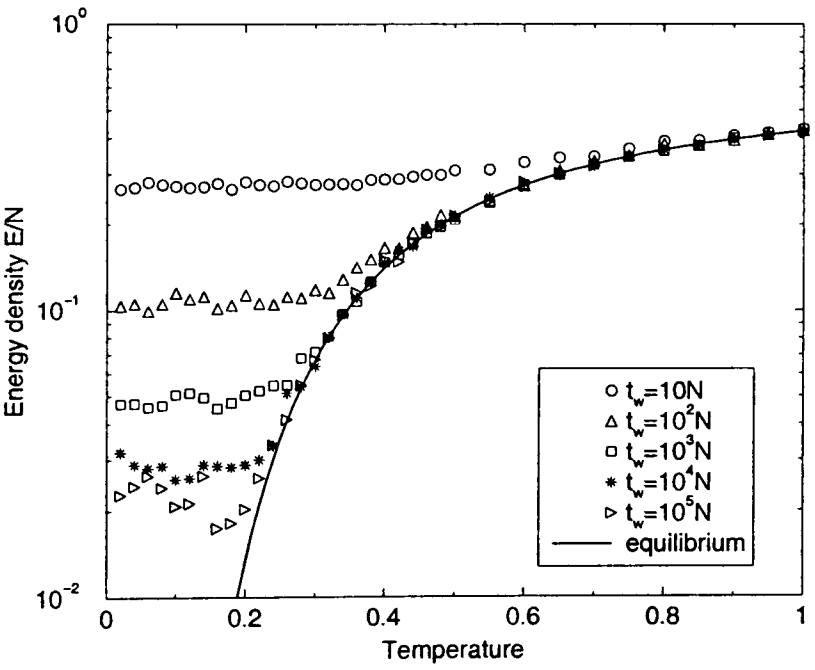

(b) The energy density, E/N, measured at time t_w subsequent to a rapid quench from $\beta = 0$.

Figure 5.4: The energy density for both cooling and rapidly quenching.

ulation, the results of which are shown in Figure 5.4(a). We see the typical glassy signature, with the system unable to reach equilibrium at the slowest cooling rate; the equilibrium curve is given by Equation (3.2.1). Note, however, as expected the temperatures at which this effect comes into play are considerably lower than in the two-dimensional case (Figure 3.2(a)); the 3d system possesses far more routes to relaxation. Correspondingly, we would expect a 1d system to have difficulty

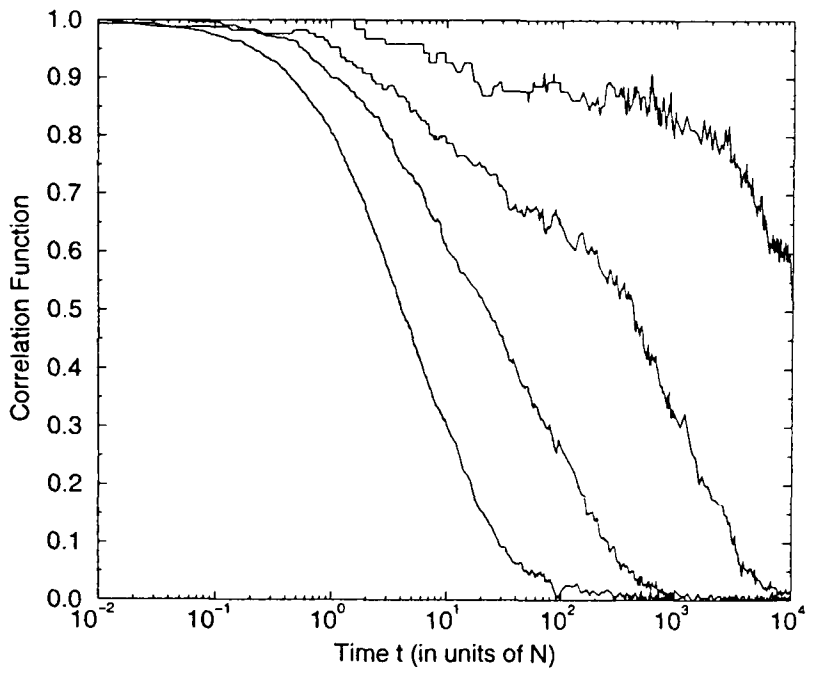

Figure 5.5: The equilibrium correlation functions for, from left to right, $\beta = 3, 4, 5$ and 6.

relaxing at much higher temperatures.

If we instead subject the system at infinite temperature to a rapid quench in order to look for the signature of activated processes (as displayed very clearly in Figures 3.2(b) and 3.22(b)), we find it difficult to show clear evidence for these processes, as one cannot feasibly run the simulations for long enough. One can see a dip developing in the data (see Figure 5.4(b)) from the longest wait-times ($t_w = 10^5$) which would deepen if one were to run for even longer wait-times, but there is no advantage to be gained from such an operation.

These two Figures, 5.4(a) and 5.4(b), show that it is extremely difficult to probe the activated regime in this three-dimensional model. One has to go to very low temperatures and wait for very long times before one finds the intermediate plateau. This makes it infeasible to investigate this system in the regime of the second time-scale, where one has slow temperature-dependent relaxation. Thus we shall limit ourselves to a discussion of the behaviour of the energy density on the fast, temperature-independent time-scale. As far as the correlation functions are concerned, although one can of course directly access an equilibrium configuration and thus measure the equilibrium correlation function $C(t)$ as given in Equation (3.2.4), one cannot obtain reasonable data at the temperatures of real interest, where the plateau begins to develop. This is because these temperatures are extremely low so the system contains very few defects and the correlation function is extremely noisy, as shown in Figure 5.5. Therefore we shall make no attempt to fit this data in any way, and merely comment that one again sees the familiar two-step relaxation.

Figure 5.6(a) shows the behaviour of the energy density subsequent to a quench from infinite temperature. Our understanding of the initial decay is that it falls into the class of annihilation-diffusion models described by the reaction scheme $A + A + A \to A$, for which the asymptotic behaviour of the energy density should

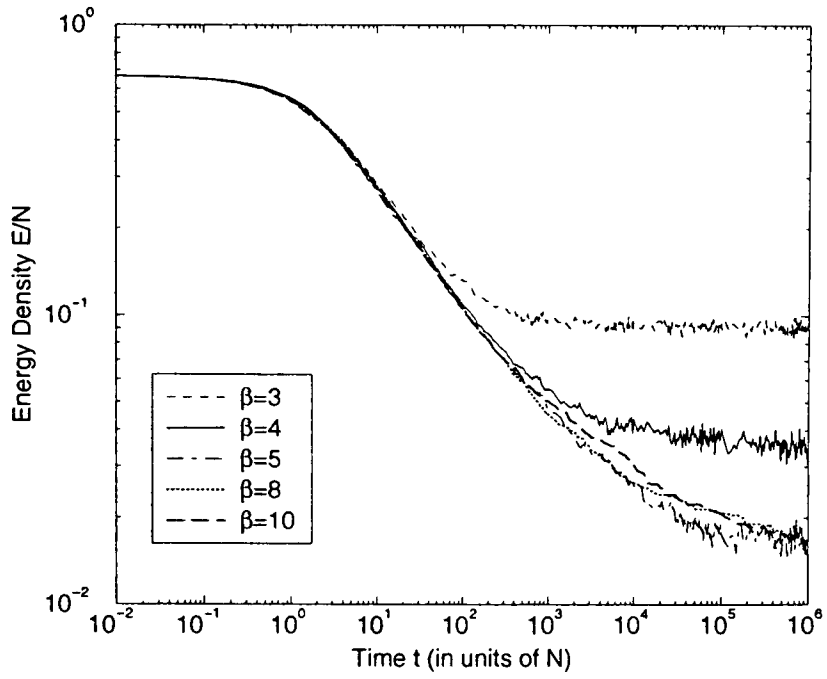

(a) The energy density for various temperatures.

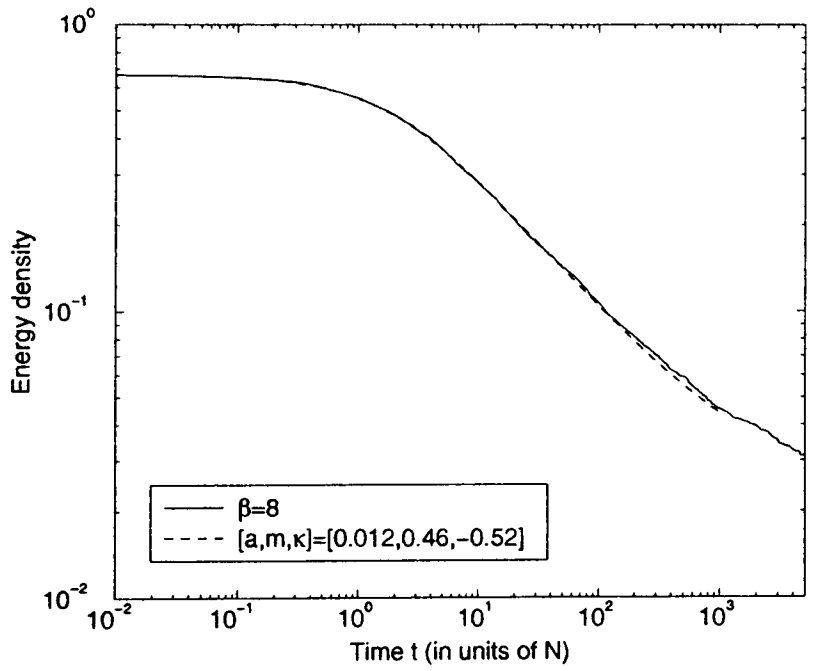

(b) A power law fit to the energy density of the form of Equation (5.2.1).

Figure 5.6: The energy density, subsequent to a quench from $T = \infty$.

be that of $t^{-0.5}$ in two dimensions and above, and thus we expect to fit this data with the following form:

$$\frac{E}{N} = (\frac{2}{3} - a)(1 + mt)^{\kappa} + a \tag{5.2.1}$$

where a, m, κ are all parameters to be fitted, although we would predict from previous discussion and data that $m \sim 0.5$ and $\kappa \sim -0.5$. We also expect a to be very small as the plateau occurs at a very low value in this model.

As we are trying to fit the initial behaviour, which is temperature-independent, it is immaterial which temperature we choose as we shall truncate the data in any case (provided, that is, the energy density does not equilibrate or come close to doing so within the range we shall be fitting to). Figure 5.6(b) shows the results of such a fit; it is clear that this power law fits the data over at least three decades. The parameters m, κ are also very close to our predicted values, providing further evidence that these systems have a short-time behaviour which can be described by the reaction-diffusion scheme $A + A + A \rightarrow A$, where the A's represent defects. As mentioned before, this behaviour may be modified at intermediate times (i.e. very close to the onset of the plateau) as the system may be better described by $A + B \rightarrow A$, where the A's are defects behaving as static traps, and the B's are dimers, but we cannot adequately investigate this conjecture, and merely wish to remind the reader of the complexity present within these models.

5.3 Conclusions

In summary, although this three-dimensional model has proved unwieldy and unsuitable for extensive analysis, it serves to further support the hypotheses we wish to investigate with regards to these models. On a qualitative note, we see the two-step relaxation in both the energy density and the correlation functions, although the temperature at which activation becomes important is very low in this model. Quantitatively, we provide further compelling evidence for the $A + A + A \rightarrow A$ scenario in the initial decay of the energy. This has been a particularly important check, as other theories could provide in 2d a $t^{-0.5}$ dependence in the asymptotic behaviour of the energy decay. One example of this is $A + B \rightarrow \emptyset$; however such a theory would predict dimensional-dependence in the first decay. We do not observe any such dependence, and conclude that $A + A + A \rightarrow A$ is indeed the correct reaction scheme for the early regime of these models.

We wish to add that one can also produce a one-dimensional version of this model, which retains the key features of facilitated diffusion, and dimer absorption/creation. We shall not present those results here as they are qualitatively very similar to those of the 2d square lattice model and the $D < 0$ hexagonal model, and do not significantly add to our understanding of these models. In particular, the form of the energy decay is still in keeping with the $A + A + A \rightarrow A$ classification for the early region, and slightly slower than the $t^{-1/4}$ behaviour predicted by an $A + B \rightarrow \emptyset$ theory for the slow temperature-dependent decay.

Chapter 6

Closing Remarks

We shall now give a brief summary of the results presented in the preceding chapters, before concluding with a short discussion on some suggestions for further work.

In this thesis we have presented results for several related models which display glassy behaviour. This research was motivated by the desire to produce a very simple model which nonetheless exhibits the signatures of glassiness. Despite the simplicity of the models discussed, we have observed rich and complex behaviour.

In Chapter 2 we studied a 2d topological froth with a non-interacting Hamiltonian which was allowed to evolve through Glauber-Kawasaki dynamics. This showed the characteristic glassy dependence of the energy on the cooling-rate, and even at the slowest cooling rate employed, equilibrium was not attained for low temperatures. We also observed two-step relaxation in both the energy decay and the correlation functions, and aging effects for non-equilibrium correlation functions. Several predictions of Mode-coupling Theory (MCT) were tested and although some agreement was found, there was no convincing evidence that a mode-coupling critical temperature could be ascribed to this system as the relaxation times fitted most closely to an offset Arrhenius law (typical of strong glasses). Thus we conclude that MCT does not appear to be the most fitting description of this system within the temperature regime investigated. Investigation of the Fluctuation-Dissipation Theorem (FDT) for non-equilibrium conditions revealed an interesting result: no deviation from the equilibrium relation was observed for waiting-times exceeding a certain threshold value, despite the fact that the system was clearly out of equilibrium.

In keeping with the ethos of minimalism, we further simplified the topological froth model to a two-dimensional hexagonally-based spin model. In Chapter 3 we studied two versions of this model — one with a unique absorbing ground state ($D > 0$) and the other with a highly degenerate disordered ground state ($D < 0$). Both models displayed the same features as the topological froth, i.e. dependence of the energy on the rate of cooling, two-step relaxation in the energy and the correlation functions, and aging in the non-equilibrium correlation functions. However, these models possess a distinct advantage over the topological froth in that the equilibrium states can be directly accessed and thus we were able to probe the behaviour more deeply. The first time-scale was found to be temperature-independent, whilst the

second was an exponential function of inverse temperature. These time-scales could be directly ascribed to different processes within the system. It was hypothesised that the early temperature-independent relaxation of the energy could be classified under the reaction-diffusion scheme $A + A + A \rightarrow A$, and fits of that region of the energy decay supported the hypothesis for both models. It was suggested that the second temperature-dependent decay was due to two-particle annihilation processes, although in both versions of the model the observed decay was somewhat slower than would be predicted by these classifications. For the $D > 0$ model, this was most likely due to clustering of defects whilst for $D < 0$, it was undoubtably due to the hindering effect of the disordered background. In the former case, one could fit the correlation functions with the sum of two exponentials, and the fitting parameters agreed well with a naïve theory of the behaviour of the system. For the model with the disordered background ($D < 0$), an exponential plus a stretched exponential was found to fit better — this was ascribed to blocking of the defects. In both models, studies of the overlap in equilibrium supported the proposed functional form of the correlation functions. It was also established that these models fall into the Type II (glassy) classification rather than Type I (coarsening).

FDT studies for $D > 0$ also yielded the equilibrium relation despite the fact that the system had not reached equilibrium. For $D < 0$ the results were less conclusive, as the disordered background led to some marked deviations from the equilibrium FDT relationship for shorter waiting-times, although one could tentatively suggest that equilibrium FDT was recovered for much longer waiting times (but still shorter than the equilibration time of the system). The waiting-time at which the deviations were no longer observed appeared to increase with decreasing temperature. We also applied a transformation from three-state spin variables to Ising spins to the $D > 0$ model, and observed FDT plots with completely different shapes, which could nontheless be understood with reference to the influence of the decaying energy.

In order to establish the influence of the lattice geometry in Chapter 4 we studied a spin model on a square lattice with the same non-interacting Hamiltonian and four-spin-flip rule, and a unique absorbing ground state. The lattice geometry was found to have a strong influence on the behaviour as it was easier for defects to become blocked than in the equivalent hexagonal case. As a result the behaviour observed was very similar to that of the hexagonal $D < 0$ model, where the jamming was provided by the disordered background rather than the lattice geometry.

The FDT results for this square-based model also had some similarity to the $D < 0$ model, with deviations from the equilibrium relationship observed for short waiting-times; again, the persistence of this effect was temperature-dependent. Above a threshold value, equilibrium FDT was clearly recovered. The approach employed throughout these FDT studies was to focus on the defect variables rather than the majority spins, and we then applied this approach to two kinetically-constrained models, the symmetrically-constrained (SCIC) and asymmetrically-constrained (ACIC) Ising chains. For the former, this approach yielded FDT plots which followed the equilibrium line up until the point at which the correlation func-

tion settled. It also completely removed all waiting-time dependence from the response, and restricted the waiting-time dependence within the correlation function to the value at which it settled. For the ACIC, the equilibrium FDT relationship was recovered above a threshold waiting-time, although longer simulations would be required to ensure there was no subsequent breaking of FDT. In addition, the simulations were performed using disconnected correlation functions, and therefore further work is required involving the use of the connected function.

An extension to three dimensions of the three-state models with constrained dynamics was investigated in Chapter 5 with regard to the energy decay, and reinforced the $A + A + A \rightarrow A$ classification. Studies of other features were deemed infeasible as this model was more computer-time intensive.

To summarise briefly, we have introduced models of increasing simplicity which nonetheless exhibit rich and complex behaviour on a microscopic level and glassy behaviour on a macroscopic level. We have succeeded in classifying the underlying processes within a reaction-diffusion framework. We have also investigated the Fluctuation-Dissipation Theorem out of equilibrium in these, and other, models; we find that under certain conditions the equilibrium relation can be recovered, a point which is deserving of much further study.

With regards to further work, our approach so far has been to perform successive iterations on the original topological froth model to further simplify it. Two essential features have emerged as necessary to retain the characteristic glassy behaviour with two-step relaxation: facilitated diffusion (i.e. diffusion is only possible for a particle if it has a neighbouring particle of the correct type) and a three particle annihilation process which leaves a single particle. With these features incorporated one finds two-step relaxation because activation has been implicitly introduced — isolated particles must either create or absorb a pair in order to move. Thus one could study a reaction-diffusion model of the type:

$$A + A + A \rightleftharpoons A$$

with a forward reaction rate of unity, and a reverse reaction rate proportional to $e^{-\beta}$, and one would obtain qualitatively similar results, *provided the diffusion was facilitated.* We suggest further investigation into such models, with a view to developing a full analytic theory.

The model upon the square lattice could be further simplified by considering instead a square-based system with Ising spins, and energy $E = \sum_{i=1}^{N} s_i$, such that the ground state is $s_i = -1, \forall i$. If one then used the Metropolis algorithm and chose to flip all four spins around a vertex, the features of free dimer (defect-pair) diffusion and dimer absorption/creation would be reproduced. As this model would not conserve the total magnetization, it would be interesting to see to what extent the results differed from those presented in Chapter 4. This model can be directly mapped to a two-dimensional Ising model with the plaquette interaction and single spin-flips [70,71], a connection which is deserving of further investigation.

Alternatively, one could retain the three-state feature and the same Hamiltonian used throughout this thesis, but instead of taking D to be uniform across the entire system, ascribe quenched values D_i to each cell. Thus the energy barriers would no longer take a single value but would vary, which would likely result in a different and exciting behaviour.

Through this thesis much attention has been paid to out of equilibrium investigations of the Fluctuation-Dissipation Theorem. We have shown that different FDT plots can be obtained through different approaches, and through focusing on the defect variables we have succeeded in reproducing equilibrium FDT in almost all the models investigated. We suggest further work on this, as it may be possible to find an approach in which one investigates degrees of freedom which are in quasi-equilibrium at that temperature and density despite the system being generally out of equilibrium.

Appendix

Overlap Functions in Equilibrium

We defined the overlap between two copies of a system cloned at time s (and subsequently evolving at the same temperature but subject to different stochastic thermal noise) in Equation (3.2.10) as:

$$Q_s(t) = \frac{\sum_{i=1}^{N} \sigma_i^1(s+t)\sigma_i^2(s+t)}{\sum_{i=1}^{N} \left(\sigma_i^1(s)\right)^2}$$

where σ is some order parameter of the system and the superscripts 1,2 refer to replicas 1,2. This is a general definition that applies to both equilibrium and non-equilibrium conditions. However, in equilibrium the overlap cannot depend on s but only on the relative time t since the clones were made (note also that the denominator will be a conserved quantity in equilibrium and thus it is immaterial at which time it is taken). We denote the equilibrium overlap by $Q(t)$.

In equilibrium, the relative time t since cloning defines the time taken to travel the route between two configurations. Thus (using time-reversal symmetry) on the diagram below the overlap between configurations B and C, which both occur at time $s+t$, is the same as that between configuration A, which occurs at time $s-t$, and either of configuration B or C. Hence we have that:

$$Q(t) = \frac{\sum_{i=1}^{N} \sigma_i^{1=2}(s-t)\sigma_i^1(s+t)}{\sum_{i=1}^{N} \sigma_i^1(s)^2}$$

If we now consider the equilibrium correlation function C(t):

$$C(t) = \frac{\sum_{i=1}^{N} \sigma_i(t)\sigma_i(0)}{\sum_{i=1}^{N} \sigma_i(0)^2}$$

we see that $Q(t) = C(2t)$ in equilibrium [67].

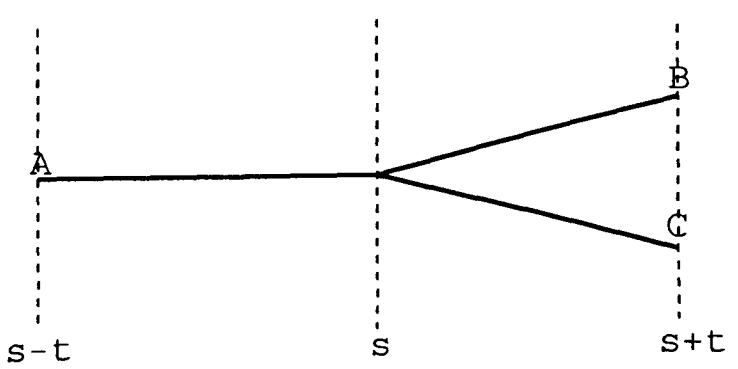

Bibliography

[1] F. Wooten and D. Weaire, Solid State Phys. **40**, 1 (1987).

[2] C. A. Angell, Science **267**, 1924 (1995).

[3] U. Bengtzelius, W. Götze, and A. Sjölander, J. Phys. C **17**, 5915 (1984).

[4] E. Leutheusser, Phys. Rev. A **29**, 2765 (1984).

[5] S. P. Das and G. F. Mazenko, Phys. Rev. A **34**, 2265 (1986).

[6] W. Götze and A. Sjölander, Z. Phys. B **65**, 415 (1987).

[7] W. Kob, p28 in *Experimental and Theoretical Approaches to Supercooled Liquids: Advances and Novel Applications*; Eds.: J. Fourkas, D. Kivelson, U. Mohanty and K. Nelson (ACS Books, Washington, 1997).

[8] W. Götze, J. Phys. Cond. Matt. **11**, A1 (1999).

[9] W. Götze and L. Sjögren, Rep. Prog. Phys. **55**, 241 (1992).

[10] W. Kob and H. C. Andersen, Phys. Rev. E **52**, 4134 (1995).

[11] J. Wuttke *et al.*, Phys. Rev. Lett. **72**, 3052 (1994).

[12] J. Wuttke, W. Petry, G. Coddens, and F. Fujara, Phys. Rev. E **52**, 4026 (1995).

[13] T. Franosch, W. G. M. R. Mayr, and A. P. Singh, Phys. Rev. E **55**, 3183 (1997).

[14] J. Horbach and W. Kob, Phys. Rev. B **60**, 3169 (1999).

[15] J. Horbach and W. Kob, cond-mat/0104322 .

[16] L. F. Cugliandolo and J. Kurchan, Phys. Rev. Lett. **71**, 173 (1993).

[17] J.-P. Bouchaud, L. Cugliandolo, J. Kurchan, and M. Mézard, p161 in *Spin Glasses and Random Fields*; Ed: A. P. Young (World Scientific, 1998).

[18] F. Ritort, Phys. Rev. Lett. **75**, 1190 (1995).

[19] S. Franz and F. Ritort, Europhys. Lett. **31**, 507 (1995).

[20] A. Crisanti, F. Ritort, A. Rocco, and M. Sellitto, J. Chem. Phys. **113**, 10615 (2000).

[21] M. Nicodemi, Phys. Rev. Lett. **82**, 3734 (1999).

[22] J. P. Garrahan and M. E. J. Newman, Phys. Rev. E **62**, 7670 (2000).

[23] L. F. Cugliandolo, J. Kurchan, and L. Peliti, Phys. Rev. E **55**, 3898 (1997).

[24] J. L. Barrat and W. Kob, Europhys. Lett. **46**, 637 (1999).

[25] R. D. Leonardo, L. Angelani, G. Parisi, and G. Ruocco, Phys. Rev. Lett. **84**, 6054 (2000).

[26] G. H. Fredrikson and H. C. Andersen, Phys. Rev. Lett. **53**, 1244 (1984).

[27] M. E. J. Newman and C. Moore, Phys. Rev. E **60**, 5068 (1999).

[28] E. Follana and F. Ritort, Phys. Rev. B **54**, 930 (1996).

[29] M. Shulz and S. Trimper, J. Stat. Phys. **94**, 173 (1999).

[30] J. Reiter and J. Jäckle, Physica A **215**, 311 (1999).

[31] A. Buhot and J. P. Garrahan, cond-mat/0104340 .

[32] J. Jäckle and S. Eisinger, Z. Phys. B **84**, 115 (1991).

[33] P. Sollich and M. R. Evans, Phys. Rev. Lett. **83**, 3238 (1999).

[34] H. Hinrichsen, Adv. in Phys. **49**, 815 (2000).

[35] J. Cardy, *Field Theory and Nonequilibrium Statistical Mechanics*, Lectures presented as part of the Troisieme Cycle de la Suisse Romande, Spring 1999. Availiable at http://www-thphys.physics.ox.ac.uk/users/JohnCardy.

[36] D. Toussaint and F. Wilczek, J. Chem. Phys. **78**, 2642 (1983).

[37] M. Bramson and J. Lebowitz, Phys. Rev. Lett. **61**, 2397 (1988).

[38] P. Grassberger and I. Procaccia, J. Chem. Phys **77**, 6281 (1982).

[39] R. F. Kayser and J. B. Hubbard, Phys. Rev. Lett. **51**, 79 (1983).

[40] V. Privman, Phys. Rev. A **10**, R6140 (1992).

[41] D. ben Avraham, Phys. Rev. Lett. **71**, 3733 (1993).

[42] P. L. Krapivsky, Phys. Rev. E **49**, 3233 (1994).

[43] B. P. Lee, J. Phys. A **27**, 2633 (1994).

[44] V. Privman, Phys. Rev. E **52**, 1866 (1995).

[45] F. Wooten, K. Winer, and D. Weaire, Phys. Rev. Lett. **54**, 1392 (1985).

[46] B. Dubertret, T. Aste, and H. Ohlenbusch, Phys. Rev. E **58**, 6368 (1998).

[47] B. Dubertret and N. Rivier, Biophys. J. **73**, 38 (1997).

[48] F. T. Lewis, Anat. Rec. **50**, 235 (1930).

[49] D. Weaire and R. Phelan, J. Phys. Cond. Mat. **8**, 9519.

[50] T. Aste and D. Sherrington, J. Phys. A **32**, 7049 (1999).

[51] H. Ohlenbusch, N. Rivier, T. Aste, and B. Dubertret, Eur. Phys. J. B **2**, 211 (1998).

[52] D. Weaire and N. Rivier, Contemp. Physics **25**, 59 (1984).

[53] J. Stavans, Rep. Prog. Mod. Phys. **56**, 733 (1993).

[54] W. Kob, J. Phys. C **11**, R85 (1999).

[55] J. Kurchan, L. Peliti, and M. Sellitto, Europhys. Lett.5 **39**, 365 (1997).

[56] A. Barrat, J. Kurchan, V. Loreto, and M. Sellitto, Phys. Rev. Lett. 85 **85**, 5034 (2000).

[57] F. H. Stillinger and T. A. Weber, Phys. Rev. A **25**, 978 (1982).

[58] F. H. Stillinger and T. A. Weber, Science **225**, 983 (1984).

[59] F. H. Stillinger, Science **267**, 1935 (1995).

[60] S. Sastry, P. G. Debenedetti, and F. H. Stillinger, Nature **393**, 554 (1998).

[61] F. Sciortino, W. Kob, and P. Tartaglia, Phys. Rev. Lett. **83**, 3214 (1999).

[62] A. Crisanti and F. Ritort, Europhys. Lett. **52**, 640 (2000).

[63] W. Kob, F. Sciortino, and P. Tartaglia, Europhys. Lett. **49**, 590 (2000).

[64] F. Sciortino, W. Kob, and P. Tartaglia, J. Phys. Cond. Mat. **12**, 6525 (2000).

[65] W. Kob, J. Barrat, F. Sciortino, and P. Tartaglia, Phys. Rev. Lett. **12**, 6385 (2000).

[66] L. Davison and D. Sherrington, J. Phys. A **33**, 8615 (2000).

[67] A. Barrat, R. Burioni, and M.Mézard, J. Phys. A **29**, 1311 (1996).

[68] A. J. Bray, Adv. in Phys. **43**, 357 (1994).

[69] R. G. Palmer, D. L. Stein, E. Abrahams, and P. W. Anderson, Phys. Rev. Lett. **53**, 958 (1984).

[70] A. Lipowski, J. Phys. A **30**, 7365 (1997).

[71] D. Alvarez, S. Franz, and F. Ritort, Phys. Rev. B **54**, 9756 (1996).